Dissertation
submitted to the
Combined Faculties for the Natural Sciences and for Mathematics
of the Ruperto-Carola University of Heidelberg, Germany
for the degree of
Doctor of Natural Sciences

Put forward by

Dipl.-Phys. Univ. Alexander Merle
Born in: Arad, Romania

Oral Examination: December 9th 2009

The Mysteries of Leptons:
New Physics and unexplained Phenomena

Referees:
Prof. Dr. Manfred Lindner
&
Prof. Dr. Tilman Plehn

Zusammenfassung

Diese Doktorarbeit beschäftigt sich mit den Mysterien des leptonischen Sektors des Standardmodells der Elementarteilchenphysik. Nach einem kurzen Überblick über das Standardmodell beginnt der Text mit einer Einführung der so genannten "GSI-Anomalie", der Beobachtung einer periodischen Modullierung des exponentiellen Zerfallsgesetzes, welche noch immer unerklärt ist und fälschlicherweise Neutrinooszillationen zugeschrieben wurde. Es wird argumentiert weshalb diese Interpretation falsch ist und einige weitere Apekte des Phänomens werden diskutiert. Danach werden zwei Themen der Neuen Physik jenseits des Standardmodells behandelt, Doppel-beta-Prozesse und Leptonfamilienzahlverletzung. Einige wichtige phänomenologische Aspekte des ersteren Punktes werden diskutiert, bevor eine detaillierte Berechnung des radiativen Prozesses des neutrinolosen Doppel-Elektroneneinfangs durchgeführt wird. Trotz der winzigen Raten ist ein detailliertes Verständnis dieses Prozesses wichtig, um korrekte experimentelle Untergrenzen festzulegen. Der letzte Teil der Arbeit beginnt mit sehr allgemeinen (und fast modellunabhängigen) Bedingungen für die Erhaltung der Leptonfamilienzahl. Daraufhin wird das Zusammenspiel von Struktur und Freiheit im Yukawa-Sektor eines Modells in Konfrontation mit der Phänomenologie untersucht. Schließlich kommentieren wir noch einen neuen Mechanismus, der in der Tat realistische Strukturen erzeugen kann, welche zu leptonfamilienzahlverletzenden Effekten führen.

Abstract

This doctoral thesis deals with the mysteries of the leptonic sector of the Standard Model of Elementary Particle Physics. After giving a short overview about the Standard Model itself, the text starts with introducing the so-called "GSI anomaly", the observation of a periodic modulation of the exponential decay law, which is still unexplained and has erroneously been attributed to neutrino oscillations. It is argued why this interpretation is incorrect and several further aspects of the phenomenon are discussed. Afterwards two topics of New Physics beyond the Standard Model are treated, double beta processes and lepton flavour violation. Some important phenomenological aspects of the former are discussed before performing a detailed calculation of the radiative process of neutrino-less double electron capture. In spite of the tiny rates, a detailed understanding of this process is important for setting proper experimental limits. The last part of the thesis starts with very general (and nearly model-independent) constraints for lepton flavour conservation, before discussing the interplay of structure and freedom in the Yukawa sector when a model is confronted with phenomenology. We also comment on a new mechanism that can indeed introduce some realistic structures leading to lepton flavour violating effects.

Dedicated to S.
For all the joy you brought in my life

R.I.P.

Contents

Chapter 1

Introduction

Already Goethe's Faust wanted to know in the legendary German drama "what the world contains, In its innermost heart and finer veins" [1]. But he also doubted if science actually can provide such an insight – and it indeed could not at that time.

Meanwhile, we have made a lot of progress in our understanding of Nature. One of the most fundamental branches in science is Elementary Particle Physics, which has contributed significantly to this progress in the last and present century. Amazingly, our theories in the sub-nuclear domain seem to be among the most successfull descriptions of phenomena we observe, although it is in some sense far beyond the limits of our imagination. Still, scientists have found ways to describe and explain the outcome of very many exciting experiments and we seem to be on the right track towards a real understanding of what is going on.

In fact, we have a working model which is suitably called *Standard Model*. Among the great predictions of this model that have later on been verified experimentally are the existence of the Z^0-boson [2], the existence of the t-quark [3], or the extremely precise calculation of the anomalous magnetic moment of the electron, that agrees with experiments at the level of 10 decimals [4] – an agreement which is one of the most precise in all of physics!

Still we know that some building blocks are missing and that our praised Standard Model cannot be the end of the story: For example, it gives us no candidate particle for the so-called *Dark Matter* that has been observed in our Universe [5], it cannot explain the baryon asymmetry [6], and no mechanism to stabilize the Higgs mass against radiative corrections is provided [7]. Part of these questions may be solved by the upcoming LHC experiment [8], among them hopefully the discovery of the last particle of the Standard Model that has not been seen yet, the famous Higgs boson.

In this thesis, some of the mysteries of the leptonic sector of the Standard Model are discussed. Leptons are the "light" fermions, i.e., the charged leptons (*electron*, *muon*, and *tau*) as well as the neutral leptons (*neutrinos*). The leptonic sector is especially well-suited for the quest of finding New Physics beyond the Standard Model, as leptons can (different from quarks) appear as free particles and, since they do not take part in strong interactions, more or less all relevant processes can (at least in principle) be calculated in perturbation theory. Especially neutrinos turn out to have very interesting properties, as we will see in the course of the text. However, also charged leptons may well serve as window to the world of New Physics.

The text is structured as follows: After giving a short overview of the Standard Model and theories beyond in Chapter 2, we start in Chapter 3 with a phenomenon that is currently still unexplained, namely the observation of a non-exponential decay law in single Electron Capture decays, that has erroneously been attributed to neutrino oscillations. After that we investigate radiative neutrino-less double Electron Capture in Chapter 4, which will clearly lead us beyond the Standard Model since it is related to the possible identity of the neutrino to its anti-particle. Then, in Chapter 5, we will extend our considerations to the charged lepton sector by discussing

lepton flavour violation, which results in other rare processes different from neutrino-less double beta decay modes. We finally conclude in Chapter 6.

Note that parts of this thesis have already been published in Refs. [9–14].

Chapter 2

The Standard Model and beyond

Let us start with a short introduction to the Standard Model of Elementary Particle Physics (SM) [15].

Essentially, the SM is a Quantum Field Theory model based in the gauge group $SU(3)_C \times SU(2)_L \times U(1)_Y$, where C stands for *color*, L for *left*, and Y is the so-called *hypercharge*. All particles in the SM are parts of different representations of this gauge group, which obey certain transformation laws. *Gauge invariance* means that the full Lagrangian density of the SM has to be invariant under all gauge transformations, which then imposes many restrictions onto its form and hence onto the possible interactions that can appear between particles.

As an $SU(N)$-group has (N^2-1) generators (and a $U(1)$ has one), we have eight so-called *gluons* (G_a, with $a = 1, ..., 8$) from $SU(3)_C$, three *W-bosons* (W_c, with $c = 1, 2, 3$) from $SU(2)_L$, and one *B-boson* (B^0) from $U(1)_Y$, which are the mediators of the strong and electroweak interactions. These mediators are called *gauge bosons*. Gauge invariance forces the gauge bosons, which all have a spin of 1, to be massless. Furthermore, we have certain fermions (with a spin of $\frac{1}{2}$) in the SM, the so-called *quarks* and *leptons*. Both these groups of fermions can be divided further: We know three generations of *up-type quarks* (u, c, t) and three *down-type quarks* (d, s, b), as well as three neutral leptons called *neutrinos* $(\nu_e, \nu_\mu, \nu_\tau)$ and three *charged leptons* (e, μ, τ), known as *electron*, *muon*, and *tau*. The left- and right-handed fermions sit in different representations of the gauge group $SU(3)_C \times SU(2)_L \times U(1)_Y$:

$$
\begin{aligned}
& q_L = \begin{pmatrix} u_L \\ d_L \end{pmatrix}, \ \begin{pmatrix} c_L \\ s_L \end{pmatrix}, \ \begin{pmatrix} t_L \\ b_L \end{pmatrix} \sim (\underline{\mathbf{3}}, \underline{\mathbf{2}}, +\frac{1}{3}), \\
& u_R, \ c_R, \ t_R \sim (\underline{\mathbf{3}}, \underline{\mathbf{1}}, +\frac{4}{3}), \\
& d_R, \ s_R, \ b_R \sim (\underline{\mathbf{3}}, \underline{\mathbf{1}}, -\frac{2}{3}), \\
& l_L = \begin{pmatrix} (\nu_e)_L \\ e_L \end{pmatrix}, \ \begin{pmatrix} (\nu_\mu)_L \\ \mu_L \end{pmatrix}, \ \begin{pmatrix} (\nu_\tau)_L \\ \tau_L \end{pmatrix} \sim (\underline{\mathbf{1}}, \underline{\mathbf{2}}, -1), \\
& (\nu_e)_R, \ (\nu_\mu)_R, \ (\nu_\tau)_R \sim (\underline{\mathbf{1}}, \underline{\mathbf{1}}, 0), \text{ and} \\
& e_R, \ \mu_R, \ \tau_R \sim (\underline{\mathbf{1}}, \underline{\mathbf{1}}, -2).
\end{aligned} \tag{2.1}
$$

Note that in Eq. (2.1), we have already done a first step beyond the SM, as it does not contain right-handed neutrinos in its pure version.

There is one more part of the SM that has not been detected directly yet, the well known scalar (spin 0) Higgs boson $H \sim (\underline{\mathbf{1}}, \underline{\mathbf{2}}, 1)$. This particle is somehow special, because it is the key point for matching the SM with many of the experiments we have done. The problem is that, according to gauge invariance, not only the gauge bosons but also all particles in Eq. (2.1)

should be massless.[1] We indeed know that the gluons are massless and we have found one colorless gauge boson (namely the photon) which is massless, but it does not correspond to one of the two neutral bosons W^0 and B^0. Furthermore, the quark and charged lepton masses have been determined to be

$$\begin{aligned}
&m_u = 2.55^{+0.75}_{-1.05}\ \text{MeV},\ m_c = 1.27^{+0.07}_{-0.11}\ \text{GeV},\ m_t = 171.3^{+1.1}_{-1.1}\ \text{GeV},\\
&m_d = 5.04^{+0.96}_{-1.54}\ \text{MeV},\ m_s = 105^{+25}_{-35}\ \text{MeV},\ m_b = 4.20^{+0.17}_{-0.07}\ \text{GeV},\\
&m_e = 0.510998910^{+0.000000013}_{-0.000000013}\ \text{MeV},\ m_\mu = 105.6583668^{+0.0000038}_{-0.0000038}\ \text{MeV},\\
&\text{and } m_\tau = 1776.84^{+0.17}_{-0.17}\ \text{MeV}.
\end{aligned} \tag{2.2}$$

For neutrinos, there are just upper limits ($\lesssim 1$ eV) known on the masses (cf. Chapter 4), but we can still be sure that they are massive, as we will see in a moment. Furthermore, we know two electrically charged massive vector bosons $W^\pm$ and the electrically neutral Z^0, which is massive as well:

$$M_W = (80.398 \pm 0.025)\ \text{GeV and } M_Z = (91.1876 \pm 0.0021)\ \text{GeV}. \tag{2.3}$$

The reason for these mysterious masses is the Higgs boson: It can couple to the other particles of the model in a gauge-invariant way (like, e.g., $(-\overline{q_L} H Y_u u_R + h.c.)$ or $(-\overline{q_L}\tilde{H} Y_d d_R + h.c.)$ with $\tilde{H} = i\sigma^2 H^*$ and the so-called *Yukawa matrices* Y_i). By obtaining a *vacuum expectation value* (VEV) $\sqrt{\langle H^\dagger H\rangle}$ (which is often sloppily denoted $\langle H^0\rangle$), these couplings result in effective (*Dirac-*) mass terms for the fermions and also in mass terms for some of the bosons in the model. Since these mass terms are, however, still not invariant under the SM-gauge group $SU(3)_C \times SU(2)_L \times U(1)_Y$ but just under the smaller group $SU(3)_C \times U(1)_{\text{em}}$, the Higgs-VEV leads to a phenomenon called *spontaneous symmetry breaking*. This breaking serves a double purpose: It gives masses to certain particles, but it also yields a residual symmetry $U(1)_{\text{em}}$ which still needs one massless gauge bosons. This is a certain superposition of W^0 & B^0 and is just the particle that we know as photon.

There is one more point about all that: Since the mass terms of, e.g., the up-like and the down-like quarks are both built using the same quark $SU(2)_L$ doublet q_L, the corresponding mass matrices $M_u = vY_u$ and $M_d = vY_d$ cannot be diagonalized simultaneously. This means when, e.g.,

$$-\overline{q_L} M_u u_R + h.c. = -(\overline{u_L}, \overline{c_L}, \overline{t_L}) \begin{pmatrix} m_u & 0 & 0 \\ 0 & m_c & 0 \\ 0 & 0 & m_t \end{pmatrix} \begin{pmatrix} u_R \\ c_R \\ t_R \end{pmatrix} + h.c., \tag{2.4}$$

then M_d cannot have the form $M_d = \text{diag}(m_d, m_s, m_b)$. This is what is called *quark mixing*. One can, e.g., go into the mass basis of the up-like quarks, like in Eq. (2.4). But then the states (d, s, b) have no definite masses. The mass eigenstates (d', s', b') can be obtained by a transformation with the so-called *CKM-matrix* V_{CKM} (Cabibbo-Kobayashi-Maskawa) by the formula

$$\begin{pmatrix} d' \\ s' \\ b' \end{pmatrix} = V_{\text{CKM}}^\dagger \begin{pmatrix} d \\ s \\ b \end{pmatrix}. \tag{2.5}$$

A common parameterization for this matrix is

$$V_{\text{CKM}} = \begin{pmatrix} c_{12}c_{13} & s_{12}c_{13} & s_{13}e^{-i\delta} \\ -s_{12}c_{23} - c_{12}s_{23}s_{13}e^{i\delta} & c_{12}c_{23} - s_{12}s_{23}s_{13}e^{i\delta} & s_{23}c_{13} \\ s_{12}s_{23} - c_{12}c_{23}s_{13}e^{i\delta} & -c_{12}s_{23} - s_{12}c_{23}s_{13}e^{i\delta} & c_{23}c_{13} \end{pmatrix}, \tag{2.6}$$

[1] Note, however, that the right-handed neutrinos could actually form a mass term. We will discuss this possibility in a minute.

with $s_{ij} = \sin\theta_{ij}$ and $c_{ij} = \cos\theta_{ij}$. The parameters are three so-called *mixing angles* θ_{ij} and one *Dirac CP-phase* δ. The values of the quark mixing parameters are approximately given by

$$\theta_{12} = 13.0^\circ,\ \theta_{13} = 0.2^\circ,\ \theta_{23} = 2.4^\circ,\ \text{and}\ \delta = 59.7^\circ. \tag{2.7}$$

Note that all three mixing angles are quite small, so that V_{CKM} is actually close to unity. There exists an analogous matrix in the lepton sector, which is called *Pontecorvo-Maki-Nagakawa-Sakata (PMNS-) matrix* (see Eq. (4.4)).

Giving masses to neutrinos is a more subtle issue: Glancing at Eq. (2.2), we see that all fermion masses are roughly of the order of GeV or MeV. The reason for this is the scale of the Higgs-VEV, which is $v = 174$ GeV. The neutrinos are, however, at least six orders of magnitude lighter than the electron, which is the lightest of all other fermions. This leads us to the question if the neutrinos obtain their masses at all from the same Higgs mechanism as the other fermions. Indeed, there might be more options: The right-handed neutrino is a total singlet under the SM gauge group, so for this field we have the unique opportunity to form an allowed mass term which is given by

$$\mathcal{L}_{\text{Majorana}} = -\overline{(\nu_R)^C} M_R \nu_R. \tag{2.8}$$

This term is called *Majorana mass term*, and it is possible for fermions which are identical to their anti-particles after electroweak symmetry breaking. The charge conjugation C allows for the correct chiral structure of this term and since ν_R is a total singlet, this term is automatically gauge-invariant. Furthermore, since there is the same field to the left and to the right of the mass matrix M_R, it must actually be real and symmetric.[2] The entries of M_R are not generated by the Higgs mechanism, so they can have any values. But that makes the small neutrino masses even more puzzling, since M_R could be extremely large and could very well be much higher than the scale of the electroweak VEV v. There is a very elegant way out of this dilemma, which is known as *seesaw mechanism* [16–20]. In this framework, one allows for left-handed neutrinos ν_L (which are part of the lepton $SU(2)_L$ doublets in Eq. (2.1)), as well as for singlet right-handed neutrinos N_R (which are capitalized in order to make clear that they obtain large masses). The most general mass term is then a combination of a Dirac and a Majorana mass term,

$$\mathcal{L}_{\text{mass}} = -(\overline{\nu_L} m_D N_R + h.c.) - \overline{(N_R)^C} M_R N_R = -(\overline{\nu_L}, \overline{(N_R)^C}) \left(\begin{array}{c|c} 0 & m_D \\ \hline m_D^T & M_R \end{array}\right) \begin{pmatrix} (\nu_L)^C \\ N_R \end{pmatrix}. \tag{2.9}$$

Note that m_D obtains its entries from the Higgs mechanism, so they have to be around the electroweak scale, while M_R can have arbitrarily large entries. The resulting mass eigenstates are superpositions of ν_L and $(N_R)^C$ with mass matrices for the light and heavy neutrinos that are given by

$$m_L = -m_D M_R^{-1} m_D^T \text{ and } M_H \approx M_R. \tag{2.10}$$

If the entries of m_D are, e.g., of $\mathcal{O}(100\text{ GeV})$, while the entries of M_R are of $\mathcal{O}(10^{16}\text{ GeV})$, the masses of the light neutrinos will naturally be around 1 meV.

How do we actually know that neutrinos are indeed massive? From a phenomenon called *neutrino oscillations* [21–24]. These oscillations are periodic transitions between the three types of neutrinos, which depend on the so-called *baseline* L, the distance between production and detection of the neutrino. In a simplified 2-flavour picture, where only two flavour-eigenstate neutrinos (ν_e, ν_μ) exist (and also two mass eigenstates (ν_1, ν_2), which are non-trivial superpositions of the flavour eigenstates that are parameterized by a mixing angle θ), the oscillation probability is given as

$$P(\nu_e \to \nu_\mu, L) = \sin^2(2\theta) \sin^2\left(\frac{\Delta m^2 L}{4E}\right), \tag{2.11}$$

[2] Strictly speaking, it does not have to be real, as long as one also adds the Hermitian conjugate of the mass term as well. It can, however, always be rearranged to look exactly like Eq. (2.8).

where $\Delta m^2 = m_2^2 - m_1^2$ and E is the energy of the neutrino. Since this probability is only sensitive to the mass square difference Δm^2, an observation of neutrino oscillations yields the information that neutrinos are indeed massive, but it gives no clue about their absolute mass scale. We have measured two mass square differences in neutrino oscillation experiments, the *solar* $\Delta m^2_\odot = m_2^2 - m_1^2$ and the *atmospheric* $\Delta m^2_A = m_3^2 - m_1^2$, from which we can conclude that there are three active neutrinos in Nature (in accordance with the measurement of the Z^0-boson decay width, see Ref. [25]). Note further that, different from the quark sector, some neutrino mixing angles in the PMNS-matrix turn out to be relatively large, one is even maximal (cf. Sec. 4.2).

Although the SM is a very nicely working and consistent description of the particles in Nature, it must be incomplete, unfortunately. As briefly mentioned in Chapter 1, there are several observations that the SM cannot explain, and it has inherent problems, too. Apart from the things already mentioned, these are for example the hierarchies of the masses (which seem to become larger with the generation number without a reason) or the values of the mixing angles, for which there is also no explanation (this belongs to the so-called *flavour sector* of the SM). If one takes all these quantities as input parameters, one can still make a lot of predictions which are consistent with experiments, so the structure of our interactions seems to be well described by the SM. Nevertheless, the current situation is somehow unsatisfying and a working extension of the model is desirable. The only problem is that no one knows at the moment in which direction one should extend the SM. Common possibilities are extensions of the scalar sector (see, e.g., Ref. [26]), the gauge sector (see, e.g., Ref. [27]), the spatial dimensions (see, e.g., Ref. [28]), or the global symmetries (the most popular being the so-called *Supersymmetry* (SUSY), see Ref. [7]). Several such models and their connection to the flavour sector will be treated in Chapter 5.

Having reviewed some of the most important points in what concerns the SM and its extensions, we are prepared to enter some of the mysterious aspects of the leptonic sector in more detail. This is what will be done in the next three chapters.

Chapter 3

The GSI anomaly

The first phenomenon that we discuss is currently still unexplained. At GSI (*GSI Helmholtzzentrum für Schwerionenforschung*; before: *Gesellschaft für Schwerionenforschung*) in Darmstadt, Germany, the life-time of several highly charged (in fact hydrogen-like) ions with respect to single electron capture (EC) decay has been measured [29]. What has been found there was not the expected purely exponential decay law, but rather an additional superimposed periodic modulation, as can be seen from Fig. 3.1. After that, a huge debate arose about whether it could be related to neutrino mixing [30–40], or not [10, 13, 41–51]. Alternative attempts for an explanation involve spin-rotation coupling [52–54], the interference of the final states [55], or hyperfine excitation [56]. From the experimental side, two test-experiments (with, however, different systematics [57]) have been performed [58, 59].

In the following, we first discuss the experiment at GSI and the results that have been obtained. We will then shortly comment on experimental difficulties and oddities associated with the experiment, before we calculate the process using the methods of Quantum Field Theory (QFT). Afterwards, we will prove that several approaches indeed justify our treatment of the EC process and also comment on the discussion of Quantum Beats (QBs), which have been mentioned as possible cause of the phenomenon. Finally, we will briefly discuss several articles, in which this treatment has not been done correctly.

3.1 The experiment at GSI

Let us start by briefly explaining the measurement at GSI. For a more detailed explanation of the experiment, the original paper (Ref. [29]) should be consulted. As shown schematically in Fig. 3.2, Sm-projectiles hit a Be-target and produce a bunch of ions from several isotopes (actually, most of them are completely stripped [60]). The next stage is the so-called Fragment Separator (FRS): A suitable magnetic field selects ions of a certain mass over charge ratio M/Q, that are then separated in flight. Note that the latter separation is done by sending the ions through an aluminum foil, inside of which the energy loss of the respective ions is proportional to Q^2. Then, by using another magnetic field for one more M/Q-selection, in average two ions are injected into the Experimental Storage Ring (ESR), which is drawn in more detail in Fig. 3.3. After applying electron cooling in the first few seconds and also by applying a permanent stochastic cooling, the velocity spread $\frac{\Delta v}{v}$ of the ions is reduced to only about 10^{-7}. Then the revolution frequency is only a function of M/Q and can be used as an identification of the respective ion.

The frequency is monitored by using so-called Schottky pickups [61]. The strength of the Schottky signal is proportional to the number of ions of the same frequency, and for up to three ions, the number of ions can be read off from diagrams like the ones in Fig. 3.4 (for larger

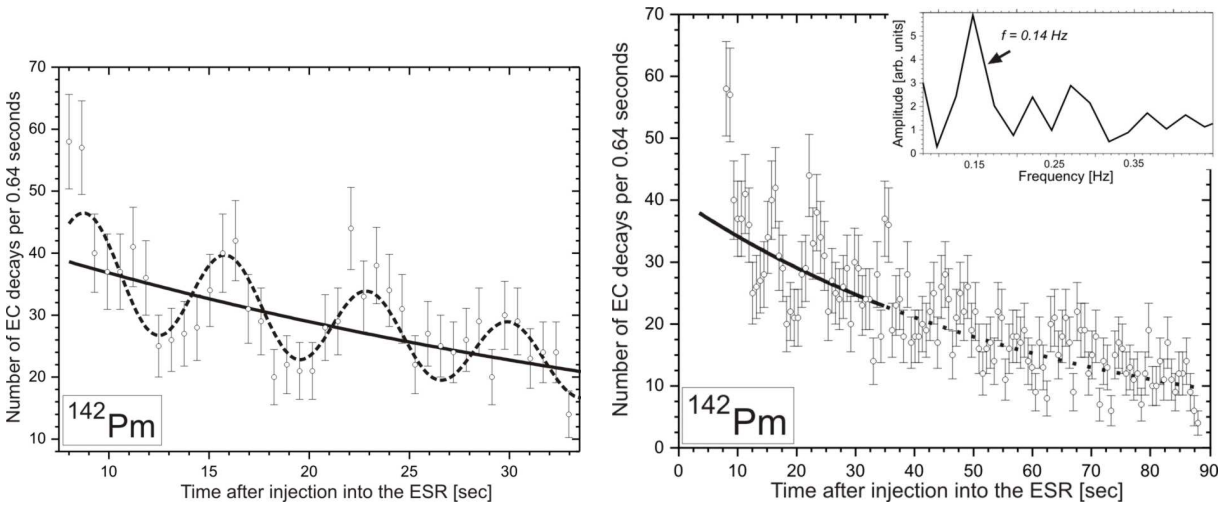

Figure 3.1: The periodic modulation of the exponential decay law, as measured at GSI. The left panel shows only the data from the first 33 seconds, which exhibits the oscillatory behavior. If one looks at the full data set, however, which is presented on the right, the oscillations are much less pronounced and the amplitude seems to shrink considerably for less statistics. (Plots taken from Ref. [29].)

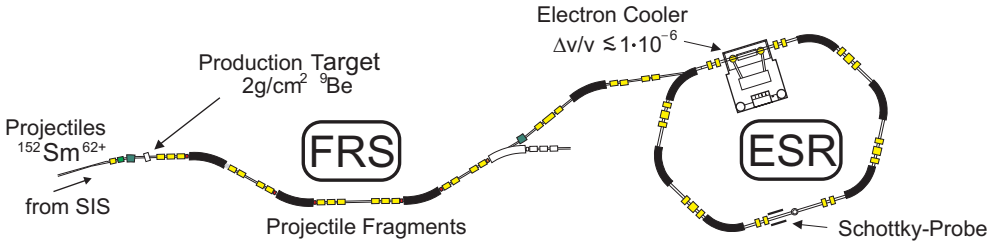

Figure 3.2: The way to the ESR (cf. Fig. 3.3) at GSI. (Picture taken from Ref. [60].)

numbers, the fluctuations of the signal get too large to do that).[1] By time-resolved monitoring of these signals for a certain band of frequencies, the disappearance times of the mother ions as well as the appearance times of the daughter nuclei can be determined very accurately.

3.2 The results of the measurements

The results for $^{142}\mathrm{Pm}^{60+}$ can be found in Fig. 3.1. If fitted with a cos-modulation, the corresponding oscillation period has been determined to be $T = (7.10 \pm 0.22)$ s [29,39]. Further data has been taken for $^{140}\mathrm{Pr}^{58+}$, which resulted in $T = (7.06 \pm 0.08)$ s [29,39]. The zero hypothesis of a purely exponential decay is rejected at 99% C.L. [29]. There is also preliminary data on $^{122}\mathrm{I}^{52+}$, which has, however, not been fully analyzed yet. The current status seems to confirm the oscillatory behavior with a period of $T = (6.11 \pm 0.03)$ s [39].

In the original work, this puzzling result has been attributed to neutrino oscillations [29], which was also claimed as cause of the measurement by several other authors [30, 31, 33–35, 37–39]. This approach was, however, criticized by several authors and shown to be physically incorrect [10, 13, 13, 41–50]. Furthermore, the corresponding neutrino mass square difference as believed to be extracted from the data has been determined to be $\Delta m^2 = (2.18 \pm 0.03) \cdot$

[1] Actually, the strength of the signal is below the thermal noise by a factor of $\sim 10^{-4}$, which means that $\sim 10^4$ circulations are necessary to see a signal.

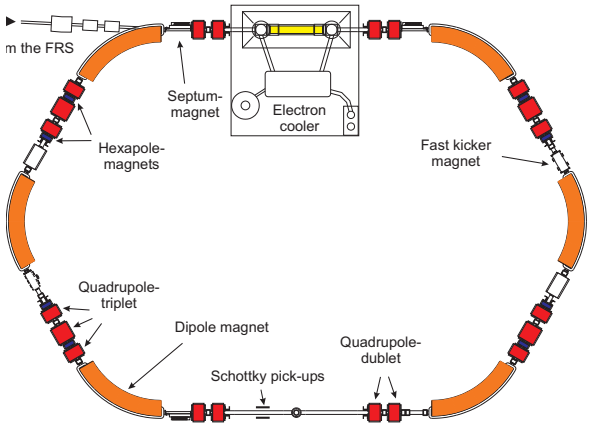

Figure 3.3: The Experimental Storage Ring (ESR) at GSI. (Picture taken from Ref. [60].)

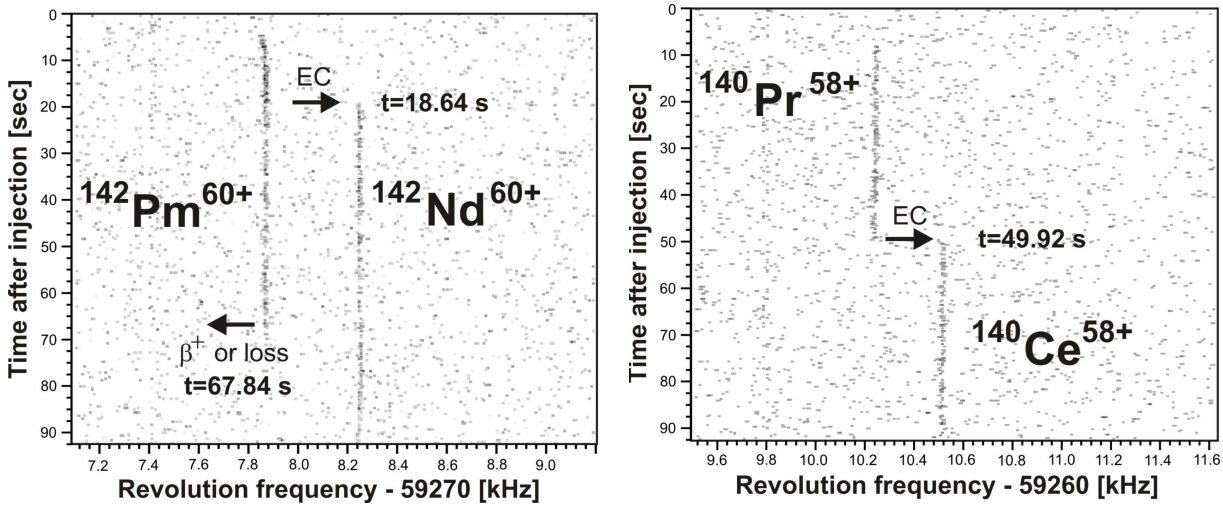

Figure 3.4: The monitoring of the ions. The revolution frequency is clearly a function of the mass over charge ratio, which makes the identification of the respective ions possible. An EC decay slightly changes the mass of the ion, which causes a small jump in the frequency. A β^+ decay in turn changes the mass and the charge, which causes a much larger jump in the opposite direction. (Pictures taken from Ref. [29].)

10^{-4} eV^2 [31], a value which is in conflict with the solar, as well as with the atmospheric Δm^2, both well-known from neutrino oscillation experiments [23].

If one tries to relate the oscillation period of roughly 7 s to a level splitting in the initial state of the decay (see Sec. 3.8.2), the resulting energy difference is about 10^{-15} eV! This scale is extremely tiny, and it is not at all clear where such a splitting should originate from. Furthermore, it seems that the oscillation frequency scales with $1/M$, where M is the mass of the ion [39]. This is one more puzzling feature, since everything that has to do with, e.g., a magnetic moment (such as hyperfine splitting) should scale with Q/M rather than $1/M$. The mass over charge ratio Q/M is, however, nearly the same for all three isotopes considered and it is highly non-trivial to find suitable effects that indeed scale with $1/M$.

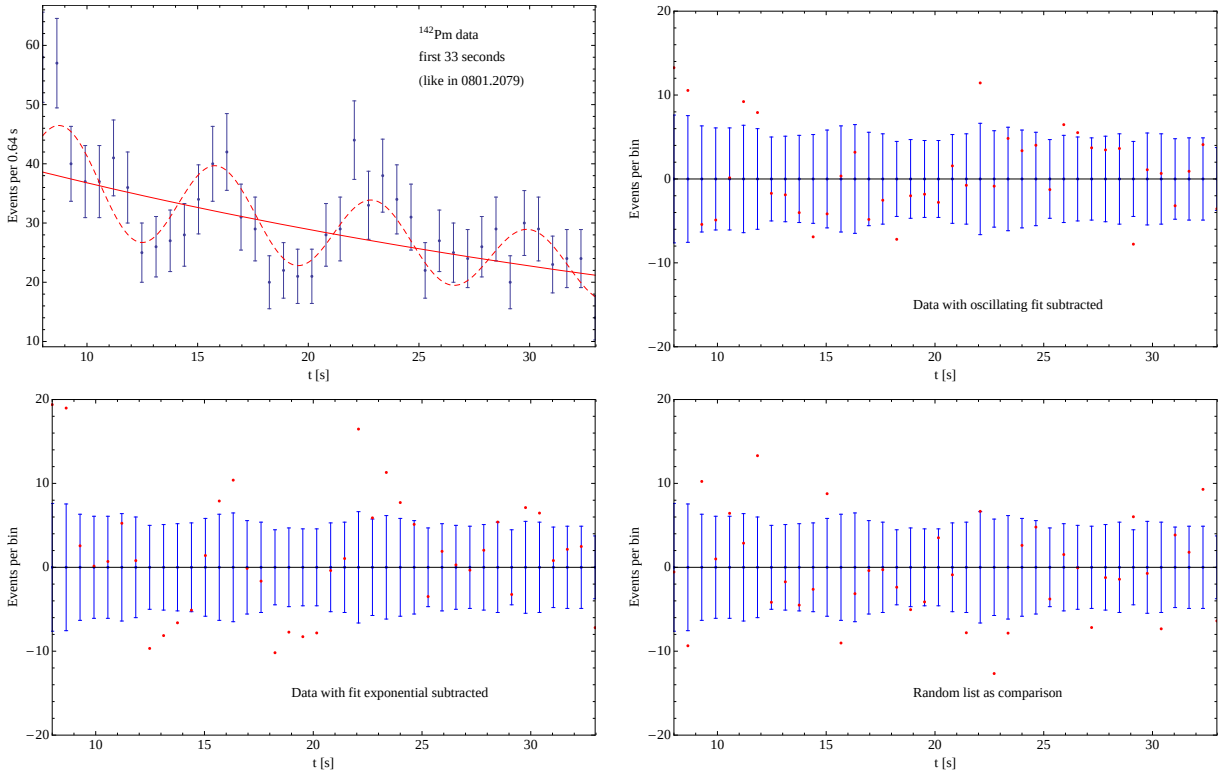

Figure 3.5: Statistical oddities in the Pm-data. It seems that, after subtracting the oscillatory fit, the data would cluster too much around zero.

3.3 Experimental difficulties and oddities

Of course, the first response to such a puzzling observation would be to check the functionality of all ingredients of the experiment, which has been done extensively [62]. We do not want to go into experimental details here, but there is one peculiarity about the Pm-run that should be mentioned.

Looking at the upper left panel of Fig. 3.5 (which is a reproduction of the left panel in Fig. 3.1, where the same features are visible), one can get the impression that the errors of data points seem to nearly always include the fitting curve. Of course, this is just an observation by eye, but one can go further an subtract the best-fit curve for the oscillatory fit (upper right panel) as well as for the exponential fit (lower left panel). The spread of the resulting data points should then be distributed as a Gaussian (actually: Poisson) around zero, with a standard deviation of $\sqrt{N}$ for a bin with N events. As comparison, such a random list is plotted in the lower right panel of Fig. 3.5. Again, it seems that the data points after subtraction of the oscillatory fit lie too often inside the error bars (which can be seen in all of the plots).

The question is, how such an observation can be quantified. One possibility is the so-called *Mann-Whitney test* [63]. This test essentially compares two data lists and gives a statement about the probability that these two lists arise from the same distribution. The main point is that the lists are combined, the result is ordered, and by this ordering one can assign a rank to the combined list. By this rank, one can obtain a probability for how well the two lists fit together.

We have tried to compare the data with the fit (oscillatory or exponential) subtracted with a list of random numbers that was indeed generated by Gaussian distributions in every bin with standard deviations given by $\sqrt{N}$. The result does, of course, depend on the random list, but not too much. The essential outcome is that the probability for the data with the oscillatory

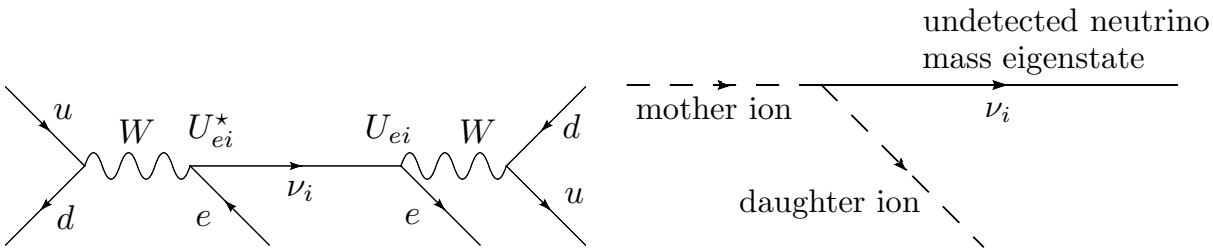

Figure 3.6: The Feynman diagrams for neutrino oscillations (left) and for the process at GSI (right).

fit subtracted to be consistent with a random list turns out to be roughly 3-7%. The data with the exponential fit subtracted gives about 15-20%, while the test, comparing two random lists, yields about 30%.

There might be even better statistical tests than Mann-Whitney, but the principle feature is clear: While the χ^2-fit is only sensitive to an overall agreement of a data set with a certain fit, it cannot resolve correlations between points, since it only sums over all data points. Accordingly, it might well be that, even if the χ^2-fit looks good (or even too good), more information is hidden in the data points.

To be fair, we should also mention that this statistical peculiarity is not present for the cases of Pr and I. So it might be that what looks like something odd is indeed just a random fluctuation of the data point, which could occur with a probability of 1 out of 20.

But let us come back to facts harder than statistics and think about the actual situation at GSI, before performing a detailed calculation of the *EC* process.

3.4 Intuitive thoughts

We start with a general argument why the GSI anomaly is distinct from neutrino oscillations. A possible Feynman diagram for neutrino oscillations is drawn on the left panel of Fig. 3.6, where we look in that case at the $\nu_e \to \nu_e$-channel. In order to get a valid and unambiguous description of the process, it is necessary to include the production as well as the detection process of the neutrino. In that way, there is no need to assume a certain form for an external wave packet that describes the neutrino, but one can rather treat it as virtual particle with a Dirac propagator,

$$\frac{i(\not{p} + m_i)}{p^2 - m_i^2 + i\epsilon}. \tag{3.1}$$

Important features of the above diagram are the following: At the production vertex, the neutrino is produced by weak interaction, which couples to flavour eigenstates. Since the outgoing charged lepton is a positron e^+ (or, equivalently, an anti-electron), the corresponding neutrino has to have electron flavour, too. If neutrino and anti-neutrino are indeed distinct (a question that will re-arise in Chapter 4), then the corresponding neutrino is an electron-neutrino, ν_e. The next point is the propagation of the neutrino: Because of Eq. (3.1), we need a mass eigenstate to propagate (only such a state can have a definite 4-momentum and the particle's mass is explicitly included in the propagator). The ν_e is, however, no mass eigenstate. There is nothing like a "ν_e-mass", but an electron neutrino is rather a superposition of different mass eigenstates ν_i (which are orthogonal, since they correspond to different mass eigenvalues), from which we currently know that there are three,

$$|\nu_e\rangle = \sum_{i=1}^{3} U^*_{ei} |\nu_i\rangle. \tag{3.2}$$

Category	Double Slit	$e^+e^- \to \mu^+\mu^-$	GSI-experiment
1	No slit-monitoring at all	e^+e^--collider	N/A
2A	Monitoring & read out	New Physics required	GSI-like experiment with more kinematical accuracy
2B	Monitoring without read out	New Physics, but no read out	Actual GSI-experiment

Table 3.1: The classification of the three examples.

Here, U_{ei} is an element of the unitary leptonic mixing matrix that we will discuss in more detail later on (cf. Eq. (4.4)). At the detection vertex, the neutrino is detected in connection with an electron, so it is again a ν_e. Obviously, there are three possible ways to reach the same final state from the same initial state – and hence we have to sum the partial amplitudes before squaring the total amplitude (*coherent summation*):

$$A_{ee} = \sum_i |U_{ei}|^2 e^{-ip_i^\mu x_\mu}. \tag{3.3}$$

Since there was propagation in between, the different mass eigenstates will, however, have obtained different phases, and interference terms appear when calculating the square of the total amplitude. These phases depend on the space-time coordinates of the detection, and accordingly this procedure will lead to the standard formula for neutrino oscillations.

But how is the situation at the GSI-experiment? This is drawn in the right panel of Fig. 3.6. The production process is essentially the same: Since there was an electron in the initial state, the neutrino produced is again a ν_e. There is, however, a clear difference in the process: The neutrino that is produced escapes undetected, and there is *no second flavour measurement*. Feynman diagrams describe transitions between states of definite energy and momentum. Thus the final state neutrino must be a mass eigenstate ν_i due to energy-momentum conservation. In a hypothetical situation where the energies and momenta of the mother and daughter ions are measured with infinite precision, it would even be possible to tell from kinematics which neutrino mass eigenstate has been produced. Only this mass eigenstate, i.e., only one Feynman diagram would contribute and the rate would be proportional to

$$|U_{ei} e^{-ip_i^\mu x_\mu}|^2 = |U_{ei}|^2, \tag{3.4}$$

but there would be no oscillations. However, this is far from the real kinematical situation in the setup at GSI.

Realistic values for the energy and momentum uncertainties imply that it is not possible to tell which mass eigenstate was produced, so that all of them have to be taken into account, and they must be treated as distinct final states. They contribute to the total rate as an *incoherent sum* of the amplitudes (which is just a sum over probabilities), since the mass eigenstates are orthogonal vectors in Hilbert space. The total rate is then proportional to $\sum_i |U_{ei} e^{-ip_i x}|^2 = 1$, implying that in principle there cannot be any mixing effects. Of course, this cannot change in a quantum mechanical approximation of QFT. This orthogonality can also not be changed by a large energy uncertainty [22], since the only feature that is relevant is the fact that the mass eigenstates are in principle distinguishable.

3.5 Comparisons to other processes

Let us again go through these arguments is greater detail. The starting point for the discussion is the superposition principle in QM. One common formulation is [64]: “When a process can

happen in alternative ways, we *add the amplitudes* for each possible way." The problem in the interpretation arises in the term "alternative ways", because it is not a priori clear what the word *way* actually means. A second problem of interpretation is connected to the word *process*, which exhibits similar ambiguities.

Let us use the following terminology: *Process* means a reaction with a well-defined initial and final state, whereas *way* is a particular intermediate state of a process. E.g., the scattering reaction $e^+e^- \to \mu^+\mu^-$ is one single process, no matter by which way (γ-, Z^0-, or H^0-exchange at tree-level in the Standard Model (SM) of elementary particles) it is mediated. $Z^0 \to \nu_e\overline{\nu}_e$ and $Z^0 \to \nu_\mu\overline{\nu}_\mu$ are, however, two distinct processes.

Using this terminology, the superposition principle can be formulated in the following way:

1. If different ways lead from the same initial to the same final state in one particular process, then one has to add the respective partial amplitudes to obtain the total amplitude. The probability of the process to happen is then proportional to the absolute square of this total amplitude (*coherent summation*).

2. If a reaction leads to physically distinct final states, then one has to add the probabilities for the different processes (*incoherent summation*).

If a certain situation belongs to category 1, an interference pattern will be visible (or oscillations, in case the interfering terms have different phases as functions of time), while if it belongs to category 2, there will be no interference. The remaining question is at which point the measurement comes in. This can be trivially said for point 2: Either the experimental apparatus is sufficiently good to distinguish between the different final states (2A) – then no summation whatsoever is necessary simply because one can divide the data set into two (or more), one for each of the different final states. If this is not the case (2B), the experiment will be able to lead to either of the final states, but one would not know which one had been the actual result – then the probabilities for the different final states to occur have to be added in order to obtain the total probability.

What if we do such a measurement for category 1? If we can indeed distinguish several ways that a process can happen, then this has to be done by some measurement. Since this measurement then has selected one particular way, we have actually transformed a situation belonging to category 1 into a situation of category 2. However, then there would be no terms to interfere with – the interference would have been "killed".

Let us now turn to Table 3.1, that illustrates how our three examples fit into the categories 1, 2A, and 2B. These three examples will be discussed one by one in the following.

3.5.1 The Double Slit experiment with photons

This is the "classical" situation of an experiment that reveals the nature of QM. It has first been performed by Thomas Young [65] and has later been used as the major example to illustrate the laws of QM. It works as follows: Light emitted coherently by some source (e.g., a laser) hits a wall with two slits, both with widths comparable to the wavelength of the light. If it hits a screen behind the wall, one will observe an interference pattern, as characteristic for wave-like objects (category 1). There is, however, the interpretation of light as photons, i.e., quanta of a well-defined energy. Naturally, one could ask which path such a photon has taken, i.e., through which of the two slits it has travelled. The amazing observation is that, as soon as one can resolve this by monitoring the slits accurately enough, the interference pattern will vanish, no matter if one actually reads out the information of the monitoring (2A), or not (2B). The reason is that, regardless of using the information or not, the measurement itself has disturbed the QM process in a way that the interference pattern is destroyed [66].

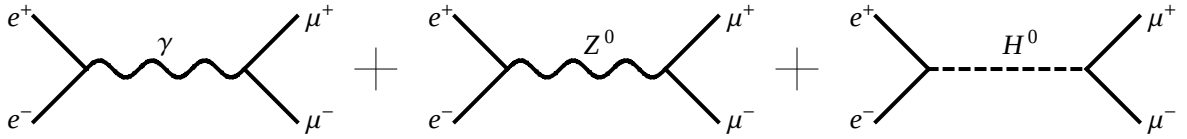

Figure 3.7: The diagrams contributing to $e^+e^- \to \mu^+\mu^-$ in the SM.

The key point is that one cannot even say that the photon takes only one way: In the QM-formulation, amplitudes are added (and not probabilities), and hence the photon does not take one way or the other (and we simply sum over the results), but it rather has a total amplitude that includes way 1 as well as way 2. By taking the absolute square of this amplitude interference terms appear. A QFT-formulation involving elementary fields only would be completely different: One would sum over the amplitudes for the photon to interact with each electron and each quark in the matter the slits are made of, after having propagated to this particular particle and before propagating further to a certain point on the screen. Of course, by using an effective formulation of the theory, one can find a much more economical description and the easiest one is to simply comprise all possible interactions into two amplitudes, one for going through the first and one for going through the second slit.

If there is monitoring, one actually "kills" one of these two amplitudes, the other one remains, and the interference pattern is destroyed. Whenever there has been such a measurement, the interference will vanish. As we will see, the question is if in a certain situation a measurement has been performed (or is implicitly included in the process considered), no matter if the corresponding information is read out or not.

The situation at GSI can actually be compared to the double slit experiment: They key point for dividing the situations described above into category 1 and 2 was that we need a screen (or any other apparatus) to measure the photons after the double slit. In the GSI case, this "screen" would be the second flavour tag (the right vertex in the diagram on the left panel of Fig. 3.6). Since this is missing, however, there can be no interference terms (and hence no oscillations in the lifetime), no matter if the "slits" are monitored or not.

3.5.2 $e^+e^- \to \mu^+\mu^-$ scattering at a collider

Let us now consider the scattering of e^-e^+ to form a pair of muons. This is, differently from the Double Slit experiment, a fundamental process where only a small number of elementary particles is involved. If one wants to calculate the scattering probability, the amplitude for the process is again decisive. In the SM, there are only three possibilities for this process to happen at tree-level and in all three of them the e^+e^- pair annihilates to some intermediate (virtual) boson which in the end decays again, but this time into a $\mu^+\mu^-$ pair. The intermediate particle can either be a photon, a Z^0-boson, or a Higgs scalar, see Fig. 3.7.

Here, we have three different *ways* to form the process. The difference to the Double Slit experiment, however, is that these three ways cannot be separated easily. In a real collider-experiment we are not able to say that the reaction $e^+e^- \to \mu^+\mu^-$ has taken place by the exchange of, e.g., a photon only, but it will always be the sum of the three diagrams (and a lot more, in case we include higher orders). Hence, this process will always fall into category 1 and interference terms will appear.

This might be different once we postulate New Physics: If, e.g., there were three strong background fields that couple only to the photon, to the Z^0-boson, and to the Higgs, respectively, and do not disturb each other, then one could (by a suitable experimental device) distinguish

the three diagrams and would end up in category 2. Depending on whether the corresponding information is read out or not, the experiment could belong to 2A or 2B, but in both cases interference would be lost.

3.5.3 The situation in the GSI-experiment

The remaining question is what the situation looks like for the GSI-experiment. Even though the QFT-calculation of what happens is pretty straightforward, fitting everything in the language used above might be a bit more subtle. We will, however, see in Sec. 3.6 that the formulation in terms of amplitudes leads to the same result anyway.

Let us go back to the Feynman diagram (right panel of Fig. 3.6): Here, in the absence of extreme kinematics, the neutrino is produced as electron neutrino. What happens to this neutrino? Since it is not detected, it escapes to infinity in the view of QFT (in the picture of second quantization). Physically, it loses its coherence after some propagation distance and travels as a unique mass eigenstate.

The key point is the following: Since the neutrino will not interact before it loses its coherence, it must be asymptotically a mass eigenstate. This can be shown easily: The coherence length of a (relativistic) neutrino is given by [67]

$$L_{\text{coh}} = 2\sqrt{2}\sigma_x \cdot \frac{2p^2}{(\Delta m^2)_\odot}, \tag{3.5}$$

where σ_x is the size of the neutrino wave packet, p is the mean value neutrino momentum in the limit $m_\nu = 0$, and $(\Delta m^2)_\odot = 7.67 \cdot 10^{-5}$ eV^2 [23] is the solar neutrino mass square difference as known from neutrino oscillation experiments. The question is how to obtain an estimate for σ_x: If the nucleus that undergoes the EC was inside a lattice, one could estimate a width like the typical interatomic distance, $\sigma_x \sim 1$Å, which would lead to $L_{\text{coh}} \sim 2 \cdot 10^8$ m. Of course, this precision cannot be reached in the GSI-experiment. However, at least during the electron cooling [68], the nucleus will be localized to some precision. Since the velocity of the nucleus is known, this information could in principle be extrapolated for each run. A fair estimate would then be the average distance between two electrons in the cooling process, which is roughly given by $1/\sqrt[3]{n} \sim 0.1$ mm, where n is the electron density [69]. This would lead to a more realistic coherence length of $L_{\text{coh}} \sim 2 \cdot 10^{14}$ m. The pessimistic case, where σ_x is taken to be the approximate diameter 108.36 m/π [70] of the ESR produces $L_{\text{coh}} \sim 6 \cdot 10^{19}$ m. The mean free path of a neutrino in our galaxy, however, is roughly $1 \cdot 10^{40}$ m (for an assumed matter density in the Milky Way of $1 \cdot 10^{-23}$ g/cm^3), so the assumption that the neutrino does not interact before losing its coherence is completely safe.

Even if we do not know in which of the three mass eigenstates it actually is, we know that it has to be in one of them. This knowledge is somehow obtained "a posteriori", since the mass eigenstate only reveals its identity after some propagation. But, by conservation of energy and momentum, one could treat the process as if the kinematical selection had already been present at the production point of the neutrino. This "measurement" is enforced by the physical conservation laws.

An analogous reasoning is given by Feynman and Hibbs [66], using the example of neutron scattering: Neutrons prepared to have all spin up scatter on a crystal. If one of the scattered neutrons turns out to have spin down, one knows by angular momentum conservation that it must have been scattered by a certain nucleus. In principle, by noting down the spin state of every nucleus in the crystal before and after the measurement, one could find the corresponding scattering partner of the neutron without disturbing it. No matter if this would be difficult practically, by a physical conservation law one knows that a particular scattering must have

been present, even if the corresponding nucleus is not "read out". Accordingly, the corresponding interference vanishes and the neutrons that have spin down after the scattering come out diffusely in all directions.

This can also be formulated in the language of wave packets: We have complete 4-momentum conservation for each single component (which is a plane wave!) of the wave packets, but if we consider the whole wave packet, its central momentum does not have to be conserved [22, 71]. However, all the different components can produce both possible neutrino mass eigenstates, but for a certain kinematical configuration of mother and daughter components only one of the mass eigenstates will actually be produced.

The rest is easy: If the GSI-experiment had infinite kinematical precision, one could read out which of the mass eigenstates has been produced and it would clearly fall into category 2A. Since, however, this information is not read out but could in principle have been obtained (e.g. by detecting the escaping neutrino), the GSI-experiment falls into category 2B and one has to sum over probabilities. This logic works because we know that the neutrino is, after some propagation, no superposition of mass eigenstates anymore, but just one particular eigenstate with a completely fixed mass.

A viewpoint closer to the amplitude formulation would be: If the neutrino finally interacts, it has to "decide" which mass eigenstate it has, even if it was a superposition of several mass eigenstates before. This is then equivalent to the image of having produced one particular mass eigenstate from the beginning.

3.6 Amplitudes - probably the easiest language to use

In this section, we use time-dependent amplitudes for the different basis states to describe another example, namely charged pion decay, which is then compared to neutrino oscillations (referring again to the actual situation in the GSI-experiment). This description is clear enough to account for very different situations, and allows for an easy and nearly intuitive understanding of the various cases.

3.6.1 Charged pion decay

It is well-known that a charged pion (e.g. π^+) can decay into either a positron in combination with an electron neutrino, or into the corresponding pair of μ-like particles. Let us consider the case of a pure (and normalized) initial state pion $|\pi^+\rangle$. As this state evolves with time (and is not monitored), it will become a coherent superposition of the mother-state, as well as all possible daughter states:

$$|\pi^+(t)\rangle = \mathcal{A}_\pi(t)|\pi^+\rangle + \mathcal{A}_\mu(t)|\mu^+\nu_\mu\rangle + \mathcal{A}_e(t)|e^+\nu_e\rangle, \tag{3.6}$$

where all time-dependence is inside the partial amplitudes $\mathcal{A}_i$. Of course, this state has to be normalized correctly:

$$|\mathcal{A}_\pi(t)|^2 + |\mathcal{A}_\mu(t)|^2 + |\mathcal{A}_e(t)|^2 = 1, \tag{3.7}$$

with $\mathcal{A}_\pi(0) = 1$ and $\mathcal{A}_\mu(0) = \mathcal{A}_e(0) = 0$. One can understand Eq. (3.6) in the following way: The state at time t is a coherent superposition of the basis states $\{|\pi^+\rangle, |\mu^+\nu_\mu\rangle, |e^+\nu_e\rangle\}$ with time-dependent coefficients. Note that the basis states are orthogonal, since they are clearly distinguishable. The outcome of a certain measurement is some state $|\Psi\rangle$. If one wants to know the probability for measuring that particular state, one has to calculate it according to the standard formula,

$$P(\Psi) = |\langle\Psi|\pi^+(t)\rangle|^2. \tag{3.8}$$

The question is what $|\Psi\rangle$ looks like. To make that clear, let us discuss several cases:

- The (trivial) case is that there has been no detection at all: Then we have gained no information. This means that the projected state is just the time-evolved state itself (we do not know anything except for the time passed since the experiment has started), and we get
$$|\langle\Psi|\pi^+(t)\rangle|^2 = |\langle\pi^+(t)|\pi^+(t)\rangle|^2 = 1. \tag{3.9}$$
This result is trivial, since the probability for anything to happen always has to be equal to 1.

- The next situation is when our experimental apparatus can give us only the information that the pion has decayed, but we do not know the exact final state. This can be either $|\mu^+\nu_\mu\rangle$ or $|e^+\nu_e\rangle$ and we remain with a superposition of these two states. The only information that we have gained is that the amplitude for the initial pion to be still there is now zero, $\mathcal{A}_\pi = 0$ in Eq. (3.6). Then, the properly normalized state $|\Psi\rangle$ is given by
$$|\Psi\rangle = \frac{\mathcal{A}_\mu(t)|\mu^+\nu_\mu\rangle + \mathcal{A}_e(t)|e^+\nu_e\rangle}{\sqrt{|\mathcal{A}_\mu(t)|^2 + |\mathcal{A}_e(t)|^2}}. \tag{3.10}$$
The absolute value square of the corresponding projection is
$$\begin{aligned}|\langle\Psi|\pi^+(t)\rangle|^2 &= \left|\frac{|\mathcal{A}_\mu(t)|^2\langle\mu^+\nu_\mu|\mu^+\nu_\mu\rangle + |\mathcal{A}_e(t)|^2\langle e^+\nu_e|e^+\nu_e\rangle| + 0}{\sqrt{|\mathcal{A}_\mu(t)|^2 + |\mathcal{A}_e(t)|^2}}\right|^2 = \\ &= |\mathcal{A}_\mu(t)|^2 + |\mathcal{A}_e(t)|^2. \end{aligned}\tag{3.11}$$
If there is any oscillatory phase in the amplitudes, $\mathcal{A}_k(t) = \tilde{\mathcal{A}}_k(t)e^{i\omega_k t}$, it will have no effect due to the absolute values.

- What if we know that the initial pion is still present? This sets $\mathcal{A}_\mu(t) = \mathcal{A}_e(t) = 0$, and $|\Psi\rangle$ is just $\mathcal{A}_\pi(t)|\pi^+\rangle/\sqrt{|\mathcal{A}_\pi(t)|^2}$. The projection yields
$$|\langle\Psi|\pi^+(t)\rangle|^2 = |\mathcal{A}_\pi(t)|^2, \tag{3.12}$$
which again does not oscillate.

- If one particular final state, let us say $|e^+\nu_e\rangle$, is detected, then we have $\mathcal{A}_\pi(t) = \mathcal{A}_\mu(t) = 0$ and we get another term free of oscillations:
$$|\langle\Psi|\pi^+(t)\rangle|^2 = |\mathcal{A}_e(t)|^2. \tag{3.13}$$

The question remains when we indeed get oscillations. The answer is: It depends on what our detector measures. If the detector, e.g., measures not exactly the state $|\mu^+\nu_\mu\rangle$ or $|e^+\nu_e\rangle$, but instead some (hypothetical) superposition (e.g., some quantum number which is not yet known, under which neither μ^+ nor e^+ is an eigenstate, but some superposition of them), then one could, e.g., measure the following (correctly normalized!) state:
$$|\Psi\rangle = \frac{1}{\sqrt{2}}\left(|\mu^+\nu_\mu\rangle + |e^+\nu_e\rangle\right). \tag{3.14}$$
The squared overlap is
$$|\langle\Psi|\pi^+(t)\rangle|^2 = \frac{1}{2}\left[|\mathcal{A}_\mu(t)|^2 + |\mathcal{A}_e(t)|^2 + 2\Re\left(\mathcal{A}_\mu^*(t)\mathcal{A}_e(t)\right)\right], \tag{3.15}$$
where the $2\Re\left(\mathcal{A}_\mu^*(t)\mathcal{A}_e(t)\right)$-piece will, in general, contain oscillatory terms.

What has been done differently than before? This time we have done more than simply killing one or more amplitudes in Eq. (3.6), and this is the cause of oscillations: Whenever we are in a situation, in which the state playing the role of $|\Psi\rangle$ in Eq. (3.14) is physical, the corresponding projection will yield oscillatory terms.

3.6.2 Neutrino oscillations and the GSI-experiment

Let us now turn to neutrino oscillations. Here, as we will see, a state like $|\Psi\rangle$ in Eq. (3.14) can indeed be physical in some situations. To draw a clean analogy to the experiment done at GSI, we consider a hydrogen-like ion as initial state $|M\rangle$ that can decay to the state $|D\nu_e\rangle$ via electron capture. Since there was an electron in the initial state, we know that the amplitude for producing the mass eigenstate $|\nu_i\rangle$ is just proportional to U_{ei}. If there is no relative phase between the two mass eigenstates, the neutrino produced in the decay is exactly the particle that we call *electron neutrino*. In any case, due to different kinematics, the two mass eigenstates will develop different phases in the time-evolution. This means that, in spite of the mixing matrix elements U_{ei} being time-independent, there will be a phase between the two neutrino mass eigenstates.

Completely analogous to Eq. (3.6), the time-evolution of the initial state will be given by:

$$|M(t)\rangle = \mathcal{A}_M(t)|M\rangle + U_{e1}\mathcal{A}_1(t)|D\nu_1\rangle + U_{e2}\mathcal{A}_2(t)|D\nu_2\rangle, \tag{3.16}$$

with $|\mathcal{A}_M(t)|^2 + |U_{e1}\mathcal{A}_1(t)|^2 + |U_{e2}\mathcal{A}_2(t)|^2 = 1$ and $\mathcal{A}_M(0) = 1$. We can immediately look at different cases:

- The mother is seen: This kills all daughter amplitudes, $\mathcal{A}_{1,2}(t) = 0$. With the proper normalization for $|\Psi\rangle$ one gets no oscillation again:

$$|\langle\Psi|M(t)\rangle|^2 = |\mathcal{A}_M(t)|^2. \tag{3.17}$$

- The next case corresponds to the actual GSI-experiment: One sees only the decay, but cannot tell which of the two neutrino mass eigenstates has been produced. This leads to $\mathcal{A}_M(t) = 0$ and hence

$$|\Psi\rangle = \frac{U_{e1}\mathcal{A}_1(t)|D\nu_1\rangle + U_{e2}\mathcal{A}_2(t)|D\nu_2\rangle}{\sqrt{|U_{e1}\mathcal{A}_1(t)|^2 + |U_{e2}\mathcal{A}_2(t)|^2}}. \tag{3.18}$$

  Projecting this state on $|M(t)\rangle$ from Eq. (3.16) yields

$$|\langle\Psi|M(t)\rangle|^2 = \left|\frac{|U_{e1}\mathcal{A}_1(t)|^2\cdot 1 + |U_{e2}\mathcal{A}_2(t)|^2\cdot 1}{\sqrt{|U_{e1}\mathcal{A}_1(t)|^2 + |U_{e2}\mathcal{A}_2(t)|^2}}\right|^2 = |U_{e1}\mathcal{A}_1(t)|^2 + |U_{e2}\mathcal{A}_2(t)|^2, \tag{3.19}$$

  which exhibits no oscillation, but is rather an incoherent sum over probabilities.

- The GSI-experiment with infinite kinematic precision: In this case, one could actually distinguish the states $|D\nu_1\rangle$ and $|D\nu_2\rangle$. If one knows that $|D\nu_1\rangle$ is produced (e.g., by having very precise information about the kinematics), one will again have no oscillation,

$$|\langle\Psi|M(t)\rangle|^2 = |\mathcal{A}_1(t)U_{e1}|^2. \tag{3.20}$$

These are in principle all cases that can appear. One can, however, have a closer look at the realistic situation in the GSI-experiment. Let us re-consider Eq. (3.16): In reality, the mother ion will be described by a wave packet with a finite size or, equivalently, a finite spreading in momentum space, due to the Heisenberg uncertainty relation. If this wave-packet is broad enough that each component can equivalently decay into $|D\nu_1\rangle$ or $|D\nu_2\rangle$, then both of the corresponding amplitudes will actually have the same phase ($\mathcal{A}_1(t) = \mathcal{A}_2(t)$), since they have the same energy, and one can write Eq. (3.16) as

$$|M(t)\rangle = \mathcal{A}_M(t)|M\rangle + \mathcal{A}(t)\underbrace{\left[U_{e1}|D\nu_1\rangle + U_{e2}|D\nu_2\rangle\right]}_{=|D\nu_e\rangle}. \tag{3.21}$$

Since the knowledge of the momentum of the mother ion is not accurate enough at the GSI-experiment to make a distinction between both final states $|D\nu_k\rangle$, this is a realistic situation. Of course, this does not at all change the above argumentation, since the final state $|\Psi\rangle$ will experience the same modification. The neutrino produced is an electron-neutrino, as expected.

The question remains, why some authors come to the conclusion that there should be oscillations? The answer is simple: If the correspondence between time-evolved initial state and detected state is wrong, then oscillations may appear. As example we will consider the situation that the kinematics of the mother and daughter are fixed so tightly, that indeed the production amplitudes for $|D\nu_1\rangle$ and $|D\nu_2\rangle$ are not equal. This would correspond to an extremely narrow wave packet in momentum space. Let us, e.g, have in mind the extreme case when by kinematics only the production of the lightest mass eigenstate ν_1 is possible. This is no problem in principle and we would be used to it if neutrinos had larger masses, so that the Q-value of the capture was only sufficient to produce the lightest neutrino. If only the disappearance of the mother is seen, the corresponding state $|\Psi\rangle$, which is detected, is given by Eq. (3.18) (with $\mathcal{A}_2(t) = 0$ in the extreme case, but in any case with $\mathcal{A}_1(t) \neq \mathcal{A}_2(t)$). The corresponding neutrino is, however, no electron-neutrino anymore (which would be $U_{e1}|\nu_1\rangle + U_{e2}|\nu_2\rangle$, with the same phase for both states)! Indeed this is no surprise at all, since the kinematics in the situation considered is so tight that it changes the neutrino state which is emitted. This is a clear consequence of quantum mechanics, since for obtaining the necessary pre-knowledge (the very accurate information about the kinematics), one has to do a measurement that is precise enough to have an impact on the QM state.

If one now projects onto an electron neutrino instead of correctly projecting onto the state which is emitted, oscillations will appear:

$$|\langle D, \nu_e|M(t)\rangle|^2 = |(U_{e1}^*\langle D\nu_1| + U_{e2}^*\langle D\nu_2|) \cdot (\mathcal{A}_M(t)|M\rangle + U_{e1}\mathcal{A}_1(t)|D\nu_1\rangle + U_{e2}\mathcal{A}_2(t)|D\nu_2\rangle)|^2 =$$
$$= |\mathcal{A}_1(t)|^2 + |\mathcal{A}_2(t)|^2 + 2\Re(\mathcal{A}_1(t)\mathcal{A}_2^*(t)). \tag{3.22}$$

This is, however, wrong: One has not used all the information that one could in principle have obtained! But Nature does not care about if one uses information or not, so this treatment does simply not correspond to what has happened in the actual experiment. The oscillations, however, only arise due to the incorrect projection, and have no physical meaning.

The remaining question is if the neutrino that is emitted in the GSI-experiment oscillates. The answer is yes, of course. But to see that, we will have to modify our formalism a bit. Knowing that the neutrino that has been emitted corresponds to $\mathcal{A}_M(t) = 0$ in Eq. (3.21), the remaining (normalized) state is:

$$|\Psi\rangle = \frac{\mathcal{A}(t)}{|\mathcal{A}(t)|}\left[U_{e1}|D\nu_1\rangle + U_{e2}|D\nu_2\rangle\right]. \tag{3.23}$$

Rephasing this state and measuring the time from t on gives as initial state:

$$|\Psi\rangle = U_{e1}|D\nu_1\rangle + U_{e2}|D\nu_2\rangle. \tag{3.24}$$

This is the state which will undergo some evolution in time according to

$$|\Psi(t')\rangle = \mathcal{A}_1'(t')U_{e1}|D\nu_1\rangle + \mathcal{A}_2'(t')U_{e2}|D\nu_2\rangle, \tag{3.25}$$

with $|\mathcal{A}_1'(t')U_{e1}|^2 + |\mathcal{A}_2'(t')U_{e2}|^2 = 1$ and $\mathcal{A}_1'(0) = \mathcal{A}_2'(0) = 1$. If we ask what happens to this neutrino if it is detected after some macroscopic distance, it is necessary to take into account what has happend to the daughter nucleus that has been produced together with the neutrino, due to entanglement. The daughter nucleus, which is accurately described by a wave packet, is detected, but not with sufficient kinematical accuracy to distinguish the different components

$|D\rangle$ of the wave packet. The effect of such a non-measurement is studied most easily in the density matrix formalism. The density matrix ρ' corresponding to Eq. (3.25) is given by

$$|\Psi(t')\rangle\langle\Psi(t')| = |\mathcal{B}_1(t')|^2|D\rangle|\nu_1\rangle\langle\nu_1|\langle D| + |\mathcal{B}_2(t')|^2|D\rangle|\nu_2\rangle\langle\nu_2|\langle D| + [\mathcal{B}_1(t')\mathcal{B}_2^*(t')|D\rangle|\nu_1\rangle\langle\nu_2|\langle D| + h.c.], \tag{3.26}$$

where $\mathcal{B}_k(t') = \mathcal{A}'_k(t')U_{ek}$. If the exact kinematics of the daughter is not measured, then one has to calculate the trace over the corresponding states. That gives

$$\rho \equiv \int dD\langle D|\rho'|D\rangle = |\mathcal{B}_1(t')|^2|\nu_1\rangle\langle\nu_1| + |\mathcal{B}_2(t')|^2|\nu_2\rangle\langle\nu_2| + \left(\mathcal{B}_1(t')\mathcal{B}_2^*(t')|\nu_1\rangle\langle\nu_2| + h.c.\right). \tag{3.27}$$

If we want to know the probability to detect, e.g., a muon neutrino, $|\nu_\mu\rangle = U_{\mu 1}|\nu_1\rangle + U_{\mu 2}|\nu_2\rangle$, then the corresponding projection operator is given by

$$\mathcal{P}_\mu = |\nu_\mu\rangle\langle\nu_\mu|, \tag{3.28}$$

and the probability to detect this state is

$$P_\mu = \mathrm{Tr}(\mathcal{P}_\mu\rho) = \langle\nu_1|\mathcal{P}_\mu\rho|\nu_1\rangle + \langle\nu_2|\mathcal{P}_\mu\rho|\nu_2\rangle. \tag{3.29}$$

Note that, however, the neutrino states $|\nu_{1,2}\rangle$ will always be orthogonal, since they correspond to eigenstates of different masses (like an electron is in that sense orthogonal to a muon). The result is

$$P_\mu = |U_{\mu 1}|^2|\mathcal{B}_1(t')|^2 + |U_{\mu 2}|^2|\mathcal{B}_2(t')|^2 + [U_{\mu 1}U_{\mu 2}^*\mathcal{B}_1^*(t')\mathcal{B}_2(t') + c.c.], \tag{3.30}$$

where the term in brackets contains oscillatory contributions in general.

3.7 The correct Quantum Field Theory treatment of EC decay

After having argued in great detail why one indeed needs an *incoherent sum* over probabilities, it is time to perform a detailed calculation of the process at GSI, using the density matrix formalism for a proper theoretical treatment of the detection process. This calculation will show explicitly that no interference terms can appear in the EC decay, as long as there is just one initial state and no coherent superposition of more than one.

First we have to take into account that the GSI detector is sensitive to the daughter ion, but not to the neutrino. Using again the density matrix formalism, the detection of a daughter state $|\psi_{D,k}\rangle$ is described by the operator

$$\hat{P}^{(k)} = \sum_{j=1}^{3}\int d^3p_\nu\ |\psi_{D,k};\nu_j,\mathbf{p}_\nu\rangle\langle\psi_{D,k};\nu_j,\mathbf{p}_\nu|. \tag{3.31}$$

The sum and the integral run over a complete set of neutrino mass eigenstates $|\nu_j\rangle$ with momenta $\mathbf{p}_\nu$. With the density matrix for the time-evolved mother state $|\psi_M\rangle$, given by $\rho = |\psi_M\rangle\langle\psi_M|$, the probability for the observation of $|\psi_{D,k}\rangle$ becomes

$$\mathcal{P}_k = \mathrm{Tr}\left[\hat{P}^{(k)}\rho\right] = \sum_{j=1}^{3}\int d^3p_\nu\ \left|\langle\psi_{D,k};\nu_j,\mathbf{p}_\nu|\psi_M\rangle\right|^2. \tag{3.32}$$

The sum over neutrino states is incoherent. Therefore, if $\mathcal{P}_k$ contains oscillatory interference terms, they cannot be due to neutrino mixing, but must originate from somewhere else. Accordingly, they would even occur in a hypothetical model with only one neutrino flavour. All attempts to explain the GSI anomaly in terms of neutrino mixing are thus invalid.

One might, however, imagine that different components of the mother wave packet $|\psi_M\rangle$ obtain relative phase differences during the propagation. If several such components could decay into *the same* daughter state $|\psi_{D,k};\nu_j,\mathbf{p}_\nu\rangle$, they would induce interference terms in $\mathcal{P}_k$. This would correspond exactly to a situation of category 1 in the language of Sec. 3.5: Different ways lead to the same final state. To see under which conditions such a mechanism could explain the GSI anomaly, we will now compute the matrix element $\langle\psi_{D,k};\nu_j,\mathbf{p}_\nu|\psi_M\rangle$ in the wave packet formalism [22]. This is necessary, since the mother and daughter ions are constrained to be inside the ESR. Accordingly, they cannot be described by plane waves (that would have equal probability to appear anywhere in space), but rather by a more complicated function. In turn, they also cannot be momentum eigenstates, but will have some certain spreading.

The states $|\psi_M\rangle$ and $|\psi_D\rangle$ of the mother and daughter ions are described by Gaussian wave packets

$$\psi_A(\mathbf{x},t)=\left(\frac{2\pi}{\sigma_A^2}\right)^{3/4}\int\frac{d^3p_A}{(2\pi)^3\sqrt{2E_A}}\exp\left[-\frac{(\mathbf{p}_A-\mathbf{p}_{A0})^2}{4\sigma_A^2}-iE_A(t-t_A)+i\mathbf{p}_A(\mathbf{x}-\mathbf{x}_A)\right], \quad (3.33)$$

where $A=M,D$. Here, $\mathbf{p}_{M0}$ and $\mathbf{p}_{D0}$ are the central momenta of the wave packets, and $\sigma_{M,D}$ are their momentum space widths.[2] The energies are given by $E_A=\sqrt{\mathbf{p}_A^2+m_A^2}$. Furthermore, the wave packets are defined such that at the injection time t_M, the peak of ψ_M is located at $\mathbf{x}_M$ (and analogous for the detection time t_D and ψ_D).

Using coordinate space Feynman rules, one can easily write down the decay amplitude into a specific final state $|\psi_D;\nu_j,\mathbf{p}_\nu\rangle$:

$$i\langle\psi_D;\nu_j,\mathbf{p}_\nu|\psi_M\rangle=\int d^3x dt\; U_{ej}\mathcal{M}_j^{EC}(E_M,E_D,E_\nu)\psi^*_{\nu_j}(\mathbf{x},t)\psi^*_D(\mathbf{x}_D,t_D)\psi_M(\mathbf{x}_M,t_M), \quad (3.34)$$

where U_{ej} is an element of the PMNS-matrix and $\mathcal{M}_j^{EC}(E_M,E_D,E_\nu)$ is the transition amplitude between plane wave states, as computed in [72, 73]. Inserting Eq. (3.33) for the ions and describing the neutrino as plane wave, we obtain

$$\begin{aligned}i\langle\psi_D;\nu_j,\mathbf{p}_\nu|\psi_M\rangle=&\int\frac{d^3p_M}{(2\pi)^3\sqrt{2E_M}}\int\frac{d^3p_D}{(2\pi)^3\sqrt{2E_D}}\int d^3x dt\left(\frac{2\pi}{\sigma_M\sigma_D}\right)^{\frac{3}{2}}U_{ej}\mathcal{M}_j^{EC}(E_M,E_D,E_\nu)\\&\cdot\exp\left[-\frac{(\mathbf{p}_D-\mathbf{p}_{D0})^2}{4\sigma_D^2}+iE_D(t-t_D)-i\mathbf{p}_D(\mathbf{x}-\mathbf{x}_D)\right]\\&\cdot\exp\left[-\frac{(\mathbf{p}_M-\mathbf{p}_{M0})^2}{4\sigma_M^2}-iE_M(t-t_M)+i\mathbf{p}_M(\mathbf{x}-\mathbf{x}_M)\right]\exp\left[iE_{\nu,j}t-i\mathbf{p}_\nu\mathbf{x}\right], \quad (3.35)\end{aligned}$$

where $E_{\nu,j}$ is the energy of the mass eigenstate ν_j. Now we apply several approximations that will simplify the calculation considerably, but will not affect the general argumentation:

- First, we expand the energies E_A up to first order in the momentum difference $(\mathbf{p}_A-\mathbf{p}_{A0})$, which leads to

$$E_A\approx E_{A0}+\frac{\mathbf{p}_{A0}}{E_{A0}}(\mathbf{p}_A-\mathbf{p}_{A0})=E_{A0}+\mathbf{v}_{A0}(\mathbf{p}_A-\mathbf{p}_{0A}), \quad (3.36)$$

  where $\mathbf{v}_{A0}$ is the group velocity of the wave packet and $E_{A0}=\sqrt{\mathbf{p}_{A0}^2+m_A^2}$.

[2] Note that is not always easy to assign an exact value to these widths, but the argumentation in this section is not changed for any of the plausible assumptions about the σ's, cf. Sec. 3.5.3.

- Furthermore, we assume the pre-factors $\frac{1}{\sqrt{2E_A}}$ to vary slowly over the width of the wave packet, which leads to the replacement

$$\frac{1}{\sqrt{2E_A}} \to \frac{1}{\sqrt{2E_{A0}}}. \tag{3.37}$$

- Finally, we also assume the matrix element $\mathcal{M}_j^{EC}(E_M, E_D, E_\nu)$ to vary slowly with energy:

$$\mathcal{M}_j^{EC}(E_M, E_D, E_\nu) \approx \text{const.} \tag{3.38}$$

As we will see in Sec. 3.8.2, these approximations cannot destroy an oscillatory behavior and are indeed simply a technical simplification of the computation. We then have to evaluate integrals of the following form:

$$\begin{aligned}
&\int \frac{d^3p_A}{(2\pi)^3\sqrt{2E_A}} \exp\left[-\frac{(\mathbf{p}_A - \mathbf{p}_{A0})^2}{4\sigma_A^2} \pm iE_A(t-t_A) \mp i\mathbf{p}_A(\mathbf{x}-\mathbf{x}_A)\right] \approx \\
&\approx e^{\pm iE_{A0}(t-t_A)\mp i\mathbf{p}_{A0}} \int \frac{d^3p_A}{(2\pi)^3\sqrt{2E_A}} \exp\left[-\frac{(\mathbf{p}_A - \mathbf{p}_{A0})^2}{4\sigma_A^2}\right] e^{\mp i(\mathbf{p}_A-\mathbf{p}_{A0})[\mathbf{x}-\mathbf{x}_A-\mathbf{v}_{A0}(t-t_A)]} = \\
&= e^{\pm iE_{A0}(t-t_A)\mp i\mathbf{p}_{A0}} \left(\frac{\sigma_A^2}{2\pi}\right)^{3/2} \frac{2}{\sqrt{E_{A0}}} e^{-\sigma_A^2[\mathbf{x}-\mathbf{x}_A-\mathbf{v}_{A0}(t-t_A)]^2},
\end{aligned} \tag{3.39}$$

where we have used the formula

$$\int d^3x\ e^{-\mathbf{x}^T A\mathbf{x}+\mathbf{b}^T\mathbf{x}} = \frac{\pi^{3/2}}{\sqrt{\det A}} e^{\mathbf{b}^T A^{-1}\mathbf{b}/4}. \tag{3.40}$$

Having done that, Eq. (3.35) becomes

$$\begin{aligned}
i\langle\psi_D;\nu_j,\mathbf{p}_\nu|\psi_M\rangle = \frac{4}{\sqrt{E_{M0}E_{D0}}} \left(\frac{\sigma_M\sigma_D}{2\pi}\right)^{3/2} \int d^3x dt\ U_{ej}\mathcal{M}_j^{EC}(E_{M0}, E_{D0}, E_\nu) \cdot \\
\cdot \exp\left[-iE_{M0}(t-t_M) + i\mathbf{p}_{M0}(\mathbf{x}-\mathbf{x}_M) - (\mathbf{x}-\mathbf{x}_M-\mathbf{v}_{M0}(t-t_M))^2\,\sigma_M^2\right] \cdot \\
\cdot \exp\left[+iE_{D0}(t-t_D) - i\mathbf{p}_{D0}(\mathbf{x}-\mathbf{x}_D) - (\mathbf{x}-\mathbf{x}_D-\mathbf{v}_{D0}(t-t_D))^2\,\sigma_D^2\right] \exp\left[iE_{\nu,j}t - i\mathbf{p}_\nu\mathbf{x}\right].
\end{aligned} \tag{3.41}$$

The remaining integrals over $\mathbf{x}$ and t are Gaussian as well. Doing the $\mathbf{x}$-integral first yields for $i\langle\psi_D;\nu_j,\mathbf{p}_\nu|\psi_M\rangle$:

$$\frac{2}{\sqrt{2E_{M0}E_{D0}}} \left(\frac{\sigma_M\sigma_D}{\sigma_M^2+\sigma_D^2}\right)^{3/2} \int dt\ U_{ej}\mathcal{M}_j^{EC}(E_{M0}, E_{D0}, E_\nu) e^{-At^2+(B_R+iB_{I,j})t+(C_R+iC_I)}, \tag{3.42}$$

where

$$\begin{aligned}
A &= \frac{-\boldsymbol{\tau}^2}{\sigma_M^2+\sigma_D^2} + \tau^2, \\
B_R &= \frac{2\boldsymbol{\sigma}\boldsymbol{\tau}}{\sigma_M^2+\sigma_D^2} + 2\sigma^2, \\
B_{I,j} &= -\frac{\mathbf{p}\boldsymbol{\tau}}{\sigma_M^2+\sigma_D^2} - E_j, \\
C_R &= \frac{1}{\sigma_M^2+\sigma_D^2}\left(\boldsymbol{\sigma}^2 - \frac{\mathbf{p}^2}{4}\right) - v^2, \\
C_I &= \frac{-\boldsymbol{\sigma}\mathbf{p}}{\sigma_M^2+\sigma_D^2} + (z_M - z_D),
\end{aligned} \tag{3.43}$$

and

$$\begin{aligned}
&\boldsymbol{\sigma} = \sigma_M^2 \mathbf{y}_M + \sigma_D^2 \mathbf{y}_D,\\
&\boldsymbol{\tau} = \sigma_M^2 \mathbf{v}_{M0} + \sigma_D^2 \mathbf{v}_{D0},\\
&\sigma^2 = \sigma_M^2 \mathbf{v}_{M0}^2 t_M + \sigma_D^2 \mathbf{v}_{D0}^2 t_D,\\
&\tau^2 = \sigma_M^2 \mathbf{v}_{M0}^2 + \sigma_D^2 \mathbf{v}_{D0}^2,\\
&\upsilon^2 = \sigma_M^2 \mathbf{v}_{M0}^2 t_M^2 + \sigma_D^2 \mathbf{v}_{D0}^2 t_D^2,\\
&\mathbf{y}_{M,D} = \mathbf{x}_{M,D} - \mathbf{v}_{M0,D0} t_{M,D},\\
&z_{M,D} = E_{M0,D0} t_{M,D} - \mathbf{p}_{M0,D0} \mathbf{x}_{M,D},\\
&\mathbf{p} = \mathbf{p}_{M0} - \mathbf{p}_{D0} - \mathbf{p}_\nu,\ E_j = E_{M0} - E_{D0} - E_{\nu,j}.
\end{aligned} \tag{3.44}$$

Performing the t-integration in Eq. (3.42) yields the final result:

$$i\langle \psi_D; \nu_j, \mathbf{p}_\nu | \psi_M \rangle = C U_{ej} \mathcal{M}_j^{EC}(E_{M0}, E_{D0}, E_\nu) e^{f_j} e^{i\phi_j}, \tag{3.45}$$

where

$$\begin{aligned}
C &= \frac{2}{\sqrt{2E_{M0}E_{D0}}} \left(\frac{\sigma_M \sigma_D}{\sigma_M^2 + \sigma_D^2} \right)^{3/2} \sqrt{\frac{\pi}{A}},\\
f_j &= \frac{B_R^2 - B_{I,j}^2}{4A} + C_R, \text{ and } \phi_j = \frac{B_R B_{I,j}}{2A} + C_I.
\end{aligned} \tag{3.46}$$

The real factor e^{f_j} enforces sufficient overlap of the wave packets, but is non-oscillatory for Gaussian wave packets (it might be oscillatory for pathological forms of the wave packet, but then this oscillation would be extremely fast and always averaged out in any real physical situation [74]; in particular, the frequency would not match the scale obtained in the GSI-experiment). The complex phase factor $e^{i\phi_j}$ is oscillatory, but is irrelevant for the modulus of the matrix element appearing in Eq. (3.32). Accordingly, there can be no oscillatory terms in the final result.

3.8 Quantum Beats and the GSI anomaly

The last point to discuss are the so-called Quantum Beats (QBs) [75]. There, atomic levels are considered for the discussion, and we will stick to that here and give the relation to the GSI-experiment at the end of each case.

As has been pointed out in Refs. [10,41,42,45], the only possibility where QBs might explain the GSI anomaly, is a splitting in the initial state. We will argue (using the language of Ref. [75]), why this is true and also give a short derivation of the explicit expression for the one successfull case. This case, however, has its problems, too.

3.8.1 Single atom of type I

Let us start with the classical example of QBs, namely one atom in a coherent superposition of three states $|a\rangle$, $|b\rangle$, and $|c\rangle$, where the first two states are above and closely spaced compared to $|c\rangle$. This setting is drawn on the left panel of Fig. 3.8 and is referred to as *type I*. First note that the three levels correspond to different (but fixed) eigenvalues of the energy and are hence orthogonal vectors in Hilbert space. This is not at all changed by an energy uncertainty which, however, makes it possible to have a coherent superposition of the three states. Initially, we assume the atom to be in such a superposition of these states, but having emitted no photon

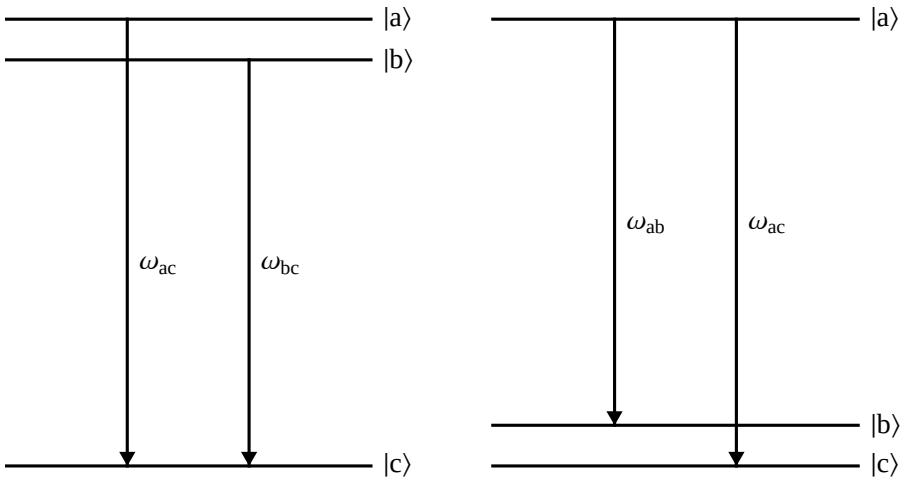

Figure 3.8: Type I (left) and type II (right) of the Quantum Beats settings.

yet. Accordingly, the photon state can only be the vacuum $|0\rangle_\gamma$. Then, the initial state of this system can be written as

$$|\Psi(0)\rangle = \mathcal{A}_0|a\rangle|0\rangle_\gamma + \mathcal{B}_0|b\rangle|0\rangle_\gamma + \mathcal{C}_0|c\rangle|0\rangle_\gamma, \tag{3.47}$$

where $|\mathcal{A}_0|^2 + |\mathcal{B}_0|^2 + |\mathcal{C}_0|^2 = 1$. If this system undergoes a time-evolution, the lower state might be populated by de-excitation of the upper ones, which is done by photon emission.[3] If the state $|1_x\rangle_\gamma = a_x^\dagger|0\rangle_\gamma$ is assumed to describe a state with one photon of frequency ω_x, then the state at time t can be written as

$$|\Psi(t)\rangle = \mathcal{A}(t)|a\rangle|0\rangle_\gamma + \mathcal{B}(t)|b\rangle|0\rangle_\gamma + \mathcal{C}(t)|c\rangle|0\rangle_\gamma + \mathcal{C}_1(t)|c\rangle|1_{ac}\rangle_\gamma + \mathcal{C}_2(t)|c\rangle|1_{bc}\rangle_\gamma, \tag{3.48}$$

where $\mathcal{A}(0) = \mathcal{A}_0$, $\mathcal{B}(0) = \mathcal{B}_0$, $\mathcal{C}(0) = \mathcal{C}_0$, $\mathcal{C}_{1,2}(0) = 0$, and $|\mathcal{A}(t)|^2 + |\mathcal{B}(t)|^2 + |\mathcal{C}(t)|^2 + |\mathcal{C}_1(t)|^2 + |\mathcal{C}_2(t)|^2 = 1$. Under the assumption that all levels are equally populated, the radiated intensity will be proportional to

$$\langle\Psi(t)|\mathbf{E}^2(\mathbf{0},t)|\Psi(t)\rangle, \tag{3.49}$$

where

$$\mathbf{E}(\mathbf{x},t) = \sum_{\mathbf{k},\lambda} \boldsymbol{\epsilon}_{\mathbf{k},\lambda}\left(a_{\mathbf{k},\lambda}e^{-ikx} + a^\dagger_{\mathbf{k},\lambda}e^{+ikx}\right) \tag{3.50}$$

is the electric field operator and $\boldsymbol{\epsilon}_{\mathbf{k},\lambda}$ is the electric field per photon of momentum $\mathbf{k}$ and polarization λ. Note that the creation and annihilation operators have only one non-trivial commutation relation, namely $[a_{\mathbf{k},\lambda}, a^\dagger_{\mathbf{k}',\lambda'}] = \delta_{\mathbf{k},\mathbf{k}'}\delta_{\lambda,\lambda'}$. In our case we obtain effectively:

$$\mathbf{E}^2(\mathbf{0},t) = \epsilon_{ac}^2(1 + 2a^\dagger_{ac}a_{ac}) + \epsilon_{bc}^2(1 + 2a^\dagger_{bc}a_{bc}) + 2\epsilon_{ac}\epsilon_{bc}(a^\dagger_{ac}a_{bc}e^{i\Delta t} + a^\dagger_{bc}a_{ac}e^{-i\Delta t}), \tag{3.51}$$

where $\Delta = \omega_{ac} - \omega_{bc}$. Here, we have already used that terms like, e.g., a_{ac}^2 give no contribution with $|\Psi\rangle$ from Eq. (3.48). Remember now, that the atomic states are orthonormal. This means that one can, e.g., combine a term proportional to $\langle b|$ in $\langle\Psi(t)|$ only with the corresponding term $|b\rangle$ in $|\Psi(t)\rangle$. The corresponding combination of amplitudes $|\mathcal{B}(t)|^2$ does, however, not oscillate, since any phase will be killed by the absolute value. This is also true for every term involving one

[3] Note that we neglect transitions from $|a\rangle$ to $|b\rangle$ due to the different energy of the corresponding photons.

of the time-independent parts of Eq. (3.51): E.g., the term proportional to $\mathcal{C}^*(t)\mathcal{C}_1(t)$ involves a factor

$$ {}_\gamma\langle 0|a^\dagger_{ac}a_{ac}a^\dagger_{ac}|0\rangle_\gamma = 0, \tag{3.52}$$

because of $a^\dagger_{ac}$ acting on the left. There are, however, remaining oscillatory terms such as $\mathcal{C}^*_1(t)\mathcal{C}_2(t)e^{i\Delta t}$, which is proportional to

$$ {}_\gamma\langle 0|a_{ac}a^\dagger_{ac}a_{bc}a^\dagger_{bc}|0\rangle_\gamma = {}_\gamma\langle 0|(1+a^\dagger_{ac}a_{ac})(1+a^\dagger_{bc}a_{bc})|0\rangle_\gamma = {}_\gamma\langle 0|0\rangle_\gamma = 1. \tag{3.53}$$

These terms cause the Quantum Beats for a type I atom. Actually, one could have expected this result intuitively: Both of the coherently excited upper levels can decay into *the same* state $|c\rangle$ via the emission of a photon. Hence, one cannot in any way determine the photon energy without measuring it directly. Without such a measurement, interference terms will appear.

The relation to the GSI-experiment is simple: One just has to replace the photon by the neutrino, which is also undetected, and interference terms will show up, too.

3.8.2 A hypothetical splitting in the initial state

We will explicitly calculate the *hypothetical* situation introduced in Sec. 3.8.1, in which the GSI oscillations can be explained by quantum beats of the mother ion. This has been mentioned in Refs. [10, 41, 42, 45].

Let us assume that the state of the mother ion is split into several sublevels $|\psi^{(n)}_M\rangle$, and that, for some reason, the production process creates the mother ion in a superposition

$$ |\psi_M\rangle = \sum_n \alpha_n |\psi^{(n)}_M\rangle, \tag{3.54}$$

where the coefficients α_n have to fulfill the normalization condition $\sum_n |\alpha_n|^2 = 1$. With this modification, Eq. (3.45) turns into

$$ i\langle\psi_D;\nu_j,\mathbf{p}_\nu|\psi_M\rangle^{(n)} = \alpha_n C U_{ej}\mathcal{M}^{EC}_j(E_{M0},E_{D0},E_\nu)e^{f^{(n)}_j}e^{i\phi^{(n)}_j} \tag{3.55}$$

where $f^{(n)}_j$ and $\phi^{(n)}_j$ are defined as in Eq. (3.46), but including an upper index (n) for the quantities E_{0M}, $\mathbf{p}_{0M}$, $\mathbf{v}_{0M}$, E_j, $\mathbf{p}$, $\boldsymbol{\sigma}$, $\boldsymbol{\tau}$, σ^2, τ^2, υ^2, $\mathbf{y}_M$, and z_M. For simplicity, we have neglected the n-dependence of the normalization factors and of the matrix element. Typically, also the wave packet overlap factor $\exp[f^{(n)}_j]$ will be almost independent of n, so we can safely omit it in the following, assuming it to be absorbed in the overall normalization constant.

Upon squaring $|\langle\psi_D;\nu_j,\mathbf{p}_\nu|\psi_M\rangle|$, we now obtain interference terms proportional to

$$ \exp\left[i(\phi^{(n)}_j - \phi^{(m)}_j)\right]. \tag{3.56}$$

To simplify this expression, we can go to the rest frame of the daughter nucleus, in which $\mathbf{v}_{0D} = 0$ and $\mathbf{p}_{0D} = 0$, and we can freely set $\mathbf{x}_M = 0$ and $t_M = 0$. Moreover, we can choose $\sigma_D = \sigma_M \equiv \overline{\sigma}$ and expand $\left(\phi^{(n)}_j - \phi^{(m)}_j\right)$ up to first order in the small quantities

$$ \Delta E^{(nm)}_{M0} \equiv E^{(n)}_{M0} - E^{(m)}_{M0} \simeq \xi\frac{\Delta m^2_{nm}}{2E^{(m)}_{M0}},\ \Delta\mathbf{p}^{(nm)}_{M0} \equiv \mathbf{p}^{(n)}_{M0} - \mathbf{p}^{(m)}_{M0} \simeq -(1-\xi)\frac{\Delta m^2_{nm}\mathbf{p}^{(m)}_{M0}}{2|\mathbf{p}^{(m)}_{M0}|^2}. \tag{3.57}$$

Here, ξ is a real parameter that is determined by the details of the production process and $\Delta m^2_{nm} = (m_n - m_m)(m_n + m_m)$ is the squared energy difference between different components in the initial state from Eq. (3.54). If we finally neglect all higher order corrections, we find

$$ |\langle\psi_D;\nu_j,\mathbf{p}_\nu|\psi_M\rangle|^2 \propto \sum_{n,m}\alpha_n\alpha^*_m \exp\left[-i\mathbf{x}_D\left(\frac{\Delta m^2_{nm}\mathbf{p}^{(m)}_{M0}}{2|\mathbf{p}^{(m)}_{M0}|^2}\right)\right]. \tag{3.58}$$

Using the relation $\mathbf{x}_D \simeq \mathbf{v}_{M0}^{(m)} t_D$, which is a good approximation for sufficiently well localized wave packets, the phase factor can equivalently be written as

$$\exp\left[\frac{-it_D \Delta m_{nm}^2}{2E_{M0}^{(m)}}\right], \tag{3.59}$$

which indeed leads to an oscillatory behavior [10].

The splitting, however, would have to be tiny, $\sim 10^{-15}$ eV, a value which can hardly be explained. As has been pointed out in [76], there is also no known reason why the production process should create a coherent superposition of substates at all. Furthermore, there exists preliminary data on the lifetimes of $^{142}\mathrm{Pm}^{60+}$ with respect to β^+ decay that shows no oscillatory behavior [39]. An initial splitting in the nucleus will lead to an oscillatory rate in this case, too. Accordingly, if such a splitting is present in the initial state, it could be in the levels of the single bound electron, since this would then effect EC decays while leaving β^+ decays untouched.

3.8.3 Single atom of type II

Let us go on and study a similar setting as in Sec. 3.8.1, namely and atom of type II, shown on the right panel of Fig. 3.8. The corresponding initial state would again be described by Eq. (3.47), but its time-evolution would now look like

$$|\Psi(t)\rangle = \mathcal{A}(t)|a\rangle|0\rangle_\gamma + \mathcal{B}(t)|b\rangle|0\rangle_\gamma + \mathcal{C}(t)|c\rangle|0\rangle_\gamma + \mathcal{B}'(t)|b\rangle|1_{ab}\rangle_\gamma + \mathcal{C}'(t)|c\rangle|1_{ac}\rangle_\gamma, \tag{3.60}$$

where $\mathcal{A}(0) = \mathcal{A}_0$, $\mathcal{B}(0) = \mathcal{B}_0$, $\mathcal{C}(0) = \mathcal{C}_0$, $\mathcal{B}'(0) = 0$, $\mathcal{C}'(0) = 0$, and $|\mathcal{A}(t)|^2 + |\mathcal{B}(t)|^2 + |\mathcal{C}(t)|^2 + |\mathcal{B}'(t)|^2 + |\mathcal{C}'(t)|^2 = 1$. The square of the electric field has again the form of Eq. (3.51), just with $bc \to ab$. Due to the orthogonality of the atomic states, there are not too many combinations which are possible:

- 0-photon state coupled with itself:
  If we take, e.g., the term $|\mathcal{A}(t)|^2$, it does not oscillate anyway. Hence, only the time-dependent parts in Eq. (3.51) (with $bc \to ab$) could lead to oscillations. But they are proportional to
  $$_\gamma\langle 0|a_{ac}^\dagger a_{ab}|0\rangle_\gamma = {}_\gamma\langle 0|a_{ab}^\dagger a_{ac}|0\rangle_\gamma = 0.$$

- 1-photon state coupled with itself:
  $|\mathcal{B}'(t)|^2$ does not oscillate, too, and the time-dependent terms from the electric field yield
  $$_\gamma\langle 1_{ab}|a_{ac}^\dagger a_{ab}|1_{ab}\rangle_\gamma = {}_\gamma\langle 0|a_{ab}a_{ac}^\dagger a_{ab}a_{ab}^\dagger|0\rangle_\gamma = 0 \text{ and}$$
  $$_\gamma\langle 1_{ab}|a_{ab}^\dagger a_{ac}|1_{ab}\rangle_\gamma = {}_\gamma\langle 0|a_{ab}a_{ab}^\dagger a_{ac}a_{ab}^\dagger|0\rangle_\gamma = 0,$$
  which follows immediately from the action of $a_{ac}^\dagger$ to the left and of a_{ac} to the right, respectively.

- 0-photon state coupled with 1-photon state:
  This is the only possibility, which is left. If we take for instance the term $\mathcal{B}^*(t)\mathcal{B}'(t)$, this will oscillate in any case, so we will also have to check the constant terms in Eq. (3.51). The ones proportional to 1 are naturally zero, ${}_\gamma\langle 0|1_{ab}\rangle_\gamma = {}_\gamma\langle 0|a_{ab}^\dagger|0\rangle_\gamma = 0$. The other terms are
  $$_\gamma\langle 0|\underbrace{a_{ac}^\dagger}_{0\leftarrow} a_{ac}|1_{ab}\rangle_\gamma = 0,\ {}_\gamma\langle 0|\underbrace{a_{ab}^\dagger}_{0\leftarrow} a_{ab}|1_{ab}\rangle_\gamma = 0, {}_\gamma\langle 0|\underbrace{a_{ac}^\dagger}_{0\leftarrow} a_{ab}|1_{ab}\rangle_\gamma = 0, \text{ and}$$
  $$_\gamma\langle 0|\underbrace{a_{ab}^\dagger}_{0\leftarrow} a_{ac}|1_{ab}\rangle_\gamma = 0, \tag{3.61}$$

where the action of the operators to give zero is always indicated by the arrow. The argumentation is analogous for the complex conjugated term.

Hence, there can be no Quantum Beats for a single atom of type II! The intuitive reason is that, by waiting long enough, one could reach an accuracy in energy that is good enough to distinguish the possible final states $|b\rangle$ and $|c\rangle$. This would then be a way to determine the energy of the emitted photon without disturbing it.

To give an analogous reasoning for the GSI-experiment, one has to turn the comparison given in Sec. 3.8.1 around and replace the *atom by the neutrino* and the *photon by the ion*. The reason is that what is claimed to interfere in this situation is the neutrino states themselves (see, e.g., Ref. [30]). This neutrino is not expected to interact before losing its coherence (cf. Sec. 3.5.3). However, once it interacts it has to "decide" for a certain mass eigenstate. By monitoring this interaction, it would be no principle problem to determine the neutrino's mass (e.g., by exploiting the spatial separation of the mass eigenstates far away from the source) and from this one could easily reconstruct the kinematics of the daughter ion in the GSI-experiment. Accordingly, no QBs are to be expected.

3.8.4 Two atoms of type II

On the other hand there is a situation in which we can expect QBs even for atoms of type II, namely if we have two of them. If these two atoms are separated by a distance which is smaller than the wavelength of the emitted photons, there is no way to resolve their separation in space and we have to write down a combined initial state for both atoms, 1 and 2:

$$|\Psi(0)\rangle = \mathcal{A}_0|a\rangle_1|a\rangle_2|0\rangle_\gamma + \mathcal{B}_0|b\rangle_1|b\rangle_2|0\rangle_\gamma + \mathcal{C}_0|c\rangle_1|c\rangle_2|0\rangle_\gamma + \mathcal{D}_{1,0}|a\rangle_1|b\rangle_2|0\rangle_\gamma + \mathcal{D}_{2,0}|b\rangle_1|a\rangle_2|0\rangle_\gamma + \\ + \mathcal{E}_{1,0}|a\rangle_1|c\rangle_2|0\rangle_\gamma + \mathcal{E}_{2,0}|c\rangle_1|a\rangle_2|0\rangle_\gamma + \mathcal{F}_{1,0}|b\rangle_1|c\rangle_2|0\rangle_\gamma + \mathcal{F}_{2,0}|c\rangle_1|b\rangle_2|0\rangle_\gamma. \tag{3.62}$$

The corresponding time-evolution $|\Psi(t)\rangle$ looks a bit complicated:

$$\mathcal{A}(t)|a\rangle_1|a\rangle_2|0\rangle_\gamma + \mathcal{B}(t)|b\rangle_1|b\rangle_2|0\rangle_\gamma + \mathcal{C}(t)|c\rangle_1|c\rangle_2|0\rangle_\gamma + \mathcal{D}_1(t)|a\rangle_1|b\rangle_2|0\rangle_\gamma + \mathcal{D}_2(t)|b\rangle_1|a\rangle_2|0\rangle_\gamma + \\ + \mathcal{E}_1(t)|a\rangle_1|c\rangle_2|0\rangle_\gamma + \mathcal{E}_2(t)|c\rangle_1|a\rangle_2|0\rangle_\gamma + \mathcal{F}_1(t)|b\rangle_1|c\rangle_2|0\rangle_\gamma + \mathcal{F}_2(t)|c\rangle_1|b\rangle_2|0\rangle_\gamma + \\ + \mathcal{G}_1(t)|b\rangle_1|a\rangle_2|1_{ab}\rangle_\gamma + \mathcal{G}_2(t)|a\rangle_1|b\rangle_2|1_{ab}\rangle_\gamma + \mathcal{H}_1(t)|c\rangle_1|a\rangle_2|1_{ac}\rangle_\gamma + \mathcal{H}_2(t)|a\rangle_1|c\rangle_2|1_{ac}\rangle_\gamma + \\ + \mathcal{I}_1(t)|b\rangle_1|b\rangle_2|1_{ab}\rangle_\gamma + \mathcal{I}_2(t)|c\rangle_1|c\rangle_2|1_{ac}\rangle_\gamma + \mathcal{J}_1(t)|b\rangle_1|c\rangle_2|1_{ab}\rangle_\gamma + \mathcal{J}_2(t)|c\rangle_1|b\rangle_2|1_{ab}\rangle_\gamma + \\ + \mathcal{K}_1(t)|b\rangle_1|c\rangle_2|1_{ac}\rangle_\gamma + \mathcal{K}_2(t)|c\rangle_1|b\rangle_2|1_{ac}\rangle_\gamma. \tag{3.63}$$

One oscillatory term would then be, e.g., $\mathcal{J}_1^*(t)\mathcal{K}_1(t)e^{-i\Delta t}$, which is proportional to

$$\gamma\langle 1_{ab}|a_{ab}^\dagger a_{ac}|1_{ac}\rangle_\gamma = \gamma\langle 0|a_{ab}a_{ab}^\dagger a_{ac}a_{ac}^\dagger|0\rangle_\gamma = \gamma\langle 0|(1+\underbrace{a_{ab}^\dagger}_{0\leftarrow}a_{ab})(1+a_{ac}^\dagger\underbrace{a_{ac}}_{\rightarrow 0})|0\rangle_\gamma = \gamma\langle 0|0\rangle_\gamma = 1. \tag{3.64}$$

An simple picture is that one cannot determine the photon energy, because one does not know which atom has emitted the radiation – which holds only if the spatial separation is indeed less than the photon's wavelength. Accordingly, we expect QBs.

For the GSI-case, this possibility has to be taken into account, because even for runs with one single EC only, there can have been more ions in that ring that were lost or decayed via β^+. In this case (comparing the neutrino again with the photon), one has to replace the wavelength of the photon by the de Broglie wavelength of the neutrino. The neutrino energy should be of the same order as the Q-value of the EC-reaction, which is roughly 1 MeV [29]. The corresponding wavelength is, however, $\lambda = \frac{2\pi\hbar c}{Ec} \sim 10^{-12}$ m, while the average distance between two ions should be of the order of the diameter of the storage ring [77], which is roughly 100 m [70]. Hence, this possibility is excluded for the GSI-experiment.

3.9 Wrong and doubtful approaches in the literature

Let us finally have a look at why several papers on the GSI anomaly that have appeared in the last months do not agree with the above results. More detailed comments are given in Ref. [10], but here we only want to mention the main points.

The main point where we disagree with Refs. [30, 32–35, 76] is Eq. (3.32), the incoherent summation, while coherent summation over amplitudes appears in the references cited. As we have argued in great detail in Secs. 3.6 and 3.7, this cannot be the case and incoherent summation is the correct treatment.

Furthermore, if one believes the neutrino oscillation explanation for a moment, to match the observed oscillation period $T \sim 7$ s, a value of $\Delta m^2_{21} \sim 2.18(3) \cdot 10^{-4}$ eV^2 is required for the solar mass squared difference, in conflict with KamLAND results (cf. Sec. 3.2). In Ref. [31], the authors relate this discrepancy to loop-induced Coulomb interactions of the neutrino, but give no explanation why the same effect does not appear in ordinary neutrino oscillation experiments.

Similar arguments have also been given by Giunti [41, 42], by Burkhardt et al. [44], and by Peshkin [45].[4] Moreover, Giunti has shown another problem, namely that the decay rate computed in [30] does not reduce to the Standard Model result if the neutrino masses are set to zero [42].

Finally, it has been claimed in Ref. [39] that a splitting in the initial state cannot explain the GSI-oscillations at all. As has been pointed out in Secs. 3.8.1 and 3.8.2, this mechanism indeed has its problems, but is still far from being excluded.

[4] Note that Ivanov et al. have replied to some of Giunti's remarks in [76, 78].

Chapter 4

Neutrino-less double Electron Capture

The next topic that we will treat is the rare process of neutrino-less double electron capture. This process is one of several possible double β decay modes that might occur if, and only if, the neutrino is a Majorana particle, meaning that it is identical to its anti-particle. This property is peculiar to $SU(3)_C \times U(1)_{\text{em}}$-singlets and the neutrino has exactly the right gauge quantum numbers. This is, however, not only the case for SM-particles. If we, e.g., look at the MSSM, then the neutralinos (which are the SUSY-partners of the neutral electro-weak gauge and Higgs bosons) would also be Majorana fermions [7].

An observation of any double β process would always prove the Majorana nature of the neutrino, since in Fig. 4.1, the external electrons could always be combined with the external quarks by W-bosons, yielding a Majorana mass term for the neutrinos. This observation is well known under the name *Schechter-Valle theorem* [79]. Hence, such an observation would clearly prove the existence of Physics beyond the Standard Model, which has not been seen directly yet.[1]

4.1 Neutrino-less double beta decay

The generic double β process is neutrino-less double β^- decay ($0\nu\beta\beta$), as seen in Fig. 4.1, which might be observable for (even-even) nuclei, where single β decay is forbidden. The net reaction is

$$(A, Z) \rightarrow (A, Z + 2) + e^- + e^-, \tag{4.1}$$

while the exact underlying mechanism is actually unknown [81]. The option mostly considered is the so-called 2-nucleon mechanism [82], where a Majorana neutrino propagator connects two SM-vertices for ordinary β^- decay. One can interpret this as follows: An electron anti-neutrino $\overline{\nu}_e$ is emitted in an ordinary β^- decay, $n^0 \rightarrow p^+ + e^- + \overline{\nu}_e$. Since it is identical to its anti-particle, it can also play the role of a neutrino ν_e and can induce a second β^- decay as $\nu_e + n^0 \rightarrow p^+ + e^-$. In order to do this it has, however, to flip its helicity/chirality which is the key feature of a mass term and leads to the proportionality of the decay rate to the square of the (effective) neutrino mass m_{ee}. The "problem" is that neutrino masses are small and accordingly the rate for the above process will be small, too, which makes it hard to observe (in fact, it has not been observed yet). Current limits on the half-life are $T_{1/2} \geq 1.9 \cdot 10^{25}$ y for Ge-76 [83],

[1] Actually, the existence of non-zero neutrino masses already points quite strongly into a direction beyond the SM. Since they might, however, still be Dirac fermions and the extension of the SM by only right-handed Dirac neutrinos does not add any new concept to the SM, we consider it here as not being strictly beyond the SM.

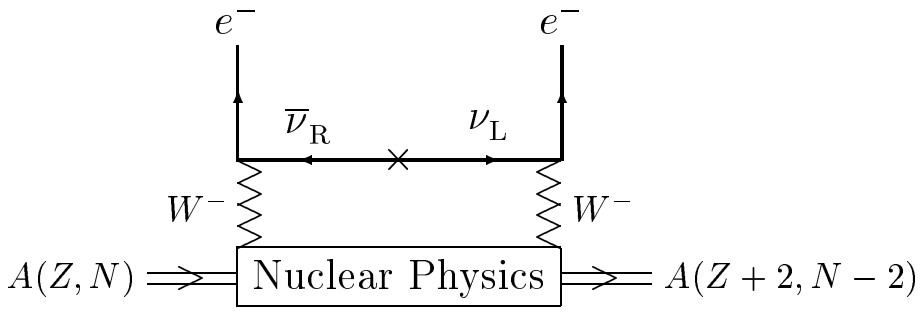

Figure 4.1: A schematic view of neutrino-less double β decay. Note the the exact mechanism of the process is actually unknown, which is indicated by the box called "Nuclear Physics". (Figure taken from Ref. [80].)

$T_{1/2} \geq 3.0 \cdot 10^{24}$ y for Te-130 [84], $T_{1/2} \geq 5.8 \cdot 10^{23}$ y for Mo-100, and $T_{1/2} \geq 2.1 \cdot 10^{23}$ y for Se-82 [85], all at 90 % C.L.

In general, the decay rate for the above process will have the form [86]

$$\Gamma = G_0 |M^{0\nu}|^2 |m_{ee}|^2, \tag{4.2}$$

where G_0 is a phase space factor that also contains all constants, m_{ee} is the effective mass, and $M^{0\nu}$ is the so-called nuclear matrix element (NME), which is an $\mathcal{O}(1)$-number that is the essential remnant of the underlying nuclear physics involved. A calculation of the NME involves very complicated nuclear physics and there is still some debate in literature how to do it best (see for example Refs. [87–90]). Fortunately, the calculated values for the NME in case of $0\nu\beta\beta$ seem to converge meanwhile [88]. A generic cross-check of the methods applied is to calculate the NME for the related process of 2-neutrino double beta decay, which has already been observed [91]. One should, however, keep in mind that this decay mode contains different systematics, so it is not a priori clear how well the validity of the methods applied can be extrapolated to the neutrino-less case.

4.2 Phenomenology of the effective neutrino mass

Let us now consider the phenomenology of the effective neutrino mass a bit closer. This quantity is given by [92]

$$m_{ee} = \sum_{i=1}^{3} U_{ei}^2 m_i, \tag{4.3}$$

where m_i are the (light) neutrino mass-eigenvalues and U is the PMNS-matrix (Pontecorvo-Maki-Nagakawa-Sakata matrix), which is given by

$$U = \begin{pmatrix} c_{12}c_{13} & s_{12}c_{13} & s_{13}e^{-i\delta} \\ -s_{12}c_{23} - c_{12}s_{23}s_{13}e^{i\delta} & c_{12}c_{23} - s_{12}s_{23}s_{13}e^{i\delta} & s_{23}c_{13} \\ s_{12}s_{23} - c_{12}c_{23}s_{13}e^{i\delta} & -c_{12}s_{23} - s_{12}c_{23}s_{13}e^{i\delta} & c_{23}c_{13} \end{pmatrix} \cdot \mathrm{diag}(1, e^{i\alpha}, e^{i(\beta+\delta)}). \tag{4.4}$$

Here, α and β are the so-called Majorana phases, while $s_{ij} = \sin\theta_{ij}$ and $c_{ij} = \cos\theta_{ij}$. Recent values of these mixing angles are, e.g., $\theta_{12} = \left(34.5^{+1.4,+4.8}_{-1.4,-4.0}\right)^\circ$, $\theta_{13} = \left(0.0^{+7.9,+12.9}_{-0.0,-0.0}\right)^\circ$, and $\theta_{23} = \left(42.3^{+5.1,+11.3}_{-3.3,-7.7}\right)^\circ$ [23], where the best-fit values as well as the 1σ- and 3σ-errors are given. The Dirac CP-phase δ is currently unknown.

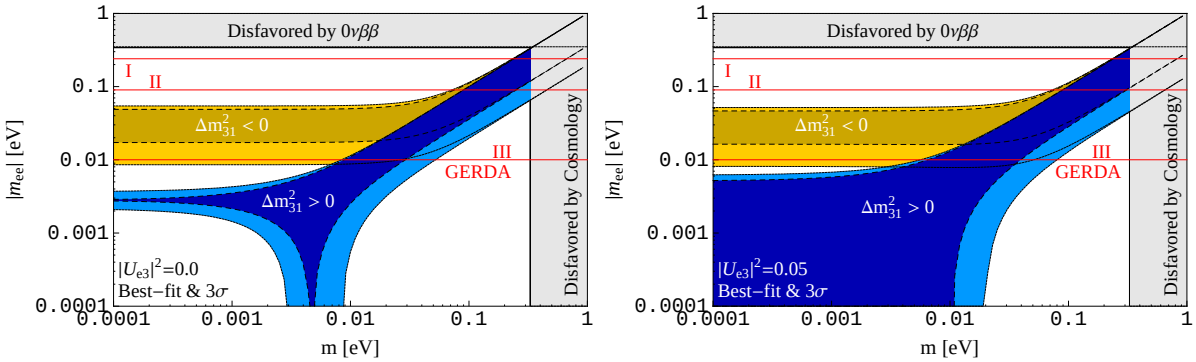

Figure 4.2: The dependence of the effective neutrino mass on the smallest neutrino mass eigenvalues for $|U_{e3}|^2 = 0.0$ and $|U_{e3}|^2 = 0.05$. The blue bands stand for normal mass ordering while the yellow ones stand for inverted ordering. In both cases, the dark parts are allowed for variation of the Majorana phases only, while for the light bands all oscillation parameters involved (except θ_{13}) have been varied within their 3σ-ranges as well. The reach for the different phases of the upcoming GERDA experiment is taken from Refs. [94, 95].

4.2.1 Special regions in the parameter space

As can be seen from Fig. 4.2, the variation of $|m_{ee}|$ with U_{e3} (and hence θ_{13}) is not too strong for most of the curve [93]. There is, however, one feature that changes considerably for a larger value of this mixing angle, namely the region where $|m_{ee}|$ can become zero. Unfortunate values of the Majorana phases can indeed pull the effective mass down to zero [92], which would lead, according to Eq. (4.2), to a zero rate for $0\nu\beta\beta$, even if the neutrino is indeed a Majorana particle. This would of course be disastrous when searching for such a decay. Fortunately, this region of the parameter space seems to be a very peculiar one and one would expect it to be relatively unnatural, if the Majorana phases had indeed just the values to yield a zero rate. However, even in that case, there might be possible cross-checks with cosmology. They could still give information about whether the neutrino can be a Dirac particle, or not [92]. This leads us to an important point in the interpretation of $0\nu\beta\beta$-results, namely to the question of how to combine several pieces of information on the neutrino mass coming from different experiments and observations.

4.2.2 The interplay with other future data: statistical analysis

Apart from $0\nu\beta\beta$, the major information on the neutrino mass comes from cosmology [96], where the sum Σ of all neutrino masses is measured,

$$\Sigma = m_1 + m_2 + m_3, \tag{4.5}$$

as well as from single β decay measurements [97], which measure the kinematic neutrino mass

$$m_\beta \equiv \sqrt{\sum_{i=1}^{3} |U_{ei}|^2 m_i^2}. \tag{4.6}$$

The future KATRIN experiment has a 5σ discovery potential of 0.35 eV for m_β, and a null result will lead to a 90 % C.L. limit of 0.2 or 0.17 eV [98], while the next cosmological limit will probe Σ down to the 0.1 eV range [96]. As one can see from Fig. 4.3, the dependences of these variables on the smallest neutrino mass eigenvalue also clearly differ for normal ($m_1 < m_2 < m_3$) or inverted

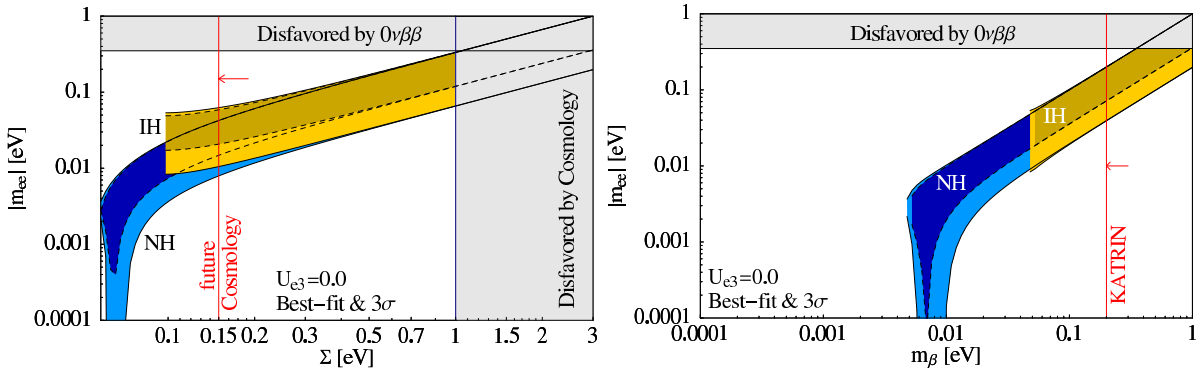

Figure 4.3: The dependence of the sum of neutrino masses and the kinematic neutrino mass on the smallest neutrino mass eigenvalue for $U_{e3} = 0$. The color code is the same as in Fig. 4.2.

Scenario	m_3 [eV]	m_{ee} [eV]	m_β [eV]	Σ [eV]
$\mathcal{QD}$	0.3	$0.11 - 0.30$	0.30	0.91
$\mathcal{INT}$	0.1	$0.04 - 0.11$	(0.11)	0.32
$\mathcal{IH}$	0.003	$0.02 - 0.05$	(0.05)	(0.10)

Table 4.1: The three different scenarios that we consider for our statistical analysis.

mass ordering ($m_3 < m_1 < m_2$). From this figure as well as from Fig. 4.2, one can see that in the near future the only region that we will be able to test in the next generation of experiments is the one for inverted mass ordering, where m_3 is the smallest mass eigenvalue. Therefore we will concentrate on this region in the following analysis. If one uses m_3 to parameterize the neutrino masses, the other mass eigenvalues are given by

$$m_1 = \sqrt{m_3^2 + |\Delta m_A^2|} \text{ and } m_2 = \sqrt{m_3^2 + |\Delta m_A^2| + \Delta m_\odot^2}, \tag{4.7}$$

where $\Delta m_\odot^2 = (7.67^{+0.22,+0.67}_{-0.21,-0.61}) \cdot 10^{-5}$ eV^2 and $|\Delta m_A^2| = (2.37^{+0.15,+0.46}_{-0.15,-0.43}) \cdot 10^{-3}$ eV^2 (for inverted mass ordering) are the mass square differences that can be obtained from neutrino oscillation experiments [23], again with their 1σ- and 3σ-errors.

Now we perform a statistical analysis [11] to investigate how well different realistic physical scenarios can be reconstructed by future experiments. For definiteness, we consider three different scenarios called $\mathcal{QD}$ (quasi-degenerate), $\mathcal{INT}$ (intermediate), and $\mathcal{IH}$ (inverted hierarchy), which are defined by different values of the smallest neutrino mass m_3. The corresponding values for the observables are given in Tab. 4.1 and are fixed except for $|m_{ee}|$, where one still has the freedom of varying the Majorana phases. Note that some values are put in paratheses, which indicate that these cannot be measured with the next generation of experiments. E.g., the upcoming KATRIN experiment will be able to measure m_β for the case of the $\mathcal{QD}$-scenario, while for the others, it will only provide an upper limit.

The next step is to explain the analysis that we are doing. At first, there are several uncertainties involved in the respective observables and the question is how to deal with them. Let us therefore start with the effective mass $|m_{ee}|$. As already explained in Sec. 4.1, experiments measure only a rate Γ_{obs}. Since this rate depends quadratically on the effective mass, cf. Eq. (4.2), one can express the experimental error $\sigma(\Gamma_{\text{obs}})$ on this rate by

$$\sigma(|m_{ee}|_{\text{exp}}) = \frac{|m_{ee}|_{\text{exp}}}{2} \frac{\sigma(\Gamma_{\text{obs}})}{\Gamma_{\text{obs}}}, \tag{4.8}$$

where $|m_{ee}|_{\rm exp}$ is the measured value of $|m_{ee}|$. If we look at the future GERDA experiment, the ratio that can be achieved will be about $\frac{\sigma(\Gamma_{\rm obs})}{\Gamma_{\rm obs}} \simeq 23.3\%$ [94]. There is, however, also a "theoretical uncertainty" on the NME involved, which has to be included as well. A possible procedure is to parameterize this error by a quantity $\zeta \geq 0$ and write the total error on the effective mass as

$$\sigma(|m_{ee}|) = (1+\zeta)\,(|m_{ee}| + \sigma(|m_{ee}|_{\rm exp})) - |m_{ee}|. \tag{4.9}$$

Following Ref. [99], we can define a covariance matrix

$$S_{ab} \equiv \delta_{ab}\sigma^2(a) + \sum_i \frac{\partial T_a}{\partial x_i}\frac{\partial T_b}{\partial x_i}\sigma_i^2, \tag{4.10}$$

where $T_1 = |m_{ee}|$, $T_2 = \Sigma$, and $T_3 = m_\beta^2$. Furthermore, $\sigma^2(a)$ is the error on T_a, and (a,b) label the entries in the covariance matrix. x_i are the oscillation parameters (mixing angles and mass square differences) that enter $|m_{ee}|$ (and m_β, though in the observable range of m_β they have basically no influence). The errors on $T_{2,3}$ are given by $\sigma(m_\beta^2) = 0.025\ \ {\rm eV}^2$ [97, 98] and $\sigma(\Sigma) = 0.05$ eV [96].

Defining $v_a = T_a - (T_a)_{\rm exp}$, where $(T_a)_{\rm exp}$ denotes the experimental value of T_a, our χ^2-function to be minimized is

$$\chi^2 = v^T S^{-1} v. \tag{4.11}$$

All oscillation parameters are set to their best-fit values and their (symmetrized) standard deviations are determined from their 1σ-ranges, which is a good approximation for future 3σ-ranges. Anyway, the impact of different numerical values here would not lead to qualitatively different results. Assuming different values for $|m_{ee}|_{\rm exp}$, we first have to minimize the χ^2-function with respect to the Majorana phases α and β, which results in a new function $\chi^2_{\rm res} = \min_{\alpha,\beta}\chi^2$. We can then further minimize with respect to m_3 to obtain its best-fit point and determine the corresponding 1σ-, 2σ-, and 3σ-ranges by setting $\Delta\chi^2 = \chi^2_{\rm res} - \chi^2_{\rm res,min}$ equal to 1, 4, and 9. The minimum in the $|m_{ee}|_{\rm exp}$-m_3 plane is then fixed such that $\Delta\chi^2$ is zero in the true region of the respective scenario. Note that these plots are no two-dimensional χ^2-plots, but rather many one-dimensional plots next to each other, one for each value of $|m_{ee}|_{\rm exp}$.

4.2.3 The interplay with other future data: numerical results

The numerical results of our analysis are shown as the solid lines in the upper rows of Figs. 4.4, 4.5, and 4.6. In all cases, we have calculated the result for a consistent measurement (i.e., m_β and Σ are measured at their true values in the corresponding scenarios, cf. Tab. 4.1) and the NME uncertainties are $\zeta = 0$ (which corresponds to the case of no uncertainty), 0.25, and 0.5. We have checked that large values of $\zeta > 0.5$ will lead to results which are not too different from the ones for $\zeta = 0.5$. In either case, the 1σ-, 2σ-, and 3σ-ranges are shown in green, yellow, and red, respectively.

The true values of $|m_{ee}|$ and m_3 for all three scenarios are marked by the vertical black lines. The plots illustrate how well we can reconstruct the different scenarios for the certain values of the NME uncertainty. Looking at Fig. 4.4, one can see that the $\mathcal{QD}$ scenario can be reconstructed quite well. This is no surprise since in that case the KATRIN experiment as well as the cosmological observation will provide a non-trivial signal. E.g., for $|m_{ee}|_{\rm exp} = 0.20$ eV, the 1σ-, 2σ-, and 3σ-ranges for m_3 are $0.28 - 0.32$ eV, $0.27 - 0.33$ eV, and $0.25 - 0.35$ eV, while the true value is 0.30 eV. Therefore, the reconstruction is adequate. This remains true when the uncertainty in NME is non-zero. Still, the reconstructed regions are narrow around the true value of m_3 (the numerical values suffer nearly no change) even though, with a larger NME uncertainty, higher values of $|m_{ee}|_{\rm exp}$ are also plausible. This is true for all three scenarios under consideration.

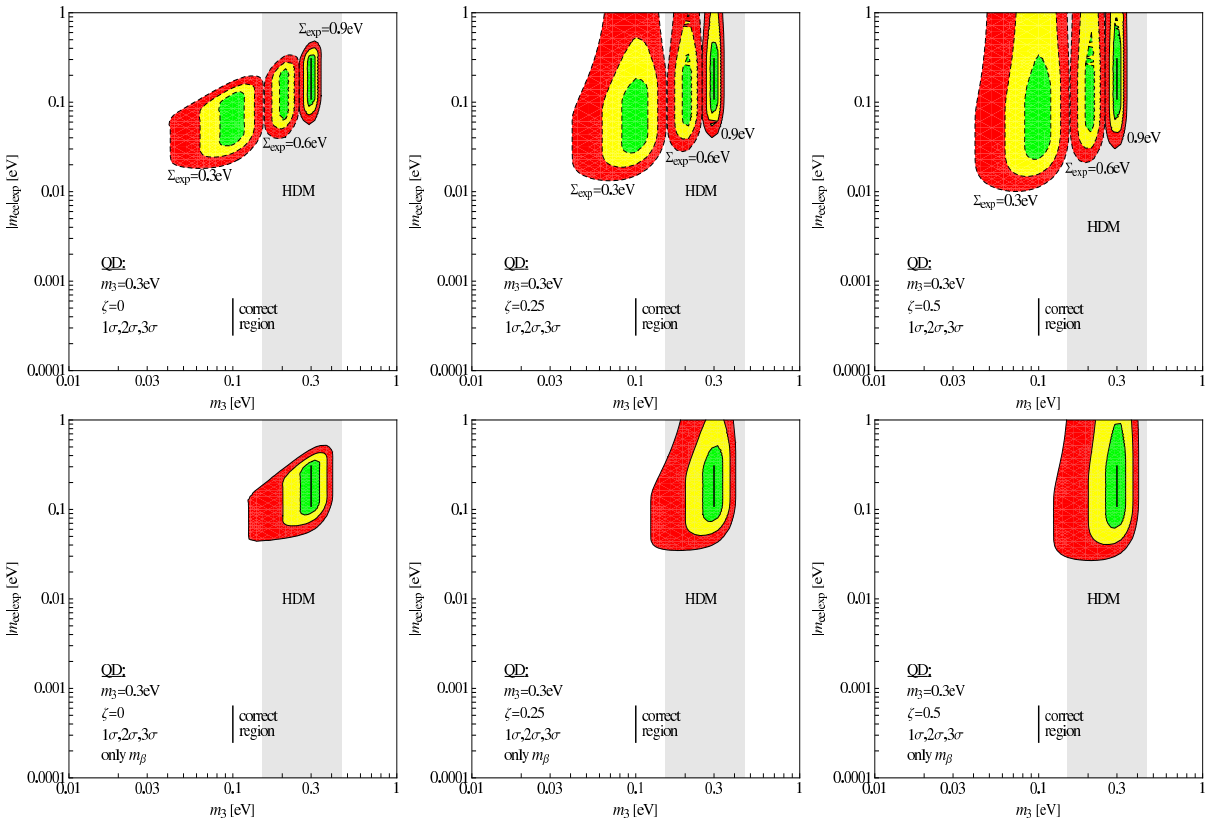

Figure 4.4: 1σ, 2σ and 3σ regions in the m_3-$|m_{ee}|_{\rm exp}$ plane for the $\mathcal{QD}$ scenario. The upper row shows the correct (solid line) as well as two possible incorrect cosmological measurements (dashed lines). The less desirable case, i.e. only taking into account a KATRIN measurement, is shown in the plots in the lower row. The area denoted HDM is the range of $|m_{ee}|$ from the claim of part of the Heidelberg-Moscow collaboration.

Similar statements hold for the $\mathcal{INT}$ scenario shown in Fig. 4.5, even though m_β cannot be measured anymore. However, there will still be a measurement of Σ, so we have sufficient information on the neutrino mass in order to make the reconstruction work. In case the measured central value is $|m_{ee}|_{\rm exp} = 0.08$ eV and $\zeta = 0$, the ranges are $0.08 - 0.12$ eV at 1σ and $0.05 - 0.15$ eV at 3σ. In case of $\zeta = 0.5$, we find $0.08 - 0.12$ eV at 1σ and $0.04 - 0.15$ eV at 3σ, which illustrates that the numerical values barely change. The mass scale has now a 3σ uncertainty of 50 %, to be compared with roughly 15 % in the $\mathcal{QD}$ scenario.

For $\mathcal{IH}$, in turn, there is no measurement at all that gives information on m_3. Hence, it is only possible to give an upper limit on the smallest neutrino mass, as illustrated by the long horizontal band in the upper left of Fig. 4.6. Note that this band corresponds directly to the yellow band marking the inverted mass ordering in Fig. 4.2. This upper limit is almost trivial, i.e., it corresponds to the neutrino mass limit obtainable from $0\nu\beta\beta$ alone. To give some numerical values, for $|m_{ee}|_{\rm exp} = 0.04$ eV one would have the 1 (3)σ ranges $m_3 < 0.03$ (0.07) eV for $\zeta = 0$ and for $\zeta = 0.5$. Due to the bound on Σ, there is very little dependence on ζ.

Up to now, the discussion has focused on the case in which all measurements are compatible. This might, however, just be a physicist's dream, and it might well be that some inconsistencies will be seen. As example for such an inconsistency, we discuss here a possible clash between results from KATRIN and from cosmology. To show this, we leave $(m_\beta)_{\rm exp}$ equal to the true value of the corresponding scenario (new physics is not expected to influence m_β too much [100]).

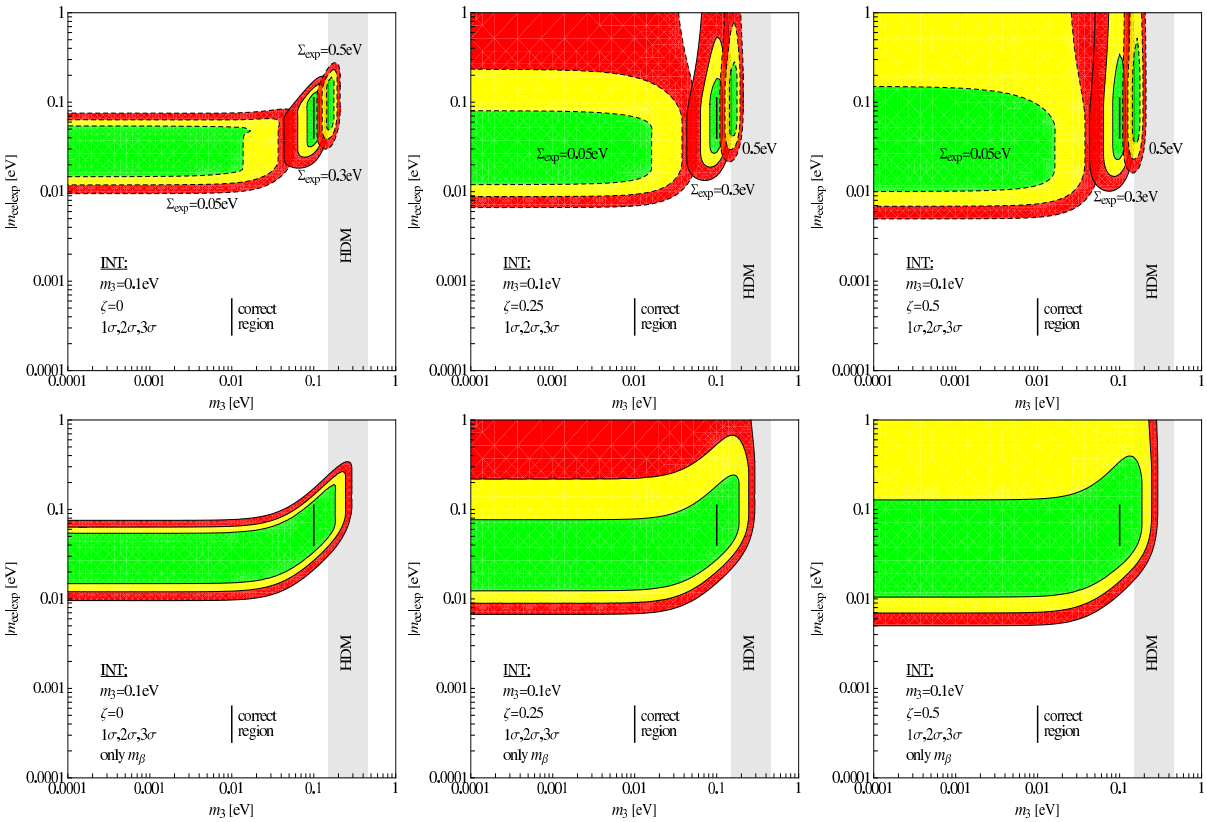

Figure 4.5: Same as Fig. 4.4 for the $\mathcal{INT}$ scenario.

For $\Sigma_{\rm exp}$, we take example values that are smaller or larger than the true value in the respective scenario. There are many models in the literature which can indeed lead to wrong values of Σ, see, e.g., Refs. [101, 102]. The result is shown by the areas within the dashed lines in the upper rows of Figs. 4.4-4.6. Having a look at the $\mathcal{QD}$-scenario first, we can see immediately that the physical range of m_3 is reconstructed incorrectly! Hence, if there are systematic errors in the cosmological measurement, or unknown features in cosmology which we are currently unaware of, a wrong neutrino mass could be reconstructed. In the $\mathcal{QD}$-case there is still information from the KATRIN-experiment available, which leads to a reconstructed neutrino mass at most one order away from the true value, even if a relatively bad value of Σ is taken into account. For the $\mathcal{INT}$ scenario, however, there is no information from KATRIN. Consequently, it might be that one derives a *wrong* upper limit on m_3! This is illustrated by the long band for $\Sigma_{\rm exp} = 0.05$ eV in the upper left plot of Fig. 4.5. This is an example for the case when one could draw a wrong conclusion by taking the cosmological measurement at face value. Even worse cases may exist for the $\mathcal{IH}$ scenario. E.g., in the upper left plot of Fig. 4.6 one would, for $\Sigma_{\rm exp} = 0.3$ eV, reconstruct an m_3 of roughly 0.1 eV, while the true value is 0.003 eV. For the $\mathcal{IH}$ scenario, one might not even realize that there is an inconsistency, since in that case the KATRIN experiment can only provide an upper limit which is too far away from the true value of m_3, in case there is no further information from another source.

One possible cross-check (or the possible consequence if one indeed discovers inconsistencies between the results from KATRIN and from cosmology) would be to dismiss the cosmological data completely. We have analyzed this case, too. Here, S_{ab} from Eq. (4.10) as well as v_a would change from 3-dimensional to 2-dimensional objects (since the part that corresponds to the sum of neutrino masses Σ is simply kicked out) while the rest of the procedure remains

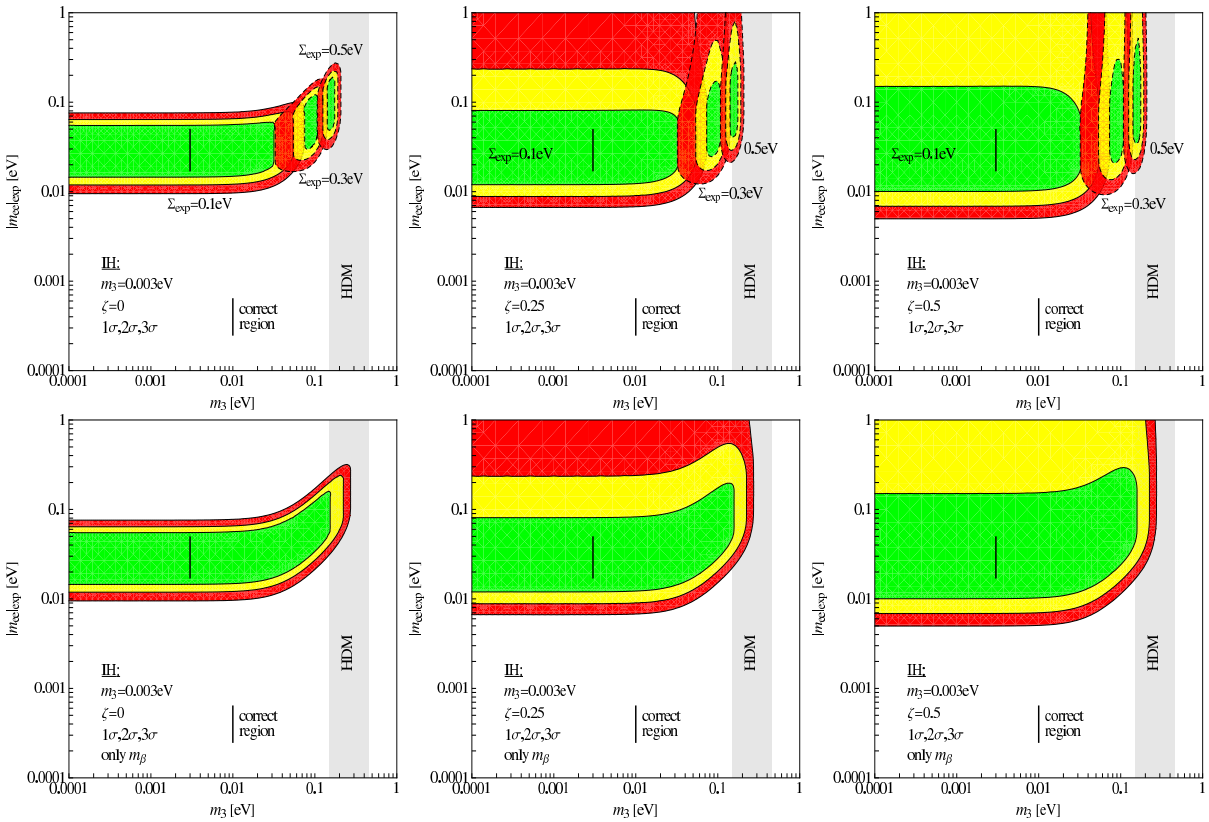

Figure 4.6: Same as Fig. 4.4 for the $\mathcal{IH}$ scenario.

the same. The results for this analysis are plotted in the lower rows of Figs. 4.4-4.6, again for different values of the NME uncertainty. For $\mathcal{QD}$, the most optimal scenario in what concerns the next generation experiments, neglecting cosmology, would simply increase the errors in the determination of m_3: E.g., for $|m_{ee}|_{\rm exp} = 0.20$ eV and $\zeta = 0$, the ranges are $0.26 - 0.34$ eV at 1σ and $0.16 - 0.41$ eV at 3σ, while for $\zeta = 0.5$, we find $0.26 - 0.34$ eV at 1σ and $0.13 - 0.41$ eV at 3σ. This was to be expected, since the KATRIN experiment will in that case yield a measurement of the neutrino mass. However, the NME uncertainty has a slightly bigger impact, and the error on m_3 increases by a factor of three (now it is about 50 % while it was roughly 15 % when cosmology had been included in the analysis). For the $\mathcal{INT}$-scenario, however, there is a major difference to the former case: Now there is no other measurement besides $|m_{ee}|_{\rm exp}$ providing information on m_3. Accordingly, one can only derive an upper limit instead of determining a certain range for m_3. This is indicated by the band in the lower left plot of Fig. 4.5. Finally for $\mathcal{IH}$, the limit on m_3 gets only slightly worse compared to the case of a Σ which is too small to be measured. Then there would not even be a real drawback in taking into account the KATRIN result only, since here cosmology can also only yield an upper limit on the neutrino mass. It remains to be said that (in all cases) an uncertainty higher than $\zeta = 0.5$ for the NME would not significantly modify the conclusions concerning the value of m_3, which makes clearly visible how important the improvements of these highly non-trivial calculations of the NME will be to extract the essential physics from future experiments. Finally, it is worth mentioning that if, in the $\mathcal{QD}$-scenario, the error on Σ is decreased (increased), the resulting error on the neutrino mass is decreased (increased) by approximately the same factor.

With our analysis we can also compare the compatibility of our three benchmark scenarios with the range $0.15 - 0.46$ eV for m_3, calculated as the (global fit) 2σ range in Refs. [103, 104]

from the claim in Ref. [105]. The implied range for m_3 is given by the gray band labeled by "HDM" (Heidelberg-Moscow) in Figs. 4.4, 4.5, and 4.6. We see that scenario $\mathcal{QD}$ is consistent with the claim, even for a measurement of $\Sigma = 0.6$ eV, to be compared with the true value $\Sigma = 0.9$ eV. The $\mathcal{INT}$ scenario ($\mathcal{IH}$ scenario) is slightly (very) incompatible for measured "true" values. However, an exceedingly high value of $\Sigma_{\rm exp}$ can lead again to compatibility. This shows that, depending on the actual results of future experiments, it might be very difficult to test or verify the above claim.

4.3 Alternative double beta processes

Let us now turn our focus to double β processes other than neutrino-less double β^- decay. Of course, there can also be isotopes which might undergo the corresponding double β^+ decay, both with [106] and without [82] the emission of neutrinos. Since electron capture (EC) is always a competing process to β^+-emission, the double β^+-modes can actually not only be $\beta^+\beta^+$, but also $EC\beta^+$ and $ECEC$. If the latter process occurs without the emission of neutrinos, we will have no particle in the final state except for the daughter atom. Since this can, however, not work due to energy and momentum conservation, we need (at least) one more particle to be emitted in that case. The obvious choice is the emission of one single photon ($ECEC\gamma$). This particular decay mode will, however, have its problems: In a calculation for ordinary EC, one assumes the contribution of the $1s$-electrons to the capture as largest, since these have the highest probability to be found inside the nucleus. However, if both $1s_{1/2}$-electrons are captured and only one photon is emitted, this can only work if the photon gets orbital angular momentum, so this process is forbidden. The reason is that a real photon always has a spin of 1, but the two electrons in the $1s_{1/2}$-orbital couple to a spin of zero. Accordingly, if one electron is captured from the $1s$-shell, the other electron has to come from a different orbital, which will then, in turn, have a smaller probability to be found inside the nucleus. This might, however, change for the next possible mode, $ECEC\gamma\gamma$. Naively, one expects this process to be suppressed by a factor of $\alpha \approx 1/137$, but since the emission of only one photon has disadvantages, this naive expectation might be incorrect.

We will investigate the ratio between these two processes for the first time. Note that, in spite of having the generic problem of uncertainties in the NME of such processes (cf. Sec. 4.2), the ratio between the two should (at least to a certain extent) be independent of the NME. The reason is that, as we will see, the angular momentum as well as the energy balances are the same for the nucleus, no matter if one or two photons are emitted. In that sense, the nucleus should not "care" about which of the two decay modes ($ECEC\gamma$ or $ECEC\gamma\gamma$) is chosen. This is something peculiar about the double EC mode and might be different for the others. We will, however, not go into details about the calculation of the NMEs, so this quasi-equality of the NMEs will have to be tested at another time.

We will exemplify in Sec. 4.5.6 why this ratio is decisive for setting accurate experimental limits on the half-life. There, we also comment on the perspectives to really detect neutrino-less double electron capture in an experiment.

4.4 The one-photon mode

Let us first focus on the emission of only one photon when capturing two electrons without emitting a neutrino. The corresponding Feynman diagrams under the assumption of the 2-nucleon mechanism (which is always assumed here) are depicted in Fig. 4.7. Two electrons are captured by the nucleus and connected by a Majorana neutrino propagator in a way that no neutrino is emitted in the end. This, however, would violate energy conservation, which is why

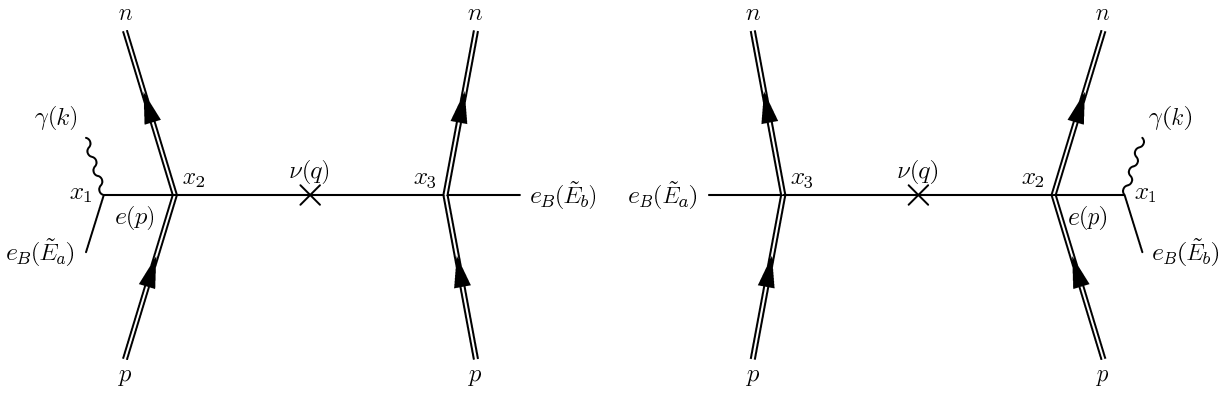

Figure 4.7: The two Feynman diagrams contributing to $ECEC\gamma$ under the assumption of the two-nucleon mechanism.

one needs to attach an additional photon to the diagram. This photon can be attached to one of the captured electrons or to the nucleus itself. The latter process is, however, subdominant for $0^+ \to 0^+$-transitions that we want to consider [107] (mainly due to angular momentum conservation, but also to the high mass of the nucleus [108]), so we neglect this possibility and consider only the diagrams of Fig. 4.7.

We use the formalism of Quantum Field Theory to calculate these diagrams. The nuclear physics part will be factored out (leading to the decay amplitude being proportional to the NME) and we will be left with the essential γ-structure of the process times a form factor originating from the bound electron wave functions.

In the whole rest of this section we use, unless stated otherwise, the chiral representation for γ-matrices (and spinors):

$$\gamma^\mu = \begin{pmatrix} 0 & \sigma^\mu \\ \overline{\sigma}^\mu & 0 \end{pmatrix} \text{ and } \gamma_5 = \gamma^5 = -i\gamma_0\gamma_1\gamma_2\gamma_3 = i\gamma^0\gamma^1\gamma^2\gamma^3 = \begin{pmatrix} -\mathbb{1} & 0 \\ 0 & \mathbb{1} \end{pmatrix}, \tag{4.12}$$

where $\sigma^\mu = (\mathbb{1}, \sigma^1, \sigma^2, \sigma^3)$ and $\overline{\sigma}^\mu = (\mathbb{1}, -\sigma^1, -\sigma^2, -\sigma^3)$. These matrices fulfill the Clifford-algebra:

$$\{\gamma^\mu, \gamma^\nu\} = 2g^{\mu\nu}\mathbb{1}. \tag{4.13}$$

Adjoint γ-matrices are given by

$$(\gamma^\mu)^\dagger = \gamma^0\gamma^\mu\gamma^0 \Rightarrow (\gamma^0)^\dagger = \gamma^0,\ (\gamma^i)^\dagger = -\gamma^i,\ (\gamma_5)^\dagger = \gamma_5, \tag{4.14}$$

the σ-matrices are defined as

$$\sigma^{\mu\nu} \equiv \frac{i}{2}[\gamma^\mu, \gamma^\nu], \tag{4.15}$$

and projection operators for left- and right-handed states are

$$P_L \equiv \frac{1}{2}(1-\gamma_5) = \begin{pmatrix} \mathbb{1} & 0 \\ 0 & 0 \end{pmatrix}, P_R \equiv \frac{1}{2}(1+\gamma_5) = \begin{pmatrix} 0 & 0 \\ 0 & \mathbb{1} \end{pmatrix}. \tag{4.16}$$

The charge conjugate $\Psi^{\mathcal{C}}$ of a spinor Ψ is given by $\Psi^{\mathcal{C}} = C\overline{\Psi}^T$, with the charge conjugation matrix

$$C \equiv i\gamma^0\gamma^2 = \begin{pmatrix} -i\sigma^2 & 0 \\ 0 & i\sigma^2 \end{pmatrix},\ C^{-1} = C^T = C^\dagger = i\gamma^2\gamma^0 = \begin{pmatrix} i\sigma^2 & 0 \\ 0 & -i\sigma^2 \end{pmatrix}. \tag{4.17}$$

Finally, we often use transposed and complex conjugated γ-matrices, which obey the relations

$$\gamma^2(\gamma^\mu)^*\gamma^2 = \gamma^\mu,\ C^{-1}(\gamma^\mu)^T C = -\gamma^\mu,\ (\gamma_5)^* = (\gamma_5)^T = \gamma_5. \tag{4.18}$$

Whenever we use spherical coordinates for a vector $\mathbf{r} = (x, y, z)^T$ in Cartesian coordinates, we define spherical coordinates (r, θ, ϕ) such that $x = r\sin\theta\cos\phi$, $y = r\sin\theta\sin\phi$, and $z = r\cos\theta$, where $r = |\mathbf{r}|$.

4.4.1 The basics of the calculation

Let us start by writing down the basic Hamiltonians that are required to describe $ECEC\gamma$. The processes involved are the emission of a photon by a bound electron, which has the Hamiltonian

$$\mathcal{H}^{e\gamma} = -e\bar{e}_B(x)\gamma^\alpha e_B(x)A_\alpha(x), \tag{4.19}$$

and the capture of a single bound electron,

$$\mathcal{H}^{EC} = \frac{G_F}{\sqrt{2}}\left\{[\bar{\nu}_L(x)\gamma^\mu(1-\gamma_5)e_B(x)]\,\mathcal{J}_\mu^\dagger(x) + h.c.\right\}. \tag{4.20}$$

Here, e_B denotes an electron bound in a shell of the atom, while the rest of the notation follows standard conventions. Using Feynman rules, we can immediately write down the S-matrix element corresponding to Fig. 4.7:

$$\begin{aligned}\langle A'|S^{(3)}|A\rangle = {}& (-i)\frac{(-i)^2}{2!}(-e)\left(\frac{G_F}{\sqrt{2}}\right)^2\int d^4x_1 d^4x_2 d^4x_3\,\cdot\\ &\cdot\Big[e_B^T(x_1,\tilde{E}_a)(\gamma^\alpha)^T\;\overline{\bar{e}_B^T(x_1)}e_B^T(x_2)(1-\gamma_5)^T(\gamma^\mu)^T\,\overline{\bar{\nu}_L^T(x_2)}\bar{\nu}_L(x_3)\gamma^\nu(1-\gamma_5)e_B(x_3,\tilde{E}_b)\,\cdot\\ &\cdot A_\alpha(x_1)\langle A'|T\left\{\mathcal{J}_\mu^\dagger(x_2)\mathcal{J}_\nu^\dagger(x_3)\right\}|A\rangle - (\tilde{E}_a\leftrightarrow\tilde{E}_b)\Big].\end{aligned} \tag{4.21}$$

Here, $\tilde{E}_{a,b}$ are the absolute values of the binding energies of the electrons, the $\mathcal{J}$'s are the (time-ordered) nuclear currents, and A_α denotes the outgoing photon. A and A' are the atomic initial and final state. Note that, due to the Pauli principle, there has to be a minus sign between both diagrams. In a consistent formulation, no additional factors are required [109].

The internal fermion propagators will be treated as follows: The bound electron propagators can be approximated by free electron propagators,

$$\overline{\bar{e}_B^T(y,E)}e_B^T(x,E) \approx \overline{\bar{e}^T(y,E)}e^T(x,E) = iS_F^T(x-y), \tag{4.22}$$

which are given by

$$S_F(x-y) = \int\frac{d^4p}{(2\pi)^4}\frac{\not{p}+m}{p^2-m^2+i\epsilon}e^{-ip(x-y)}. \tag{4.23}$$

For the transposed propagator, one can make use of $C^{-1}S_F^T(x-y)C = S_F(y-x)$.

The neutrino propagator has to be written down for a superposition of the neutrino mass eigenstates, because an electron neutrino is given by $\nu \equiv \nu_e = \sum_{i=1}^3 \tilde{U}_{ei}\nu_i$, where ν_i are the mass eigenstates and $\tilde{U}$ is the leptonic mixing matrix with all Majorana phases set to zero (cf. Eq. (4.4)). These come in by inserting $\mathbb{1} = C^{-1}C$ and applying the Majorana condition $C\bar{\nu}_i^T e^{-i\phi_i} \stackrel{!}{=} \nu_i$, with $\phi_1 = 0$, $\phi_2 = 2\alpha$, and $\phi_3 = 2\beta$ in our conventions. This allows to write the contraction of electron neutrinos as

$$\overline{\bar{\nu}_L^T(x)}\bar{\nu}_L(y) = P_R C^{-1}\sum_{i,j=1}^3 \tilde{U}_{ei}^*\tilde{U}_{ej}^* e^{i\phi_i}\underbrace{\overline{\bar{\nu}_i^T(x)}\bar{\nu}_j(y)}_{=iS_F(x-y)\delta_{ij}}P_R. \tag{4.24}$$

Inserting the propagator for each mass eigenstate, neglecting m_i^2 with respect to q^2 in the denominator, and realizing that the projection operators kill the $\not{q}$-contribution in the numerator, one ends up with

$$\overbrace{\overline{\nu}_L^T(x)\overline{\nu}_L}(y) \approx -im_{ee} \underbrace{\int \frac{d^4q}{(2\pi)^4} \frac{e^{-iq(x-y)}}{q^2+i\epsilon}}_{\equiv S_\nu(x-y)} CP_R, \tag{4.25}$$

where m_{ee} is just given by Eq. (4.3). Note that, after having done this (and making use of Eq. (4.18)), it is easy to put the two γ-matrices γ^μ and γ^ν next to each other in Eq. (4.21).

4.4.2 Factoring out the nuclear part

In this section, we factor out the nuclear physics part from the γ-structure, as done, e.g., in Ref. [110]. Then, it will be possible to do all those computations that involve spinors and matrices separately.

First, one can write out the time-ordered product of the nuclear currents explicitly and insert a complete set $\{|n\rangle\}$ of intermediate states:

$$\begin{aligned}
&\langle A'|T\left\{\mathcal{J}_\mu^\dagger(x_2)\mathcal{J}_\nu^\dagger(x_3)\right\}|A\rangle = \\
=\ & \theta(t_2-t_3)\sum_n \langle A'|\mathcal{J}_\mu^\dagger(x_2)|n\rangle\langle n|\mathcal{J}_\nu^\dagger(x_3)|A\rangle + \theta(t_3-t_2)\sum_n \langle A'|\mathcal{J}_\nu^\dagger(x_3)|n\rangle\langle n|\mathcal{J}_\mu^\dagger(x_2)|A\rangle = \\
=\ & \theta(t_2-t_3)\sum_n e^{it_2(E_n-E_f)}\langle A'|\mathcal{J}_\mu^\dagger(t_2=0,\mathbf{x}_2)|n\rangle\langle n|\mathcal{J}_\nu^\dagger(t_3=0,\mathbf{x}_3)|A\rangle\, e^{it_3(E_i-E_n)} + \\
+\ & \theta(t_3-t_2)\sum_n e^{it_3(E_n-E_f)}\langle A'|\mathcal{J}_\nu^\dagger(t_3=0,\mathbf{x}_3)|n\rangle\langle n|\mathcal{J}_\mu^\dagger(t_2=0,\mathbf{x}_2)|A\rangle\, e^{it_2(E_i-E_n)}.
\end{aligned} \tag{4.26}$$

E_i, E_f, and E_n denote the energies of the nuclear initial, final, and intermediate states. We then make use of the following approximations:

- the closure approximation: $E_n \to \langle E_n\rangle$
  The energies E_n of the intermediate states are replaced by some average value $\langle E_n\rangle$, which allows us to use $\sum_n |n\rangle\langle n| = \mathbb{1}$ in Eq. (4.26).

- we assume the 2-nucleon mechanism and use the non-relativistic approximation for the nuclear currents:

  $$\mathcal{J}_\mu^\dagger(\mathbf{x}) \approx \sum_m (g_V g_{\mu 0}\tau_m^+ + g_A g_{\mu j}\tau_m^+\sigma_m^j)\delta^{(3)}(\mathbf{x}-\mathbf{r}_m), \tag{4.27}$$

  where the sum runs over all nucleons. $\mathbf{r}_m$ denotes the position of the m-th nucleon. Details on the nuclear operators can be found in Ref. [111]. This approximation renders the integrations over $\mathbf{x}_2$ and $\mathbf{x}_3$ trivial and allows for the evaluation of part of the bound electron wave functions at the origin.[2]

- the long-wavelength approximation: $e^{\pm i\mathbf{px}} \sim 1$
  The value of $\mathbf{x}$, which points into the nucleus (due to the δ-functions), should be roughly of the order of the nuclear radius R, whose inverse is much larger than the size of typical internal momenta $|\mathbf{p}|$ ($\mathbf{p}$ is the momentum from the electron propagator over which we integrate in the end).

[2] Note that at this point we have actually lost the covariance of our expressions, since by this approximation, we have chosen a certain frame (namely the rest frame of the atom). Hence, whenever we make some approximations in the following that rely on a certain frame, we will have to check if the respective frame is identical to the rest frame chosen for this simplification.

Using $\mathcal{J}^\dagger_\nu(\mathbf{x}_3)\mathcal{J}^\dagger_\mu(\mathbf{x}_2) = \mathcal{J}^\dagger_\mu(\mathbf{x}_2)\mathcal{J}^\dagger_\nu(\mathbf{x}_3)$ [110] allows us to write Eq. (4.26) as

$$\begin{aligned}
&\langle A'|T\left\{\mathcal{J}^\dagger_\mu(x_2)\mathcal{J}^\dagger_\nu(x_3)\right\}|A\rangle \approx \qquad (4.28)\\
&\approx \left[\theta(t_2-t_3)e^{it_2(\langle E_n\rangle - E_f)}e^{it_3(E_i-\langle E_n\rangle)} + \theta(t_3-t_2)e^{it_2(E_i-\langle E_n\rangle)}e^{it_3(\langle E_n\rangle - E_f)}\right]\cdot\\
&\cdot\langle A'|\sum_{m,m'}(g_V g_{\mu 0}\tau^+_m + g_A g_{\mu j}\tau^+_m\sigma^j_m)(g_V g_{\nu 0}\tau^+_{m'} + g_A g_{\nu k}\tau^+_{m'}\sigma^k_{m'})|A\rangle\cdot\delta^{(3)}(\mathbf{x}_2-\mathbf{r}_m)\delta^{(3)}(\mathbf{x}_3-\mathbf{r}_{m'}).
\end{aligned}$$

Note that $\mathbf{r}_m$ and $\mathbf{r}_{m'}$ can also be exchanged due to the summation over both indices. Writing $\gamma^\mu\gamma^\nu = g^{\mu\nu} + \frac{1}{2}[\gamma^\mu,\gamma^\nu]$ after having simplified Eq. (4.21) allows us to divide the sum over Lorentz indices into a symmetric and an anti-symmetric part. We are left with only two parts, one proportional to the square of the vector-coupling g_V^2 (Fermi part) and the other one proportional to g_A^2 (Gamow-Teller part), as long as we restrict ourselves to the case of $0^+ \to 0^+$ transitions. The reason is that the mixed parts, using $g_{\mu 0}g_{\nu j}g^{\mu\nu} = 0$ and $\frac{1}{2}g_{\mu 0}g_{\nu j}[\gamma^\mu,\gamma^\nu] = \gamma^j\gamma^0$, lead to a term proportional to $(\sum_{m,m'}\tau^+_m\tau^+_{m'}\boldsymbol{\sigma}_{m'}\boldsymbol{\gamma})$. The operator $\boldsymbol{\sigma}_{m'}$ changes the spin for only one of the two states (either the initial or the final one), but this is not allowed in a pure $0^+ \to 0^+$ transition (which is the dominant contribution) and hence these operators yield zero when sandwiched between $\langle A'|$ and $|A\rangle$. The remaining two terms are:

$$\text{Fermi part:}\quad g_V^2\langle A'|\textstyle\sum_{m,m'}\tau^+_m\tau^+_{m'}|A\rangle\delta^{(3)}(\mathbf{x}_2-\mathbf{r}_m)\delta^{(3)}(\mathbf{x}_3-\mathbf{r}_{m'}),\ \text{and}$$

$$\text{Gamow-Teller part:}\quad -g_A^2\langle A'|\textstyle\sum_{m,m'}\tau^+_m\tau^+_{m'}\boldsymbol{\sigma}_m\boldsymbol{\sigma}_{m'}|A\rangle\delta^{(3)}(\mathbf{x}_2-\mathbf{r}_m)\delta^{(3)}(\mathbf{x}_3-\mathbf{r}_{m'}).$$

Now we have already reached our goal, since only the $g^{\mu\nu}$-part of $\gamma^\mu\gamma^\nu$ survives, which can simply be factored out from Eq. (4.21). The final expression looks like

$$\begin{aligned}
&\gamma^\mu\gamma^\nu\langle A'|T\left\{\mathcal{J}^\dagger_\mu(x_2)\mathcal{J}^\dagger_\nu(x_3)\right\}|A\rangle \to\\
&\to \sum_{m,m'}\langle A'|\tau^+_m\tau^+_{m'}(g_V^2 - g_A^2\boldsymbol{\sigma}_m\boldsymbol{\sigma}_{m'})|A\rangle\delta^{(3)}(\mathbf{x}_2-\mathbf{r}_m)\delta^{(3)}(\mathbf{x}_3-\mathbf{r}_{m'})\cdot\\
&\cdot\left[\theta(t_2-t_3)e^{it_2(\langle E_n\rangle - E_f)}e^{it_3(E_i-\langle E_n\rangle)} + \theta(t_3-t_2)e^{it_3(\langle E_n\rangle - E_f)}e^{it_2(E_i-\langle E_n\rangle)}\right]. \qquad (4.29)
\end{aligned}$$

4.4.3 The nuclear matrix element

The next step is to perform the integrations over t_1, t_2, and t_3. This will also allow us to check if the condition for energy conservation that we get is indeed correct. In order to do this, we first perform the momentum integrations over the 0-components, which leads to

$$\begin{aligned}
S_F(x_1-x_2) = \frac{-i}{2^4\pi^3}\int\frac{d^3p}{E-i\epsilon'}\Big[&\theta(t_1-t_2)(\not{p}+m_e)e^{-i(E-i\epsilon')(t_1-t_2)}e^{+i\mathbf{p}(\mathbf{x}_1-\mathbf{x}_2)} +\\
&+\theta(t_2-t_1)(-\not{p}+m_e)e^{+i(E-i\epsilon')(t_1-t_2)}e^{-i\mathbf{p}(\mathbf{x}_2-\mathbf{x})_2}\Big] \qquad (4.30)
\end{aligned}$$

and

$$S_\nu(x_2-x_3) = \frac{-i}{2^4\pi^3}\int\frac{d^3q}{|\mathbf{q}|-i\epsilon'}e^{+i\mathbf{q}(\mathbf{x}_2-\mathbf{x}_3)}\left[\theta(t_2-t_3)e^{-i|\mathbf{q}|(t_2-t_3)} + \theta(t_3-t_2)e^{+i|\mathbf{q}|(t_2-t_3)}\right], \qquad (4.31)$$

where ϵ' always indicates the correct ϵ-prescription. Furthermore, the time-dependence can be factored out from the bound electron wave functions,

$$e_B(x,\tilde{E}) = e^{+i(m_e-\tilde{E})t}e_B(\mathbf{x},\tilde{E}), \qquad (4.32)$$

and the outgoing photon with 4-momentum $k = (k_0, \mathbf{k})$ can be written as

$$A_\alpha(x_1) = \sqrt{\frac{1}{2k_0 V}}\epsilon^*_\alpha(\mathbf{k})e^{-ik_0t_1}e^{+i\mathbf{k}\mathbf{x}_1}, \tag{4.33}$$

where $\epsilon^*_\alpha(\mathbf{k})$ is the polarization vector. Note that the photon wave is normalized such that A_α has exactly the energy k_0. Furthermore, the identities $k^2 = 0$ (zero mass) and $k\epsilon = 0$ (transversality) hold for real photons. This leads to $\epsilon^*_0 = \epsilon^*_3 = 0$, which reflects the fact that time-like and longitudinal polarizations are forbidden for real photons. Having done all this yields

$$\begin{aligned}
\langle A'|S^{(3)}|A\rangle = {} & \frac{ieG_F^2 m_{ee}}{2^8\pi^6\sqrt{2k_0V}}\int d^3x_1 dt_1 dt_2 dt_3 \int \frac{d^3p}{E - i\epsilon'}\frac{d^3q}{|\mathbf{q}| - i\epsilon'}\sum_{m,m'}\tilde{g}_{mm'}e^{+i\mathbf{q}(\mathbf{r}_m - \mathbf{r}_{m'})}\cdot \\
& \cdot\Big\{\epsilon^*_\alpha(\mathbf{k})e^{-ik_0t_1}e^{+i\mathbf{k}\mathbf{x}_1}e^{+i(m_e-\tilde{E}_a)t_1}e^{+i(m_e-\tilde{E}_b)t_2}\Big[\underbrace{\theta(t_2-t_3)e^{i\tilde{E}_f t_2}e^{i\tilde{E}_i t_3}}_{\to N_1} + \underbrace{\theta(t_3-t_2)e^{i\tilde{E}_f t_3}e^{i\tilde{E}_i t_2}}_{\to N_2}\Big]\cdot \\
& \cdot\Big[\underbrace{\theta(t_1-t_2)e^{-i(E-i\epsilon')(t_1-t_2)}e^{+i\mathbf{p}\mathbf{x}_1}\cdot e_B^T(\mathbf{x}_1,\tilde{E}_a)C\gamma^\alpha(+\not{p}+m_e)P_L e_B(0,\tilde{E}_b)}_{\to L_1} + \\
& + \underbrace{\theta(t_2-t_1)e^{+i(E-i\epsilon')(t_1-t_2)}e^{-i\mathbf{p}\mathbf{x}_1}\cdot e_B^T(\mathbf{x}_1,\tilde{E}_a)C\gamma^\alpha(-\not{p}+m_e)P_L e_B(0,\tilde{E}_b)}_{\to L_2}\Big] - \\
& -(\tilde{E}_a \leftrightarrow \tilde{E}_b)\Big\},
\end{aligned} \tag{4.34}$$

where $\tilde{g}_{mm'} = \langle A'|\tau^+_m\tau^+_{m'}(g_V^2 - g_A^2\boldsymbol{\sigma}_m\boldsymbol{\sigma}_{m'})|A\rangle$, $\tilde{E}_i = |\mathbf{q}| + E_i - \langle E_n\rangle$, $\tilde{E}_f = \langle E_n\rangle - E_f - |\mathbf{q}|$, and $e_B(0,\tilde{E})$ is the spatial part of the bound electron wave function, evaluated at the origin.

To proceed, one only needs to write the θ-functions in their Fourier representation,

$$\theta(t-t') = \frac{i}{2\pi}\int\frac{da_0}{a_0 + i\epsilon}e^{-ia_0(t-t')}, \tag{4.35}$$

and then evaluate the integrals over t_1, t_2, and t_3 first to get δ-functions. We will do this explicitly for N_1L_1 and just list the results for the rest. The whole contribution reads:

$$\int dt_1dt_2dt_3\frac{dr_0}{r_0}\frac{ds_0}{s_0}e^{-ir_0(t_2-t_3)}e^{i\tilde{E}_f t_2}e^{i\tilde{E}_i t_3}e^{-is_0(t_1-t_2)}e^{-i(E-i\epsilon')(t_1-t_2)}e^{-ik_0t_1}e^{+i(m_e-\tilde{E}_a)t_1}e^{+i(m_e-\tilde{E}_b)t_3}. \tag{4.36}$$

The integration over the t's gives $(2\pi)^3$ times

$$\delta(m-k_0-\tilde{E}_a-(E-i\epsilon')-s_0)\delta(\tilde{E}_b-m_e-E_i+\langle E_n\rangle-|\mathbf{q}|-r_0)\delta(-r_0+\langle E_n\rangle-E_f-|\mathbf{q}|+s_0+(E-i\epsilon')). \tag{4.37}$$

Using these δ-functions to evaluate the integrals over r_0 and s_0, one obtains, altogether,

$$N_1L_1 = \frac{2\pi\delta[(E_i+2m_e-\tilde{E}_a-\tilde{E}_b)-(E_f+k_0)]}{(m_e-k_0-\tilde{E}_a-(E-i\epsilon'))(|\mathbf{q}|+m_e+E_i-\tilde{E}_b-\langle E_n\rangle)}. \tag{4.38}$$

The other 3 contributions are

$$\begin{aligned}
N_2L_1 &= \frac{2\pi\delta[(E_i+2m_e-\tilde{E}_a-\tilde{E}_b)-(E_f+k_0)]}{(m_e-k_0-\tilde{E}_a-(E-i\epsilon'))(|\mathbf{q}|-m_e+E_f+\tilde{E}_b-\langle E_n\rangle)}, \\
N_1L_2 &= \frac{2\pi\delta[(E_i+2m_e-\tilde{E}_a-\tilde{E}_b)-(E_f+k_0)]}{(k_0+\tilde{E}_a-(E-i\epsilon')-m_e)(|\mathbf{q}|+m_e+E_i-\tilde{E}_b-\langle E_n\rangle)}, \text{ and} \\
N_2L_2 &= \frac{2\pi\delta[(E_i+2m_e-\tilde{E}_a-\tilde{E}_b)-(E_f+k_0)]}{(k_0+\tilde{E}_a-(E-i\epsilon')-m_e)(|\mathbf{q}|-m_e+E_f+\tilde{E}_b-\langle E_n\rangle)}.
\end{aligned} \tag{4.39}$$

By this, we have indeed obtained the desired energy denominators. One can have a closer look at the energy conservation, enforced by the δ-functions in the numerators in Eqs. (4.38) and (4.39). The energy conservation looks like

$$\delta((E_i + 2m_e - \tilde{E}_a - \tilde{E}_b) - E_f - k_0), \tag{4.40}$$

where $E_{i,f}$ are the initial and final state energies. A short calculation leads to

$$E_i = M_i + (Z-2)m_e - BE(Z) + \tilde{E}_a + \tilde{E}_b \text{ and } E_f = M_f + (Z-2)m_e - BE(Z-2) + \tilde{E}'_a + \tilde{E}'_b, \tag{4.41}$$

where $M_{i,f}$ are the masses of the initial and final nucleus, $BE(Z)$ is the absolute value of the binding energy of the electrons for a neutral atom with atomic number Z (where we neglect correlation effects of the electrons), and $\tilde{E}'_{a,b}$ are the binding energies for electrons in the same orbitals as the captured electrons, but for the daughter nucleus. The connection to the Q-value of the reaction is simply that the photon energy k_0 has to be equal to

$$\tilde{Q} \equiv (Q - \tilde{E}'_a - \tilde{E}'_b). \tag{4.42}$$

The Q-value has to be corrected by the binding energies that correspond to the holes in the electron shell of the final state [112]. This is because the characteristic time-scale for the atomic shell to react and re-arrange itself is much longer than the time-scale for the nucleus to decay. Thus, the final state atom will not be in its ground state, but will rather have holes corresponding to the orbitals of the captured electrons. The binding energies of the captured electrons in the mother state do not affect the overall energy conservation; they are, however, important for the internal dynamics (as, e.g., for the calculation of the corresponding NME).

Then, by using neutrino "potential" functions [110],

$$H(|\mathbf{x}|, a) \equiv \frac{1}{2\pi^2} \int \frac{e^{i\mathbf{q}\mathbf{x}} d^3q}{|\mathbf{q}|(|\mathbf{q}| + a)}, \tag{4.43}$$

we can define the Fermi and Gamow-Teller NMEs:

$$M_{\mathrm{F}} \equiv \langle A' | \sum_{m,m'} h(|\mathbf{r}_m - \mathbf{r}_{m'}|) \tau_m^+ \tau_{m'}^+ | A \rangle \text{ and } M_{\mathrm{GT}} \equiv \langle A' | \sum_{m,m'} h(|\mathbf{r}_m - \mathbf{r}_{m'}|) \tau_m^+ \tau_{m'}^+ \boldsymbol{\sigma}_m \boldsymbol{\sigma}_{m'} | A \rangle, \tag{4.44}$$

where $h(|\mathbf{r}_m - \mathbf{r}_{m'}|) \approx h_{a,b}(|\mathbf{r}_m - \mathbf{r}_{m'}|)$, with

$$h_{a,b}(|\mathbf{r}_m - \mathbf{r}_{m'}|) \equiv \frac{R}{2} H(|\mathbf{r}_m - \mathbf{r}_{m'}|, E_i + m_e - \tilde{E}_{a,b} - \langle E_n \rangle) + H(|\mathbf{r}_m - \mathbf{r}_{m'}|, E_f - m_e - \tilde{E}_{a,b} - \langle E_n \rangle), \tag{4.45}$$

and R being the nuclear radius. Note that we assume the NMEs to vary slowly with energy, so that a small difference in the energy of the bound electron is not important. Finally, one can factor out the NME

$$M^{0\nu} \equiv M_{\mathrm{GT}} - \frac{g_V^2}{g_A^2} M_{\mathrm{F}} \tag{4.46}$$

and define the function

$$A(k_0, \tilde{E}) = m_e - k_0 - \tilde{E} \tag{4.47}$$

to obtain

$$\langle A' | S^{(3)} | A \rangle = \frac{-ieG_F^2 m_{ee} g_A^2 M^{0\nu}}{2^5 \pi^3 \sqrt{2k_0 V} R} \delta(k_0 - \tilde{Q}) \int d^3x_1 \epsilon_\alpha^*(\mathbf{k}) e^{+i\mathbf{k}\mathbf{x}_1} \int \frac{d^3p}{E - i\epsilon'} \cdot \tag{4.48}$$

$$\cdot \Big\{ \Big[\frac{e^{+i\mathbf{p}\mathbf{x}_1}}{A(k_0, \tilde{E}_a) - (E - i\epsilon')} \cdot e_B^T(\mathbf{x}_1, \tilde{E}_a) C\gamma^\alpha (+E\gamma^0 - \mathbf{p}\boldsymbol{\gamma} + m_e) P_L e_B(0, \tilde{E}_b) +$$

$$+ \frac{e^{+i\mathbf{p}\mathbf{x}_1}}{-A(k_0, \tilde{E}_a) - (E - i\epsilon')} \cdot e_B^T(\mathbf{x}_1, \tilde{E}_a) C\gamma^\alpha (-E\gamma^0 - \mathbf{p}\boldsymbol{\gamma} + m_e) P_L e_B(0, \tilde{E}_b) \Big] - (\tilde{E}_a \leftrightarrow \tilde{E}_b) \Big\},$$

where we have used $\mathbf{p} \to -\mathbf{p}$ in the second summand. The notation $e_B(\mathbf{x}, \tilde{E})$ means that the structure of the bound electron wave, implicitly contained in the symbolic writing "$\tilde{E}$", still has to be taken into account. [3]

4.4.4 The low Q region

In this section, we illustrate the dependence of the process on the magnitude of the Q-value of the reaction. As we shall see, the calculation proceeds differently, depending on whether the Q-value is small or large (and we will also specify what that means in this case).

In order to do this, we start with the integration over $\mathbf{p}$ in Eq. (4.48). Clearly, we have three parts, one with a factor E, one with $\mathbf{p}$, and one with m_e inside the γ-structure:

- Let us start with the E-part, which is proportional to

$$\Gamma_E = e_B^T(\mathbf{x}_1, \tilde{E}_a) C\gamma^\alpha \gamma^0 P_L e_B(0, \tilde{E}_b). \tag{4.49}$$

The part which is relevant for the integration is given by

$$\int \frac{d^3p}{E} e^{+i\mathbf{p}\mathbf{x}_1} E \left[\frac{1}{A - (E - i\epsilon')} - \frac{1}{-A - (E - i\epsilon')} \right] = 2A \cdot \int \frac{d^3p\ e^{+i\mathbf{p}\mathbf{x}_1}}{A^2 - E^2 + i\epsilon'}. \tag{4.50}$$

Writing out E^2 in the denominator leads to the following expression for the E-part (where $p = |\mathbf{p}|$):

$$-2A\Gamma_E \int \frac{d^3p\ e^{+i\mathbf{p}\mathbf{x}_1}}{p^2 + (m_e^2 - A^2) - i\epsilon'}. \tag{4.51}$$

From this, one can clearly see that the $\mathbf{p}$-integration depends on $(m_e^2 - A^2)$ being larger or less than zero. Using Eq. (4.47), one can easily see that $(m_e^2 - A^2) > 0$ for $k_0 < 2m_e - \tilde{E}_a$ and $(m_e^2 - A^2) < 0$ otherwise. Because of $k_0 = \tilde{Q}$, the first case corresponds to the low Q region, while the second one stands for a high Q-value. The physical difference between both cases comes from the fact that emitting the photon decreases the energy of the electron. For a photon momentum smaller than $(2m_e - \tilde{E}_a)$, the "rest" energy of the bound electrons is enough to create the photon – the electron that emits the photon (electron a for the first diagram in Fig. 4.7) and the other captured electron do not lose their full energy. A higher Q-value in turn requires a higher virtuality of the electrons (they will have negative energy after having emitted the photon), which causes the difference in the integration.

To simplify the notation, we can define the following auxiliary quantities:

$$\begin{aligned} &B^2 \equiv m_e^2 - A^2 \text{ for } k_0 < 2m_e - \tilde{E}_a \text{ (small } Q,\ m_e^2 - A^2 > 0) \text{ and} \\ &D^2 \equiv A^2 - m_e^2 \text{ for } k_0 > 2m_e - \tilde{E}_a \text{ (high } Q,\ A^2 - m_e^2 > 0). \end{aligned} \tag{4.52}$$

For low Q, this allows us to write the integral in Eq. (4.51) as

$$I_1(x_1) \equiv \int \frac{d^3p\ e^{+i\mathbf{p}\mathbf{x}_1}}{p^2 + B^2(k_0, \tilde{E}_a) - i\epsilon'}. \tag{4.53}$$

Evaluating this integral is easy: One can write $\mathbf{p}\mathbf{x}_1 = px_1 \cos\theta$ and then integrate over the angles ϕ and θ, which yields

$$I_1(x_1) = \frac{-2\pi i}{x_1} \left(\int_{p=0}^{+\infty} \frac{dp\ pe^{+ipx_1}}{p^2 + B^2} - \int_{p=0}^{-\infty} \frac{dp\ pe^{-ipx_1}}{p^2 + B^2} \right) = \frac{-2\pi i}{x_1} \int_{p=-\infty}^{+\infty} \frac{dp\ pe^{+ipx_1}}{p^2 + B^2}, \tag{4.54}$$

[3] Actually, the bound electron wave does not depend on $\tilde{E}$ anymore, since this dependence has been factored out in Eq. (4.32). Still, one should keep in mind that the γ-structure of the corresponding spinor will depend on the orbital that contains the electron. This is accounted for by using the notation "$e_B(\mathbf{x}, \tilde{E})$".

with poles at $p = \pm iB$. Since $x_1 = |\mathbf{x}_1|$, it is possible to close the integration contour in the upper half-plane (which leads to a mathematically positive orientation of the integral) and use the residue theorem for the pole at $+iB$. The simple result is

$$I_1(x_1) = \frac{2\pi^2}{x_1} e^{-B(k_0, \tilde{E}_a)x_1}, \tag{4.55}$$

which gives

$$E\text{-part}: \ -2A\Gamma_E I_1(x_1) = \frac{-4\pi^2 A}{x_1} e^{-Bx_1}\Gamma_E. \tag{4.56}$$

- The **p**-part is proportional to

$$\mathbf{\Gamma}_p = e_B^T(\mathbf{x}_1, \tilde{E}_a) C\gamma^\alpha \boldsymbol{\gamma} P_L e_B(0, \tilde{E}_b), \tag{4.57}$$

and the integration reads

$$2\int \frac{d^3p \ e^{+i\mathbf{p}\mathbf{x}_1}}{p^2 + B^2}\mathbf{p} = -2i\boldsymbol{\nabla}_{x_1} I_1(x_1), \tag{4.58}$$

which leads to (neglection higher order corrections that are suppressed by the exponential)

$$\mathbf{p}\text{-part}: \ \frac{4\pi^2 i}{x_1^2} e^{-Bx_1}\hat{\mathbf{x}}_1 \mathbf{\Gamma}_p, \tag{4.59}$$

where $\hat{\mathbf{x}}_1$ is the unit vector in x_1-direction. Here, we have also used $\boldsymbol{\nabla}_{x_1} = \hat{\mathbf{x}}_1 \frac{\partial}{\partial x_1} + ...$

- The m_e-part finally is proportional to

$$\Gamma_m = e_B^T(\mathbf{x}_1, \tilde{E}_a) C\gamma^\alpha P_L e_B(0, \tilde{E}_b), \tag{4.60}$$

and leads to

$$m_e\text{-part}: \ \frac{-4\pi^2 m_e}{x_1} e^{-Bx_1}\Gamma_m. \tag{4.61}$$

Finally, all our efforts yield

$$\begin{aligned}\langle A'|S^{(3)}|A\rangle = {} & \frac{ieG_F^2 m_{ee} g_A^2 M^{0\nu}}{2^3\pi\sqrt{2k_0 V}R}\delta(k_0 - \tilde{Q})\int \frac{d^3x_1}{x_1}\epsilon_\alpha^*(\mathbf{k})e^{+i\mathbf{k}\mathbf{x}_1} \cdot \\ & \cdot\Big[e_B^T(\mathbf{x}_1, \tilde{E}_a) C\gamma^\alpha \left(A\gamma^0 - \frac{i}{x_1}\hat{\mathbf{x}}_1\boldsymbol{\gamma} + m_e\right) P_L e_B(0, \tilde{E}_b)\Big] - (\tilde{E}_a \leftrightarrow \tilde{E}_b).\end{aligned} \tag{4.62}$$

Next we look at the structure of the bound electron wave functions. Note that the spinors in this part are first written down in the *Dirac representation* for economical reasons and will be transformed into the corresponding expressions in the chiral representation later. We restrict ourselves here to electrons from the $1s_{1/2}$ (abbreviated "$1s$"), from the $2s_{1/2}$ (abbreviated "$2s$"), and from the $2p_{1/2}$ (abbreviated "$2p$") shells, since those can be treated analogously. In principle, there could also be contributions like, e.g., one $1s_{1/2}$-electron and one $2p_{3/2}$-electron for the emission of one single photon. We neglect those in the following, since they require a much more complicated mathematical apparatus. In principle, it might however be that they also contribute in a non-negligible way.

According to Ref. [113], the structure of the bound electron waves close to the nucleus in the Dirac representation is approximately given by

$$e_B(\mathbf{x}_1, \tilde{E}_a) = R_a(|\mathbf{x}_1|)C_a Y_{00}\Gamma_a, \tag{4.63}$$

	Schrödinger	Dirac
$1s$	$2\left(\frac{Z}{a}\right)^{3/2} e^{-Zr/a}$	$N_+\sqrt{\Gamma(2\gamma+1)}\left[Z_+F(0,2\gamma+1,2\lambda r)\right]$
$2s$	$2\left(\frac{Z}{2a}\right)^{3/2}(1-\frac{Zr}{2a})e^{-Zr/(2a)}$	$N_+\sqrt{\Gamma(2\gamma+2)}\left[Z_+F(-1,2\gamma+1,2\lambda r)-F(0,2\gamma+1,2\lambda r)\right]$
$2p$	$\frac{1}{\sqrt{3}}\left(\frac{Z}{2a}\right)^{3/2}\frac{Zr}{a}e^{-Zr/(2a)}$	$N_-\sqrt{\Gamma(2\gamma+2)}\left[Z_-F(-1,2\gamma+1,2\lambda r)+F(0,2\gamma+1,2\lambda r)\right]$

Table 4.2: The radial parts of the wave functions that we use, both normalized such that the integral over the radial part gives 1. r is the radial coordinate and a is the Bohr radius. The abbreviations used above are $N_\pm = \frac{(2\lambda)^{3/2}}{\Gamma(2\gamma+1)}\sqrt{\frac{(m_e\pm\epsilon)\lambda}{4Z\alpha m_e^2 Z_\pm}}(2\lambda r)^{\gamma-1}e^{-\lambda r}$, $Z_\pm = \frac{Z\alpha m_e}{\lambda}\pm 1$, $\lambda = \sqrt{m_e^2-\epsilon^2}$, $\epsilon = m_e - \tilde{E}$, and $\gamma = \sqrt{1-Z^2\alpha^2}$ with the fine structure constant α and the atomic number Z. Γ is the Euler Γ-function and F is the confluent hypergeometric Kummer function.

where $R_a(|\mathbf{x}_1|)$ contains all the radial dependence, C_a is a constant (with $C_{1s} = C_{2s} = 1$ and $C_{2p} = \frac{1}{\sqrt{3}}$), Y_{00} is the lowest spherical harmonic, and Γ_a is the spinor part. Actually, this spinor part involves spherical spinors Ω_{jlm_j} to account for spin-orbit coupling, but if one neglects the subdominant component of the spinor, the bound electron waves reduce to the form given in Eq. (4.63). Close to the origin, the spinors are

$$\Gamma_{1s,2s} = \begin{pmatrix}\chi_{m_j}\\ 0\end{pmatrix} \text{ and } \Gamma_{2p} = \begin{pmatrix}0\\ \sigma^3\chi_{m_j}\end{pmatrix}, \tag{4.64}$$

where $m_j = \pm\frac{1}{2}$ is the projection of the total spin ($\frac{1}{2}$ in all three cases). The explicit form of the 2-spinors is

$$\chi_{+1/2} = \begin{pmatrix}1\\ 0\end{pmatrix} \text{ and } \chi_{-1/2} = \begin{pmatrix}0\\ 1\end{pmatrix}. \tag{4.65}$$

Note that neglecting the smaller spinor-component (whose relative important would increase further away from the nucleus) in Eq. (4.64) is well justified by Eq. (4.55): If the bound electron wave is not evaluated at the origin (as for $e_B(0,\tilde{E}_b)$ in Eq. (4.62)), the exponential function e^{-Bx_1} suppresses all contributions which are far away from the nucleus. The "decay length" of this exponential is $1/B$, which corresponds to about 100 fm ($B = \mathcal{O}(m_e)$), and this is is still far below the Bohr radius. This might be different for a larger Q-value, so our approximation might be worse for that case. We will, however, further use it keeping in mind that it might be less suited for the high Q region.

Let us go back to the present case now: We have not specified yet what the radial wave function R_a in Eq. (4.63) actually is. We will use two different versions for this function: First, we approximate it by the solution of the non-relativistic Schrödinger equation for the corresponding orbital, but we also use the exact solution of the Dirac equation in a Coulomb potential for the corresponding component [113], summarized in Tab. 4.2. The former has the advantage that in this approximation, we will obtain fully analytical results. In contrast, the Dirac case can only be solved numerically, but will yield more accurate results. Furthermore, the comparison with the Schrödinger case is also a confirmation of the numerics. In case these wave functions are evaluated at the origin, one can simply set the radial coordinate equal to $\frac{1}{V}\int d^3r\ r = \frac{3}{4}R$, which is the mean radial value of r and is of the order of the nuclear radius (and hence essentially zero if compared to the Bohr radius). The values of the wave functions at the origin are shown in Fig. 4.8. One can see nicely that the Schrödinger waves approximately reproduce the Dirac results for $1s$ and $2s$, while they clearly underestimate the $2p$-contribution.

We can now proceed as follows: The exact way would be to simply evaluate the integrations and γ-structure arising from Eq. (4.63). One can, however, also make use of an approxima-

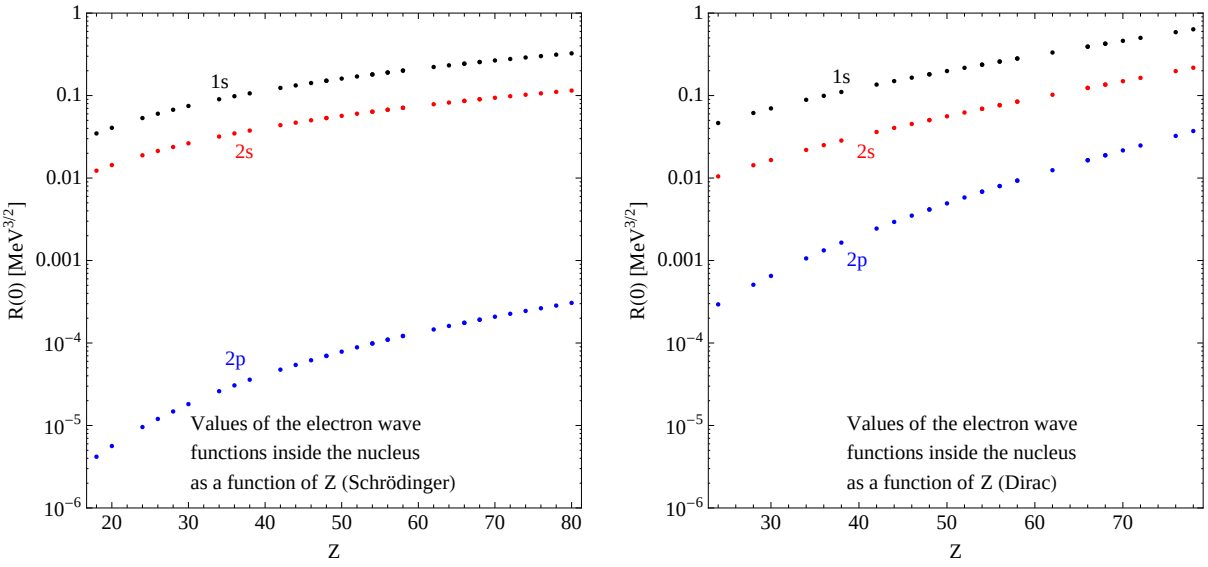

Figure 4.8: The solutions of the Schrödinger and Dirac equation, evaluated at the origin for several isotopes.

tion: Since the Q-values involved are small and $k_0 = \tilde{Q}$, one can perform a long wavelength approximation in Eq. (4.62), $e^{+i\mathbf{k}\mathbf{x}_1} \approx 1$. We will do both to be able to check the validity of this approximation that way. We are left with four cases in total: Either with or without long wavelength approximation, and for each way we use the Schrödinger and the Dirac wave functions.

Let us first do the evaluation in the easiest case, applying the long wavelength approximation. The x_1-integration in Eq. (4.62) is then actually trivial: For the E- and m_e-part, there is no angular dependence at all in the integrand and what remains is the function

$$f_S^a(k_0, \tilde{E}_a) = 4\pi C_a \int\limits_{x_1=0}^{\infty} dx_1 \; x_1 R_a(x_1) e^{-B(k_0,\tilde{E}_a)x_1}. \tag{4.66}$$

For the Schrödinger wave functions, these integrals can be performed analytically, yielding

$$f_S^{1s} = \frac{8\pi\sqrt{aZ^3}}{(aB+Z)^2}, \; f_S^{2s} = \frac{8\sqrt{2}\pi(2B(aZ)^{3/2} - 3\sqrt{aZ^5})}{(2aB+Z)^3}, \text{ and } f_S^{2p} = \frac{16\sqrt{2}\pi\sqrt{aZ^5}}{3(2aB+Z)^3}. \tag{4.67}$$

The $\mathbf{p}$-part is killed by the integration, since $\int\limits_0^{2\pi} \sin\phi d\phi = \int\limits_0^{2\pi} \cos\phi d\phi = \int\limits_0^{\pi} \cos\theta d\theta = 0$.

The calculation without the long wavelength approximation is a bit more elaborate, but can be simplified considerably using several tricks: First, we can expand the exponential into spherical Bessel functions and spherical harmonics,

$$e^{i\mathbf{k}\mathbf{x}_1} = 4\pi \sum_{l=0}^{\infty} \sum_{m=-l}^{+l} i^l j_l(k_0 x_1) Y_{lm}^*(\Omega_{\mathbf{k}}) Y_{lm}(\Omega_{\mathbf{x}_1}). \tag{4.68}$$

Exploiting the orthogonality relation $\int d\Omega \, Y_{lm}^*(\Omega) Y_{l'm'}(\Omega) = \delta_{ll'}\delta_{mm'}$ with the Y_{00} from Eq. (4.63), one can use $j_0(r) = \frac{\sin r}{r}$ to arrive at a function

$$\tilde{f}_S^a(k_0, \tilde{E}_a) = \frac{4\pi}{k_0} C_a \int\limits_{x_1=0}^{\infty} dx_1 \; \sin(k_0 x_1) R_a(x_1) e^{-B(k_0,\tilde{E}_a)x_1} \tag{4.69}$$

instead of Eq. (4.66), which is still solvable analytically for the Schrödinger wave functions. This leads to

$$\tilde{f}_S^{1s} = \frac{8\pi\sqrt{aZ^3}}{a^2k_0^2 + (aB+Z)^2},\ \tilde{f}_S^{2s} = \frac{8\sqrt{2}\pi(4(aZ)^{3/2}(a(B^2+k_0^2) - BZ) - 3\sqrt{aZ^7})}{(4(B^2+k_0^2)a^2 + 4BZa + Z^2)^2},\ \text{and}$$
$$\tilde{f}_S^{2p} = \frac{16\sqrt{2}\pi\sqrt{aZ^5}(2aB+Z)}{3(4(B^2+k_0^2)a^2 + 4BZa + Z^2)^2}. \tag{4.70}$$

The corresponding function for the **p**-part can be obtained by an analogous calculation. The remaining angular dependence gives a vector [4]

$$\mathbf{v}^T = (Y_{11}(\Omega_\mathbf{k}) - Y_{1,-1}(\Omega_\mathbf{k}), i(Y_{11}(\Omega_\mathbf{k}) + Y_{1,-1}(\Omega_\mathbf{k})), \sqrt{2}Y_{10}(\Omega_\mathbf{k})), \tag{4.71}$$

to be multiplied with $\boldsymbol{\gamma}$. The radial part can be written as

$$\tilde{f}_V^a(k_0, \tilde{E}_a) = (4\pi)^{3/2} C_a \int_{x_1=0}^{\infty} dx_1\ j_1(k_0x_1) R_a(x_1) e^{-B(k_0,\tilde{E}_a)x_1}, \tag{4.72}$$

where $j_1(r) = \frac{\sin r}{r^2} - \frac{\cos r}{r}$. The analytic solutions for the case of Schrödinger wave functions are

$$\tilde{f}_V^{1s} = \frac{-\left[16\left(\frac{Z\pi}{a}\right)^{3/2}\left((B+\frac{Z}{a})\arctan\left(\frac{ak_0}{aB+Z}\right) - k_0\right]}{k_0^2},$$
$$\tilde{f}_V^{2s} = \frac{4\sqrt{2}(Z\pi)^{3/2}\left[\frac{ak_0(4a^2(B^2+k_0^2)+8BZa+3Z^2)}{4a^2(B^2+k_0^2)+4BZa+Z^2} - \frac{1}{2}(2aB+3Z)\arctan\left(\frac{2ak_0}{2aB+Z}\right)\right]}{a^{5/2}k_0^2},\ \text{and}$$
$$\tilde{f}_V^{2p} = \frac{2\sqrt{2}\pi^{3/2}\left(\frac{Z}{a}\right)^{5/2}\left[\arctan\left(\frac{2ak_0}{2aB+Z}\right) - \frac{2ak_0(2aB+Z)}{4(B^2+k_0^2)a^2+4BZa+Z^2}\right]}{3k_0^2}. \tag{4.73}$$

It is easy to show that all three functions in Eq. (4.73) tend to zero for $k_0 \to 0$, which is consistent with them being absent in the long wavelength approximation. All functions are plotted for the $1s$-example in Figs. 4.9 and 4.10. One can immediately see that the long wavelength approximation is good for small k_0, but in total the non-relativistic approximation does not seem to work very well (it does, however, reproduce the correct order of magnitude and is suited for a cross-check).

Finally, we can now also write down the exchange term corresponding to $(\tilde{E}_a \leftrightarrow \tilde{E}_b)$ in Eq. (4.62). For the E-part (cf. Eq. (4.56)), this gives

$$A_a f_S^a C_b R_b(0) \cdot \Gamma_a^T C\gamma^\alpha\gamma^0 P_L \Gamma_b - A_b f_S^b C_a R_a(0) \cdot \Gamma_b^T C\gamma^\alpha\gamma^0 P_L \Gamma_a. \tag{4.74}$$

The second γ-structure yields

$$\Gamma_b^T C\gamma^\alpha\gamma^0 P_L\Gamma_a \equiv (\Gamma_b^T C\gamma^\alpha\gamma^0 P_L\Gamma_a)^T = \Gamma_a^T C\gamma^\alpha\gamma^0 P_L\Gamma_b, \tag{4.75}$$

so the pre-factor in front of the structure $\Gamma_a^T C\gamma^\alpha\gamma^0 P_L\Gamma_b$ will simply be

$$F_-(k_0) \equiv A_a(k_0) f_S^a(k_0) C_b R_b(0) - A_b(k_0) f_S^b(k_0) C_a R_a(0). \tag{4.76}$$

One can perform an analogous calculation for the m_e-part yielding

$$m_e f_S^a C_b R_b(0) \cdot \Gamma_a^T C\gamma^\alpha\gamma^0 P_L\Gamma_b - (\tilde{E}_a \leftrightarrow \tilde{E}_b) = f_-(k_0)\Gamma_a^T C\gamma^\alpha\Gamma_b - f_+(k_0)\Gamma_a^T C\gamma^\alpha\gamma_5\Gamma_b, \tag{4.77}$$

[4] This can again be shown by expanding the exponential function like in Eq. (4.68) and applying orthogonality.

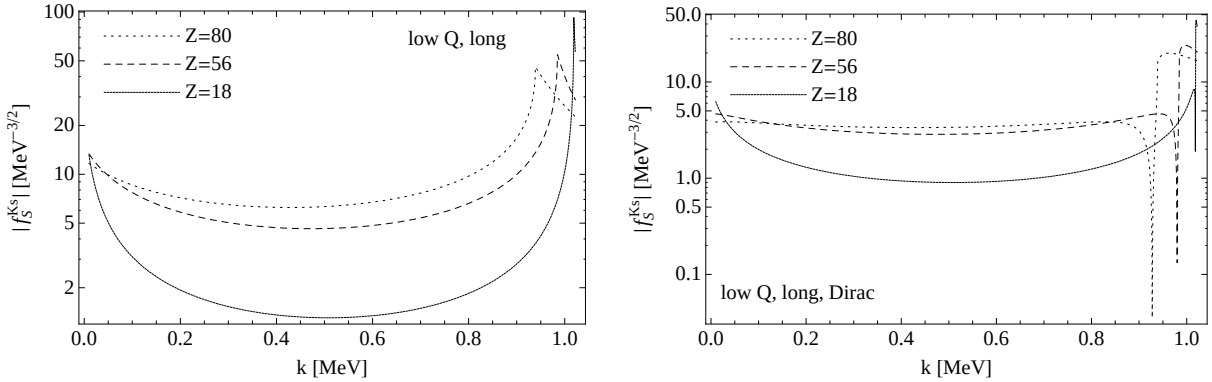

Figure 4.9: The form of the f-functions (for the $1s$-orbital as example) for the Schrödinger (left panel) and Dirac (right panel) wave functions in the long wavelength approximation. This approximation reproduces the exact solution (cf. Fig. 4.10) very well for $k_0 \lesssim 0.25$ MeV. As expected, the contributions are larger for a higher value of the atomic number Z.

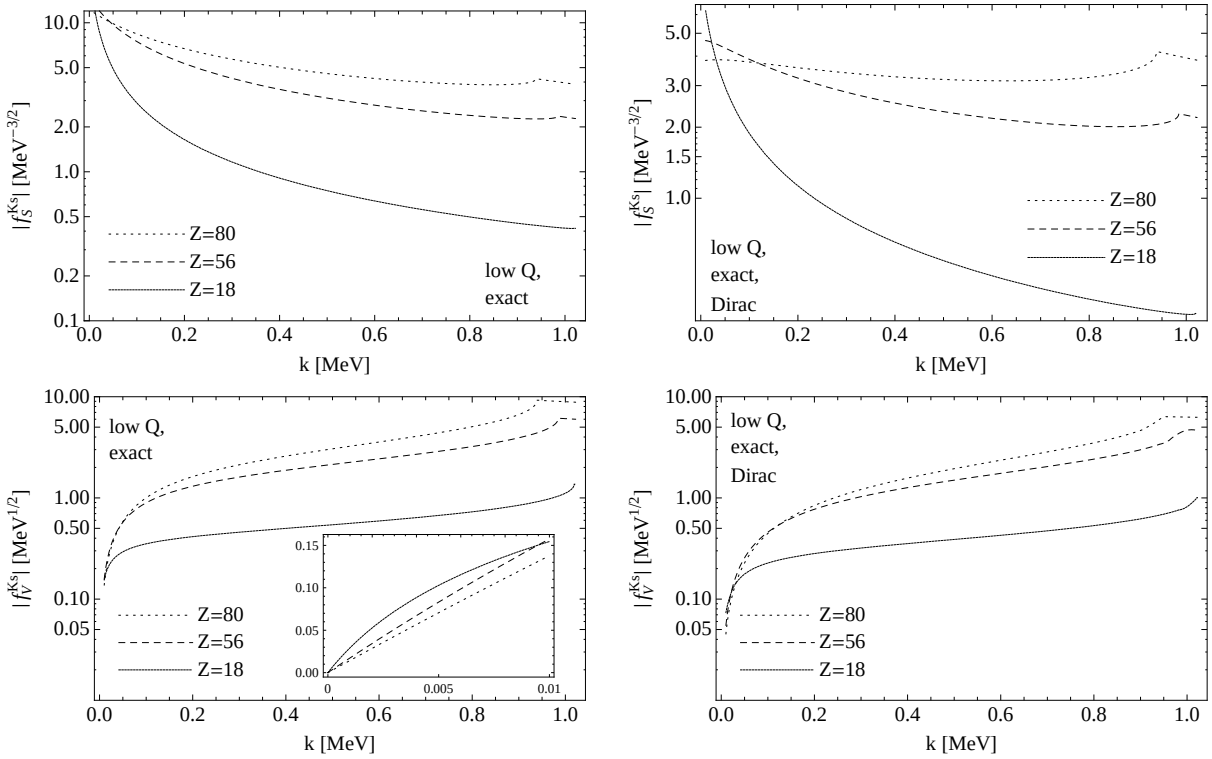

Figure 4.10: The form of the f-functions (for the $1s$-orbital as example) for the Schrödinger (left column) and Dirac (right column) wave functions without the long wavelength approximation.

where

$$f_{\pm}(k_0) \equiv \frac{m_e}{2}\left[f_S^a(k_0)C_bR_b(0) \pm f_S^b(k_0)C_aR_a(0)\right]. \tag{4.78}$$

The γ-structure of the **p**-part is of the form $\Gamma_a^T C\gamma^\alpha(\mathbf{v}\boldsymbol{\gamma})\gamma^0 P_L\Gamma_b$, which effectively reduces to

$$v_3\Gamma_a^T C\gamma^\alpha\gamma^3\gamma^0 P_L\Gamma_b, \tag{4.79}$$

as we shall see later, with a pre-factor

$$\tilde{F}_-(k_0) \equiv f_V^a(k_0)C_bR_b(0) - f_V^b(k_0)C_aR_a(0). \tag{4.80}$$

We are now ready to insert explicit expressions for the spinors from Eq. (4.64). First, we transform them into the chiral representation, which is done by the unitary transformation [114]

$$\Psi_{\text{chiral}} = \frac{1}{\sqrt{2}}\begin{pmatrix}\mathbb{1} & -\mathbb{1}\\ \mathbb{1} & \mathbb{1}\end{pmatrix}\Psi_{\text{Dirac}}, \tag{4.81}$$

in order to be able to use the explicit γ-matrices from Eq. (4.12). This leads to

$$\Gamma_{1s,2s} \to \frac{1}{\sqrt{2}}\begin{pmatrix}\chi_{m_j}\\ \chi_{m_j}\end{pmatrix} \text{ and } \Gamma_{2p} \to \frac{1}{\sqrt{2}}\begin{pmatrix}-\sigma^3\chi_{m_j}\\ \sigma^3\chi_{m_j}\end{pmatrix} = -\gamma^3\frac{1}{\sqrt{2}}\begin{pmatrix}\chi_{m_j}\\ \chi_{m_j}\end{pmatrix}, \tag{4.82}$$

which suggests the replacement $\Gamma_c \to \gamma^c_{\text{shell}}\Gamma_c$ in Eqs. (4.74), (4.77), and (4.79), where $\gamma^{1s,2s}_{\text{shell}} = \mathbb{1}$ and $\gamma^{2p}_{\text{shell}} = \gamma^3$.

These explicit forms can now be inserted directly. Furthermore, we make use of the actions of Pauli matrices on 2-spinors,

$$\mathbb{1}\chi_{m_j} = \chi_{m_j},\ \sigma^1\chi_{m_j} = \chi_{-m_j},\ \sigma^2\chi_{m_j} = 2im_j\chi_{-m_j},\ \text{and } \sigma^3\chi_{m_j} = 2m_j\chi_{m_j}. \tag{4.83}$$

For capturing two s-electrons a and b, this leads to

$$\Gamma_a^T C\gamma^\alpha\gamma^0 P_L\Gamma_b = -\frac{1}{2}z^\alpha, \Gamma_a^T C\gamma^\alpha\Gamma_b = -z^\alpha,\ \text{and } \Gamma_a^T C\gamma^\alpha\gamma_5\Gamma_b = 0, \tag{4.84}$$

where

$$z^\alpha \equiv \chi^T_{-m_a}\sigma^\alpha\chi_{m_b}. \tag{4.85}$$

Capturing one s- and one p-electron gives

$$\Gamma_a^T C\gamma^\alpha\gamma^0 P_L\Gamma_b = \frac{1}{2}z^\alpha, \Gamma_a^T C\gamma^\alpha\Gamma_b = 0,\ \text{and } \Gamma_a^T C\gamma^\alpha\gamma_5\Gamma_b = z^\alpha, \tag{4.86}$$

where we have explicitly verified that it does not matter which electron (a or b) is taken to be s and which to be p. We still lack the part with $\boldsymbol{\gamma}$. For both cases, it yields a structure proportional to $\mathbf{v}\chi^T_{-m_a}\sigma^\alpha\boldsymbol{\sigma}\chi_{m_b}$. Since $\epsilon_0^* = 0$, one can write this as $v_j\delta^{\alpha i}\chi^T_{-m_a}\sigma^i\sigma^j\chi_{m_b}$ and use $\sigma^i\sigma^j = \delta^{ij} + i\epsilon^{ijk}\sigma^k$. The first part leads to a term proportional to $\chi^T_{-m_a}\chi_{m_b} = \delta_{-m_a,m_b}$, which is forbidden by angular momentum conservation. We are left with $iv_j\delta^{\alpha i}\epsilon^{ijk}\chi^T_{-m_a}\sigma^k\chi_{m_b}$. For a real photon, we can only have $i = 1$ or $i = 2$, leading to

$$iv_j(\delta^{\alpha 1}\epsilon^{1jk} + \delta^{\alpha 2}\epsilon^{2jk})(\delta^{k1}\chi^T_{-m_a}\sigma^1\chi_{m_b} + \delta^{k2}\chi^T_{-m_a}\sigma^2\chi_{m_b} + \delta^{k3}\underbrace{\chi^T_{-m_a}\sigma^3\chi_{m_b}}_{\propto\delta_{-m_a,m_b}\to 0}). \tag{4.87}$$

The only possible combinations are $(2m_av_3\delta^{\alpha 1}\delta_{m_am_b})$ and $(iv_3\delta^{\alpha 2}\delta_{m_am_b})$. Since v_3 is proportional to $\cos\theta_k$, the phase space integration kills all interference terms with Eqs. (4.84) and (4.86). This is still true for the terms proportional to $v_{1,2}$ that appear in the quadratic

contribution originating from that term. Therefore, we set $\boldsymbol{\gamma} \to \gamma^3$ in the **p**-part. Effectively, this leads to a structure of

$$\mathbf{v}\chi^T_{-m_a}\sigma^\alpha \boldsymbol{\sigma}\chi_{m_b} \to v_3 \cdot \frac{z^\alpha}{2}, \tag{4.88}$$

where we have dropped a factor with absolute value 1, since it does not matter in the absence of interference terms.

Finally, we can define the following form factors:

$$g_\pm(k_0) \equiv f_\pm(k_0) + \frac{1}{2}F_-(k_0) \text{ and } \tilde{g}_- \equiv \frac{1}{2\sqrt{3}}\tilde{F}_-(k_0). \tag{4.89}$$

The numerical factor in the latter definition allows for a convenient way of writing down the final decay rate in the end. The final matrix element is

$$\langle A'|S^{(3)}|A\rangle = \mathcal{M}\delta(k_0 - \tilde{Q}) = \mp iC\delta(k_0 - \tilde{Q})\epsilon^*_\alpha(\mathbf{k})[g_\mp(k_0) + \sqrt{3}\cos\theta_k \tilde{g}_-(k_0)]z^\alpha, \tag{4.90}$$

where the upper sign is valid for the capture of two s-electrons, while the lower one holds for the capture of one s- and one p-electron. The constant is given by

$$C = \frac{eG_F^2 g_A^2 m_{ee} M^{0\nu}}{2^5\pi^2\sqrt{2k_0 V}R}. \tag{4.91}$$

Note that $\tilde{g}_-(k_0 \to 0) \to 0$, and that there will be no interference terms between $g_\mp$ and $\tilde{g}_-$.

Having done all that, one can square the amplitude in Eq. (4.90), where we apply the usual trick for the δ-function,

$$\left[\delta(k_0 - \tilde{Q})\right]^2 \to \frac{T}{2\pi}\delta(k_0 - \tilde{Q}). \tag{4.92}$$

The result then has to be summed over the possible photon polarizations, where we can use

$$\sum_{(i)} \epsilon^{(i)*}_\alpha \epsilon^{(i)}_\beta \to -g_{\alpha\beta}. \tag{4.93}$$

This leads to a proportionality to (cf. Eq. (4.83))

$$|z^3|^2 + |z^2|^2 + |z^1|^2 - |z^0|^2 = 2\delta_{m_a,m_b}. \tag{4.94}$$

As it should be, the contributions coming from longitudinal and time-like photon polarizations exactly cancel each other and the final result requires the two captured electrons to have parallel spins, as required by angular momentum conservation. Finally, the square of the amplitude has to be summed over all possible electron pairs that can be captured in a certain decay mode [107].

In the end, one can use Fermi's Golden Rule to obtain the decay width,

$$\Gamma = 2\pi\frac{V/T}{(2\pi)^3}\int d^3k|\mathcal{M}|^2 \cdot \frac{T}{2\pi}\delta(k_0 - \tilde{Q}). \tag{4.95}$$

The final expression for the decay rate reads:

$$\begin{aligned}
\Gamma_{1s\&2s} &= \frac{\alpha G_F^4 g_A^4}{2^8\pi^5 R^2}|M^{0\nu}|^2|m_{ee}|^2\tilde{Q}\left[|g_-(\tilde{Q})|^2 + |\tilde{g}_-(\tilde{Q})|^2\right] \text{ and} \\
\Gamma_{1s(2s)\&2p} &= \frac{\alpha G_F^4 g_A^4}{2^8\pi^5 R^2}|M^{0\nu}|^2|m_{ee}|^2\tilde{Q}\left[|g_+(\tilde{Q})|^2 + |\tilde{g}_-(\tilde{Q})|^2\right],
\end{aligned} \tag{4.96}$$

where $\tilde{Q} = Q - \tilde{E}'_a - \tilde{E}'_b$ is the corrected Q-value and $\alpha = \frac{e^2}{4\pi}$ is the fine structure constant. The actual dependence of the decay rate on $\tilde{Q}$ and the form factors is plotted in Fig. 4.11 for the Schrödinger case. As expected, the contribution to the rate grows with the atomic number Z and is largest for the capture of two s-electrons. The variation with $\tilde{Q}$ is relatively moderate for generic photon energies. We have furthermore plotted a more detailed comparison of the exact calculation with the long wavelength approximation in Fig. 4.12. For very small $\tilde{Q}$, the long wavelength approximation turns out to be extremely good, too, as we shall see later when looking at the numerical values.

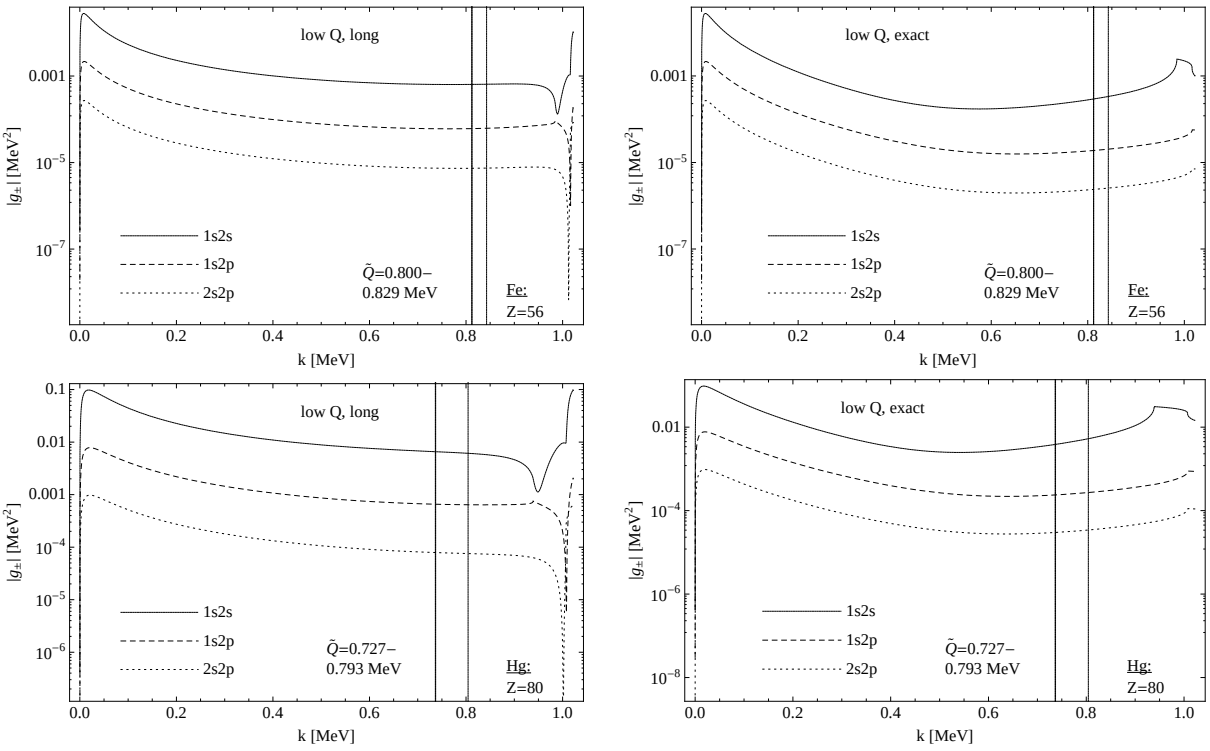

Figure 4.11: The actual dependence of the decay rate from Eq. (4.96) on $\tilde{Q}$ and on the form factors (for the Schrödinger solutions as example). The left column shows the long wavelength approximation, while the right one shows the exact calculation, each for two exemplary isotopes.

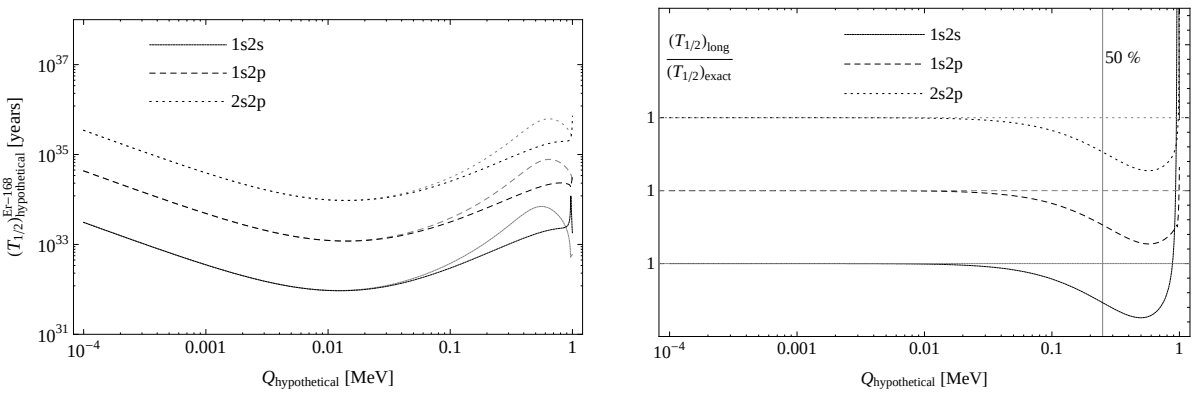

Figure 4.12: Example plots for Er-168 for a hypothetical Q-value to demonstrate the validity of the long wavelength approximation for small k_0. On the left, one can find the hypothetical half-life for the exact calculation (gray) and the long wavelength approximation (black). On the right panel, one can see that the ratio between both is exactly 1 in the domain where the approximation works. For $k_0 \lesssim 0.25$ MeV, the approximation differs from the exact calculation by at most 50%.

4.4.5 The high Q region

Let us now turn to the region of larger Q-values. For this, we go back to Eq. (4.52) and repeat the analysis using the real and positive quantity D^2.

Of course, the structure is all the same for the high Q-region. The major physical difference is that here, of course, it makes no sense to use the long wavelength approximation, since the photon energies are too large for that. In the calculation, the integral from Eq. (4.53) will, however, look differently:

$$I_2(x_1) \equiv \int \frac{d^3p\ e^{+i\mathbf{p}\mathbf{x}_1}}{p^2 - D^2(k_0, \tilde{E}_a) - i\epsilon'}. \tag{4.97}$$

The contour can still be closed above the real axis, but the pole which is now decisive is the one at $p = D + i\epsilon'$. Apart from this, the calculation remains the same and the result for the integral is

$$I_2(x_1) = \frac{2\pi^2}{x_1} e^{iD(k_0,\tilde{E}_a)x_1}, \tag{4.98}$$

so the only difference from the formulae in Sec. 4.4.4 is the replacement $e^{-B(k_0,\tilde{E}_a)x_1} \longrightarrow e^{iD(k_0,\tilde{E}_a)x_1}$. The functions from Eq. (4.70) now change to

$$\begin{aligned}
\tilde{f}_S^{1s} &= \frac{8\pi \left(\frac{Z}{a}\right)^{3/2}}{k_0^2 - \frac{(aD+iZ)^2}{a^2}},\ \tilde{f}_S^{2s} = \frac{8\sqrt{2a}\pi Z^{3/2}\left(4(k_0^2 - D^2)a^2 + 4iDZa - 3Z^2\right)}{(4(k_0^2 - D^2)a^2 - 4iDZa + Z^2)^2},\ \text{and} \\
\tilde{f}_S^{2p} &= \frac{16\sqrt{2a}\pi Z^{5/2}(Z - 2iaD)}{3\left(4(k_0^2 - D^2)a^2 - 4iDZa + Z^2\right)^2},
\end{aligned} \tag{4.99}$$

and the ones from Eq. (4.73) now look like

$$\begin{aligned}
\tilde{f}_V^{1s} &= \frac{-16\left(\frac{Z\pi}{a}\right)^{3/2}\left[\left(D + \frac{iZ}{a}\right)\arctan\left(\frac{ak_0}{aD+iZ}\right) - k_0\right]}{k_0^2}, \\
\tilde{f}_V^{2s} &= \frac{4\sqrt{2}(Z\pi)^{3/2}\left[\frac{ak_0\left(4(k_0^2-D^2)a^2-8iDZa+3Z^2\right)}{4(k_0^2-D^2)a^2-4iDZa+Z^2} - \frac{1}{2}(2aD + 3iZ)\arctan\left(\frac{2ak_0}{2aD+iZ}\right)\right]}{a^{5/2}k_0^2},\ \text{and} \\
\tilde{f}_V^{2p} &= \frac{2\sqrt{2}\pi^{3/2}\left(\frac{Z}{a}\right)^{5/2}\left(i\arctan\left(\frac{2ak_0}{2aD+iZ}\right) - ak_0\left(\frac{1}{Z-2ia(D-k_0)} + \frac{i}{2a(D+k_0)+iZ}\right)\right.}{3k_0^2},
\end{aligned} \tag{4.100}$$

both once again for the Schrödinger wave functions. Apart from that, all formulae stay the same and the final decay rate in Eq. (4.96) will look exactly the same, too.

4.4.6 Numerical results

Finally, we present the results of the numerical analysis of Eq. (4.96). One major difficulty is, of course, the exact value of the nuclear matrix element $|M^{0\nu}|$. Since we do not want to enter this discussion, we simply present our results as functions of this value, i.e., we simply calculate the rate $\Gamma/|M^{0\nu}|^2$ and the half-life $T_{1/2} \cdot |M^{0\nu}|^2$ (where we use $T_{1/2} = \frac{\ln 2}{\Gamma}$ and $m_e = 0.511$ MeV $= 2.45 \cdot 10^{28}$/years). The nuclear radii are calculated according to $R \approx 1.4\ \text{fm} \cdot \sqrt[3]{A}$, where A is the atomic mass number. The Q-values for the different reactions are taken from Ref. [91].

Our numerical input is summarized in Tab. 4.3. We have listed everything in units of MeV and have assumed typical values for the quantities used that are no Constants of Nature. The exemplary isotopes and their characteristic values are given in Tab. 4.4. The atomic binding energies are taken from Ref. [115].

Quantity	Symbol	Value
Electron mass	m_e	0.511 MeV
Bohr radius	a	$5.29 \cdot 10^{-11}$ m $= 268.53/\text{MeV}$
Fermi constant	G_F	$1.166 \cdot 10^{-11}/\text{MeV}^2$
Fine structure constant	α	1/137
Axial vector coupling	g_A	1.25
Effective neutrino mass	$\lvert m_{ee}\rvert$	1 eV $= 1.0 \cdot 10^{-6}$ MeV

Table 4.3: The numerical input and physical constants we use. Note that we write everything in units of MeV.

Element	Z	$E_{1s}(E'_{1s})$ [MeV]	$E_{2s}(E'_{2s})$ [MeV]	$E_{2p}(E'_{2p})$ [MeV]
Ar-36	18	0.003(0.002)	0.0003 (<0.001)	0.0003 (<0.001)
Ca-40	20	0.004(0.003)	0.0004 (<0.001)	0.0004 (<0.001)
Cr-50	24	0.006(0.005)	0.0007 (0.001)	0.0006 (<0.001)
Fe-54	26	0.007(0.006)	0.0008 (0.001)	0.0007 (0.001)
Ni-58	28	0.008(0.007)	0.001 (0.001)	0.0009 (0.001)
Zn-64	30	0.010(0.008)	0.001 (0.001)	0.001 (0.001)
Se-74	34	0.013(0.011)	0.002 (0.001)	0.001 (0.001)
Kr-78	36	0.014(0.013)	0.002 (0.002)	0.002 (0.001)
Sr-84	38	0.016(0.014)	0.002 (0.002)	0.002 (0.002)
Mo-92	42	0.020(0.018)	0.003 (0.003)	0.003 (0.002)
Ru-96	44	0.022(0.020)	0.003 (0.003)	0.003 (0.003)
Pd-102	46	0.024(0.022)	0.004 (0.003)	0.003 (0.003)
Cd-106	48	0.027(0.024)	0.004 (0.004)	0.004 (0.003)
Cd-108	48	0.027(0.024)	0.004 (0.004)	0.004 (0.003)
Sn-112	50	0.029(0.027)	0.004 (0.004)	0.004 (0.004)
Te-120	52	0.032(0.029)	0.005 (0.004)	0.005 (0.004)
Xe-124	54	0.035(0.032)	0.005 (0.005)	0.005 (0.005)
Xe-126	54	0.035(0.032)	0.005 (0.005)	0.005 (0.005)
Ba-130	56	0.037(0.035)	0.006 (0.005)	0.006 (0.005)
Ba-132	56	0.037(0.035)	0.006 (0.005)	0.006 (0.005)
Ce-136	58	0.040(0.037)	0.007 (0.006)	0.006 (0.005)
Ce-138	58	0.040(0.037)	0.007 (0.006)	0.006 (0.006)
Sm-144	62	0.047(0.044)	0.008 (0.007)	0.007 (0.006)
Gd-152	64	0.050(0.047)	0.008 (0.008)	0.008 (0.007)
Dy-156	66	0.054(0.050)	0.009 (0.008)	0.009 (0.007)
Dy-158	66	0.054(0.050)	0.009 (0.008)	0.009 (0.008)
Er-162	68	0.057(0.054)	0.010 (0.009)	0.009 (0.008)
Er-164	68	0.057(0.054)	0.010 (0.009)	0.009 (0.009)
Yb-168	70	0.061(0.057)	0.010 (0.010)	0.010 (0.010)
Hf-174	72	0.065(0.061)	0.011 (0.010)	0.011 (0.009)
W-180	74	0.070(0.065)	0.012 (0.011)	0.012 (0.011)
Os-184	76	0.074(0.070)	0.013 (0.012)	0.012 (0.012)
Pt-190	78	0.078(0.074)	0.014 (0.013)	0.013 (0.012)
Hg-196	80	0.083(0.078)	0.015 (0.014)	0.014 (0.013)

Table 4.4: The atomic number Z and the binding energies [115] for one electron in the $1s_{1/2}$-, $2s_{1/2}$-, and $2p_{1/2}$-shell in MeV (Ref. [91]) for the isotopes considered.

		Schr.		Dirac	
Element	Q [MeV]	long	exact	long	exact
Ar-36	0.434	7.87^{36}	3.99^{37}	2.65^{37}	1.11^{38}
Ca-40	0.194	1.18^{36}	2.42^{36}	3.61^{36}	6.49^{36}
Fe-54	0.680	8.93^{35}	4.77^{36}	2.21^{36}	1.00^{37}
Cd-108	0.269	5.58^{33}	1.25^{34}	7.77^{33}	1.21^{34}
Xe-126	0.897	7.68^{33}	1.51^{34}	9.04^{33}	1.92^{34}
Ba-132	0.840	6.36^{33}	1.50^{34}	6.81^{33}	1.48^{34}
Ce-138	0.693	4.93^{33}	1.75^{34}	4.67^{33}	1.12^{34}
Gd-152	0.056	3.21^{32}	3.22^{32}	6.56^{34}	6.61^{34}
Dy-158	0.283	7.74^{32}	1.52^{33}	7.50^{32}	9.44^{32}
Er-164	0.024	1.11^{34}	1.11^{34}	2.31^{35}	2.31^{35}
W-180	0.146	1.28^{32}	1.46^{32}	2.94^{32}	2.89^{32}
Hg-196	0.820	7.96^{32}	1.47^{33}	3.42^{32}	5.12^{32}

Table 4.5: The total half-lives (for all three combinations) in years (modulo their dependence on the NME) for the isotopes in the low Q region. The notation x^y always stands for $x \cdot 10^y$.

Let us start with the low Q-region, where we have 12 exemplary isotopes. The half-lives in years, modulo their dependence on the nuclear matrix element, are given in Tab. 4.5, where the notation x^y always stands for $x \cdot 10^y$. The first thing to observe is that, as expected, the half-lives are generically smaller for larger atomic number Z, which is simply a reflection of the electrons being closer to the nucleus in average for higher Z. The only exception is Er-164. This can, however, be explained by its extremely small Q-value: If one corrects that value by the energies of the holes in the atomic final states, one will see that capture from the $1s$-shell is actually forbidden, so there is only one contribution for this element instead of three ($1s2s$, $1s2p$, and $2s2p$). It can also be seen that the long-wavelength approximation works well for really small Q-values, especially for Gd-152 and Er-164, but also for Ca-40 and W-180. The non-relativistic approximation gives fair estimates that differ from the Dirac results by a factor of $\mathcal{O}(1)$. Turning this around, they confirm the results that have been obtained from numerics.

In general, the half-lives are extremely high. This is partially a reflection of the fact that the emission of only one photon might be disfavored, but in general double EC is a very rare process, so one could not have expected really nice numbers. This might, however, considerably change for other, more exotic, mechanisms that could potentially mediate this decay.

For completeness, we also list the results for the high Q region in Tab. 4.6. The general tendencies seem to be the same, but it is important to keep in mind that our method of calculation might not be as accurate in this sector as it is for low Q (due to the absence of the factor e^{-Bx_1} in the integral, cf. Eqs. (4.55) and (4.98)).

4.5 The two-photon mode

The next task is to do the corresponding calculation for the case of two photons emitted ($ECEC\gamma\gamma$). This calculation is much more involved than the last one, which is why we will restrict ourselves to the long wavelength approximation, as used in Sec. 4.4.4. This approximation is valid for low Q-values and we have shown that, for the 1γ-case, the region $\tilde{Q} \lesssim 0.25$ MeV is reproduced well. Since in the present case two photons are emitted, we can expect this approximation to be applicable also for slightly higher values of the effective Q-value up to about $\tilde{Q} \sim 0.5$ MeV. Furthermore, also in the region below 0.25 MeV it should work better than for

Element	Q [MeV]	Schrödinger	Dirac
Cr-50	1.171	3.11^{35}	6.54^{36}
Ni-58	1.926	1.76^{35}	3.05^{36}
Zn-64	1.096	1.32^{35}	9.10^{35}
Se-74	1.209	9.67^{34}	3.62^{35}
Kr-78	2.866	7.12^{34}	2.63^{35}
Sr-84	1.787	7.22^{34}	1.82^{35}
Mo-92	1.649	6.58^{34}	7.28^{34}
Ru-96	2.719	3.96^{34}	4.39^{34}
Pd-102	1.172	1.07^{35}	2.23^{34}
Cd-106	2.771	3.10^{34}	1.91^{34}
Sn-112	1.922	6.23^{34}	1.44^{34}
Te-120	1.698	1.11^{35}	1.01^{34}
Xe-124	2.866	2.20^{34}	6.08^{33}
Ba-130	2.611	2.51^{34}	4.77^{33}
Ce-136	2.400	2.79^{34}	3.49^{33}
Sm-144	1.781	2.15^{34}	1.87^{33}
Dy-156	2.011	7.41^{33}	1.00^{33}
Er-162	1.845	4.08^{33}	7.39^{32}
Yb-168	1.422	1.59^{33}	4.67^{32}
Hf-174	1.101	4.13^{32}	2.27^{32}
Os-184	1.452	4.53^{32}	2.02^{32}
Pt-190	1.383	2.82^{32}	1.46^{32}

Table 4.6: The same as Tab. 4.5 for the high Q region.

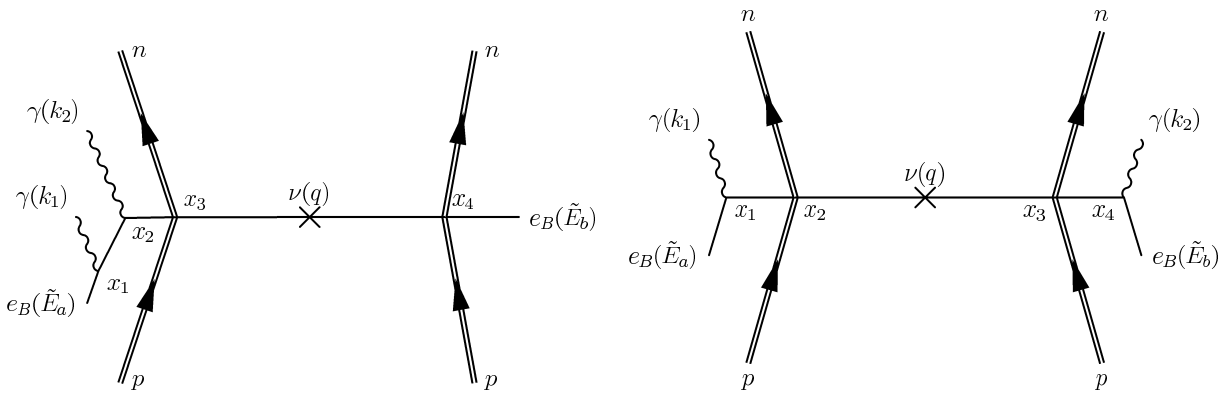

Figure 4.13: The different Feynman diagrams contributing to $ECEC\gamma\gamma$ under the assumption of the two-nucleon mechanism. The left diagram is referred to as "A", while the right one is called "B".

$ECEC\gamma$. Glancing at Tab. 4.5, we expect the approximation to work well for Ca-40, Gd-152, Er-164, and W-180, but it should also be applicable to Ar-36, Cd-108, and Dy-158.

In the following we will perform the calculation and give in the end the ratio of $ECEC\gamma\gamma$ to $ECEC\gamma$ for the seven isotopes for which we expect the approximation to work.

4.5.1 The Feynman diagrams and the starting point of the calculation

We start with the Feynman diagrams for the process. Assuming the 2-nucleon mechanism again, one can draw two topologically different diagrams, which are depicted in Fig. 4.13: Either one of the captured electrons emits both photons (diagram of type A, left panel) or both of the captured electrons emit one photon each (diagram of type B, right panel).

Using Eqs. (4.19) and (4.20), the corresponding S-matrix elements are given by

$$\begin{aligned}\langle A'|S_A^{(4)}|A\rangle = &\left(\frac{(-i)^2}{2!}\right)^2 (-e)^2 \left(\frac{G_F}{\sqrt{2}}\right)^2 \int d^4x_1 d^4x_2 d^4x_3 d^4x_4 \cdot \\ &\cdot e_B^T(x_1,\tilde{E}_a)(\gamma^\alpha)^T \overline{e_B^T(x_1)} e_B^T(x_2)(\gamma^\beta)^T \overline{e_B^T(x_2)} e_B^T(x_3)(1-\gamma_5)^T(\gamma^\mu)^T \overline{\nu_L^T(x_3)}\overline{\nu}_L(x_4)\gamma^\nu \cdot \\ &\cdot(1-\gamma_5)e_B(x_4,\tilde{E}_b)\cdot\langle A'|T\left\{\mathcal{J}_\mu^\dagger(x_3)\mathcal{J}_\nu^\dagger(x_4)\right\}|A\rangle \cdot N\left\{A_\alpha(x_1)A_\beta(x_2)\right\} + (\text{rest}), \end{aligned} \tag{4.101}$$

and

$$\begin{aligned}\langle A'|S_B^{(4)}|A\rangle = &\left(\frac{(-i)^2}{2!}\right)^2 (-e)^2 \left(\frac{G_F}{\sqrt{2}}\right)^2 \int d^4x_1 d^4x_2 d^4x_3 d^4x_4 \cdot \\ &\cdot e_B^T(x_1,\tilde{E}_a)(\gamma^\alpha)^T \overline{e_B^T(x_1)} e_B^T(x_2)(1-\gamma_5)^T(\gamma^\mu)^T \overline{\nu_L^T(x_2)}\overline{\nu}_L(x_3)\gamma^\nu(1-\gamma_5)\overline{e_B(x_3)}\overline{e}_B(x_4)\cdot \\ &\cdot\gamma^\beta e_B(x_4,\tilde{E}_b)\cdot\langle A'|T\left\{\mathcal{J}_\mu^\dagger(x_2)\mathcal{J}_\nu^\dagger(x_3)\right\}|A\rangle \cdot N\left\{A_\alpha(x_1)A_\beta(x_4)\right\} + (\text{rest}), \end{aligned} \tag{4.102}$$

using the same notation as in Sec. 4.4. Note that the normal ordering has no effect on the photon creation operators (they commute anyway). The term "+(rest)" means that we still have to add (subtract) the diagrams with the two photon (electron) lines exchanged to ensure obedience to the Pauli principle. Schematically, this means

$$+(\text{rest}) = -(\tilde{E}_a \leftrightarrow \tilde{E}_b) + (k_1 \leftrightarrow k_2) - (\tilde{E}_a \leftrightarrow \tilde{E}_b, k_1 \leftrightarrow k_2). \tag{4.103}$$

Eqs. (4.101) and (4.102) can be simplified using Eqs. (4.17) and (4.18). For the propagators, we make use of Eqs. (4.22), (4.23), and (4.25). The nuclear physics part can again be factored out as in Sec. 4.4.2 and we use Eqs. (4.30), (4.31), (4.32), (4.33), and (4.35) to be able to integrate over the times. This calculation again yields an energy-conserving δ-function for both types of diagrams, which is given by

$$\delta\left[(E_i + 2m_e - \tilde{E}_a - \tilde{E}_b) - (E_f + \omega_1 + \omega_2)\right], \tag{4.104}$$

where $\omega_{1,2} = (k_{1,2})_0 = |\mathbf{k}_{1,2}|$. Using arguments very similar to the ones that led us to Eq. (4.41), one can rewrite this as

$$\delta(\omega_1 + \omega_2 - \tilde{Q}), \tag{4.105}$$

where $\tilde{Q}$ is defined exactly as in Eq. (4.42). Having done all that and having defined an NME analogously to Eqs. (4.44) and (4.46), one obtains

$$\begin{aligned}\langle A'|S_A^{(4)}|A\rangle = &-\frac{i\alpha G_F^2 g_A^2 m_{ee} M^{0\nu}}{2^{10}\pi^5 V R\sqrt{\omega_1\omega_2}}\delta(\omega_1+\omega_2-\tilde{Q})\epsilon_\alpha^*(\mathbf{k}_1)\epsilon_\beta^*(\mathbf{k}_2)\int d^3x_1 d^3x_2 \frac{d^3p_1}{E_1}\frac{d^3p_2}{E_2}\cdot \\ &\cdot e^{i\mathbf{k}_1\mathbf{x}_1}e^{i\mathbf{k}_2\mathbf{x}_2}\cdot e_B^T(\mathbf{x}_1,\tilde{E}_a)C\gamma^\alpha\Gamma_A^\beta P_L e_B(0,\tilde{E}_b) + (\text{rest}) \end{aligned} \tag{4.106}$$

for diagram A, where

$$\Gamma_A^\beta \equiv \frac{e^{-i\mathbf{p}_1(\mathbf{x}_1-\mathbf{x}_2)}e^{-i\mathbf{p}_2\mathbf{x}_2}}{(\omega_1+\tilde{E}_a-m_e-E_1)(\omega_1+\omega_2+\tilde{E}_a-m_e-E_2)}\cdot(-\not{p}_1+m_e)\gamma^\beta(-\not{p}_2+m_e) -$$
$$-\frac{e^{-i\mathbf{p}_1(\mathbf{x}_1-\mathbf{x}_2)}e^{+i\mathbf{p}_2\mathbf{x}_2}}{(\omega_1+\tilde{E}_a-m_e-E_1)(\omega_1+\omega_2+\tilde{E}_a-m_e+E_2)}\cdot(-\not{p}_1+m_e)\gamma^\beta(+\not{p}_2+m_e) -$$
$$-\frac{e^{+i\mathbf{p}_1(\mathbf{x}_1-\mathbf{x}_2)}e^{-i\mathbf{p}_2\mathbf{x}_2}}{(\omega_1+\tilde{E}_a-m_e+E_1)(\omega_1+\omega_2+\tilde{E}_a-m_e-E_2)}\cdot(+\not{p}_1+m_e)\gamma^\beta(-\not{p}_2+m_e) +$$
$$+\frac{e^{+i\mathbf{p}_1(\mathbf{x}_1-\mathbf{x}_2)}e^{+i\mathbf{p}_2\mathbf{x}_2}}{(\omega_1+\tilde{E}_a-m_e+E_1)(\omega_1+\omega_2+\tilde{E}_a-m_e+E_2)}\cdot(+\not{p}_1+m_e)\gamma^\beta(+\not{p}_2+m_e). \quad (4.107)$$

The analogous expression for diagram B is given by

$$\langle A'|S_B^{(4)}|A\rangle = +\frac{i\alpha G_F^2 g_A^2 m_{ee} M^{0\nu}}{2^{11}\pi^6 V R\sqrt{\omega_1\omega_2}}\delta(\omega_1+\omega_2-\tilde{Q})\epsilon_\alpha^*(\mathbf{k}_1)\epsilon_\beta^*(\mathbf{k}_2)\int d^3x_1 d^3x_4 \frac{d^3p_1}{E_1}\frac{d^3p_2}{E_2}\cdot$$
$$\cdot e^{i\mathbf{k}_1\mathbf{x}_1}e^{i\mathbf{k}_2\mathbf{x}_4}\cdot e_B^T(\mathbf{x}_1,\tilde{E}_a)C\gamma^\alpha\Gamma_B\gamma^\beta e_B(\mathbf{x}_4,\tilde{E}_b) + (\text{rest}), \quad (4.108)$$

with

$$\Gamma_B \equiv \frac{e^{-i\mathbf{p}_1\mathbf{x}_1}e^{+i\mathbf{p}_2\mathbf{x}_4}}{(\omega_1+\tilde{E}_a-m_e-E_1)(m_e-\omega_2-\tilde{E}_b-E_2)}\left[\not{p}_1P_L\not{p}_2 - m_e(\not{p}_1P_L+P_L\not{p}_2)+m_e^2P_L\right] +$$
$$+\frac{e^{-i\mathbf{p}_1\mathbf{x}_1}e^{-i\mathbf{p}_2\mathbf{x}_4}}{(\omega_1+\tilde{E}_a-m_e-E_1)(\omega_2+\tilde{E}_b-m_e-E_2)}\left[-\not{p}_1P_L\not{p}_2 + m_e(\not{p}_1P_L-P_L\not{p}_2)+m_e^2P_L\right] +$$
$$+\frac{e^{+i\mathbf{p}_1\mathbf{x}_1}e^{+i\mathbf{p}_2\mathbf{x}_4}}{(m_e-\omega_1-\tilde{E}_a-E_1)(m_e-\omega_2-\tilde{E}_b-E_2)}\left[-\not{p}_1P_L\not{p}_2 + m_e(-\not{p}_1P_L+P_L\not{p}_2)+m_e^2P_L\right] +$$
$$+\frac{e^{+i\mathbf{p}_1\mathbf{x}_1}e^{-i\mathbf{p}_2\mathbf{x}_4}}{(m_e-\omega_1-\tilde{E}_a-E_1)(\omega_2+\tilde{E}_b-m_e-E_2)}\left[\not{p}_1P_L\not{p}_2 + m_e(\not{p}_1P_L+P_L\not{p}_2)+m_e^2P_L\right] \quad (4.109)$$

As already argued, we now make use of the long wavelength approximation,

$$e^{+i\mathbf{k}_1\mathbf{x}_1} \approx e^{+i\mathbf{k}_2\mathbf{x}_{2,4}} \approx 1. \quad (4.110)$$

4.5.2 The low Q region for diagram A

Let us first apply Eq. (4.110) to Eqs. (4.106) and (4.107). The first point to realize is that the integration over $\mathbf{x}_2$ is actually trivial and leads to a δ-function $\delta(\mathbf{p}_2 \pm \mathbf{p}_1)$. We can further use the substitution $\mathbf{p}_1 \to -\mathbf{p}_1$ in the third and fourth line of Eq. (4.107) to obtain a common factor $e^{-i\mathbf{p}_1\mathbf{x}_1}$. Defining

$$A(\omega_1,\tilde{E}_a) \equiv \omega_1+\tilde{E}_a-m_e \text{ and } B(\omega_1,\omega_2,\tilde{E}_a) \equiv \omega_2 + A(\omega_1,\tilde{E}_a) \quad (4.111)$$

we arrive a the following integral:

$$\int d^3p_1 \frac{e^{-i\mathbf{p}_1\mathbf{x}_1}}{(A^2-E_1^2)(B^2-E_1^2)} e_B^T(\mathbf{x}_1,\tilde{E}_a)C\gamma^\alpha(-A\gamma^0+\mathbf{p}_1\boldsymbol{\gamma}+m_e)\gamma^\beta(-B\gamma^0+\mathbf{p}_1\boldsymbol{\gamma}+m_e)P_L e_B(0,\tilde{E}_b). \quad (4.112)$$

This integral will again split into different parts, just as the ones in Secs. 4.4.4 and 4.4.5. Let us first discuss the parts that will vanish in the integration. From Eq. (4.112), we can get a contribution which is proportional to $(\mathbf{p}_1\boldsymbol{\gamma})\gamma^\beta(\mathbf{p}_1\boldsymbol{\gamma})$, which can also be written as $2\delta^{\beta i}(\mathbf{p}_1)_i(\mathbf{p}_1\boldsymbol{\gamma}) + (\mathbf{p}_1)^2\gamma^\beta$. Exactly as in Eq. (4.58), we can trade the factor $\mathbf{p}_1$ for a $i\boldsymbol{\nabla}_{x_1}$ in front of the integral.

Since there is one more factor with directional information (which will be proportional to $\mathbf{k}_1$ (or $\mathbf{k}_2$) in the end) included in this term, it will give a subdominant contribution after the phase-space integration (as the functions in Eq. (4.100) in the long wavelength approximation), and we skip it here. What remains is the effective replacement $(\mathbf{p}_1\boldsymbol{\gamma})\gamma^\beta(\mathbf{p}_1\boldsymbol{\gamma}) \to (\mathbf{p}_1)^2\gamma^\beta$. The terms in Eq. (4.112) which are proportional to $\mathbf{p}_1$ will cancel out in the integration. Effectively, we can set

$$(-A\gamma^0 + \mathbf{p}_1\boldsymbol{\gamma} + m_e)\gamma^\beta(-B\gamma^0 + \mathbf{p}_1\boldsymbol{\gamma} + m_e) \to (-A\gamma^0 + m_e)\gamma^\beta(-B\gamma^0 + m_e) + p_1^2\gamma^\beta, \quad (4.113)$$

and remain with two types of integrals,

$$I_1(x_1) \equiv \int d^3p_1 \frac{e^{-i\mathbf{p}_1\mathbf{x}_1}}{(A^2 - E_1^2)(B^2 - E_1^2)} \text{ and } I_2(x_1) \equiv \int d^3p_1 \frac{p_1^2 e^{-i\mathbf{p}_1\mathbf{x}_1}}{(A^2 - E_1^2)(B^2 - E_1^2)}. \quad (4.114)$$

In either case, the integration is quite similar to the one leading from Eq. (4.53) to Eq. (4.55). Defining the two quantities

$$\tilde{A}^2 \equiv m_e^2 - A^2 \text{ and } \tilde{B}^2 \equiv m_e^2 - B^2, \quad (4.115)$$

which are both positive in the low $\tilde{Q}$ region, we have the four poles $\pm i\tilde{A}$ and $\pm i\tilde{B}$, from which only the ones above the real axis are relevant. Applying the residue theorem leads to

$$I_1(x_1) = \frac{-i\pi}{x_1(A^2 - B^2)}\left(e^{-\tilde{B}x_1} - e^{-\tilde{A}x_1}\right) \text{ and } I_2(x_1) = \frac{+i\pi}{x_1(A^2 - B^2)}\left(\tilde{B}^2 e^{-\tilde{B}x_1} - \tilde{A}^2 e^{-\tilde{A}x_1}\right). \quad (4.116)$$

Using Eq. (4.63), we can define the following two functions:

$$f_{1,2}^a(\omega_1, \omega_2) \equiv 4\pi C_a \int_{x_1=0}^{\infty} dx_1 x_1^2 I_{1,2}(x_1) R_a(x_1). \quad (4.117)$$

Just as in Sec. 4.4.4, these functions can be calculated analytically if one uses the Schrödinger wave functions from Tab. 4.2 as approximation, which results in

$$\begin{aligned}
f_1^{1s}(\omega_1, \omega_2) &= \frac{8i(\tilde{A} - \tilde{B})\pi^2(aZ)^{3/2}\left(a(\tilde{A} + \tilde{B}) + 2Z\right)}{(A^2 - B^2)(a\tilde{A} + Z)^2(a\tilde{B} + Z)^2}, \\
f_1^{2s}(\omega_1, \omega_2) &= -\frac{8i\sqrt{2a}\pi^2 Z^{3/2}\left[4Z\left(\frac{1}{(2a\tilde{A}+Z)^3} - \frac{1}{(2a\tilde{B}+Z)^3}\right) - \frac{1}{(2a\tilde{A}+Z)^2} + \frac{1}{(2a\tilde{B}+Z)^2}\right]}{B^2 - A^2}, \text{ and} \\
f_1^{2p}(\omega_1, \omega_2) &= -\frac{16i\sqrt{2aZ^5}\pi^2\left(\frac{1}{(2a\tilde{A}+Z)^3} - \frac{1}{(2a\tilde{B}+Z)^3}\right)}{3(A^2 - B^2)},
\end{aligned} \quad (4.118)$$

and also in

$$\begin{aligned}
f_2^{1s}(\omega_1, \omega_2) &= \frac{8i(\tilde{A} - \tilde{B})\pi^2\sqrt{aZ^5}\left(2a\tilde{A}\tilde{B} + (\tilde{A} + \tilde{B})Z\right)}{(A^2 - B^2)(a\tilde{A} + Z)^2(a\tilde{B} + Z)^2}, \\
f_2^{2s}(\omega_1, \omega_2) &= \frac{8i\sqrt{2a}\pi^2 Z^{3/2}\left[\frac{(3Z-2a\tilde{A})\tilde{A}^2}{(2a\tilde{A}+Z)^3} + \frac{\tilde{B}^2(2a\tilde{B}-3Z)}{(2a\tilde{B}+Z)^3}\right]}{B^2 - A^2}, \text{ and} \\
f_2^{2p}(\omega_1, \omega_2) &= \frac{16i\sqrt{2aZ^5}\pi^2\left(\frac{\tilde{A}^2}{(2a\tilde{A}+Z)^3} - \frac{\tilde{B}^2}{(2a\tilde{B}+Z)^3}\right)}{3(A^2 - B^2)}.
\end{aligned} \quad (4.119)$$

To cope with the γ-structure in the amplitude, we can further define

$$\begin{aligned}
g_0^a(\omega_1,\omega_2) &\equiv A(\omega_1,\tilde{E}_a)B(\omega_1,\omega_2,\tilde{E}_a)f_1^a(\omega_1,\omega_2),\\
g_1^a(\omega_1,\omega_2) &\equiv m_e^2 f_1^a(\omega_1,\omega_2) + f_2^a(\omega_1,\omega_2),\\
g_A^a(\omega_1,\omega_2) &\equiv -m_e A(\omega_1,\tilde{E}_a)f_1^a(\omega_1,\omega_2), \text{ and}\\
g_B^a(\omega_1,\omega_2) &\equiv -m_e B(\omega_1,\omega_2,\tilde{E}_a)f_1^a(\omega_1,\omega_2).
\end{aligned} \tag{4.120}$$

This allows us to write Eq. (4.106) as

$$\begin{aligned}
\langle A'|S_A^{(4)}|A\rangle = &-\frac{i\alpha G_F^2 g_A^2 m_{ee} M^{0\nu}}{2^7\pi^3 V R\sqrt{\omega_1\omega_2}}\delta(\omega_1+\omega_2-\tilde{Q})\epsilon_\alpha^*(\mathbf{k}_1)\epsilon_\beta^*(\mathbf{k}_2)\cdot\\
\cdot &C_b R_b(0)\tilde{\Gamma}_a^T C\gamma^\alpha[g_0^a\gamma^0\gamma^\beta\gamma^0 + g_1^a\gamma^\beta + g_A^a\gamma^0\gamma^\beta + g_B^a\gamma^\beta\gamma^0]\tilde{\Gamma}_b + (\text{rest}),
\end{aligned} \tag{4.121}$$

where $\tilde{\Gamma}_a \equiv \gamma^a_{\text{shell}}\Gamma_a$.

The remaining task is to write down the term "(rest)" and we start with the electron anti-symmetrization. Realizing that $\beta = 0$ gives no contribution due to $\epsilon_0^* = 0$, one can effectively anti-commute γ^β and γ^0, which simplifies the γ-structure. We also define

$$h_1^a(\omega_1,\omega_2) \equiv g_1^a(\omega_1,\omega_2) - g_0^a(\omega_1,\omega_2) \text{ and } h_2^a(\omega_1,\omega_2) \equiv g_B^a(\omega_1,\omega_2) - g_A^a(\omega_1,\omega_2). \tag{4.122}$$

The anti-symmetrization can be done as, e.g., in Eq. (4.74). It is again useful to define functions that will later on translate into the form factors. These functions are

$$\begin{aligned}
k_\pm^1(\omega_1,\omega_2) &\equiv C_b R_b(0)h_1^a(\omega_1,\omega_2) \pm C_a R_a(0)h_1^b(\omega_1,\omega_2) \text{ and}\\
k_\pm^2(\omega_1,\omega_2) &\equiv \frac{1}{2}\left(C_b h_2^a(\omega_1,\omega_2) \pm C_a h_2^b(\omega_1,\omega_2)\right).
\end{aligned} \tag{4.123}$$

The final form of the S-matrix element is

$$\begin{aligned}
\langle A'|S_A^{(4)}|A\rangle = &-\frac{i\alpha G_F^2 g_A^2 m_{ee} M^{0\nu}}{2^7\pi^3 V R\sqrt{\omega_1\omega_2}}\delta(\omega_1+\omega_2-\tilde{Q})\epsilon_\alpha^*(\mathbf{k}_1)\epsilon_\beta^*(\mathbf{k}_2)\cdot\\
\cdot\Big[&g^{\alpha\beta}\left(k_+^1\tilde{\Gamma}_a^T C P_L\tilde{\Gamma}_b + \tilde{\Gamma}_a^T C\gamma^0(k_-^2 - k_+^2\gamma_5)\tilde{\Gamma}_b\right) -\\
&-i\left(k_-^1\tilde{\Gamma}_a^T C\sigma^{\alpha\beta}P_L\tilde{\Gamma}_b\right) + \tilde{\Gamma}_a^T C\sigma^{\alpha\beta}\gamma^0(k_+^2 - k_-^2\gamma_5)\tilde{\Gamma}_b\Big] + (k_1\leftrightarrow k_2).
\end{aligned} \tag{4.124}$$

Before we add the photon-exchange term, too, we first revisit diagram B and try to bring the corresponding S-matrix element into a similar form.

4.5.3 The low Q region for diagram B

Let us go back to Eq. (4.108) and bring it to a form similar to the one of $\langle A'|S_A^{(4)}|A\rangle$ in Eq. (4.124). We again start by applying Eq. (4.110) and define

$$A_i^c = \omega_i + \tilde{E}_c - m_e. \tag{4.125}$$

To clean up the γ-structure a bit, it is useful to remark that also in this case all contributions, which are proportional to only $\mathbf{p}_{1,2}$ will vanish, as in the long wavelength approximation in Sec. 4.4.4. Furthermore one can include substitutions $\mathbf{p}_{1,2} \to -\mathbf{p}_{1,2}$ to have a common pre-factor $e^{-i\mathbf{p}_1\mathbf{x}_1}e^{-i\mathbf{p}_2\mathbf{x}_4}$. Doing all that and performing some cumbersome algebra, one finally arrives at an effective expression for Γ_B from Eq. (4.109):

$$\Gamma_B \to \frac{4e^{-i\mathbf{p}_1\mathbf{x}_1}e^{-i\mathbf{p}_2\mathbf{x}_4}}{[(A_1^a)^2 - E_1^2][(A_2^b)^2 - E_2^2]}\left[-E_1E_2A_1^aA_2^bP_R + E_1E_2m_e^2P_L - E_1^2m_eA_2^b\gamma^0P_L + E_2^2m_eA_1^a\gamma^0P_R\right]. \tag{4.126}$$

Starting again with the integration over $\mathbf{p}_{1,2}$, this leads to three different integrals that we have to compute:

$$\left.\begin{matrix} I_3(x,A) \\ I_4(x,A) \\ I_5(x,A) \end{matrix}\right\} \equiv \int \frac{d^3p}{E} \frac{e^{-i\mathbf{px}}}{A^2-E^2} \cdot \left\{\begin{matrix} 1 \\ E \\ E^2 \end{matrix}\right. \tag{4.127}$$

To evaluate these integrals, we use once again the residue theorem. Performing the integration over the angular part first and writing $E^2 = p^2 + m_e^2$, all these integrals have poles at $\pm i\sqrt{m_e^2 - A^2}$, from which only the one above the real axis is relevant. This is, however, not all, since I_3 also has singularities at $\pm im_e$. We can make use of the following theorem: If a complex function $f(z)$ is of the form $\frac{g(z)}{h(z)}$ and $h(z)$ is zero at $z = z_0$, then the corresponding residue is given by

$$\mathrm{res}_{z_0} f(z) = \frac{g(z_0)}{h'(z_0)}. \tag{4.128}$$

Comparing this to Eq. (4.127), we can simply set

$$g(p) = \frac{pe^{+ipx}}{p^2 + (m_e^2 - A^2)} \text{ and } h(p) = \sqrt{m_e^2 + p^2}, \tag{4.129}$$

which leads immediately to $1/h'(+ip) = 0$, so we do not have to care about this pole. Then, the rest of the integration is done easily and we end up with

$$\left.\begin{matrix} I_3(x,A) \\ I_4(x,A) \\ I_5(x,A) \end{matrix}\right\} = \frac{-2\pi^2}{x} e^{-\sqrt{m_e^2 - A^2}x} \cdot \left\{\begin{matrix} 1/A \\ 1 \\ A \end{matrix}\right. \tag{4.130}$$

The integration over the spatial coordinates leads to one more form factor, which can be defined as

$$\phi_a(\omega_i) \equiv 4\pi C_a \int_{x=0}^{\infty} dx\ xR_a(x) e^{-\sqrt{m_e^2 - (A_i^a)^2}x}. \tag{4.131}$$

This can again be calculated analytically for the Schrödinger wave functions from Tab. 4.2 yielding

$$\begin{aligned} \phi_a^{1s}(\omega_i) &= \frac{8\pi\sqrt{aZ^3}}{\left(\sqrt{m_e^2 - (A_i^a)^2}a + Z\right)^2},\ \phi_a^{2s}(\omega_i) = \frac{8\sqrt{2a}\pi\left(2a\sqrt{m_e^2 - (A_i^a)^2} - 3Z\right)Z^{3/2}}{\left(2\sqrt{m_e^2 - (A_i^a)^2}a + Z\right)^3}, \text{ and} \\ \phi_a^{2p}(\omega_i) &= \frac{16\pi\sqrt{2aZ^5}}{3\left(2\sqrt{m_e^2 - (A_i^a)^2}a + Z\right)^3}. \end{aligned} \tag{4.132}$$

Using two more abbreviations,

$$M_\pm^{ab}(\omega_1,\omega_2) \equiv \frac{1}{2}\left(m_e^2 \pm A_1^a A_2^b\right) \text{ and } N_\pm^{ba}(\omega_1,\omega_2) \equiv \frac{m_e}{2}(A_2^b \pm A_1^a), \tag{4.133}$$

we can write down Eq. (4.108) as

$$\begin{aligned} \langle A'|S_B^{(4)}|A\rangle = &+\frac{i\alpha G_F^2 g_A^2 m_{ee} M^{0\nu}}{2^9\pi^3 V R\sqrt{\omega_1\omega_2}} \delta(\omega_1 + \omega_2 - \tilde{Q})\epsilon_\alpha^*(\mathbf{k}_1)\epsilon_\beta^*(\mathbf{k}_2)\phi_a(\omega_1)\phi_b(\omega_2) \cdot \\ &\cdot\tilde{\Gamma}_a^T C\gamma^\alpha\gamma^\beta\left[M_-^{ab} + M_+^{ab}\gamma_5 - N_-^{ba}\gamma^0 + N_+^{ba}\gamma^0\gamma_5\right]\tilde{\Gamma}_b + (\text{rest}). \end{aligned} \tag{4.134}$$

Using Eqs. (4.13) and (4.15) allows us to write $\gamma^\alpha\gamma^\beta = g^{\alpha\beta} - i\sigma^{\alpha\beta}$, which makes it possible to decompose Eq. (4.134) into parts which are symmetric and anti-symmetric under the exchange

of the Lorentz indices α and β. This renders the calculation of the electron exchange term trivial. Abbreviating

$$\begin{aligned}
l^1_\pm(\omega_1,\omega_2) &\equiv \phi_a(\omega_1)\phi_b(\omega_2)M^{ab}_- \pm \phi_b(\omega_1)\phi_a(\omega_2)M^{ba}_-,\\
l^2_\pm(\omega_1,\omega_2) &\equiv \phi_a(\omega_1)\phi_b(\omega_2)M^{ab}_+ \pm \phi_b(\omega_1)\phi_a(\omega_2)M^{ba}_+,\\
l^3_\pm(\omega_1,\omega_2) &\equiv \phi_b(\omega_1)\phi_a(\omega_2)N^{ab}_- \pm \phi_a(\omega_1)\phi_b(\omega_2)N^{ba}_-, \text{ and}\\
l^4_\pm(\omega_1,\omega_2) &\equiv \phi_b(\omega_1)\phi_a(\omega_2)N^{ab}_+ \pm \phi_a(\omega_1)\phi_b(\omega_2)N^{ba}_+,
\end{aligned} \tag{4.135}$$

one can write

$$\begin{aligned}
\langle A'|S^{(4)}_B|A\rangle = &+\frac{i\alpha G_F^2 g_A^2 m_{ee} M^{0\nu}}{2^9\pi^3 V R\sqrt{\omega_1\omega_2}}\delta(\omega_1+\omega_2-\tilde{Q})\epsilon^*_\alpha(\mathbf{k}_1)\epsilon^*_\beta(\mathbf{k}_2)\cdot\\
&\cdot\Big[g^{\alpha\beta}\tilde{\Gamma}^T_a C(l^1_- + l^2_-\gamma_5)\tilde{\Gamma}_b - i\tilde{\Gamma}^T_a C\sigma^{\alpha\beta}(l^1_+ + l^2_+\gamma_5)\tilde{\Gamma}_b +\\
&+g^{\alpha\beta}\tilde{\Gamma}^T_a C\gamma^0(l^3_- + l^4_-\gamma_5)\tilde{\Gamma}_b + i\tilde{\Gamma}^T_a C\sigma^{\alpha\beta}\gamma^0(l^3_+ + l^4_+\gamma_5)\tilde{\Gamma}_b\Big] + (k_1\leftrightarrow k_2).
\end{aligned} \tag{4.136}$$

4.5.4 The final form of the decay rate

Finally, we have to calculate the total amplitude from Eqs. (4.124) and (4.136). The total S-matrix element is given by

$$\langle A'|S^{(4)}|A\rangle = \langle A'|S^{(4)}_A|A\rangle + \langle A'|S^{(4)}_B|A\rangle, \tag{4.137}$$

since both amplitudes lead to the same final state (cf. Secs. 3.4, 3.5, and 3.6). To write everything with one constant factor in front, it is useful to define

$$\begin{aligned}
&r_1(\omega_1,\omega_2) \equiv -k^1_+(\omega_1,\omega_2) + \frac{1}{2}l^1_-(\omega_1,\omega_2),\ r_2(\omega_1,\omega_2) \equiv k^1_+(\omega_1,\omega_2) + \frac{1}{2}l^2_-(\omega_1,\omega_2),\\
&r_3(\omega_1,\omega_2) \equiv 2k^2_+(\omega_1,\omega_2) - \frac{1}{2}l^1_+(\omega_1,\omega_2),\ r_4(\omega_1,\omega_2) \equiv -2k^2_-(\omega_1,\omega_2) - \frac{1}{2}l^2_+(\omega_1,\omega_2),\\
&r_5(\omega_1,\omega_2) \equiv -2k^2_-(\omega_1,\omega_2) + \frac{1}{2}l^3_-(\omega_1,\omega_2),\ r_6(\omega_1,\omega_2) \equiv 2k^2_+(\omega_1,\omega_2) + \frac{1}{2}l^4_+(\omega_1,\omega_2),\\
&r_7(\omega_1,\omega_2) \equiv 2k^2_+(\omega_1,\omega_2) + \frac{1}{2}l^3_+(\omega_1,\omega_2), \text{ and } r_8(\omega_1,\omega_2) \equiv -2k^2_-(\omega_1,\omega_2) + \frac{1}{2}l^4_-(\omega_1,\omega_2).
\end{aligned} \tag{4.138}$$

Furthermore, we need to symmetrize (or anti-symmetrize) these functions,

$$r^s_{1,2,5,6}(\omega_1,\omega_2) \equiv r_{1,2,5,6}(\omega_1,\omega_2)+r_{1,2,5,6}(\omega_2,\omega_1),\ r^a_{3,4,7,8}(\omega_1,\omega_2) \equiv r_{3,4,7,8}(\omega_1,\omega_2)-r_{3,4,7,8}(\omega_2,\omega_1), \tag{4.139}$$

in order to write down the final version of the S-matrix element:

$$\begin{aligned}
\langle A'|S^{(4)}|A\rangle = &+\frac{i\alpha G_F^2 g_A^2 m_{ee} M^{0\nu}}{2^8\pi^3 V R\sqrt{\omega_1\omega_2}}\delta(\omega_1+\omega_2-\tilde{Q})\epsilon^*_\alpha(\mathbf{k}_1)\epsilon^*_\beta(\mathbf{k}_2)\cdot\\
&\cdot\Big[g^{\alpha\beta}\tilde{\Gamma}^T_a C(r^s_1 + r^s_2\gamma_5)\tilde{\Gamma}_b + i\tilde{\Gamma}^T_a C\sigma^{\alpha\beta}(r^a_3 + r^a_4\gamma_5)\tilde{\Gamma}_b +\\
&+g^{\alpha\beta}\tilde{\Gamma}^T_a C\gamma^0(r^s_5 + r^s_6\gamma_5)\tilde{\Gamma}_b + i\tilde{\Gamma}^T_a C\sigma^{\alpha\beta}\gamma^0(r^a_7 + r^a_8\gamma_5)\tilde{\Gamma}_b\Big].
\end{aligned} \tag{4.140}$$

The next step is to square this expression and to sum over polarizations. Starting with the summation over the polarizations of the photons, one can immediately see that there are now interference terms between the parts proportional to $g^{\alpha\beta}$ and to $\sigma^{\alpha\beta}$. Using Eq. (4.92) and

taking into account that only the physical photon polarizations can matter in the end (which we have checked explicitly for the 1-photon case in Eq. (4.94)), we arrive at

$$|\langle A'|S^{(4)}|A\rangle|^2 \to |\tilde{C}|^2 \frac{T}{2\pi}\delta(\omega_1+\omega_2-\tilde{Q})2[|\Gamma_1|^2+|\Gamma_2^{12}|^2], \tag{4.141}$$

where $\tilde{C} \equiv \frac{\alpha G_F^2 g_A^2 m_{ee} M^{0\nu}}{2^8\pi^3 V R\sqrt{\omega_1\omega_2}}$,

$$\begin{aligned}\Gamma_1 &\equiv \tilde{\Gamma}_a^T C(r_1^s + r_2^s\gamma_5)\tilde{\Gamma}_b + \tilde{\Gamma}_a^T C\gamma^0(r_5^s + r_6^s\gamma_5)\tilde{\Gamma}_b, \text{ and}\\ \Gamma_2^{12} &\equiv \tilde{\Gamma}_a^T C\sigma^{12}(r_3^a + r_4^a\gamma_5)\tilde{\Gamma}_b + \tilde{\Gamma}_a^T C\sigma^{12}\gamma^0(r_7^a + r_8^a\gamma_5)\tilde{\Gamma}_b\Big].\end{aligned} \tag{4.142}$$

We still have to sum over the electron polarizations in Eq. (4.141). Using $\Gamma_a^* = \Gamma_a$, this will always lead to the expression

$$\sum_{s=\pm 1/2}\Gamma_s\Gamma_s^T = \frac{1}{2}\cdot\left[\begin{pmatrix}1&0&1&0\\0&0&0&0\\1&0&1&0\\0&0&0&0\end{pmatrix}+\begin{pmatrix}0&0&0&0\\0&1&0&1\\0&0&0&0\\0&1&0&1\end{pmatrix}\right] = \frac{1}{2}(1+\gamma^0), \tag{4.143}$$

where we have used Eqs. (4.82) and (4.65). Doing this explicitly for Γ_1, one arrives at

$$|\Gamma_1|^2 \to \frac{1}{4}\cdot\left(-T^1+T^2-T^3+T^4\right), \tag{4.144}$$

where

$$\begin{aligned}T^1 &\equiv \mathrm{Tr}\left[(1+\gamma^0)(\gamma^a_{\text{shell}})^T C(r_1^s+r_2^s\gamma_5)\gamma^b_{\text{shell}}(1+\gamma^0)(\gamma^b_{\text{shell}})^T C(r_1^{s*}+r_2^{s*}\gamma_5)\gamma^a_{\text{shell}}\right],\\ T^2 &\equiv \mathrm{Tr}\left[(1+\gamma^0)(\gamma^a_{\text{shell}})^T C(r_1^s+r_2^s\gamma_5)\gamma^b_{\text{shell}}(1+\gamma^0)(\gamma^b_{\text{shell}})^T C(r_5^{s*}-r_6^{s*}\gamma_5)\gamma^a_{\text{shell}}\right],\\ T^3 &\equiv \mathrm{Tr}\left[(1+\gamma^0)(\gamma^a_{\text{shell}})^T C(r_5^s+r_6^s\gamma_5)\gamma^b_{\text{shell}}(1+\gamma^0)(\gamma^b_{\text{shell}})^T C(r_1^{s*}+r_2^{s*}\gamma_5)\gamma^a_{\text{shell}}\right], \text{and}\\ T^4 &\equiv \mathrm{Tr}\left[(1+\gamma^0)(\gamma^a_{\text{shell}})^T C(r_5^s+r_6^s\gamma_5)\gamma^b_{\text{shell}}(1+\gamma^0)(\gamma^b_{\text{shell}})^T C(r_5^{s*}-r_6^{s*}\gamma_5)\gamma^a_{\text{shell}}\right].\end{aligned} \tag{4.145}$$

The other contribution is given by

$$|\Gamma_2^{12}|^2 \to \frac{1}{4}\cdot\left(T^5+T^6-T^7-T^8\right), \tag{4.146}$$

where

$$\begin{aligned}T^5 &\equiv \mathrm{Tr}\left[(1+\gamma^0)(\gamma^a_{\text{shell}})^T\gamma^0\gamma^1(r_3^a+r_4^a\gamma_5)\gamma^b_{\text{shell}}(1+\gamma^0)(\gamma^b_{\text{shell}})^T C(r_3^{a*}+r_4^{a*}\gamma_5)\gamma^a_{\text{shell}}\right],\\ T^6 &\equiv \mathrm{Tr}\left[(1+\gamma^0)(\gamma^a_{\text{shell}})^T\gamma^0\gamma^1(r_3^a+r_4^a\gamma_5)\gamma^b_{\text{shell}}(1+\gamma^0)(\gamma^b_{\text{shell}})^T C(r_7^{a*}-r_8^{a*}\gamma_5)\gamma^a_{\text{shell}}\right],\\ T^7 &\equiv \mathrm{Tr}\left[(1+\gamma^0)(\gamma^a_{\text{shell}})^T\gamma^0\gamma^1(r_7^a+r_8^a\gamma_5)\gamma^b_{\text{shell}}(1+\gamma^0)(\gamma^b_{\text{shell}})^T C(r_3^{a*}+r_4^{a*}\gamma_5)\gamma^a_{\text{shell}}\right], \text{and}\\ T^8 &\equiv \mathrm{Tr}\left[(1+\gamma^0)(\gamma^a_{\text{shell}})^T\gamma^0\gamma^1(r_7^a+r_8^a\gamma_5)\gamma^b_{\text{shell}}(1+\gamma^0)(\gamma^b_{\text{shell}})^T C(r_7^{a*}-r_8^{a*}\gamma_5)\gamma^a_{\text{shell}}\right].\end{aligned}$$

We can capture the two electrons either both from s-shells ($\gamma^{a,b}_{\text{shell}} = \mathbb{1}$), both from the $2p$-shell ($\gamma^{a,b}_{\text{shell}} = -\gamma^3$), or one from an s-shell and one from a p-shell ($\gamma^a_{\text{shell}} = \mathbb{1}$ and $\gamma^b_{\text{shell}} = -\gamma^3$, or vice versa, which leads to the same result).

Let us do this calculation explicitly for one example, namely for T^1 in case of capturing two s-electrons. Then, $\gamma^{a,b}_{\text{shell}} = \mathbb{1}$ leads from Eq. (4.145) to

$$T^1 = \mathrm{Tr}[(1+\gamma^0)C(r_1^s+r_2^s\gamma_5)(1+\gamma^0)C(r_1^{s*}+r_2^{s*}\gamma_5)]. \tag{4.147}$$

Since $C(r_1^s + r_2^s\gamma_5)$ and $C(r_1^{s*} + r_2^{s*}\gamma_5)$ contain an even number of γ-matrices, only the contributions with both factors 1 or with both γ^0 will survive,

$$T^1 = \mathrm{Tr}[C(r_1^s + r_2^s\gamma_5)C(r_1^{s*} + r_2^{s*}\gamma_5)] + \mathrm{Tr}[\gamma^0 C(r_1^s + r_2^s\gamma_5)\gamma^0 C(r_1^{s*} + r_2^{s*}\gamma_5)]. \tag{4.148}$$

Bringing all γ^0 to the left in the second trace gives a minus sign when anti-commuting with γ_5 or C and nothing else, since $(\gamma^0)^2 = \mathbb{1}$. All C's can also be brought to the left and be eliminated using $C^2 = -\mathbb{1}$. $\mathrm{Tr}(\gamma_5) = 0$ and $(\gamma_5)^2 = \mathbb{1}$ then yields

$$T^1 = -\mathrm{Tr}[(|r_1^s|^2 + |r_2^s|^2)\mathbb{1}] + \mathrm{Tr}[(|r_1^s|^2 - |r_2^s|^2)\mathbb{1}] = -8|r_2^s|^2. \tag{4.149}$$

Computing the remaining traces for all cases can be done in a long but finite time-interval, and the result is

$$|\Gamma_1|^2 \to \begin{Bmatrix} 2|r_2^s - r_6^s|^2 \\ 2|r_1^s - r_5^s|^2 \\ 2|r_2^s + r_6^s|^2 \end{Bmatrix} \text{ and } |\Gamma_2^{12}|^2 \to \begin{Bmatrix} 2|r_4^a - r_8^a|^2 \\ 2|r_3^a - r_7^a|^2 \\ 2|r_4^a + r_8^a|^2 \end{Bmatrix} \text{ for capture of } \begin{Bmatrix} 2\times s \\ s\ \&\ p \\ 2\times p \end{Bmatrix} \tag{4.150}$$

This allows us to define the final form factor for $ECEC\gamma\gamma$, which is given by

$$|F_{ab}(\omega_1,\omega_2)|^2 \equiv \begin{cases} |r_2^s(\omega_1,\omega_2) - r_6^s(\omega_1,\omega_2)|^2 + |r_4^a(\omega_1,\omega_2) - r_8^a(\omega_1,\omega_2)|^2 \text{ for } 2\times s \\ |r_1^s(\omega_1,\omega_2) - r_5^s(\omega_1,\omega_2)|^2 + |r_3^a(\omega_1,\omega_2) - r_7^a(\omega_1,\omega_2)|^2 \text{ for } s\ \&\ p \\ |r_2^s(\omega_1,\omega_2) + r_6^s(\omega_1,\omega_2)|^2 + |r_4^a(\omega_1,\omega_2) + r_8^a(\omega_1,\omega_2)|^2 \text{ for } 2\times p \end{cases} \tag{4.151}$$

Finally, we can again make use of Fermi's Golden Rule,

$$\Gamma = \frac{2\pi}{T}\left(\frac{V}{(2\pi)^3}\right)^2 \int d^3k_1 d^3k_2\ |\mathcal{M}|^2 \frac{T}{2\pi}\delta(\omega_1 + \omega_2 - \tilde{Q})\Big|_{\omega_1+\omega_2\le\tilde{Q}}. \tag{4.152}$$

The final result for the decay rate is

$$\Gamma_{ab} = \frac{\alpha^2 G_F^4 g_A^4}{2^{16}\pi^{10}R^2}|m_{ee}|^2|M^{0\nu}|^2 \int_{\omega_1=0}^{\tilde{Q}} d\omega_1\ \omega_1(\tilde{Q} - \omega_1)|F_{ab}(\omega_1, \tilde{Q} - \omega_1)|^2, \tag{4.153}$$

where the remaining integral has to be calculated numerically. The dependence of the integrand on ω_1 is plotted exemplary in Fig. 4.14 for all s-wave contributions of Ca-40. Also there it is clearly visible that the Schrödinger bound electron wave functions indeed reproduce the qualitative form of the Dirac waves, whereas the numerical values differ.

4.5.5 The numerical results and the ratio to the 1-photon case

Finally, we can also perform a numerical analysis of Eq. (4.153) for the Schrödinger and the Dirac case. As input we again use the values from Tab. 4.3. The resulting half-lives in years are given in Tab. 4.7. These numbers are also not very promising, as expected. As already discussed, we expect the long wavelength approximation to work very well for Ca-40, Gd-152, Er-164, and W-180. For Ar-36, Cd-108, and Dy-158, it should at least be okay to use it, which is why we have written these values in parantheses. It can be seen clearly from the table, that a very low Q-value is disadvantageous. This is partially because some captures involving $1s$-electrons might be forbidden energetically (e.g., capture of both $1s$-electrons is forbidden for Gd-152), but partially also because the phase space dependence should favor two photons for a larger Q-value, which will, however, be considerably more difficult to calculate.

In Tab. 4.8, we also give the ratios of the rates for $ECEC\gamma\gamma$ to the ones for $ECEC\gamma$. Note that we have always used the exact calculation (without the long wavelength approximation)

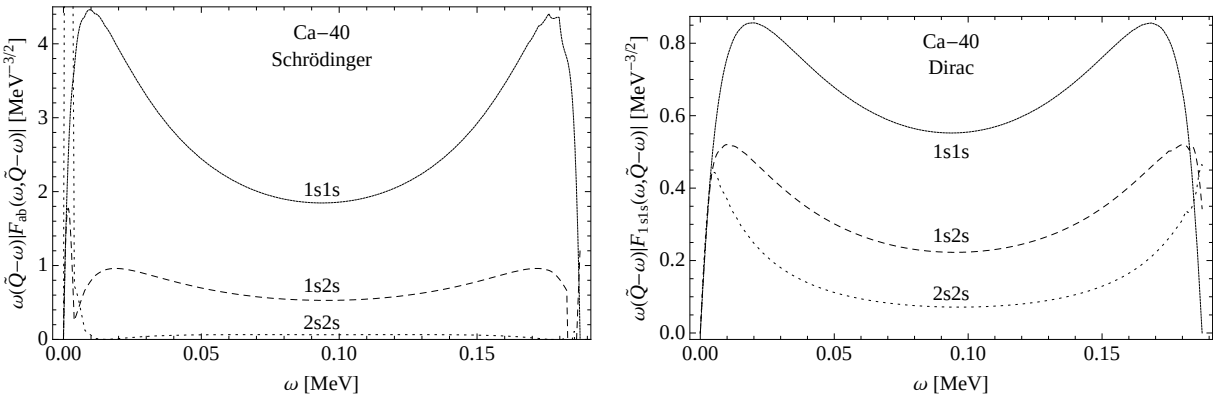

Figure 4.14: The actual dependence of the integrand in Eq. (4.153) for the s-electron contributions. Again, the form of two results is very similar if one compares the Schrödinger to the Dirac case, while the numerical values differ.

Element	Q [MeV]	Schrödinger	Dirac
Ar-36	0.434	(3.96^{36})	(1.08^{37})
Ca-40	0.194	3.09^{37}	9.53^{37}
Cd-108	0.269	(1.11^{37})	(3.63^{37})
Gd-152	0.056	1.09^{39}	3.01^{40}
Dy-158	0.283	(1.24^{37})	(3.19^{37})
Er-164	0.024	2.37^{40}	6.25^{43}
W-180	0.146	1.17^{38}	5.39^{38}

Table 4.7: The half-lives for $ECEC\gamma\gamma$ in the long wavelength approximation (modulo their dependence on the nuclear matrix elements). For those elements for which we expect the approximation to work just as an estimation, we have written the results in brackets.

for $ECEC\gamma$, because for that process this approximation is already expected to break down for $\tilde{Q} \approx 0.25$ MeV, while it should be useful also for slightly larger Q-values in the case of $ECEC\gamma\gamma$. One general tendency is that (at least in the low Q region), the ratio is larger for small Z. This is because of Eq. (4.42): For smaller Z, the capture of two electrons from the $1s$-shell is not yet energetically disfavored, while for larger Z the corrected Q-value $\tilde{Q}$ is small enough to suppress the rate for the two-photon process. Except for Ar-36 the emission of one photon is, however, always dominant by far. This might change considerably as soon as we go to larger Q-values, where we can expect $ECEC\gamma\gamma$ to win because of the stronger $\tilde{Q}$-dependence. A further observation is that this ratio is in most cases very similar, no matter if we use the Schrödinger or the Dirac wave functions. This is one more sign that uncertainties should tend to cancel out in this ratio, as already discussed for the uncertainties in the NME (cf. Sec. 4.3). Note that this ratio is also independent of G_F, g_A, R, and $|m_{ee}|$ (cf. Eqs. (4.96) and (4.153)).

Summing up, one can say that at least for some isotopes, it can be the case that the emission of two photons is advantageous compared to the 1-photon process. This is encouraging for further investigations, which might be especially interesting for higher Q-values which have, however, to be treated in a more advanced way in what regards the bound electron wave functions.

4.5.6 Comments on the experimental situation

The question if the process with emission of one or two photons dominates might be an important one from the experimental point of view, even if it may never be actually observed. Let

Element	Schrödinger	Dirac
Ar-36	10.1	10.3
Ca-40	0.078	0.068
Cd-108	0.0011	0.00033
Gd-152	$2.9 \cdot 10^{-7}$	$2.2 \cdot 10^{-6}$
Dy-158	$1.2 \cdot 10^{-4}$	$3.0 \cdot 10^{-5}$
Er-164	$4.7 \cdot 10^{-7}$	$3.7 \cdot 10^{-9}$
W-180	$1.2 \cdot 10^{-6}$	$5.4 \cdot 10^{-7}$

Table 4.8: The ratios of the rate for $ECEC\gamma\gamma$ to the rate for $ECEC\gamma$. As argued in Sec. 4.3, this ratio should be independent of the NME. Furthermore, the dependences on G_F, g_A, R, and $|m_{ee}|$ cancel out, and hence this ratio is also independent of uncertainties related to those quantities (the most dramatic of which arise from $|m_{ee}|$). Note that for $ECEC\gamma$, we have always used the exact calculation (without long wavelength approximation), since the approximation is expected to break down for even lower Q-values in that case.

us briefly discuss a recent measurement on the half-life of Ar-36 with respect to neutrino-less double electron capture [116, 117]. In this measurement, no photon has been seen above the background in the region of interest. The limit that has been obtained is

$$T_{1/2}(0^+ \to 0^+)\big|_{1\gamma} \geq 1.85 \cdot 10^{18} \text{ y at 68\% C.L.} \tag{4.154}$$

This limit is directly proportional to the full energy peak detection efficiency ϵ, which is, at the position of the peak, equal to 0.26%.

Let us do an easy estimation of the limit that could be obtained for the dominance of the 2γ-process. According to Tab. 4.8, this mode is indeed dominant by a factor of about 10. We will assume here for simplicity that this is the only possible decay mode. If ϵ is the probability to see a photon, the probability to miss it is $(1-\epsilon)$. For dominance of the 2γ-mode, the probability to see one photon is even a bit higher, because of the lower photon energy [116], but let us assume for simplicity that it is still equal to ϵ. Then, the probability to see anything if two photons are emitted is given by $2\epsilon(1-\epsilon)+\epsilon^2 \approx 2\epsilon$ instead of ϵ. This would increase the limit from Eq. (4.154) by a factor of 2. If the efficiency also increases to ϵ', which is roughly $\frac{3.5}{2.6}\epsilon$, then the increase would even be a factor of roughly 3.

In any case, it will be useful to know the dominant decay mode well. Note, however, that these considerations will change if some other process than the 2-nucleon mechanism dominates the decay rate. Unfortunately, pinning down the exact mechanism will involve measurements for different isotopes and will be a major task in the future research on double β processes [118]. In general, an experimental detection of neutrino-less double electron capture will be very tough (if not impossible), unless some more exotic mechanism is involved that causes the decay (which might well be). Nevertheless, experiments in this direction have been done and are going on (see, for example, Refs. [119–123]), and current best limits for the half-life are around 10^{20} years [124], which may further improve in the next years.

Chapter 5

Lepton Flavour Violation

The last topic that we want to discuss is Lepton Flavour Violation (LFV). The term *flavour* essentially means the generation of a fermion. In the SM, the up-like quarks appear in three flavours, (u, c, t), exactly as the down-like quarks, (d, s, b). The same is true for the charged leptons (e, μ, τ), as well as for the neutrinos $(\nu_e, \nu_\mu, \nu_\tau)$. From the experimental side, it seems to be pretty clear that fermions indeed appear in three generations, whereas from the theory side a reason for that is still lacking [64].

In the neutrino sector, lepton flavour violating processes are well-known and are called *neutrino oscillations* [24], cf. Chapter 2. These transitions like $\nu_e \leftrightarrow \nu_\mu$ can indeed, e.g., transform a state of electron-flavour into one with muon-flavour. So far, so good. The amazing point is that this flavour change does not change the charge of the particle, but rather only its flavour. In the charged current sector, flavour changing processes are well-known [125], but in the neutral current sector, the SM actually does not provide any flavour changing neutral current (FCNC) interaction at tree-level.

Even more amazing, there is actually no deeper reason for that in the SM! The absence of FCNCs is only a so-called *accidental symmetry*: When we take the SM gauge group and particle content and impose constraints like Lorentz or gauge invariance, we automatically end up with flavour conserving neutral currents only. This is also confirmed by experiments: A decay like, e.g., $\mu \to e\gamma$ would be perfectly allowed by energy, momentum, and angular momentum conservation, but nevertheless we have not observed it yet (the current best limit for the branching ratio of this decay compared to ordinary muon decay $\mu^- \to e^- \nu_\mu \overline{\nu}_e$ comes from the past MEGA-experiment [126], and amounts to $\mathrm{Br}(\mu \to e\gamma) < 1.2 \cdot 10^{-11}$). This branching ratio will be probed by the upcoming MEG experiment that is expected to reach a sensitivity of $1.2 \cdot 10^{-13}$ at 90% C.L. and a single event sensitivity of even $3.7 \cdot 10^{-14}$ [127].

Since there is no reason for the absence of LFV, models beyond the SM will generically violate lepton flavour [9]. In the SM with massive neutrinos, one can actually draw a 1-loop diagram for $\mu \to e\gamma$ (cf. Fig. 5.1), but even an optimistic prediction (with rather large values for the neutrino masses) will only lead to a branching ratio of about 10^{-47} [128].[1] In turn, if we can observe LFV in the near future, this will be an unambiguous signal of Physics beyond the Standard Model (BSM) and will be a major discovery.

5.1 The rare decay $\mu \to e\gamma$ and other lepton flavour violating processes

Let us now discuss the diagram in Fig. 5.1 for $\mu \to e\gamma$ a bit closer, before we turn to other LFV-processes. An extensive treatment of this process in the SM with massive neutrinos (and

[1] The reason why this value is so tiny will become clear in a moment.

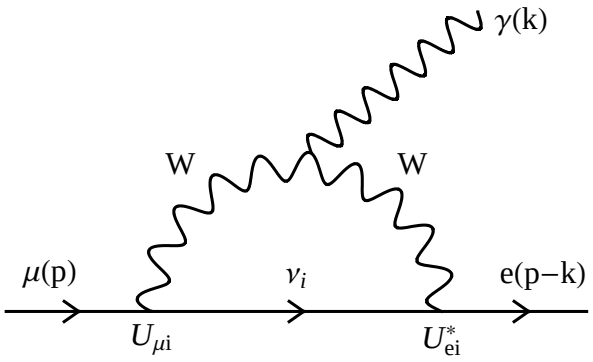

Figure 5.1: The diagram for $\mu \to e\gamma$ in the SM with massive neutrinos. It is a higher order process, which is additionally suppressed by the GIM-mechanism. The flavour violation happens on the neutrino line, since the neutrino mass eigenstates are no flavour eigenstates.

also beyond) can be found in Refs. [128–130]. Furthermore, there exists an excellent paper on the general process $f_1 \to f_2\gamma$ [131], which can also be used, e.g., for the calculation of an electric dipole moment of the neutrino. We will here only mention the most important points in the calculation of $\mu \to e\gamma$.

First, when making a general ansatz for the amplitude, one can immediately see by applying electromagnetic gauge invariance as well as by the properties of a physical photon that the resulting transition amplitude is of magnetic type:

$$\mathcal{M}(\mu \to e\gamma) = \epsilon^*_\mu(\mathbf{k})\overline{e}(p-k)\left[ik_\nu\sigma^{\mu\nu}(A + B\gamma_5)\right]\mu(p), \tag{5.1}$$

with some functions A and B. In the approximation $m_e \approx 0$ (which is always fine for the above process), one additionally obtains $A = B$ and the amplitude can be written as

$$\mathcal{M}(\mu \to e\gamma) = A\overline{e}(p-k)\left[2(p\epsilon) - m_\mu \not{\epsilon}\right]\mu(p), \tag{5.2}$$

where we have used the Gordon decomposition and the Dirac equation. As will become important later, there will always be a chirality flip somewhere on the fermion line.[2]

The most important point in the calculation for the case of the SM with massive neutrinos is that terms of the following form come in:

$$\sum_{i=1}^{3} U^*_{ei}U_{\mu i} f\left(\frac{m_i^2}{M_W^2}\right), \tag{5.3}$$

where $U_{\alpha j}$ are elements of the PMNS-matrix (cf. Eq. (4.4)), m_i is the mass of the virtual neutrino mass eigenstate ν_i, M_W is the W-boson mass, and f is some loop function that arises in the computation. They key point is that in the SM we have $m_i \ll M_W$, and we can hence expand the function f as

$$f\left(\frac{m_i^2}{M_W}\right) = f(0) + f'(0)\cdot\frac{m_i^2}{M_W^2} + ..., \tag{5.4}$$

where the first term is independent of m_i. Then, in Eq. (5.3), this leading term will be killed by the unitarity of the PMNS-matrix U and we end up with a suppressed amplitude. This theorem is commonly known as *Glashow-Iliopoulos-Maiani*- (GIM-) mechanism [132].

[2]This is necessary since the photon carries away one unit of angular momentum.

Note that this logic can also be turned around: By a non-observation of $\mu \to e\gamma$ (and similar processes), one can also obtain limits on the unitarity of the PMNS-matrix [133].

The final result for the decay rate in the SM with massive neutrinos can be written as

$$\Gamma(\mu \to e\gamma) = \frac{m_\mu^3}{8\pi}\left(|A|^2 + |B|^2\right), \text{ with } A = B = \frac{eg^2 m_\mu}{256\pi^2 M_W^2} \cdot \left(\sum_{i=1}^{3} U_{ei}^* U_{\mu i} \frac{m_i^2}{M_W^2}\right). \tag{5.5}$$

Relating this to the muon decay rate for ordinary muon decay,

$$\Gamma(e^- \nu_\mu \overline{\nu}_e) = \frac{m_\mu^5 G_F^2}{192\pi^3}, \tag{5.6}$$

which is essentially equal to the total decay rate of the muon, leads to a branching ratio of

$$\mathrm{Br}(\mu \to e\gamma) = \frac{3\alpha}{32\pi}\left(\sum_{i=1}^{3} U_{ei}^* U_{\mu i} \frac{m_i^2}{M_W^2}\right)^2. \tag{5.7}$$

Of course, there can also be LFV-processes different from $\mu \to e\gamma$. The τ-lepton might undergo similar decays, $\tau \to \mu\gamma$ or $\tau \to e\gamma$, where the current best limits are $\mathrm{Br}(\tau \to \mu\gamma) < 4.5 \cdot 10^{-8}$ at 90% C.L. (BELLE experiment, Ref. [134]) and $\mathrm{Br}(\tau \to e\gamma) < 1.1 \cdot 10^{-7}$ at 90% C.L. (Babar experiment, Ref. [135]), respectively. Further possibilities are, e.g., $\mu^+ \to e^+e^-e^+$ (with $\mathrm{Br}(\mu \to 3e) < 1.0 \cdot 10^{-12}$, SINDRUM experiment, Ref. [136]) or μ-e conversion on nuclei (with $\mathrm{Br}(\mu\mathrm{Ti} \to e\mathrm{Ti}) < 4.3 \cdot 10^{-12}$, SINDRUM II experiment, Ref. [137]). Numerous other processes and limits can be found in Refs. [138] and [139].

5.2 The necessity of general conditions for flavour violation

Up to now, only upper limits for branching ratios of LFV-processes can be given. If one tries to parameterize the bounds for their rates using effective field theory, the corresponding numerical coefficients are already quite small [140]. Especially if MEG does not observe any LFV decay, this will lead to the question whether lepton flavour conservation (at least at the tree- or 1-loop level) needs to be imposed as a general condition on extensions of the SM, too. Therefore it is useful to give such criteria, i.e., to determine sufficient and necessary conditions for the conservation of lepton flavour in a general theory which incorporates the SM. By giving necessary conditions for lepton flavour conservation, the results can also be applied if MEG does in fact observe lepton flavour violating decays: As lepton flavour violation occurs in many extensions of the SM, no single theory can be considered to be proven by such a result. By applying the criteria developed here, one can determine what is exactly necessary to obtain LFV-processes, and which features a minimal lepton flavour violating extension of the SM has to contain.

The groundbreaking paper on FCNCs has been written by Glashow and Weinberg [141], already in the late 70's. This paper only dealt with flavour violation in the quark sector and of course at that time, it was e.g. not known how many quark flavours indeed exist in our world, or what the exact structure of the weak interaction actually is. Another interesting work on this topic was done by Paschos [142]. A first application of these criteria to leptons has been performed shortly afterwards by Lee and Shrock [143]. In the light of the development of particle physics within the last three decades it is, however, worth reconsidering such criteria for flavour violation in the lepton sector. Here, general conditions necessary in order for LFV not to occur will be given. If these conditions are not fulfilled it will – in general – be possible to have LFV-processes, assuming that there are no accidental cancellations or further suppressions in the theory. Many of these results are known, or at least often used implicitly. However, a

Particle	$SU(2)_L$	T_3	Y	Q	γ_5-EV
e_L, $\overline{(e_L)^{\mathcal{C}}}$	**2**	$-\frac{1}{2}$	-1	-1	-1
e_R, $\overline{(e_R)^{\mathcal{C}}}$	**1**	0	-2	-1	1
$(e_L)^{\mathcal{C}}$, $\overline{e_L}$	**2**	$\frac{1}{2}$	1	1	1
$(e_R)^{\mathcal{C}}$, $\overline{e_R}$	**1**	0	2	1	-1

Table 5.1: The quantum numbers of the charged leptons. $SU(2)_L$-representation, weak isospin T_3, hypercharge Y, electric charge Q as obtained by $Q = T_3 + \frac{Y}{2}$, and γ_5-eigenvalue.

concise overview of these criteria and their consistent application to different extensions of the SM has not been given until recently [9].

We will only investigate renormalizable interactions and not consider higher-dimensional operators, since in a non-renormalizable theory explicit lepton flavour violating operators, such as

$$\frac{1}{\Lambda^2}(\overline{\mu}e)(\overline{e}e), \tag{5.8}$$

where Λ is the energy scale at which lepton flavour is violated, can simply be added to the Lagrangian. In addition to the general criteria, we will investigate in each section several examples and use our general results to give concrete conditions for the parameters in the respective models. For a better overview, the quantum numbers of the charged leptons are listed in Tab 5.1. A summary table of the results can be found in the Appendix.

5.3 Neutral bosons at tree-level

In general, a neutral current interaction that changes the flavour of a fermion f_i (we here speak of general fermions, as the results of this general section can also be applied to quarks) can be mediated by a neutral scalar or a neutral vector boson that couples to a fermion f_i as well as to a fermion f_j with a different flavour index $j \neq i$. Writing down the most general Lagrangians for both cases, the scalar interaction looks like

$$\mathcal{L}_{\text{scalar}} = S\overline{f}\left(C_L\mathcal{P}_L + C_R\mathcal{P}_R\right)f + h.c., \tag{5.9}$$

and the vector interaction has the form

$$\mathcal{L}_{\text{vector}} = V_\mu\overline{f}\gamma^\mu\left(C_L\mathcal{P}_L + C_R\mathcal{P}_R\right)f + h.c., \tag{5.10}$$

where $f = (f_1, f_2, ..., f_N)^T$ is a vector and C_L and C_R are numerical coefficients (matrices), all in flavour space, which obviously do not have to be the same as in the scalar case.

A mass term for a general vector of Dirac fermions in an N-dimensional flavour space is given by

$$\mathcal{L}_{\text{Dirac}} = -\overline{f_R}M_D f_L - \overline{f_L}M_D^\dagger f_R, \tag{5.11}$$

where $M_D \in \mathbb{C}^{N\times N}$ is an arbitrary matrix in the $N \times N$ flavour space. Hence, it can be diagonalized by a bi-unitary transformation leading to

$$D_D = \text{diag}(m_1, m_2, ..., m_N) = U_L M_D^\dagger U_R^\dagger = U_R M_D U_L^\dagger, \text{ with } m_i > 0, \tag{5.12}$$

where $U_{L,R}^\dagger = U_{L,R}^{-1}$ and $U_L M_D^\dagger M_D U_L^\dagger = U_R M_D M_D^\dagger U_R^\dagger = D_D^2$. Accordingly, the transformation of f (which in this work will – unless stated differently – be an eigenstate of the respective interaction) to the mass eigenstate f' is given by

$$f_R = U_R f'_R \;\&\; f_L = U_L f'_L. \tag{5.13}$$

Note that in general $U_R \neq U_L$. The mass basis is always the most useful basis to work with, as it is always uniquely defined.

The question is, how the interaction terms Eqs. (5.9) and (5.10) will look like after transforming the interaction eigenstates f into the corresponding mass eigenstates f':

S) S is a neutral scalar by assumption, hence we can define it as real by absorbing any phase in the coupling matrices. In the flavour space vector notation, the scalar interaction as written in Eq. (5.9) can be simplified giving

$$\begin{aligned}\mathcal{L}_{\text{scalar}} &= S\overline{f}\left(C_L\mathcal{P}_L + C_R\mathcal{P}_R\right)f + h.c. = S(\overline{f_R}C_L f_L + \overline{f_L}C_R f_R) + h.c. = \\ &= S\overline{f_R}\underbrace{\left[C_L + C_R^\dagger\right]}_{\equiv C} f_L + h.c. = S\overline{f_R}C f_L + h.c., \end{aligned} \tag{5.14}$$

where C is some matrix in flavour space.

The transformation to mass eigenstates leads to (viewing Ψ as vector in flavour space and keeping in mind that, e.g., γ-matrices that act on spinors and hence on the *components* of Ψ must commute with a matrix U in flavour space, since for such a matrix U they only look like scalars):

$$\begin{aligned}\Psi &= U\Psi', \\ \Psi^{\mathcal{C}} &= U^*\Psi'^{\mathcal{C}}, \\ \overline{\Psi} &= \overline{\Psi'}U^\dagger, \text{ and} \\ \overline{\Psi^{\mathcal{C}}} &= \overline{\Psi'^{\mathcal{C}}}U^T. \end{aligned} \tag{5.15}$$

Then, the scalar interaction looks like:

$$\mathcal{L}_{\text{scalar}} = S\overline{f_R}C f_L + h.c. = S\overline{f'_R}U_R^\dagger C U_L f'_L + h.c. \tag{5.16}$$

Thereby the condition for complete flavour conservation is:

$$U_R^\dagger\left[C_L + C_R^\dagger\right]U_L \stackrel{!}{=} \text{diagonal}. \tag{5.17}$$

This condition can be understood as demanding that the interaction basis is the same as the mass basis. We will refer to such basis identities as *alignment*. For the neutral scalars considered here, C_L and C_R can simultaneously be non-zero. To incorporate this interaction into an SM-invariant Lagrangian, the corresponding neutral scalar needs to be a component of an $SU(2)_L$ doublet with hypercharge $(+1)$ or (-1), i.e., a copy of the SM Higgs boson or its charge conjugate (with the possible difference of a CP phase – e.g. for the A of a two-Higgs doublet model this phase is just (-1)).

V) Here, we discuss a neutral intermediate vector boson which can again be defined as real. If it can only couple to left-handed fermions, it must be the $T_3 = 0$ component of an $SU(2)_L$ triplet, i.e., a (massive) copy of the SM W^0. If it couples to both left- and right-handed charged leptons it must be an $SU(2)$ singlet, and in fact a total singlet under the SM gauge group, i.e., a (massive) copy of the SM B^0. A vector that only couples to right-handed charged leptons is also a total singlet under the SM gauge group, and the fact that it does not couple to left-handed charged leptons needs to be explained in the full BSM theory. The interaction Lagrangian is given by

$$\begin{aligned}\mathcal{L}_{\text{vector}} &= V_\mu\overline{f}\gamma^\mu(C_L\mathcal{P}_L + C_R\mathcal{P}_R)f = V_\mu[\,\overline{f_L}\gamma^\mu C_L f_L + \overline{f_R}\gamma^\mu C_R f_R] = \\ &= V_\mu[\,\overline{f'_L}\gamma^\mu(U_L^\dagger C_L U_L)f'_L + \overline{f'_R}\gamma^\mu(U_R^\dagger C_R U_R)f'_R], \end{aligned} \tag{5.18}$$

where C_L and C_R are necessarily Hermitian. To forbid tree-level flavour change, one can demand

$$\begin{aligned} U_L^\dagger C_L U_L &\stackrel{!}{=} \text{diagonal}, \\ U_R^\dagger C_R U_R &\stackrel{!}{=} \text{diagonal}. \end{aligned} \tag{5.19}$$

A special case arises if both coefficients, C_L and C_R, are proportional to a unit matrix $\mathbb{1}_F$ in flavour space:

$$C_L = c_L \cdot \mathbb{1}_F \;\&\; C_R = c_R \cdot \mathbb{1}_F. \tag{5.20}$$

This is the *flavour universality* condition, as fulfilled, e.g., for the neutral current weak and electromagnetic interactions in the SM. In that case, one gets natural flavour conservation due to the unitarity of the transformation matrices. In case of flavour universality, alignment is automatic, as the identity matrix is the same in all bases. Flavour universality was not an option in the scalar case, as the scalar interaction connects different fermion fields (namely left- and right-handed one, which are, in general, components of different representations of the gauge group).

As the only renormalizable theories of vector bosons are gauge theories [144], in general we need to consider these hypothetical, additional vector bosons as gauge particles corresponding to broken generators of some gauge group. Additional vector bosons transforming as an $SU(2)_L$ triplet must therefore be the gauge bosons of the gauge group which is broken down to $SU(2)_L$ at some high energy scale. The minimal model in which this is possible uses an $SU(2) \times SU(2)$ gauge group, which is then broken down to its diagonal subgroup. This subgroup is then identified with $SU(2)_L$. None of the models we discuss introduce such vector bosons. They are, however, a possible extension of the SM.

Indeed, there are only three kinds of neutral particles which can transmit tree-level LFV:

S) A copy of the SM Higgs boson (or its charge conjugate), with an interaction basis different from the physical mass basis.

Va) A massive copy of the SM photon with flavour non-universal couplings that may or may not discriminate between left- and right-handed particles (which is often called Z').

Vb) A copy of the SM Z boson, which is the gauge boson of a gauge group, that is broken down to $SU(2)_L$.

In the following we discuss the SM and several of its extensions, applying the criteria we have obtained. We do not explicitly mention the cases which are equivalent to the SM case when discussing BSM models. For the discussion, we switch to denoting the involved flavoured fermions by e, as most of the results are only applicable to charged leptons. $e = (e, \mu, \tau)^T$ still denotes a vector in flavour space, whose components are Dirac spinors. $l = (\nu, e)^T$ denotes lepton doublets, whose components are vectors in flavour space with 4-spinors as their respective components.

5.3.1 The Standard Model with massive neutrinos

Standard Model: lepton flavour conservation

As none of the necessary particles is present in the Standard Model of elementary particle physics, we expect no lepton FCNCs at all at tree-level, as we know is the case. To illustrate why this is true and what is exactly "missing" in the SM, we give a short discussion.

The only neutral scalar in the SM is the usual Higgs boson H^0, while for neutral vectors, one has the photon γ, the Z^0 of weak interactions, as well as all the gluons G^a from QCD, but the latter ones do not couple to leptons. Accordingly, the following possibilities remain:

S) The only neutral scalar particle in the Standard Model is the physical Higgs boson H^0. Its interaction Lagrangian looks like [15]

$$\mathcal{L} = -\frac{gH}{2M_W}\sum_i \overline{\Psi}_i m_i \Psi_i, \tag{5.21}$$

which, e.g., for charged leptons becomes

$$\mathcal{L}_H = -\frac{gH}{2M_W}\overline{e}(m_e)e. \tag{5.22}$$

Here, $e = (e, \mu, \tau)^T$ and (m_e) is the mass matrix for the charged leptons. Other combinations, like $\overline{\nu}(m)e$ cannot occur since the physical Higgs in the SM is electrically neutral and hence such terms are forbidden by charge conservation.

Here, the flavour conservation follows trivially: In principle, the mass matrix (m_e) could have non-diagonal elements. However, since we demand to write everything in the mass basis, which is defined in a way that it diagonalizes the mass matrix, the diagonal structure of (m_e) is mandatory. As expected, the Standard Model has no scalar interaction that can cause flavour non-conservation at tree-level.

V) According to Ref. [15], the interactions of SM fermions with the photon or the Z-boson are:

$$\mathcal{L} = -e\sum_i q_i \overline{\Psi}_i \gamma^\mu \Psi_i A_\mu - \frac{g}{2\cos\theta_W}\sum_i \overline{\Psi}_i \gamma^\mu (g_V^i - g_A^i\gamma_5)\Psi_i Z_\mu. \tag{5.23}$$

As usual, q_i is the electrical charge of the fermion i in units of the elementary charge e, A_μ describes the photon field, Z_μ the Z-boson, g is the weak coupling, θ_W the Weinberg angle, and g_V^i and g_A^i are the strength of the vector and axial vector coupling, respectively, that depend on the weak isospin of the corresponding particle.

Considering charged leptons, one can easily see why no flavour changes arise: Since neutral currents are, as their name suggests, neutral, they cannot mix a ν- and an e at one vertex. Now, since all charged leptons have the same weak isospin $t_{3L} = -\frac{1}{2}$, for all of them one gets

$$\begin{aligned} g_V &\equiv g_V^i = t_{3L}(i) - 2q_i \sin^2\theta_W = -\frac{1}{2} + 2\sin^2\theta_W, \\ g_A &\equiv g_A^i = t_{3L}(i) = -\frac{1}{2}. \end{aligned} \tag{5.24}$$

Then the Lagrangians for interaction of fermions Ψ $(= u, d, e)$ with a common electrical charge $Q(\Psi)$ $(= \frac{2}{3}, -\frac{1}{3}, -1)$ with a photon and a Z-boson, respectively, look already diagonal in flavour space:

$$\mathcal{L}_A = -Qe\overline{\Psi}\gamma^\mu \mathbb{1}_F \Psi\, A_\mu, \quad \mathcal{L}_Z = -\frac{g}{2\cos\theta_W}\overline{\Psi}\gamma^\mu (g_V(Q) - g_A(Q)\gamma_5)\mathbb{1}_F\Psi\, Z_\mu. \tag{5.25}$$

Hence, according to Eqs. (5.19), one trivially has no tree-level FCNCs in the SM, as expected.

We have here implicitly retrieved the original Glashow-Weinberg criteria [141]: Criterion 1 (natural conservation of all flavours by neutral currents) and 2 (the same conservation at 1-loop level) can be understood as demanding flavour universality in the electroweak interactions, while criterion 3 (the Higgs coupling conserves all flavours) can be reformulated as demanding automatic alignment in the Yukawa sector, which is guaranteed if all fermions receive their mass from one scalar VEV only.

5.3.2 Multi Higgs Doublet Models

Multi Higgs models: $\forall k : \tilde{C}_k \stackrel{!}{=}$ diagonal

As we have seen, there are no tree-level FCNCs in the SM. The simplest extensions of the SM are those, where we simply add particles to the SM spectrum. Of the three types of particles which can transmit tree-level lepton FCNCs, a copy of the SM Higgs is the easiest one to add, as it does not require an extension of the SM gauge group. If we add an arbitrary amount of copies of the Higgs boson to the SM, our model is called for obvious reasons a Multi Higgs Doublet Model. It is easiest to add only one Higgs boson – this is then referred to as a Two Higgs Doublet Model (THDM) [26].

S) We can in principle add an arbitrary amount n of *additional* Higgs doublets to the SM particle spectrum. These will in general have arbitrary Yukawa couplings to the fermions. The Yukawa Lagrangian for the neutral scalars and charged leptons will therefore be

$$\mathcal{L} = \sum_{k=1}^{2n+1} H_k \overline{e'_R} C_k e'_L + h.c., \tag{5.26}$$

as we have a total of $(2n+2)$ neutral scalar degrees of freedom (including pseudoscalars), one of which is eaten by the Z-boson. One linear combination of all these H_k will have the couplings of the SM Higgs, but this linear combination does not necessarily need to be a mass eigenstate, i.e., it will include several different k. There is in general no basis where all the C_k's are diagonal, so we consider the above Lagrangian to be written in the mass basis of the charged leptons. The condition for absence of tree-level FCNCs is then:

$$C_k \stackrel{!}{=} \text{diagonal}, \tag{5.27}$$

for all but one k in the mass basis. The last matrix is then automatically diagonal, since we know that one linear combination must be diagonal in the mass basis. This condition leads to well-known constraints such as the THDM I and II, where an additional Z_2 symmetry is imposed, as first discussed in Ref. [141]. Our more general condition for the absence of tree-level FCNCs given above can be rephrased in the following way: We write the Lagrangian in its explicitly $SU(2)_L$ invariant form,

$$\mathcal{L} = \sum_{k=1}^{n+1} \overline{e'_R} Y_k l'_L \phi_k + h.c., \tag{5.28}$$

where l'_L is the left-handed lepton $SU(2)_L$ doublet, ϕ_k is a copy of the SM Higgs doublet, and we are in the mass basis of the charged leptons. Then C_k is diagonal for all k if and only if Y_k is diagonal for all k, i.e., all Yukawa matrices are diagonal in the mass basis. In an arbitrary basis this means that, given the structure of one Yukawa matrix Y_k, all other Yukawa matrices are defined, except for their eigenvalues. So, if we want to forbid tree-level FCNCs, the only new parameter in the Yukawa sector compared to the SM is, for each pair of Higgs boson and fermion, the fraction of the fermion's mass which is generated by the Higgs boson's VEV.

In summary one can say that the alignment which occurs automatically in the SM is lost in Multi Higgs models and must be postulated separately to exclude tree-level LFV.

5.3.3 Z'-models

$$\boxed{\underline{Z'\text{-models}}\text{: } U_L^\dagger \epsilon'^{(L)} U_L \stackrel{!}{=} \text{diagonal } \& \; U_R^\dagger \epsilon'^{(R)} U_R \stackrel{!}{=} \text{diagonal}}$$

Z'-type models are also just a very moderate modification of the Standard Model. The general idea is the introduction of an additional flavour non-universal gauge interaction, different from the interactions of the SM, which are flavourblind. The easiest example to consider is the case of one additional gauge boson, corresponding to a new Abelian gauge symmetry $U(1)'$ [27]. Of course, this may lead to further complications, such as gauge anomalies and the necessity for additional scalars which break the $U(1)'$-symmetry. However, since we here only concentrate on the lepton flavour violation sector for SM charged leptons, we assume these things to be taken care of.

From our three cases, only Va) is of relevance:

Va) One introduces a gauged non-SM symmetry $U(1)'$, under which at least two generations of charged leptons with identical chirality have different charges. This leads to a change in the gauge-covariant derivative, creating an interaction term in the Lagrangian of the form

$$\mathcal{L} = -g' \overline{e} \gamma^\mu \left[\epsilon'^{(L)} \mathcal{P}_L + \epsilon'^{(R)} \mathcal{P}_R \right] e Z'_\mu. \tag{5.29}$$

Here, g' is the coupling constant for the Z'-interaction and the charges are absorbed in the coupling matrices. Compared to Eq. (5.18), we have $V_\mu = Z'_\mu$ and real matrices $C_{L,R} = \epsilon'^{(L,R)}$, adopting the notation of Ref. [27]. The actual vector boson mass eigenstate can in general be a superposition of electroweak and non-SM gauge bosons. Flavour violating couplings can arise when going to the leptonic mass eigenbasis, if the interactions are flavour non-universal. We start in the eigenbasis of the Z'-interaction, and hence the couplings are diagonal. Then, the coupling matrices are given by

$$\epsilon'^{(L,R)}_{ij} = \epsilon'^{(L,R)}_i \delta_{ij}, \tag{5.30}$$

which is flavour non-universal, as long as the $\epsilon'^{(L,R)}_i$ are not equal. Let U_L and U_R denote the unitary matrices that transform the 3-vectors $e_{L,R}$ in flavour space into their mass eigenstates, $e'_{L,R} = U^\dagger_{L,R} e_{L,R}$. For the Z'-interaction, the Lagrangian then looks like:

$$\mathcal{L} = -g' \overline{e'} \gamma^\mu \left[U_L^\dagger \epsilon'^{(L)} U_L \mathcal{P}_L + U_R^\dagger \epsilon'^{(R)} U_R \mathcal{P}_R \right] e' Z'_\mu. \tag{5.31}$$

The conditions for flavour conservation are:

$$U_L^\dagger \epsilon'^{(L)} U_L \stackrel{!}{=} \text{diagonal } \& \; U_R^\dagger \epsilon'^{(R)} U_R \stackrel{!}{=} \text{diagonal}. \tag{5.32}$$

We can understand these conditions in the following way: If a gauge interaction is no longer flavour universal, the automatic alignment associated with flavour universality is lost, and we need to demand alignment separately in order to conserve lepton flavour.

In the next two sections, we briefly discuss two further extensions of the SM gauge group. Such theories in general lead to additional vector bosons from the extended gauge groups and additional scalars needed to break them down to the SM.

5.3.4 The 331-model

$$\boxed{\underline{331\text{-model}}\text{: } U_L^\dagger h_s U_R \stackrel{!}{=} \text{diagonal}}$$

The 331-model is one possible extension of the SM, extending the gauge group to $SU(3)_C \times SU(3)_L \times U(1)_X$, which is then broken down to the SM gauge group [145, 146].

S) To break the extended gauge group and give realistic masses to all fermions, three Higgs $SU(3)_L$-triplets (Φ, ϕ, and ϕ') are needed, together with one sextet H. Decomposed into SM representations, we are left with three copies of the SM Higgs, out of which only two can couple to leptons: Φ_1^0, which is part of the ϕ-triplet, and Φ_3^0, which is part of the sextet H. In the lepton sector, one is thereby dealing with an effective THDM. In the notation of Ref. [145], the Yukawa interaction for charged leptons is:

$$\mathcal{L} = -\overline{e_L}\left(\Phi_3^0 h_s + \Phi_1^0 h_a\right) e_R + h.c. = -\overline{e'_L} U_L^\dagger \left(\Phi_3^0 h_s + \Phi_1^0 h_a\right) U_R e'_R + h.c., \tag{5.33}$$

where h_s is a symmetric and h_a is an anti-symmetric 3×3-matrix in flavour space. As in a general THDM, one linear combination of these coupling matrices will always be diagonal in the mass basis, so we only need to demand:

$$U_L^\dagger h_s U_R \stackrel{!}{=} \text{diagonal}. \tag{5.34}$$

to prevent tree-level LFV. It should also be noted that, in the 331-model, flavour changing processes via additional neutral scalars are suppressed due to the smallness of the Yukawa couplings [147].

Va) To cancel the appearing anomalies, one has to choose one generation of quarks (the third one) to have a transformation behavior different from the other two. The corresponding flavour-changing gauge boson is called Z' and transforms as an SM singlet. No such flavour non-universality is present in the lepton sector, however, and therefore no tree-level LFV can occur.

5.3.5 LR-symmetric models

$$\boxed{\underline{LR\text{-symmetric models}}\text{: } U_L^\dagger f U_R \stackrel{!}{=} \text{diagonal}}$$

Another possible extension of the SM gauge group are Left-Right(LR)-symmetric models [148, 149] with the gauge group $SU(2)_L \times SU(2)_R \times U(1)_{B-L}$. Here, R stands for *right*, B is the baryon, and L is the lepton number. Then, $SU(2)_R \times U(1)_{B-L}$ is broken down to $U(1)_Y$, which gives the SM. Again, we end up with additional gauge bosons and additional scalars needed to break the enlarged symmetry group.

S) In order to give masses to the SM fermions, one needs to introduce a Higgs field Φ transforming as a bi-doublet under $SU(2)_L \times SU(2)_R$. Decomposed into $SU(2)_L$ this results in an adjoint Higgs boson in addition to the SM Higgs. The Yukawa interaction, in the charged lepton mass eigenbasis, is then (applying the notation of Ref. [148]):

$$\mathcal{L} = -\overline{e'_L} U_L^\dagger (f\Phi_2^0 + g\Phi_1^{0*}) U_R e'_R + h.c., \tag{5.35}$$

which is again effectively a THDM. Comparing with Sec. 5.3.2, a sufficient condition for the absence of lepton FCNCs in LR-symmetric models is

$$U_L^\dagger f U_R \stackrel{!}{=} \text{diagonal}, \tag{5.36}$$

as one linear combination of Yukawa coupling matrices must be diagonal in the mass basis.

Va) All gauge interactions are in general assumed to be flavour-universal, so we will not encounter tree-level LFVs transmitted by vector bosons here.

5.3.6 Vector-like isosinglets

$$\boxed{\underline{\text{Vector-like isosinglets}}\text{: } \tilde{U}_L^\dagger \tilde{C} \tilde{U}_L \stackrel{!}{=} \text{diagonal}}$$

This section shows that our criteria also apply in cases which may, at the first glance, not look suitable for them. This is actually the strength of these criteria, since one can transform very many cases into a form where our conditions are useful.

To show this, we discuss an extension of the SM by $2n$ vector-like (their left- and right-handed particles sit in identical representations of the gauge group) isosinglet (they have no $SU(2)$-charge) fermions $L_{L,R}$. According to Ref. [150], the most general mass term for such a setup is given by

$$\mathcal{L}_{\text{mass}} = -(\overline{l_L}, \overline{L_L}) \left(\begin{array}{c|c} m_l & J \\ \hline 0 & M \end{array}\right) \begin{pmatrix} l_R \\ L_R \end{pmatrix} + h.c. \tag{5.37}$$

We have used the freedom to rotate the right-handed leptons to reach at the zero in the lower left corner. The components m_l and J are related to the VEV of the SM-Higgs, so they should acquire masses of the same order as $\langle H \rangle$. There is, however, also the lower right component M. This component is invariant under $SU(2)_L \times U(1)_Y$ and is hence not protected by gauge-symmetry. Accordingly, it can be much larger than the other components.

Applying our criteria is easy:

Vb) If we first perform the SM-rotations, $l_{L,R} = U_{L,R} l'_{L,R}$, we will get

$$\mathcal{L}_{\text{mass}} = -(\overline{l'_L}, \overline{L_L}) \left(\begin{array}{c|c} U_L^\dagger m_l U_R & U_L^\dagger J \\ \hline 0 & M \end{array}\right) \begin{pmatrix} l'_R \\ L_R \end{pmatrix} + h.c. \tag{5.38}$$

This is the basis in which we can write down the interaction with the SM Z^0-boson:

$$\mathcal{L}_Z \propto Z_\mu (\overline{l'_L}, \overline{L_L}) \gamma^\mu \underbrace{\left(\begin{array}{c|c} \mathbb{1}_{3\times 3} & 0_{3\times n} \\ \hline 0_{n\times 3} & C_{n\times n} \end{array}\right)}_{\equiv \tilde{C}} \begin{pmatrix} l'_L \\ L_L \end{pmatrix} \tag{5.39}$$

The zero in the upper right corner arises because of the combination $\mathbf{2} \otimes \mathbf{3} \not\supseteq \mathbf{1}$ in $SU(2)$. Eq. (5.38) is, however, not written in the physical mass basis yet. To arrive there, we have to do one more rotation,

$$\begin{pmatrix} l'_L \\ L_L \end{pmatrix} = \tilde{U}_L \begin{pmatrix} l'_L \\ L_L \end{pmatrix}'. \tag{5.40}$$

In this basis, the condition for the absence of LFV reads

$$\tilde{U}_L^\dagger \tilde{C} \tilde{U}_L \stackrel{!}{=} \text{diagonal}. \tag{5.41}$$

Now it is easy to see that the case of vector-like isosinglets is just another one of the examples where flavour universality has to be demanded.

5.4 Doubly charged bosons at tree-level

For a singly charged scalar or vector with a tree-level LFV-vertex, there will be external neutrinos. We will not consider this case here, since we are interested in processes such as $\mu \to 3e$, where the flavour violation is present for charged leptons. There is only one further way different from FCNCs to mediate such processes already at tree-level, namely by exchanging doubly charged bosons, where again either scalar or vector particles can do the job:

S) For a doubly charged scalar, we will have either $C_L = 0$ or $C_R = 0$, because otherwise hypercharge would not be conserved. For $C_L \neq 0$, the scalar will be the $T_3 = 1$ component of an $SU(2)_L$ triplet with hypercharge $Y = 2$, i.e. of a triplet Higgs. For $C_R \neq 0$ the scalar will be an $SU(2)_L$ singlet with hypercharge $Y = 4$. Obviously, a given field cannot have both transformation properties at the same time.

The Lagrangian reads:

$$\mathcal{L}_{\text{scalar}} = S^{++}\overline{(f_L)^{\mathcal{C}}}C_L f_L + h.c. = S^{++}\overline{(f'_L)^{\mathcal{C}}}U_L^T C_L U_L f'_L + h.c., \tag{5.42}$$

where L can be replaced with R. Note that the "left-handed Lagrangian" given above arises from a triplet Higgs model designed to give mass to the neutrinos, and the corresponding doubly charged scalar is in general assumed to be very heavy, giving a further suppression. The condition for absence of tree-level flavour changing diagrams is:

$$U_L^T C_L U_L \stackrel{!}{=} \text{diagonal, or } U_R^T C_R U_R \stackrel{!}{=} \text{diagonal, respectively.} \tag{5.43}$$

Note that in the case of doubly charged scalars, we connect the same fermion field (e.g. f_L with $(f_L)^{\mathcal{C}}$), and therefore we could achieve automatic alignment by demanding flavour universality. For this to work, we would, however, need $U_{L/R}$ to be real.

If these conditions are not fulfilled, one can still fulfill Eq. (5.43) by demanding the corresponding type of alignment, i.e., alignment for a real U.

V) We can also have doubly charged intermediate vector bosons. These will be $SU(2)_L$ doublet vector bosons with a hypercharge of $Y = +3$. The Lagrangian is:

$$\begin{aligned}\mathcal{L}_{\text{vector}} &= V_\mu^{++}[\,\overline{(f_R)^{\mathcal{C}}}\gamma^\mu C_L f_L + \overline{(f_L)^{\mathcal{C}}}\gamma^\mu C_R f_R] + h.c. = \\ &= V_\mu^{++}[\,\overline{(f'_R)^{\mathcal{C}}}\gamma^\mu U_R^T C_L U_L f'_L + \overline{(f'_L)^{\mathcal{C}}}\gamma^\mu U_L^T C_R U_R f'_R] + h.c.\end{aligned} \tag{5.44}$$

The conditions for the absence of tree-level lepton flavour violation look like:

$$\begin{aligned}U_R^T C_L U_L &\stackrel{!}{=} \text{diagonal,} \\ U_L^T C_R U_R &\stackrel{!}{=} \text{diagonal.}\end{aligned} \tag{5.45}$$

Flavour universality is of no advantage in this case, so we can only demand the type of alignment defined in the above equation. It is important to note that, apart from leading to tree-level LFV, all the above cases actually produce lepton number violating vertices, or, in other words, the exchange boson has to carry lepton number. In this case we can list three distinct types of particles, which can mediate doubly charged tree-level LFV:

Sa) An $SU(2)_L$ triplet with hypercharge 2. This particle does not couple to right-handed particles and is equivalent to the triplet Higgs which is often used for neutrino mass generation.

Sb) An $SU(2)_L$ singlet with hypercharge 4. Of the SM fields, this particle can only couple to right-handed charged leptons.

V) An $SU(2)_L$ doublet with hypercharge 3. To ensure renormalizability, we must again demand that this vector is a gauge boson. Its gauge group will then have to contain both, $SU(2)_L$ and $U(1)_Y$, as it is charged under both gauge groups. The smallest gauge group which can contain $SU(2) \times U(1)$ is $SU(3)$. A simple realization is the 331-model, where the electroweak gauge group is embedded in an $SU(3) \times U(1)$.

Note that, after electroweak symmetry breaking, scalar particles of type Sa and Sb can mix.

5.4.1 Triplet Higgs Models

Triplet Higgs: $U_{\text{PMNS}} \stackrel{!}{=} \mathbb{1}$ (not fulfilled)

Sa) The simplest models exhibiting tree-level LFV transmitted by doubly charged bosons are again those, where the necessary particles are simply added to the SM. In Triplet Higgs models, an $SU(2)_L$ scalar triplet with hypercharge 2 is added to give Majorana masses to the left-handed neutrinos. To keep the Lagrangian $SU(2)_L$-invariant, this scalar also couples to the left-handed charged fermions,

$$\mathcal{L} = S^{++}\overline{(e_L)^{\mathcal{C}}} C_L e_L + h.c., \tag{5.46}$$

which is exactly the Lagrangian of Eq. (5.42). The interaction basis in which C_L is diagonal is that in which the neutrino Majorana mass matrix is diagonal, i.e., the neutrino mass basis. To avoid tree-level LFV, C_L should be diagonal in the charged lepton mass basis, i.e., the neutrino and charged lepton mass bases have to coincide. This would imply that U_{PMNS} is just the unit matrix, which is excluded by experiments. We can therefore say that alignment is experimentally excluded and Triplet Higgs models always induce tree-level LFV, which is, however, in general strongly suppressed by the large mass of the scalar $SU(2)_L$ triplet.

5.4.2 The 331-model

331-model:	$U_L^T h_s U_L \stackrel{!}{=}$ diagonal & $U_R^T h_s U_R \stackrel{!}{=}$ diagonal (scalars) $U_R^T U_L \stackrel{!}{=}$ diagonal (vectors)

In this model, the nearly minimal extension of the SM gauge group, that can generate doubly charged gauge bosons which in turn can mediate LFV, is incorporated. We also encounter doubly charged scalars.

Sab) In the 331-model, in general four different doubly charged scalars arise that can couple to leptons and carry a lepton number of ∓ 2, namely the $T^{\pm\pm}$ and the $\eta^{\pm\pm}$ (note that in the Higgs triplet ϕ', another bi-lepton[3] exists, $\rho^{\pm\pm}$, which does, however, not couple to leptons and gets its lepton number assignment via terms in the Higgs potential that couple e.g. a ρ^{++} and a ρ^{--} with a T^{++} and an η^{--}, cf. Ref. [145]).

Their couplings to charged leptons look like

$$\mathcal{L} = -\frac{1}{\sqrt{2}}\overline{e_L} h_s (e_L)^{\mathcal{C}} T^{++} - \frac{1}{\sqrt{2}}\overline{(e_R)^{\mathcal{C}}} h_s e_R \eta^{++} + h.c. \tag{5.47}$$

h_s has already been introduced in Sec. 5.3.4. Here, the T^{++} is equivalent to the corresponding Sa-particle in a triplet Higgs model, while the η^{++} has a hypercharge of 4 and corresponds to the case Sb. In the mass basis, this gives

$$\mathcal{L} = -\frac{1}{\sqrt{2}}\overline{e'_L} \underbrace{(U_L^\dagger h_s U_L^*)}_{=(U_L^T h_s U_L)^\dagger} (e'_L)^{\mathcal{C}} T^{++} - \frac{1}{\sqrt{2}}\overline{(e'_R)^{\mathcal{C}}} (U_R^T h_s U_R) e'_R \eta^{++} + h.c. \tag{5.48}$$

One can read off the following conditions for flavour conservation:

$$\begin{aligned} U_L^T h_s U_L &\stackrel{!}{=} \text{diagonal (Sa)}, \\ U_R^T h_s U_R &\stackrel{!}{=} \text{diagonal (Sb)}. \end{aligned} \tag{5.49}$$

[3] A bi-lepton is a particle that carries a lepton number of ± 2.

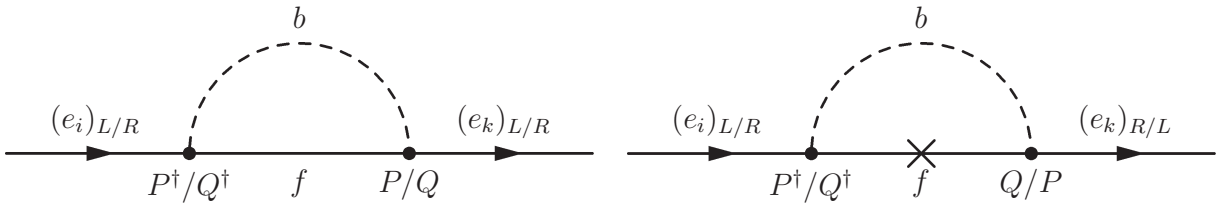

Figure 5.2: A schematic view of the cores of LFV-diagrams at 1-loop level

V) Doubly charged massive vector bosons $Y_\mu^{\pm\pm}$, which get their masses from the Φ_Y Higgs-doublet, also exist in this model. Their interaction Lagrangian with charged leptons is given by [151]

$$\mathcal{L} = -\frac{g}{\sqrt{2}}\left[\overline{(e_R)^\mathcal{C}}\gamma^\mu e_L Y_\mu^{++} + h.c.\right], \tag{5.50}$$

which reads for mass eigenstates

$$\mathcal{L} = -\frac{g}{\sqrt{2}}\left[Y_\mu^{++}\overline{(e'_R)^\mathcal{C}}\gamma^\mu (U_R^T U_L) e'_L + h.c.\right]. \tag{5.51}$$

The condition for the absence of flavour change is

$$U_R^T U_L \stackrel{!}{=} \text{diagonal}. \tag{5.52}$$

Due to the fact, that this gauge interaction couples left- and right-handed charged fermion fields, flavour universality is no longer sufficient for lepton flavour conservation.

5.4.3 LR-symmetric models

$$\boxed{\underline{LR\text{-models}}\text{: } U_{L,R}^T h_{L,R} U_{L,R} \stackrel{!}{=} \text{diagonal}}$$

Sab) In LR-symmetric models, doubly charged Higgses $H_{L,R}^{\pm\pm}$ arise. Their Yukawa couplings are given by [149]

$$\mathcal{L} = H_L^{++}\overline{e^\mathcal{C}} h_L \mathcal{P}_L e + H_R^{++}\overline{e^\mathcal{C}} h_R \mathcal{P}_R e + h.c. = H_L^{++}\overline{(e_L)^\mathcal{C}} h_L e_L + H_R^{++}\overline{(e_R)^\mathcal{C}} h_R e_R + h.c. \tag{5.53}$$

Performing the transformations into mass eigenstates and using Eq. (5.15), one obtains:

$$\mathcal{L} = H_L^{++}\overline{(e'_L)^\mathcal{C}}(U_L^T h_L U_L) e'_L + h.c. + (L \leftrightarrow R). \tag{5.54}$$

Hence, the conditions for the absence of flavour change are:

$$U_{L,R}^T h_{L,R} U_{L,R} \stackrel{!}{=} \text{diagonal}. \tag{5.55}$$

One needs to note here an important difference compared to neutrino mass generation using only a Higgs-triplet: As neutrinos also have Dirac mass terms, due to the presence of right-handed neutrinos, the Yukawa couplings to the Higgs-triplet containing H_L^{++} need not necessarily be diagonal in the neutrino mass basis.

5.5 Lepton flavour violation at 1-loop level

Let us now again think about the 1-loop process from Sec. 5.1. One of the results obtained there is, that a chirality flip has to take place during the process, i.e., the final electron must

have the opposite chirality than the one of the incoming muon. This result has been obtained without making any assumptions on the masses of the leptons involved, so that it trivially generalizes to arbitrary flavours and the process $e_i \to e_k\gamma$ (cf. Ref. [131]). For our purposes, the only interesting question is, whether this chirality flip happens on one of the external fermion lines, or arises as net effect of the loop.[4]

The first case to consider is the schematic 1-loop diagram that is depicted on the left panel of Fig 5.2 (type A: LL, type B: RR). Note that this diagram is only *very* schematic and does not contain several things: First of all, the outgoing photon is missing, that can in general couple either to the internal boson b or to the internal fermion f. The diagrams with photons connected to external particles exactly cancel, as discussed in Ref. [128]. This result is again independent of the smallness of the electron mass and of the model the process originates from, and hence generalizes to arbitrary flavours. As we are dealing with leptons of the same chirality at both vertices, we also have the same coupling constants (or matrices, in case several distinct particles can appear in the loop) at both vertices. We adopt the general convention that P denotes a coupling matrix involving left-handed leptons, while Q denotes a coupling matrix involving right-handed leptons. We will in the following refer to diagrams of the above type, i.e., with an implicit external helicity flip, as diagrams of type A (if they have external left-handed leptons) and as diagrams of type B (if they have external right-handed leptons).

The other possibility is having the chirality flip as net effect of the loop. The 1-loop LFV diagram then takes the schematic form that is depicted on the right panel of Fig. 5.2 (type C): Again, we have omitted the outgoing photon, as it can couple to either of the internal lines. The chirality flip is now explicitly shown, as a cross on the internal fermion line. We will refer to such diagrams as diagrams of type C. We do not distinguish according to the chirality of the incoming lepton, as in general, if a process where the helicity flips from left to right is possible, the reverse process will be possible as well.

Let us now try to order the conditions under which a flavour change does not occur: First of all, one needs exactly one fermion and one boson in the loop to ensure Lorentz invariance. In general this means that we will have one spin-$\frac{1}{2}$-fermion and either a scalar or a vector boson in the loop, as no renormalizable theories for particles with a higher spin are known. Furthermore, SM leptons only carry charge of the gauge groups $SU(2)_L$ and $U(1)_Y$. Hence, this must also be the case for the particle pair in the loop. The internal fermion f may carry, e.g., a color charge under $SU(3)_C$ (or some "exotic" charge in a theory beyond the SM), as long as this can be compensated by the corresponding internal boson b, so that they form a singlet under every gauge group except $SU(2)_L \times U(1)_Y$ ($\times$ possible other groups under which the charged leptons are no singlets). Therefore, another sufficient condition for the absence of flavour change at 1-loop level is

$$b \otimes f \not\supseteq \mathbf{1} \text{ (under one gauge group except } SU(2)_L \times U(1)_Y). \tag{5.56}$$

These are the obvious criteria for the absence of flavour change. The question remains which more subtle conditions can be found. Let us consider the three cases we discussed above:

A) External flip, left-handed charged lepton at both vertices:

In this case we have, at both vertices, a lepton which is the $T_3 = -\frac{1}{2}$ component of an $SU(2)_L$ doublet and has hypercharge $Y = -1$. As the photon does not carry away any of these quantum numbers, the tensor product of the internal particles must mimic the transformation properties of the left-handed SM lepton, i.e., $b \otimes f \supseteq (\mathbf{2}_L, Y = -1)$. If no pair of boson and fermion exists with these transformation properties, diagrams of type A are forbidden.

[4] A nice treatment of flavour changing loop diagrams can be found in Ref. [152].

B) External flip, right-handed charged lepton at both vertices:

Here, the situation is similar to the former case, with the only difference, that the leptons at each vertex are now right-handed. Accordingly, the quantum numbers of the internal particles must (at both vertices) fulfill $b \otimes f \supseteq (\mathbf{1}_L, Y = -2)$.

C) Internal flip:

At first sight, this situation seems to be much less straightforward than the other two. At one vertex (the one involving a left-handed external lepton) the boson and the fermion must fulfill the conditions of type A, at the other vertex they must fulfill the conditions of type B. This is naturally only possible after electroweak symmetry breaking. The difference in quantum numbers can only be brought about by a coupling to the Higgs VEV. This can correspond to the mass insertion in the diagram. In that case, the mass insertion serves a double purpose: Inducing the necessary chirality flip and the necessary change in quantum numbers. The chirality flip and the quantum number change can also be independent of each other, that is if the Higgs VEV couples to the boson line, e.g., through a dimension three term. All we definitely need is a coupling to the VEV of an SM-like Higgs somewhere in the loop.

We conclude that, for diagrams of type C to occur, a theory needs a boson and a fermion which fulfill the condition for type A diagrams and another boson-fermion pair that fulfills the condition for type B diagrams. After electroweak symmetry breaking, a superposition of the two fermions gives the mass eigenstate f which appears in the diagram, while a superposition of the two bosons gives the mass eigenstate b. Hence, one can say in general that diagrams of type C are allowed only if both diagrams of type A and of type B are allowed. Note that this condition is necessary, but not sufficient: The mixing of the relevant fermions and bosons is another necessary condition for diagrams of type C to occur.

Realizing that these are really the only cases that matter, a third sufficient condition for the absence of flavour change at 1-loop level is

$$\forall b, f: \; b \otimes f \not\supseteq (\mathbf{2}_L, Y = -1) \;\&\; b \otimes f \not\supseteq (\mathbf{1}_L, Y = -2). \tag{5.57}$$

Loop diagrams of the type discussed above even arise in the Standard Model with neutrino masses. They are, however, strongly suppressed by the GIM-mechanism [132] (as discussed in Sec. 5.1 for the case of the SM with massive neutrinos), which we will generalize in the following.

Let b and f be the two particles in the loop. Now let there be m copies of b and n copies of f, where copies means that they differ only by their mass. Let e_i denote the SM charged leptons, as before. We need to make no assumptions concerning the number of generations, but we do assume three generations for simplicity. To produce all the above loop diagrams, the Lagrangian must contain the term

$$b_A \overline{(e_L)_i} P_{iAj} f_j + b_A \overline{(e_R)_i} Q_{iAj} f_j + h.c. \tag{5.58}$$

For a fixed A, the P_{iAj} and Q_{iAj} are in general $3 \times n$-matrices, while for a fixed j they are $3 \times m$-matrices. As they cannot necessarily be diagonalized, since they do not even need to be square matrices, we assume the above term to be written in the mass basis of the SM fermions, the b_A and the f_j.

This interaction now in general leads to 1-loop flavour-changing diagrams. By a GIM-mechanism, we understand a cancellation of these diagrams, such that the matrix

$$\Gamma_{ik} = \Gamma(e_i \to e_k \gamma) \tag{5.59}$$

is approximately diagonal.[5] If it were exactly diagonal, this would imply, that the matrices

[5] Actually, its diagonal elements are strictly zero due to energy conservation.

P_{iAj} and Q_{iAj} have at most one non-zero entry per column (both for fixed A and fixed j). This means explicit conservation of lepton flavour in the interaction, or, equivalently, that we can assign a specific lepton flavour number to any given boson-fermion pair b_A and f_j. Through unitary transformations, any matrices P_{iAj} and Q_{iAj} can be brought to such a form, where they have at most one non-zero entry per column. If they have this form in the respective mass bases of the involved particles, it is another incidence of basis alignment.

GIM-mechanism means, that we can expand Γ_{ij} in some small parameter and the zeroth order coefficient in this expansion is diagonal. This is a slight deviation from our method up to now, as we have so far only considered explicit lepton flavour conservation. However, as this is the mechanism which suppresses LFV in the SM with neutrino masses, and as it relies heavily on the flavour structure of a given model, it is necessary to discuss it here, too.

We give the discussion for left-handed ($Q_{ij} = 0$) and fermionic (fixed $A = A_0$, with $b_{A_0} = b$) GIM, where the summation runs over all possible internal fermions f_j. This is the case in the SM with massive neutrinos, with b being the W-boson, and the f_j being the light massive neutrinos. It is then straightforward to generalize both to the case of bosonic GIM and to the case of both right-handed and left-handed leptons taking part in the process, i.e., $Q_{ij} \neq 0$. The partial decay width for the decay $e_i \to e_k\gamma$ in the case of left-handed fermionic GIM is [131]:

$$\Gamma_{ik} = \frac{(m_i^2 - m_k^2)^3}{16\pi m_i^3} \left(\left| \sum_{j=1}^{n} P_{ij} P_{jk}^\dagger F(m_i, m_k, m_{f_j}, m_b) \right|^2 \right), \tag{5.60}$$

where F is some loop function, similar as in Sec. 5.1. To obtain the desired result, i.e., Γ_{ik} being approximately diagonal, we need two conditions to be fulfilled. First, we need

$$PP^\dagger \stackrel{!}{=} \text{diagonal} \tag{5.61}$$

and second

$$F(m_i, m_k, m_{f_j}, m_b) \approx F(m_i, m_k, m_{f_{j'}}, m_b)\ \forall j, j' \in \{1, ..., n\} \text{ and } j \neq j'. \tag{5.62}$$

This condition is necessary, so that in a first approximation F can be taken out of the sum and we can use the first condition to diagonalize Γ. It can be considered as a condition demanding approximate mass degeneracy. What approximate mass degeneracy exactly means is, of course, ill-defined. The light neutrinos for example are not necessarily approximately degenerate in mass. However, their relative mass differences are small compared to other mass scales in the amplitude, such as the W-boson mass, because their absolute mass scale is small. We will not enter further into this discussion, as it is not connected to the main focus, namely the flavour structure and the particle content of models. It is, however, important to keep in mind, that, apart from the flavour structure, this approximate mass degeneracy is a necessary condition for the GIM-mechanism to work and thereby for the suppression of 1-loop LFV to occur.

Let us also consider the first condition in some more detail. By singular value decomposition, we can write

$$P = UP'V^\dagger, \tag{5.63}$$

where U is a 3×3 unitary matrix, V is $n \times n$ and also unitary, and P' is a "diagonal" $3 \times n$-matrix, that is its only nonzero entries are P'_{11}, P'_{22}, and P'_{33}. Our first condition can then be rewritten as

$$UP'P'^\dagger U^\dagger \stackrel{!}{=} \text{diagonal}. \tag{5.64}$$

Our first observation is, that the basis change for the fermions in the loop, given by the matrix V, drops out. This is in keeping with the second condition, as for exactly degenerate masses, there would be no uniquely defined mass basis anyhow. Secondly, we observe that $P'P'^\dagger$ is of

course diagonal. So, we are again faced with two possibilities: One is that the basis change U defined by Eq. (5.63) is trivial, that is the mass basis of the charged leptons coincides with the interaction basis, another case of alignment. The other possibility is that $P'P'^{\dagger}$ is in fact the unit matrix, in which case the above condition is automatically fulfilled – this is the 1-loop equivalent of flavour universality, as the interaction leading to the loop-diagram needs to be just that – flavour universal.

The generalization is then straightforward. In case of the most general interaction, Eq. (5.58), we need to demand

$$\begin{aligned} PP^{\dagger} &\stackrel{!}{=} \text{diagonal,} \\ QQ^{\dagger} &\stackrel{!}{=} \text{diagonal, and} \\ PQ^{\dagger} &\stackrel{!}{=} \text{diagonal} \end{aligned} \tag{5.65}$$

in the mass basis, where the matrix multiplication is to be understood in such a way, that in each case we either keep A or j fixed.

A noteworthy special case is when $f = e$: The above condition will then automatically be fulfilled if there is no tree-level LFV (where we assign a separate lepton flavour number to each generation), i.e., if P and Q are diagonal in the mass basis.

The SM with neutrino masses only has GIM-suppressed LFV. In the following discussion, we will not only check for the presence of 1-loop LFV, but we will also discuss whether they are GIM-suppressed in the general sense we just have defined.

5.5.1 The Standard Model with massive neutrinos

Standard model: Diagram A ($f = \nu_L$ & $b = W_\mu^-$) and $PP^{\dagger} = U_{\text{PMNS}}^{\dagger} U_{\text{PMNS}} = \mathbb{1}$ (GIM)

Let us start once more with the well-known process reviewed in Sec. 5.1 in order to get the connection to the generalized formalism in this section more easily. The only possibility for a 1-loop level lepton flavour violation $\mu \to e\gamma$ in the SM (with massive neutrinos) is diagram A with b being a W^-, which also emits the photon, and with f being a neutrino.

The corresponding interaction Lagrangian looks like [15]

$$\mathcal{L} = -\frac{e}{\sqrt{2}\sin\theta_W} W_\mu^- \, \overline{e_L} \gamma^\mu \nu_L + h.c. = -\frac{e}{\sqrt{2}\sin\theta_W} W_\mu^- \, \overline{e'_L} \gamma^\mu U_{\text{PMNS}}^{\dagger} \nu'_L + h.c. \tag{5.66}$$

Now let us go through our criteria: We know that $W^- \sim (\mathbf{3}_L, Y = 0)$ and $\nu_L \sim (\mathbf{2}_L, Y = -1)$ with $\nu_L \neq \nu'_L$, while they are singlets under all other gauge groups in the SM (which is just $SU(3)_C$), so the trivial sufficient condition for the absence of flavour change is not fulfilled. Also the second condition is not fulfilled, due to the quantum numbers of the internal particles. Now, in $SU(2)$, it holds that $\mathbf{3} \otimes \mathbf{2} = \mathbf{2}$ ($\oplus$ $\mathbf{4}$), so that the left-handed neutrino can serve as f, since also the hypercharge balance, namely $Y(W^-) - Y(\nu_L) = 0 - 1 = -1$ turns out to be correct. Hence there exists, as expected, lepton flavour violation in the SM, since the mixing matrix $P^{\dagger} = U_{\text{PMNS}}$ is not diagonal. So, in the SM, neutrino mixing directly leads to processes like $\mu \to e\gamma$ at loop-level.

However, the same mixing matrix also leads to GIM-suppression: Since U_{PMNS} is unitary, $PP^{\dagger} = U_{\text{PMNS}}^{\dagger} U_{\text{PMNS}} = \mathbb{1}$ and hence trivially diagonal, which exactly fulfills our condition, Eq. (5.65). This is of course again due to the fact that the weak interaction is flavour universal. As already mentioned, the condition of approximate mass degeneracy is also fulfilled due to the smallness of the absolute neutrino mass scale.

5.5.2 Multi Higgs models

Multi Higgs models:
A ($f = \nu_R$ or ν^M_{heavy} & $b = H_k^-$), GIM for $P_k P_k^\dagger \stackrel{!}{=}$ diagonal;
B ($f = \nu_L$ or ν^M_{light} & $b = H_k^-$), GIM for $Q_k Q_k^\dagger =$ diagonal;
C ($f = \nu_{\text{Dirac}}$ & $b = H_k^-$), GIM for $Q_k U^\dagger_{\text{PMNS}} P_k^\dagger \stackrel{!}{=}$ diagonal

If we have tree-level LFV in a Multi Higgs model, we can easily obtain LFV at the 1-loop level by connecting two of the external arms of the tree-level diagram with a mass insertion, giving a diagram of type C. This mass insertion can then also be moved to the two external arms giving diagrams of type A and B. This is a generic statement in models where tree-level LFV is present, so we will not consider the case of neutral scalars and charged leptons in the loop further.

We can, however, also get additional contributions with a charged scalar and a neutrino in the loop. If we do not add right-handed neutrinos to the model, the Lagrangian will contain one relevant interaction, the $SU(2)$-counterpart to the interaction given in Sec. 5.3.2,

$$\mathcal{L} = \sum_{k=1}^{n} H_k^- \overline{e'_R} Q_k \nu_L + h.c. \tag{5.67}$$

Formulated using the general conditions, we have that the additional Higgs bosons transform as $(\mathbf{2}_L, Y = -1)$ and $\nu_L \sim (\mathbf{2}_L, Y = -1)$, and again they are color singlets, thereby not satisfying the second sufficient condition for the absence of LFV. Taking the product of the representations, we find that $(\mathbf{2}_L, Y = -1) \otimes (\mathbf{2}_L, Y = -1) = (\mathbf{1}_L, Y = -2)[\oplus\, (\mathbf{3}, Y = -2)]$, allowing for diagrams of type B, with $f = \nu_L$ and $b = H_k^-$. As indicated in Eq. (5.67) we will have n negatively charged scalars: Out of the $(2n+2)$ charged degrees of freedom, half are negative, one of which is eaten by the W^-. This implies that in the mass basis no linear combination of Q_k is necessarily diagonal, as that linear combination for neutral scalars corresponds to the eaten scalar in the charged case. As the mass eigenstates of the charged scalars do not necessarily coincide with those of the neutral scalars, Q_k and the C_k of Sec. 5.3.2 (cf. Eq. (5.26)) are in general not equal. They are, however, related, since if the original Yukawa coupling matrices Y_l are diagonal for all l, then both C_k and Q_k are diagonal for all k.

This interaction is written in the charged lepton mass basis. This does not coincide with the neutrino mass basis, as we know from the fact that the PMNS-matrix is not diagonal. If we rotate the neutrinos to their mass basis, the interaction reads:

$$\mathcal{L} = \sum_{k=1}^{n} H_k^- \overline{e'_R} Q_k U^\dagger_{\text{PMNS}} \nu'_L + h.c. \tag{5.68}$$

So we find that our coupling matrix $Q_k U^\dagger_{\text{PMNS}}$ is not diagonal, i.e., diagrams of type B are allowed, even if tree-level LFV is forbidden. The condition for GIM-suppression then reads:

$$Q_k U^\dagger_{\text{PMNS}} U_{\text{PMNS}} Q_k^\dagger = Q_k Q_k^\dagger \stackrel{!}{=} \text{diagonal}. \tag{5.69}$$

This means that, if tree-level LFV is forbidden, and thereby Q_k is diagonal, these processes will always be GIM-suppressed. As in the SM this is also due to the fact, that the absolute mass scale of the light neutrinos is small compared to the mass of the scalars involved.

If we add three right-handed neutrinos to the model, there are two possibilities: One can either write down a Majorana mass term for the right-handed neutrinos and apply the Type I seesaw mechanism or one can consider neutrinos as Dirac particles.

In the first case, the mass eigenstates will be Majorana particles, a superposition of left-handed and right-handed neutrinos. We will write these as ν^M_{light} for the predominantly left-handed light neutrinos and as ν^M_{heavy} for the predominantly right-handed heavy neutrinos. As we have so far always assumed a unitary PMNS-matrix, i.e., a "perfect" seesaw, we will assume that the light neutrinos are purely left-handed and that the heavy ones are purely right-handed. We then still have the interaction of Eq. (5.68), with ν'_L replaced by ν^M_{light}, and the same conditions for LFV and GIM-suppression in diagrams of type B. The right handed or heavy neutrinos transform as total singlets under the SM gauge group, so that the product of their representations with that of the Higgs bosons is $(\mathbf{2}_L, Y = -1)$, allowing for diagrams of type A, with $f = \nu^M_{\text{heavy}}$ and $b = H^-_k$.

The corresponding couplings are then the Yukawa couplings which give the neutrinos their Dirac mass:

$$\mathcal{L} = \sum_{k=1}^{n} H^-_k \overline{e'_L} P_k \nu^M_{\text{heavy}} + h.c. \tag{5.70}$$

As the matrices P_k play no role for tree-level LFV, we make no further assumptions concerning their form. One however needs to pay close attention in which basis the above interaction is written: We have chosen the basis in which the charged lepton and the right-handed neutrino Majorana matrices are diagonal. If we had written the interaction in another basis, one would here also have to introduce a PMNS-type matrix, as was the case for the light neutrinos. LFV-processes will then occur if P_k is not diagonal and the condition for GIM-suppression is then simply

$$P_k P_k^\dagger \stackrel{!}{=} \text{diagonal}. \tag{5.71}$$

This GIM-suppression of course demands, that the heavy neutrinos are approximately degenerate in mass. Such processes are, however, strongly suppressed anyway as the heavy neutrinos decouple in the seesaw limit. Even though diagrams of type A and B are allowed, no diagrams of type C can be generated for Majorana neutrinos, as the necessary condition that the fermions of diagrams A and B mix after electroweak symmetry breaking is not fulfilled in the seesaw limit.

Things are different for the case of Dirac neutrinos. One again has the interactions of Eq. (5.68) and of Eq. (5.70), where ν^M_{heavy} must be replaced by ν'_R, the right-handed neutrinos in the neutrino mass basis. This means that diagrams of type A and type B can occur under the same conditions as above. As left- and right-handed neutrinos mix in this case to form a Dirac fermion after electroweak symmetry breaking, diagrams of type C will also be possible, if either $Q_k U^\dagger_{\text{PMNS}}$ or P_k is not diagonal. As we assume no tree-level LFV, $Q_k U^\dagger_{\text{PMNS}}$ is automatically non-diagonal and such processes can occur. The condition for GIM-suppression is then

$$Q_k U^\dagger_{\text{PMNS}} P_k^\dagger \stackrel{!}{=} \text{diagonal}. \tag{5.72}$$

We reach the conclusion that, if tree-level LFV is forbidden in a Multi Higgs model, then 1-loop LFV including left-handed neutrinos will always be GIM-suppressed. Observable LFV therefore necessitates the introduction of right-handed neutrinos. As these will approximately decouple in the Majorana case, only Dirac neutrinos lead to observable 1-loop LFV-processes. A GIM-suppression of such processes could then only be brought about by demanding the alignment conditions of Eqs. (5.71) and (5.72).

5.5.3 Universal Extra Dimensions

Universal Extra Dimensions:
A ($f = \nu_{L(n)}$ & $b = W^-_{\mu(n)}$), as for SM (GIM);
A ($f = \nu_{R(n)}$ & $b = a^-_{(n)}$), where $P = U^\dagger_{\text{PMNS}} c_R$ and $PP^\dagger \propto \mathbb{1}$ (GIM);
B ($f = \nu_{L(n)}$ & $b = a^-_{(n)}$), where $Q = U^\dagger_{\text{PMNS}} c_L$ and $QQ^\dagger \propto \text{diag}(m_e^2, m_\mu^2, m_\tau^2)$ (GIM);
C ($f = \nu_{R/L(n)}$ & $b = a^-_{(n)}$), $PQ^\dagger \propto \text{diag}(m_e, m_\mu, m_\tau)$ (GIM)

A different type of models where lepton flavour violation can occur are theories with extra spatial dimensions. There is a huge variety of them – we will only be considering the ACD-model [28], which is also often called Universal Extra Dimensions (UEDs). A key feature of this model is that the particles of the SM propagate in all 5 dimensions, where the 5th dimension is compactified.

We adopt the notation of Ref. [153]. In this model, there are two types of particles that can play the role of the boson b. First of all we have the vector bosons $W^-_{(n)}$, where n denotes the (Kaluza-Klein) (KK-) number. These KK-modes of the W-boson transform in the same way as the zero mode, which is just the SM W, under all SM gauge groups. Hence, we know from Sec. 5.5.1 that a particle transforming as a left-handed neutrino can here be used as the fermion f. UEDs lead to an additional symmetry which needs to be conserved, the conservation of the KK-number n. To ensure that the particles in the loop form a total singlet under all non-SM symmetries, we need to demand that the neutrino-like particle in the loop has the same KK-number as the boson $W_{(n)}$. Therefore the only particle that can play the role of f is the n-th KK-mode of the neutrino, $\nu_{(n)}$. Otherwise, nothing changes compared to the SM with massive neutrinos: Diagrams of type A will be allowed and GIM-suppression will always occur due to the unitarity of U_{PMNS}. The n-th KK-mode of a given neutrino ν_i will have mass $m^2_{(n)} = m_i^2 + \frac{n^2}{R^2}$, where m_i is the zero-mode mass of the neutrino and R is the compactification radius of the extra dimension. Hence, the mass degeneracy is even more explicit here, as the mass differences of neutrino KK-modes are small compared to their mass, which is approximately $\frac{n}{R}$.

UEDs also lead to scalars that can play the role of b: The higher KK-modes of the charged and pseudoscalar Higgs fields are not entirely eaten by the corresponding vector bosons, they also mix with the 5th component of those vector bosons to form physical scalars, both charged ($a^-_{(n)}$) and neutral ($a^0_{(n)}$). As these scalars transform as the SM Higgs, they can form a loop with particles transforming as neutrinos or as charged leptons, as discussed in Sec. 5.5.2. Again, we need to observe conservation of KK-number, so f can only be $\nu_{(n)}$ or the n-th KK-mode of the charged lepton, $e_{(n)}$, respectively. So, we will have the same types of diagrams as in a Multi Higgs model, with the particles in the loop replaced by their higher KK-modes. As opposed to a Multi Higgs model, the additional scalars can be considered as excitations of the same particle, and therefore all couple in the same way. They will, however, couple differently from the SM Higgs, as they also have a gauge boson contribution. All gauge interactions remain flavour universal, so we find for the coupling of left-handed charged leptons to $e_{(n)}$ and $a^0_{(n)}$:

$$P \propto (Y_e + \text{flavour universal contributions}). \tag{5.73}$$

For the coupling of the right-handed charged leptons we have no further complications from gauge interactions and the coupling matrices Q will just be proportional to the regular charged lepton Yukawa couplings Y_e. One can then see that all coupling matrices are diagonal in the charged lepton mass basis, which is also the mass basis for the KK-modes $e_{(n)}$, and we therefore have no LFV for diagrams with $e_{(n)}$ in the loop.

For neutrino KK-modes in the loop, we obtain the following Lagrangian [154]:

$$\mathcal{L} = -\frac{g_2 n}{\sqrt{2}M_{W(n)}}\left[\overline{\nu_{R(n)}}c_R e'_L + \overline{\nu_{L(n)}}c_L e'_R\right] a^-_{(n)} + h.c. \tag{5.74}$$

$$= -\frac{g_2 n}{\sqrt{2}M_{W(n)}}\left[\overline{\nu'_{R(n)}}U^\dagger_{\text{PMNS}}c_R e'_L + \overline{\nu'_{L(n)}}U^\dagger_{\text{PMNS}}c_L e'_R\right] a^-_{(n)} + h.c., \tag{5.75}$$

with $c_L = \text{diag}(m_e, m_\mu, m_\tau)$ and $c_R = M_W \cdot \mathbb{1}$. Note that, in principle, there can be a correction to c_R coming from the neutrino Yukawa coupling matrix, but we have assumed neutrinos to be purely Dirac. In that case their masses are negligible compared to M_W and can be ignored in Eq. (5.75). For comments on different methods of neutrino mass generation and their effect on LFV, see Sec. 5.5.2. The right-handed neutrinos in Eq. (5.75) are KK-modes of the left-handed neutrino and arise independently of the origin of neutrino mass. We find that the relevant coupling matrices P and Q are both the product of a flavour-diagonal matrix and the non-diagonal but unitary U_{PMNS}. We can therefore construct LFV diagrams of all types; all such processes will however be GIM-suppressed, as the mass degeneracy of the $\nu_{(n)}$ is again explicit. See Ref. [154] for a discussion of the effect of summing over a large number of GIM-suppressed amplitudes.

5.5.4 The Minimal Supersymmetric Standard Model

MSSM+ν_R:
A ($f = (\tilde{\chi}^{-/0}_{A,R})'$ & $b = \tilde{\nu}'/\tilde{e}'$), where $P = (C/N)^{R(l)}_A$, and $PP^\dagger$ = diagonal (GIM);
B ($f = (\tilde{\chi}^{-/0}_{A,L})'$ & $b = \tilde{\nu}'/\tilde{e}'$), where $Q = (C/N)^{L(l)}_A$, and $QQ^\dagger$ = diagonal (GIM);
C ($f = (\tilde{\chi}^{-/0}_{A})'$ & $b = \tilde{\nu}'/\tilde{e}'$), where $PQ^\dagger$ = diagonal (GIM)

The Minimal Supersymmetric Standard Model (MSSM) itself can only lead to 1-loop LFV diagrams (or higher), since all tree-level vertices are forbidden due to R-parity conservation. The discussion is somewhat similar to that of Sec. 5.5.3, as we again take the diagrams of the SM and Multi Higgs models, and replace the particles in the loop by other particles which transform in the same way under the SM gauge groups, thereby delegating a large part of the discussion concerning the general LFV-conditions to Secs. 5.5.1 and 5.5.2. In the case of the MSSM, the particles in the loop will be replaced by their superpartners, thereby also ensuring that there is always one boson and one fermion in the loop.

We begin by considering the supersymmetric analogon of the LFV diagrams with neutrinos in the loop. The neutrinos will be replaced by sneutrinos, which are then the bosons in the loop, $b = \tilde{\nu}$. In the MSSM, the LFV diagrams with a W in the loop (Sec. 5.5.1) and with a charged Higgs scalar in the loop (Sec. 5.5.2 – they arise as the MSSM is a THDM) are both replaced by diagrams with charginos, which are then the fermions in the loop, $f = \tilde{\chi}^-_A$ ($A = 1, 2$). This is because the two $\tilde{\chi}^-_L$'s are superpositions of the gaugino $\tilde{W}^-_L$ (the superpartner of the W) and the Higgsino $\tilde{H}^-_{uL}$ (the superpartner of one Higgs boson), and conversely the two $\tilde{\chi}^-_R$'s are superpositions of $\tilde{W}^-_R$ and $\tilde{H}^-_{dR}$. The sneutrinos will be massive, even if the neutrinos are not, due to soft SUSY breaking, so we do not need to worry about the origin of neutrino mass. The sneutrino mass basis does not need to coincide with that of the charged leptons and we expect LFV to occur. The interaction Lagrangian is[6]

$$\mathcal{L}_{\text{chargino}} = \sum_{A=1}^{2} \overline{e'_L} C^{R(l)}_A (\tilde{\chi}^-_{A,R})' \tilde{\nu}' + \overline{e'_R} C^{L(l)}_A (\tilde{\chi}^-_{A,L})' \tilde{\nu}' + h.c. \tag{5.76}$$

[6]For more details, see Refs. [155] and [156].

Here, all fields (also the bosonic ones) are written as mass eigenstates, and $C_A^{R/L(l)}$ denote the coupling matrices of the right- and left-handed chargino $(\tilde{\chi}^-_{A,R/L})'$, respectively, to the charged leptons e and the sneutrino mass eigenstates $\tilde{\nu}'$. The $C_A^{R/L(l)}$ are thereby 3×3-matrices. These matrices contain all rotations to mass eigenstates, for the left- and right-handed charginos as well as for the sneutrinos. For diagram A, one then needs $f = (\tilde{\chi}^-_{A,R})'$, and $P = C_A^{R(l)}$ has to be non-diagonal. Diagram B is possible with $f = (\tilde{\chi}^-_{A,L})'$ and $Q = C_A^{L(l)}$ non-diagonal, and diagram C with f flipping from $(\tilde{\chi}^-_{A,L})'$ to $(\tilde{\chi}^-_{A,R})'$, or vice versa, with the same P and Q as before. If all $C_A^{R/L(l)}$ turn out to be diagonal there will be no LFV at 1-loop level – this is of course a case of alignment, a term which has actually first been used for the supersymmetric case [157]. If the $C_A^{R/L(l)}$ are not diagonal, there is still the possibility of GIM-suppression, for which the conditions are

$$\begin{aligned} C_A^{R(l)} C_A^{R(l)\dagger} &\stackrel{!}{=} \text{diagonal (A)}, \\ C_A^{L(l)} C_A^{L(l)\dagger} &\stackrel{!}{=} \text{diagonal (B), and} \\ C_A^{R(l)} C_A^{L(l)\dagger} &\stackrel{!}{=} \text{diagonal (C).} \end{aligned} \tag{5.77}$$

These conditions are in fact always fulfilled: Since the chargino is a superposition of Higgsino and wino, we need to invoke the natural alignment of mass and Yukawa interaction basis as well as the flavour universality of the weak interaction. LFV only arises due to the non-trivial, unitary transformations to mass eigenstates. The critical question is therefore the approximate mass degeneracy, which can be achieved by giving approximately universal soft masses to the sneutrinos. Their mass differences, corresponding to the mass differences of the neutrinos, then become negligible. This is commonly referred to as the Super-GIM-mechanism [158] and is, in fact, covered by the generalized GIM-mechanism from the beginning of this section.

In general, LFV diagrams with charged leptons in the loop will only be allowed if tree-level LFV is also allowed (cf. Sec. 5.5.2). In UEDs, the KK-modes of the charged leptons necessarily have the same mass basis as the charged leptons themselves, which is why the "partner" diagrams do not lead to LFV (cf. Sec. 5.5.3). These things are different in the MSSM, as the superpartners of the charged leptons, the charged sleptons $\tilde{e}$, do not necessarily have the same mass basis, because their mass also arises from soft SUSY breaking terms. Basis alignment can be achieved by imposing conditions on the soft SUSY breaking terms, such as the popular mSUGRA (minimal Supergravity) boundary conditions, but in general one can construct diagrams with charged sleptons in the loop taking the role of b. The part of f is then taken by a superposition of the superpartners of the neutral electroweak gauge bosons and the neutral Higgs bosons. The mass eigenstates of these superpositions are the neutralinos $\tilde{\chi}^0_A$ $(A = 1, ..., 4)$, where the $\tilde{\chi}^0_A$ is a superposition of the bino $\tilde{B}$, the neutral wino $\tilde{W}^0$, and the two neutral Higgsinos $\tilde{H}^0_u$ and $\tilde{H}^0_d$). The corresponding interaction Lagrangian is

$$\mathcal{L}_{\text{neutralino}} = \sum_{A=1}^{4} \overline{e'_L} N_A^{R(l)} (\tilde{\chi}^0_{A,R})' \tilde{e}' + \overline{e'_R} N_A^{L(l)} (\tilde{\chi}^0_{A,L})' \tilde{e}' + h.c., \tag{5.78}$$

where the matrices $N_A^{R/L(l)}$ now contain the rotations of $(\tilde{B}, \tilde{W}^0, \tilde{H}^0_u, \tilde{H}^0_d)^T$ to mass eigenstates $((\tilde{\chi}^0_1)', ..., (\tilde{\chi}^0_4)')^T$ for both cases, R and L, and the rotations of the charged sleptons to mass eigenstates, too. The cases that can appear here are completely analogous to the ones for charginos, just with $(\tilde{\chi}^-)' \to (\tilde{\chi}^0)'$, $\tilde{\nu}' \to \tilde{e}'$, and $C \to N$ for the mixing matrices. The only difference is that there exist four different neutralinos compared to only two negatively charged charginos and six charged sleptons, making the $N_A^{R/L(l)}$ 6×3-matrices. Again the condition for GIM-suppression is automatically fulfilled, while the mass degeneracy can be achieved by approximately universal soft masses.

5.6 Constraining Models with Flavour Symmetries

As already explained at the beginning of this chapter, LFV arises very generically in BSM-Theories. In order to explain the apparent patterns in the flavour sector, so-called Discrete Flavour Symmetries are often used [159]. These symmetries impose certain relations on the otherwise in most of the cases arbitrary Yukawa matrices that couple fermions to scalars (differently from the gauge sector there is normally no symmetry principle behind Yukawa matrices – and this is exactly what is changed by imposing a certain flavour symmetry). By this relation, e.g., alignment of certain couplings could be achieved.

In this section, we turn this logic around and investigate how strongly a model with a discrete flavour symmetry can be constrained by LFV-processes. As we will see, it is generically difficult to apply conditions like Eq. (5.17), due to the remaining freedom in the Yukawa matrices. This, in turn, implies the generic existence of LFV-processes, whose limits can then be used to powerfully constrain the models in question.

5.6.1 The general arguments

A natural way to extend the SM is to add further scalar particles, which have not been discovered yet. These could, e.g., be additional $SU(2)$-singlets [160], doublets (THDM), or triplets [26]. Depending on the model, it can then be the case that more than one Higgs field contribute to the masses of all particles or that certain Higgses only give masses to a particular choice of particles [161]. These models will then, however, generically lead to flavour changing neutral currents (FCNCs) [162] and hence to LFV-processes [9], which are quite strongly constrained [139]. It is, however, also not easy to rule out these models that way, since they will in general yield complex 3×3 Yukawa coupling matrices, which hold a lot of freedom in their 18 parameters. So, in most of the cases, such a model will be able to fit all neutrino data without any problems, even if it is strongly constrained.

On the other hand, there are also ways to impose more structure onto the SM in order to get an understanding of quantities like mixing angles, or so. This is usually done by discrete flavour symmetries under which the SM-fermions (and, depending on the model, also (additional) scalars) are charged in a certain way. If, e.g., the two generations of $SU(2)_L$ doublets are components of the same doublet representation of a discrete flavour symmetry (such as the dihedral groups $D_3 \simeq S_3$ [163] or D_4 [164–166]), then this property will generically lead to μ-τ symmetry [167], by which two mixing angles are predicted: $\theta_{23} = \pi/4$ and $\theta_{13} = 0$. Moreover, in order to increase the predictivity, one can also assign the three generations of $SU(2)_L$ doublets to form a triplet of a discrete flavour symmetry (such as A_4 [168–172]). This can lead to tri-bimaximal mixing [173, 174], in which also θ_{12} is fixed to be $\tan\theta_{12} = 1/\sqrt{2}$.

Imposing such symmetries adds more structure to the model in the sense that one obtains relations between different entries of the Yukawa matrices. By that way, one can obtain the neutrino oscillation parameters as well as the charged lepton masses as functions of only a few parameters, which can then be checked on whether they are in accordance with data, or not. However, such models generically need a lot of scalars in order to break the flavour symmetry in a valid way. In case the normal Higgses are not charged under the flavour symmetry, these are additional SM-singlet scalars (*flavons*), which are only charged under the discrete symmetry and can hence break it by obtaining a VEV. These scalars will, again, lead to horribly large FCNCs, which crashes with phenomenology.

One way out is to decouple the flavons by giving them masses associated with the breaking scale of the flavour symmetry, which can be much higher than the electroweak scale. This is, of course, somehow only hiding the problem, but it will make the model fit better.

We now apply the following logic:

1. We impose a flavour symmetry and decouple the flavons in order to end up with an effective low energy model with a scalar sector that is slightly extended compared to the SM. This could, e.g., be a THDM or something similar.

2. This procedure should make the model fit better, because the possible problems that could arise by the flavons are avoided.

3. Since we have gained predictivity by imposing the flavour symmetry, we can fit the model to neutrino data, which allows us to extract certain ranges for the model parameters.

4. The model, however, still has additional scalars compared to the SM, which will be able to mediate LFV-processes, whose branching ratios can be predicted using the fitted parameter values.

5. If this prediction does not fit with present (future) LFV-bounds, we are (will be) able to exclude the particular flavour symmetry imposed (in a certain scenario). Note that this logic will also hold in the non-decoupling case if no extreme fine-tuning is involved.

In principle, this could work for any model with a slightly extended scalar sector. If the structure of the model is not extremely peculiar, which is rarely the case in the scalar sector of a theory, the additional scalars (compared to the SM) will unavoidably lead to LFV-processes, which are already strongly constrained. The key point is that these constraints are so strong that imposing some more structure by adding a flavour symmetry can easily destroy the consistency of the model with all data.

Here, we want to present such an analysis for one particular example, namely for Ma's scotogenic model [175], as this consists of a very minimal extension of the SM. Furthermore, it has not too many possible LFV-diagrams, so that our logic is not shadowed by a heavy calculational apparatus. In this model, one can see immediately the effect of certain symmetries: Without imposing a flavour symmetry, one constrains quantities like

$$|h^*_{11}h_{21} + h^*_{12}h_{22} + h^*_{13}h_{23}| \tag{5.79}$$

by LFV-processes like $\mu \to e\gamma$ [176], where h is the Yukawa coupling matrix involved. Such a combination can easily become zero for unfortunate values of some phases, exactly as the effective neutrino mass in neutrino-less double beta processes [92], cf. Sec. 4.2.1. Imposing relations between certain elements of h hinders such cancellations to appear, and the term in Eq. (5.79) will generically be much larger than zero.

We want to stress, however, that this particular model is just an example and that our idea may work for a much wider class of models.

5.7 The Ma-model

There are a lot of different models for neutrino mass generation on the market [177]. A difficult task for all of them is to explain the smallness of neutrino masses compared to other particles in Nature that we know.

One way is to forbid a tree-level mass term for neutrinos and generate neutrino masses only by radiative corrections, as done in several models [175,177–181]. Out of those, Ma's *scotogenic model* [175] (that we call *Ma-model* for simplicity) is particularly attractive: By adding only one additional Higgs doublet and heavy right-handed neutrinos to the SM, as well as imposing an additional Z_2-symmetry, it allows for sufficiently small neutrino masses. These masses are generated radiatively, because the additional neutral Higgs does not obtain a VEV that could lead to a tree-level neutrino mass term. Furthermore, due to the Z_2-symmetry, this model also

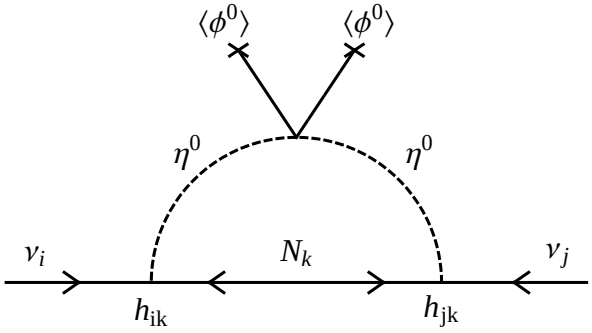

Figure 5.3: The radiative generation of a light neutrino mass term in the Ma-model.

provides a stable Dark Matter candidate, namely the lightest of the heavy neutrinos [182] or the lightest neutral scalar [183] (essentially, this Z_2-symmetry plays the same role as R-parity in SUSY). Constraints on the model arise from various different sources as, e.g., lepton flavour violation or the Dark Matter abundance [176]. In that sense, this model is very "complete". Furthermore, this model arises very naturally in a left-right symmetric framework [14].

The basic ingredients of the Ma-model apart from the SM are:

- 3 heavy right-handed (Majorana) neutrinos N_k, which are singlets under $SU(2)$ and have no hypercharge
- a second Higgs doublet η with SM-like quantum numbers that does not obtain a VEV
- an additional Z_2-parity under which all SM-particles are even, while N_k as well as η are odd

The corresponding Higgs potential looks like

$$V = m_1^2\phi^\dagger\phi + m_2^2\eta^\dagger\eta + \frac{\lambda_1}{2}(\phi^\dagger\phi)^2 + \frac{\lambda_2}{2}(\eta^\dagger\eta)^2 + \lambda_3(\phi^\dagger\phi)(\eta^\dagger\eta) + \lambda_4(\phi^\dagger\eta)(\eta^\dagger\phi) + \frac{\lambda_5}{2}\left[(\phi^\dagger\eta)^2 + h.c.\right], \tag{5.80}$$

where ϕ is the SM-Higgs. If $m_1^2 < 0$ and $m_2^2 > 0$, then only ϕ^0 will obtain a VEV $v = 174$ GeV, while $\langle\eta^0\rangle = 0$. The Yukawa Lagrangian is given by

$$\mathcal{L}_Y = f_{ij}\left(\phi^- \nu_i + (\phi^0)^* l_i\right) e_j^c + h_{ij}(\eta^0\nu_i - \eta^+ l_i)N_j + h.c., \tag{5.81}$$

which does not lead to a tree-level neutrino mass term, due to the vanishing VEV of the η^0. The neutrino masses can, however, be generated radiatively, which gives a natural suppression of the scale of the neutrino mass eigenvalues and can exploit the heaviness of the N_k (with masses M_k) as well. The mass matrix of the light neutrinos is generated from the diagram in Fig. 5.3 and reads

$$(\mathcal{M}_\nu)_{ij} = \sum_{k=1}^{3} h_{ik}h_{jk}\Lambda_k, \tag{5.82}$$

where

$$\Lambda_k = \frac{M_k}{16\pi^2}\left[\frac{m^2(H^0)}{m^2(H^0) - M_k^2}\ln\left(\frac{m^2(H^0)}{M_k^2}\right) - \frac{m^2(A^0)}{m^2(A^0) - M_k^2}\ln\left(\frac{m^2(A^0)}{M_k^2}\right)\right]. \tag{5.83}$$

Note that we have named the Higgses like in a general THDM [184], with

$$\alpha = \beta = m_{12} = \lambda_{6,7} = 0. \tag{5.84}$$

Field	$l_{1,2,3}$	e_1^c	e_2^c	e_3^c	$N_{1,2,3}$	ϕ	η	φ_S	φ_T	χ
A_4	$\underline{\mathbf{3}}$	$\underline{\mathbf{1}}$	$\underline{\mathbf{1}}''$	$\underline{\mathbf{1}}'$	$\underline{\mathbf{3}}$	$\underline{\mathbf{1}}$	$\underline{\mathbf{1}}$	$\underline{\mathbf{3}}$	$\underline{\mathbf{3}}$	$\underline{\mathbf{1}}$
Z_4^{aux}	i	i	i	i	-1	1	1	i	-1	i

Table 5.2: The particle content of Model 1. The SM particles are the three left-handed lepton $SU(2)_L$ doublets l_i, the right-handed charged leptons e_i^c, and the SM-Higgs ϕ. The BSM particles are the right-handed neutrinos N_i, the second Higgs doublet η (which does not obtain a VEV), and the flavons φ_S, φ_T, and χ, that only transform under $A_4 \times Z_4^{\text{aux}}$.

The physical Higgs masses are given by

$$m^2(h^0) = 2\lambda_1 v^2,\ m^2(H^0) = m_2^2 + (\lambda_3+\lambda_4+\lambda_5)v^2,\ m^2(A^0) = m_2^2 + (\lambda_3+\lambda_4-\lambda_5)v^2,$$
$$\text{and } m^2(H^\pm) = m_2^2 + \lambda_3 v^2. \tag{5.85}$$

5.8 Imposing discrete flavour symmetries

In the following, we will present two models which constrain the structure of the Yukawa coupling matrix h in Eq. (5.81), without discussing a particular mechanism for vacuum alignment.[7] The first one, based on Refs. [185, 186], represents the class of models which predicts tri-bimaximal mixing. The second one represents the class which predicts μ-τ symmetry. Details on the group theory of A_4 and D_4 can be found in Ref. [12].

5.8.1 The A_4-model (Model 1)

The particle content of this model is given in Tab. 5.2. The Lagrangian which is invariant under the flavour symmetry $A_4 \times Z_4^{\text{aux}}$ reads[8]

$$\begin{aligned}
\mathcal{L}_l \;=\;& y_1^e \frac{\phi}{\Lambda}(l_1\varphi_{T1} + l_2\varphi_{T3} + l_3\varphi_{T2})e_1^c + y_2^e \frac{\phi}{\Lambda}(l_3\varphi_{T3} + l_1\varphi_{T2} + l_2\varphi_{T1})e_2^c \\
&+ y_3^e \frac{\phi}{\Lambda}(l_2\varphi_{T2} + l_1\varphi_{T3} + l_3\varphi_{T1})e_1^c + \frac{\eta}{\Lambda}\Big[y_1[(2l_1N_1 - l_2N_3 - l_3N_2)\varphi_{S1} \\
&+ (2l_3N_3 - l_1N_2 - l_2N_1)\varphi_{S3} + (2l_2N_2 - l_1N_3 - l_3N_1)\varphi_{S2}] \\
&+ y_2(l_1N_1 + l_2N_3 + l_3N_2)\chi\Big] + M(N_1N_1 + N_2N_3 + N_3N_2).
\end{aligned} \tag{5.86}$$

Let us assume that the flavons obtain their VEVs as follows,

$$\begin{pmatrix} \langle\varphi_{S1}\rangle \\ \langle\varphi_{S2}\rangle \\ \langle\varphi_{S3}\rangle \end{pmatrix} = w_S \begin{pmatrix} 1 \\ 1 \\ 1 \end{pmatrix},\quad \begin{pmatrix} \langle\varphi_{T1}\rangle \\ \langle\varphi_{T2}\rangle \\ \langle\varphi_{T3}\rangle \end{pmatrix} = w_T \begin{pmatrix} 1 \\ 0 \\ 0 \end{pmatrix},\quad \text{and } \langle\chi\rangle = u\,, \tag{5.87}$$

and the SM Higgs gets the VEV $\langle\phi^0\rangle = v$. Then, the Yukawa coupling matrix and the right-handed neutrino mass matrix for Model 1 can be written as

$$h = \begin{pmatrix} 2a+b & -a & -a \\ -a & 2a & b-a \\ -a & b-a & 2a \end{pmatrix} \text{ and } M_R = M\begin{pmatrix} 1 & 0 & 0 \\ 0 & 0 & 1 \\ 0 & 1 & 0 \end{pmatrix}, \tag{5.88}$$

[7] In general, the vacuum alignment can be achieved by a minimization of the scalar potential.

[8] Here, we neglect the anti-symmetric part of the coupling between l and N or assume that the anti-symmetric coupling vanishes, which is done similarly in Ref. [186].

where $a = y_1 \frac{w_S}{\Lambda}$ and $b = y_2 \frac{u}{\Lambda}$.
The charged lepton mass matrix in this model is diagonal,

$$m_e = \frac{v}{\Lambda} y_1^e w_T,\ m_\mu = \frac{v}{\Lambda} y_2^e w_T,\ m_\tau = \frac{v}{\Lambda} y_3^e w_T. \tag{5.89}$$

Here, the hierarchies in the charged lepton masses are determined by the Yukawa couplings. Assuming that the Yukawa coupling of the τ, y_3^e, is of $\mathcal{O}(1)$ and the Higgs VEV v is 174 GeV, we can determine the ratio of the flavon over the cutoff scale Λ ($\frac{\langle f \rangle}{\Lambda}$) as being of the order of the Cabibbo angle squared, $\lambda^2 \sim 0.04$.

In order to simplify the discussion, we go to the basis where the right-handed neutrino mass matrix is diagonal. The matrix $M_R M_R^\dagger$ is diagonalized by the unitary matrix U_r

$$U_r = \begin{pmatrix} 0 & 0 & 1 \\ 0 & 1 & 0 \\ 1 & 0 & 0 \end{pmatrix}. \tag{5.90}$$

Note that the right-handed neutrino masses are degenerate, $M_{1,2,3} = M$.

The Yukawa coupling in this basis reads

$$h' = h U_r = \begin{pmatrix} -a & -a & 2a+b \\ b-a & 2a & -a \\ 2a & b-a & -a \end{pmatrix}. \tag{5.91}$$

Using Eq. (5.82), the neutrino mass matrix can be written as

$$M_\nu = \Lambda_{1,2,3} \begin{pmatrix} (6a^2+4ab+b^2) & -a(3a+2b) & -a(3a+2b) \\ -a(3a+2b) & (6a^2-2ab+b^2) & a(-3a+4b) \\ -a(3a+2b) & a(-3a+4b) & (6a^2-2ab+b^2) \end{pmatrix}, \tag{5.92}$$

where $\Lambda_{1,2,3} = \Lambda_1 = \Lambda_2 = \Lambda_3$, and the squared neutrino masses are given by the eigenvalues of $M_\nu M_\nu^\dagger$:

$$m_1^2 = (3a+b)^4 \Lambda_{1,2,3}^2,\ \ m_2^2 = b^4 \Lambda_{1,2,3}^2,\ \text{ and } m_3^2 = (-3a+b)^4 \Lambda_{1,2,3}^2, \tag{5.93}$$

which correspond to the eigenvectors $(-2,1,1)^T/\sqrt{6}$, $(1,1,1)^T/\sqrt{3}$, and $(0,-1,1)^T/\sqrt{2}$, respectively. In this model, the neutrino masses obey normal mass ordering.

The neutrino mixing observables look like:

$$\Delta m_\odot^2 = (b^4 - (3a+b)^4)\Lambda_{1,2,3}^2,\ \Delta m_A^2 = -24ab(9a^2+b^2)\Lambda_{1,2,3}^2,\ \tan\theta_{12} = \frac{1}{\sqrt{2}},\ \theta_{13} = 0,\ \text{and } \theta_{23} = \frac{\pi}{4}. \tag{5.94}$$

In this model, we have only three free parameters (a, b, M) to fit all observables. Therefore, this model is quite predictive (and hence harder to fit).

5.8.2 The D_4-model (Model 2)

The particle content of this model is given in Tab. 5.3. The Lagrangian which is invariant under the flavour symmetry $D_4 \times Z_2^{\text{aux}}$ reads

$$\begin{aligned} \mathcal{L}_l \ = \ & y_1^e l_1 e_1^c \frac{\phi}{\Lambda} \varphi_e + y_2^e (l_2 e_2^c + l_3 e_3^c) \frac{\phi}{\Lambda} \varphi_e + y_3^e (l_2 e_2^c - l_3 e_3^c) \frac{\phi}{\Lambda} \chi_e \\ & + y_1 l_1 N_1 \frac{\eta}{\Lambda} \varphi_\nu + y_2 (l_2 \psi_1 + l_3 \psi_2) N_1 \frac{\eta}{\Lambda} + y_3 (l_2 \psi_2 - l_3 \psi_1) N_2 \frac{\eta}{\Lambda} + y_4 (l_2 \psi_1 - l_3 \psi_2) N_3 \frac{\eta}{\Lambda} \\ & + \frac{1}{2} M_1 N_1 N_1 + \frac{1}{2} M_2 N_2 N_2 + \frac{1}{2} M_3 N_3 N_3. \end{aligned} \tag{5.95}$$

Field	l_1	$l_{2,3}$	e_1^c	$e_{2,3}^c$	N_1	N_2	N_3	ϕ	η	φ_e	χ_e	φ_ν	$\psi_{1,2}$
D_4	$\underline{\mathbf{1_1}}$	$\underline{\mathbf{2}}$	$\underline{\mathbf{1_3}}$	$\underline{\mathbf{2}}$	$\underline{\mathbf{1_3}}$	$\underline{\mathbf{1_2}}$	$\underline{\mathbf{1_4}}$	$\underline{\mathbf{1_1}}$	$\underline{\mathbf{1_1}}$	$\underline{\mathbf{1_3}}$	$\underline{\mathbf{1_4}}$	$\underline{\mathbf{1_3}}$	$\underline{\mathbf{2}}$
$Z_2^{\rm aux}$	1	1	1	1	-1	-1	-1	1	1	1	1	-1	-1

Table 5.3: The particle content of Model 2. Th SM particles are the three left-handed lepton $SU(2)_L$ doublets l_i, the right-handed charged leptons e_i^c, and the SM-Higgs ϕ. The BSM particles are the right-handed neutrinos N_i, second Higgs doublet η (which does not obtain a VEV),and the flavons φ_e, χ_e, φ_ν, and ψ_i, that only transform under $D_4 \times Z_2^{\rm aux}$.

Let us assume that the flavons obtain their VEVs as follows:

$$\langle\varphi_e\rangle = u_e,\ \ \langle\chi_e\rangle = -w_e,\ \ \langle\varphi_\nu\rangle = u\ ,\ \text{ and }\ \begin{pmatrix}\langle\psi_1\rangle\\ \langle\psi_2\rangle\end{pmatrix} = w\begin{pmatrix}1\\ -1\end{pmatrix}, \tag{5.96}$$

and the SM Higgs gets the VEV $\langle\phi^0\rangle = v$. Then, the Yukawa coupling matrix for Model 2 can be written as

$$h = \begin{pmatrix} a & 0 & 0\\ b & -c & d\\ -b & -c & d\end{pmatrix}, \tag{5.97}$$

where $a = y_1\frac{u}{\Lambda}$, $b = y_2\frac{w}{\Lambda}$, $c = y_3\frac{w}{\Lambda}$, and $d = y_4\frac{w}{\Lambda}$.

The charged lepton and right-handed neutrino mass matrices in this model are diagonal,

$$m_e = \frac{v}{\Lambda}y_1^e u_e,\ m_\mu = \frac{v}{\Lambda}(y_2^e u_e - y_3^e w_e),\ m_\tau = \frac{v}{\Lambda}(y_2^e u_e + y_3^e w_e). \tag{5.98}$$

Here, the hierarchy between the masses of e and (μ,τ) arises from the smallness of the Yukawa coupling y_1^e. As we did for Model 1, we assume that the ratio $(\frac{\langle f\rangle}{\Lambda})$ is of order $\lambda^2 \sim 0.04$. Using Eq. (5.82), the neutrino mass matrix can be written as

$$M_\nu = \begin{pmatrix} a^2\Lambda_1 & ab\Lambda_1 & -ab\Lambda_1\\ ab\Lambda_1 & b^2\Lambda_1 + c^2\Lambda_2 + d^2\Lambda_3 & -b^2\Lambda_1 + c^2\Lambda_2 + d^2\Lambda_3\\ -ab\Lambda_1 & -b^2\Lambda_1 + c^2\Lambda_2 + d^2\Lambda_3 & b^2\Lambda_1 + c^2\Lambda_2 + d^2\Lambda_3\end{pmatrix}. \tag{5.99}$$

The squared neutrino masses are given by the eigenvalues of $M_\nu M_\nu^\dagger$,

$$m_1^2 = 0,\ \ m_2^2 = (a^2+2b^2)^2\Lambda_1^2,\ \text{ and } m_3^2 = 4(c^2\Lambda_2 + d^2\Lambda_3)^2, \tag{5.100}$$

which correspond to the eigenvectors

$$\frac{a}{\sqrt{2(a^2+2b^2)}}(2b/a,-1,1)^T,\ \frac{b}{\sqrt{2(a^2+2b^2)}}(-b/a,1,1)^T,\ \text{and } (0,1,1)^T/\sqrt{2}, \tag{5.101}$$

respectively. In this model, the neutrino masses will obey normal ordering.

The neutrino mixing observables look like:

$$\Delta m^2_\odot = (a^2+2b^2)^2\Lambda_1^2,\ \Delta m^2_A = 4(c^2\Lambda_2+d^2\Lambda_3)^2,\ \tan\theta_{12} = \frac{a}{\sqrt{2}b},\ \theta_{13} = 0,\ \text{and } \theta_{23} = \frac{\pi}{4}. \tag{5.102}$$

In this model, we have 7 free parameters (a,b,c,d,M_1,M_2,M_3) to fit all neutrino observables. This makes Model 2 much easier to fit, but we of course pay the price of losing predictivity.

5.9 The numerical analysis

5.9.1 The general procedure

In this section, we describe the analysis procedure that has been applied. The first point to mention is that there are constraints that are required for a THDM like in Eq. (5.80) ($\lambda_1 > 0$, $\lambda_2 > 0$, $\lambda_3 > -\sqrt{\lambda_1\lambda_2}$, and $\lambda_3 + \lambda_4 - |\lambda_5| > -\sqrt{\lambda_1\lambda_2}$; they essentially keep the Higgs potential stable) as well as consistency conditions for a Ma-like model ($m_1^2 < 0$ and $m_2^2 > 0$; these are necessary in order for ϕ^0 to obtain a VEV, while η^0 obtains none). Furthermore, there are limits from direct searches at collider experiments [187]: $m(h^0) > 112.9$ GeV and $m(H^\pm) > 78.6$ GeV, both at 95% C.L.[9] Further constraints arise from the W- and Z-boson decay widths, namely $m(H^\pm) + m(H^0) > M_W$, $m(H^\pm) + m(A^0) > M_W$ and $2m(H^\pm) > M_Z$, $m(H^0) + m(A^0) > M_Z$, as well as from the requirement of perturbativity for the Higgs potential, $\lambda_2 < 1$ and $\lambda_3^2 + (\lambda_3 + \lambda_4)^2 + \lambda_5^2 < 12\lambda_1^2$ [183].

Strong constraints also come from the correction to the ρ-parameter [188]. The explicit formula for this correction reads

$$\Delta\rho = \frac{\alpha(M_Z)}{16\pi s_W^2 M_W^2} \cdot \left[F\left(m_2^2, m^2(H^0)\right) + F\left(m_2^2, m^2(A^0)\right) - F\left(m^2(H^0), m^2(A^0)\right)\right], \tag{5.103}$$

where

$$F(x,y) = \begin{cases} \frac{x+y}{2} - \frac{xy}{x-y}\ln\frac{x}{y}, & \text{for } x \neq y, \\ 0, & \text{for } x = y, \end{cases} \tag{5.104}$$

and $\alpha(M_Z) = 1/127.9$. The experimental constraint is [15]

$$\Delta\rho = -0.0006 \pm 0.0008, \tag{5.105}$$

which cuts the allowed parameter space for the Ma-model. Since we want to focus on neutrino physics and lepton flavour violation, we do not try to fit the Higgs sector as well, but rather use four different benchmark scenarios that all fulfill the consistency conditions, as well as the experimental bounds from direct searches and from the measurement of the correction to the ρ-parameter (at 3σ). In the form $(m_1, m_2, \lambda_1, \lambda_2, \lambda_3, \lambda_4, \lambda_5)$, these scenarios are:

$$\begin{aligned} \alpha: &\quad (100i\text{GeV}, 75\text{GeV}, 0.24, 0.10, 0.10, -0.15, -0.10) \\ \beta: &\quad (100i\text{GeV}, 98.5\text{GeV}, 0.24, 0.30, 0.09, -0.18, -0.11) \\ \gamma: &\quad (100i\text{GeV}, 950\text{GeV}, 0.24, 0.50, 0.02, -0.12, -0.10) \\ \delta: &\quad (100i\text{GeV}, 550\text{GeV}, 0.24, 0.30, 0.02, -0.05, -0.01) \end{aligned} \tag{5.106}$$

The corresponding Higgs masses are given in Tab. 5.4. Note that these four scenarios are also consistent with the 3σ-range of WMAP-data for H^0 being the Dark Matter candidate [183], which is why we have chosen them that way. This also leads to some more consistency conditions, as H^0 has to be the lightest of all scalars and it also has to be lighter than the heavy right-handed neutrinos.

For all these scenarios, we do the following:

1. First, the models are fitted to neutrino oscillation data, i.e., mixing angles and mass square differences [23]. This is done by the χ^2-function

$$\chi^2 = \sum_{i=1}^{N} \frac{(q_i - q_i^{\text{exp}})^2}{\sigma_i^2}, \tag{5.107}$$

[9] Note that these constraints do not apply to the *inert* Higgses H^0 and A^0. They are constrained much less severely by the current limits, differently from a normal THDM.

Scenario	$m(h^0)$	$m(H^0)$	$m(A^0)$	$m(H^\pm)$
α	120.0	32.9	84.5	93.0
β	120.0	60.4	101.5	111.5
γ	120.0	946.8	950.0	950.3
δ	120.0	548.9	549.4	550.6

Table 5.4: The Higgs masses (in GeV) for the different scenarios defined in Eq. (5.106).

Quantity	$\Delta m^2_\odot$	$(\Delta m^2_A)_{\text{nor.}}$	θ_{12}	θ_{13}	θ_{23}
Best-fit	$7.67 \cdot 10^{-5}$ eV^2	$2.46 \cdot 10^{-3}$ eV^2	$34.5°$	$0.0°$	$42.3°$
1σ	$2.15 \cdot 10^{-6}$ eV^2	$0.15 \cdot 10^{-3}$ eV^2	$1.4°$	$7.9°$	$4.2°$

Table 5.5: The neutrino mixing parameters (best-fit values and symmetrized 1σ-ranges) obtained by a global fit [23].

where q_i are the observables obtained from neutrino oscillations (θ_{12}, θ_{13}, θ_{23}, Δm^2_A, $\Delta m^2_\odot$), which are calculated in terms of the model parameters (cf. Sec. 5.8). q_i^{exp} are their measured counterparts and σ_i are the corresponding (symmetrized) standard deviations. The best-fit model parameters are determined by a minimization of the χ^2-function. By projection onto the different directions in the parameter space, we determine the 1σ- and 3σ-ranges of the model parameters.

2. Next, we calculate the maximum and minimum values of the quantities measured in different LFV-experiments ($\mu \to e\gamma$, $\tau \to \mu\gamma$, $\tau \to e\gamma$, and μ-e conversion for four different nuclei) by varying the model parameters within their 1σ- and 3σ-ranges.

3. Finally, we compare how well different past and future LFV-experiments are able to constrain or exclude the particular model in the four scenarios.

5.9.2 The χ^2-fit

After outlining the general points, we will explain the procedure in more detail using scenario α (cf. Eq. (5.106)) in connection with Model 1 (cf. Sec. 5.8.1) as example.

The χ^2-function has already been given in Eq. (5.107) and the experimental values and errors of the neutrino observables are summarized in Tab. 5.5. These observables in terms of model parameters have been given in Eq. (5.94). The minimization of the χ^2-function then yields the following best-fit values for the three parameters:

$$a = 0.0189,\ b = -0.691,\ M = 2.42 \cdot 10^6 \text{ GeV}. \tag{5.108}$$

Note that the parameter b is negative to fit the normal mass ordering, cf. Eq. (5.94). In the minimization we have required $M_{1,2,3} > m(H^0)$ and $M_{1,2,3} > M_Z/2$ for consistency reasons.

The 1σ-(3σ-) values for the model parameters are obtained by inserting all values from Eq. (5.108) into the χ^2-function, except for the one parameter that is to be constrained, and by determining the intersections of the remaining 1-dimensional function $\Delta\chi^2 \equiv \chi^2 - \chi^2_{\text{min}}$ with 1(9). For the above parameters, this yields in the form $^{+1\sigma,+3\sigma}_{-1\sigma,-3\sigma}$:

$$\begin{aligned} a:&\quad {}^{+0.0003,+0.0009}_{-0.0003,-0.0009}, \\ b:&\quad {}^{+0.003,+0.009}_{-0.003,-0.009}, \\ M:&\quad {}^{+0.02,+0.05}_{-0.02,-0.05} \cdot 10^6 \text{ GeV}. \end{aligned} \tag{5.109}$$

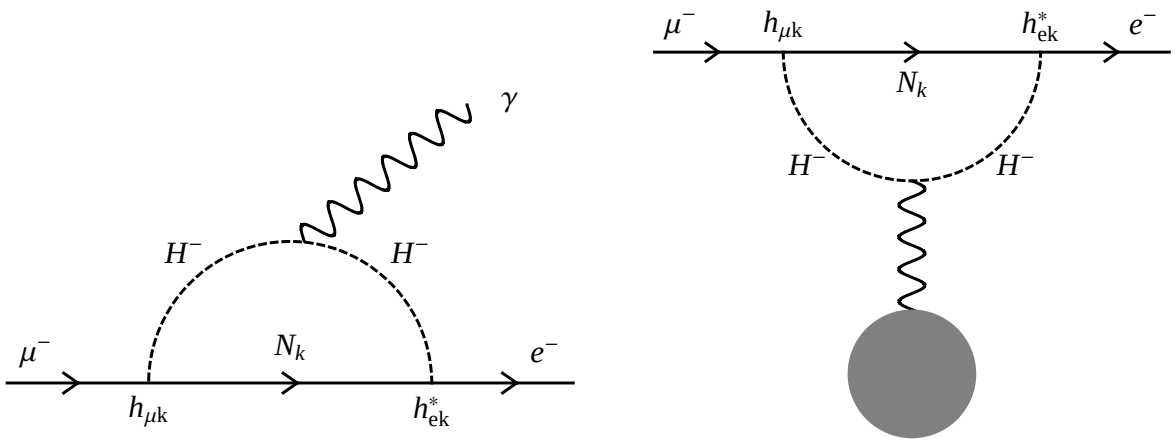

Figure 5.4: The diagrams for $\mu \to e\gamma$ and μ-e conversion in the Ma-model.

These are the ranges that we will use in the subsequent analysis. Note that in this model, they are already quite narrow, which is a manifestation of the fact that this model holds a lot of structure.

5.9.3 Predictions for various LFV-experiments

The most important types of LFV-experiments are rare lepton decays, $e_i \to e_j\gamma$, as well as conversions of a bound muon to an electron for some nucleus N, $\mu N \to eN$. In a Ma-like model, the processes of $\mu \to e\gamma$ and μ-e conversion are essentially given by the same diagram, cf. Fig. 5.4, which is in one case simply attached to a nucleus. Accordingly, the decisive quantities for both types of processes are given by [131] ($ij = e_i \to e_j\gamma$/e_i-e_j-conversion):

$$\sigma_{ij} \equiv \frac{-i}{2m^2(H^\pm)} \sum_{k=1}^{3} h^*_{jk} h_{ik} \left[(m_i + m_j) I_a \left(\frac{M_k^2}{m^2(H^\pm)} \right) + M_k I_b \left(\frac{M_k^2}{m^2(H^\pm)} \right) \right], \tag{5.110}$$

where

$$I_a(t) = \frac{1}{16\pi^2} \left[\frac{2t^2 + 5t - 1}{12(t-1)^3} - \frac{t^2 \ln t}{2(t-1)^4} \right] \text{ and } I_b(t) = \frac{1}{16\pi^2} \left[\frac{t+1}{2(t-1)^2} - \frac{t \ln t}{(t-1)^3} \right]. \tag{5.111}$$

Using these, the branching ratios are obtained as

$$\mathrm{Br}(e_i \to e_j\gamma) = \frac{m_i^3}{8\pi} \frac{|\sigma_{ij}|^2}{\Gamma(e_i \to e_j \nu_i \overline{\nu}_j)} \text{ and } \mathrm{Br}(\mu N \to eN) = \frac{\pi^2}{2^5 m_\mu^2} \frac{D_N^2}{\omega_{\mathrm{capt}}(N)} |\sigma_{\mu e}|^2. \tag{5.112}$$

Note that, in the first formula, we have neglected the final state lepton mass. The quantities D_N and $\omega_{\mathrm{capt}}(N)$, as well as a general expression for the second formula are given in Ref. [189].

We then use the parameter ranges from Eq. (5.109) to make predictions with Eq. (5.112). The result is included in Fig. 5.5. Furthermore, we have put in the limits/sensitivities of several past/future experiments, all listed in Tab. 5.6. A further discussion of the results will be given in the next section.

5.9.4 Results

We will now discuss how the general conflict between an extended scalar sector and flavour symmetries looks in our example models.

Experiment	Status	Process	BR-Limit/Sensitivity
MEGA	Past	$\mu \to e\gamma$	$1.2 \cdot 10^{-11}$
MEG	Future	$\mu \to e\gamma$	$1.0 \cdot 10^{-13}$
BELLE	Past	$\tau \to \mu\gamma$	$4.5 \cdot 10^{-8}$
Babar	Past	$\tau \to e\gamma$	$1.1 \cdot 10^{-7}$
MECO	Cancelled	$\mu\text{Al} \to e\text{Al}$	$2.0 \cdot 10^{-17}$
SINDRUM II	Past	$\mu\text{Ti} \to e\text{Ti}$	$6.1 \cdot 10^{-13}$
PRISM/PRIME	Future	$\mu\text{Ti} \to e\text{Ti}$	$5.0 \cdot 10^{-19}$
SINDRUM II	Past	$\mu\text{Au} \to e\text{Au}$	$7.0 \cdot 10^{-13}$
SINDRUM II	Past	$\mu\text{Pb} \to e\text{Pb}$	$4.6 \cdot 10^{-11}$

Table 5.6: Limits on the branching ratios for several past and future LFV-experiments [139].

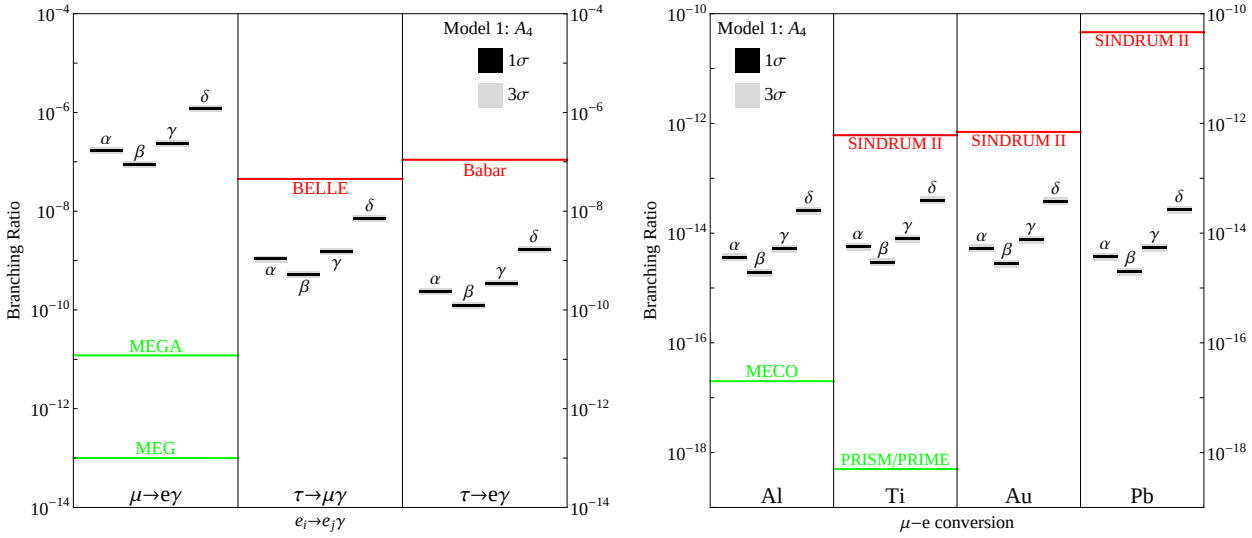

Figure 5.5: The numerical results of our analysis for Model 1.

Let us start with Model 1. The numerical results can be seen in Fig. 5.5: On the left panel, we present the 1σ (black) and 3σ (gray) predictions of Model 1 for the processes $\mu \to e\gamma$, $\tau \to \mu\gamma$, and $\tau \to e\gamma$, as well as different present and future bounds from several experiments, cf. Tab. 5.6. The right panel shows the same for μ-e conversion on the elements Al, Ti, Au, and Pb.

Model 1 is the prime example that our logic works: As explained in Sec. 5.8.1, there are only three free parameters in the model. Still, it is able to fit the neutrino data well. Actually, the only deviations from a perfect fit arise from the very accurate prediction of the mixing angles (e.g., the experimental best-fit value of θ_{23} is not exactly maximal; cf. Eq. (5.94) and Tab. 5.5). The obtained parameter ranges are, however, quite narrow, as can be seen from the example given in Sec. 5.9.2. This is exactly the point, where the experimental limits on LFV-processes get really powerful: Due to the stiffness in the model parameter space, the prediction of, e.g., the branching ratio $\mu \to e\gamma$ is so clear, that only a very narrow window is left for parameter variations. Accordingly, this model is actually already excluded by the past MEGA experiment (cf. Fig. 5.5) for all four Higgs scenarios from Eq. (5.106). We want to stress again that these four scenarios belong to the few regions in parameter space that are indeed consistent with all the data and constraints mentioned in Sec. 5.6.1. The branching ratios for μ-e conversion are in general lower, and pass all current constraints. However, in this sector PRISM/PRIME will provide another future bound that will be able to exclude this model.

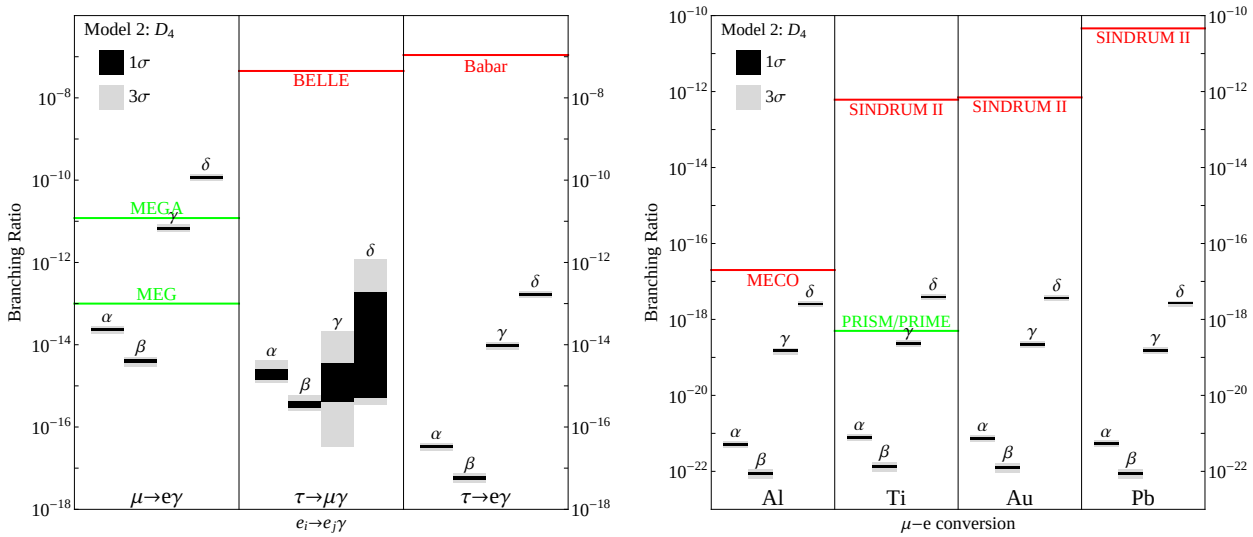

Figure 5.6: The numerical results of our analysis for Model 2.

The remaining question is how far we can stretch this logic for models with less and less predictivity. As example for that case we can use Model 2, which has seven free parameters to fit the data (cf. Sec. 5.8.2). This more than doubles the degrees of freedom in the fit.

The numerical results for this model are given in Fig. 5.6. First of all, it may look odd that here, all 1σ and 3σ regions are somehow narrow, except for $\tau \to \mu\gamma$. This is simply because all branching ratios are essentially functions of the product $|ab|$ (where a and b are model parameters), while the one for $\tau \to \mu\gamma$ is given by the sum of three contributions, which are proportional to $|b|^2$, $|c|^2$, and $|d|^2$, respectively. This numerical example nicely shows how more freedom blows up the regions which are predicted by a certain model. Turning this argumentation around, a certain limit on some observable is weaker the more free parameters there are that influence the observable in question.

However, even this model with much less predictivity than the one before can be excluded for some scenarios: Scenario δ has already been excluded by the MEGA-experiment and scenario γ can be tested by MEG. This shows the strength of our considerations: Even for a model that has a lot of freedom our logic still applies in suitable settings, which are here given by the scenarios γ and δ. Actually, even the scenarios α and β are not that far below the future MEG-bound, and especially a hypothetical future experiment aiming at $\tau \to \mu\gamma$ might be very suitable to exclude this particular model.

5.10 Radiative transmission of lepton flavour hierarchies

Finally, we also present a natural explanation of the patterns in the flavour sector that can arise in the framework of the Ma-model, when it is embedded into an LR-symmetry [14], cf. Secs. 5.3.5 and 5.4.3.

5.10.1 The basics of the model

Our model is based on the left-right (LR) symmetric group [148,149,190–192] $SU(2)_L \times SU(2)_R \times U(1)_{B-L}$, supplemented by a discrete symmetry Z_4. Quarks and leptons are assigned as in the minimal LR-model to left-right symmetric doublets. The symmetry breaking is implemented as in the minimal LR model by the Higgs fields $\Phi(2,2,0)$ and $\Delta_R(1,3,+2) \oplus \Delta_L(3,1,+2)$.

Fields	Z_4 charge
Q_R	$-i$
L_R	$+i$
Φ	$+i$
$\tilde{\Phi} \equiv \sigma_2 \Phi^* \sigma_2$	$-i$
Δ_R	-1

Table 5.7: The non-trivial Z_4-charges in the model.

In the leptonic sector, the $SU(2)_R \times U(1)_{B-L}$ breaking by the right handed triplet with $B - L = 2$ gives large Majorana masses to the heavy neutrinos [193]. Unlike in the usual implementation of the seesaw formula however, the Dirac mass for neutrinos vanishes to all orders in perturbation theory due to the Z_4 symmetry, whose effect on the various fields is given in the Tab. 5.7. This already points in the direction that the Z_4-symmetry plays a similar role like the Z_2 in the pure Ma-model, cf. Sec. 5.7. The other fields are assumed to be singlets of Z_4. The most general potential for the left-right model has been discussed in Ref. [148]. The presence of the Z_4 symmetry in our model forbids, e.g., terms linear in $\mathrm{Tr}(\tilde{\Phi}^\dagger \Phi)$ for the potential, so that the minimum energy configuration corresponds to the following special VEV-structure for the Φ field:

$$\langle \Phi \rangle = \begin{pmatrix} \kappa & 0 \\ 0 & 0 \end{pmatrix}. \tag{5.113}$$

For the $\Delta_{L,R}$ fields we have

$$\langle \Delta_R^0 \rangle = \begin{pmatrix} 0 & 0 \\ v_R & 0 \end{pmatrix}, \text{ and } \langle \Delta_L^0 \rangle = \begin{pmatrix} 0 & 0 \\ 0 & 0 \end{pmatrix}. \tag{5.114}$$

The gauge invariant Yukawa couplings of the above Z_4 supplemented LR-model look like

$$\mathcal{L}_Y = h_q \bar{q}_L \Phi q_R + h_l \bar{l}_L \tilde{\Phi} l_R + \left[f(l_R^T \Delta_R l_R + l_L^T \Delta_L l_L) + h.c. \right]. \tag{5.115}$$

By an appropriate choice of the basis, we can choose $h_{q,l}$ to be diagonal without loss of generality in this. It is easy to see that, with the above assignment, we get a zero Dirac neutrino mass m_D. The diagonal Yukawa coupling matrix h_l (cf. Eq. (5.81)) is given by $h_l = \mathrm{diag}(m_e, m_\mu, m_\tau)/v$. We also note that there is no type II seesaw [194–197] contribution to the neutrino masses, unlike in usual left-right models. The minimum of the potential is stable under radiative corrections, because after symmetry breaking, there is a remnant Z_2-symmetry present under which all fields are even except for η and N_R [14]. Hence, below the $SU(2)_R \times U(1)_{B-L}$-breaking scale, the model is a just an effective Ma-model with the correct Z_2-assignment, cf. Sec. 5.7.

5.10.2 A seesaw-like formula for Neutrino masses

At tree-level both, neutrino Dirac masses and the down quark masses vanish. As far as neutrinos are concerned, they pick up just the correct mass from the diagram in Fig. 5.3. We can first write Eq. (5.82) as

$$(\mathcal{M}_\nu)_{ij} = m_{l,i} \Lambda_{ij} m_{l,j}, \tag{5.116}$$

where $m_l = \mathrm{diag}(m_e, m_\mu, m_\tau)$, and Λ_{ij} is given by Eq. (5.83) with $M_k \to M_{ij}$ (in this basis, the heavy neutrino mass matrix is not diagonal anymore). Under the assumption $m^2(H^0) \ll M_k^2$, we effectively have

$$\Lambda_{ij}(\lambda', M_{N,ij}) \simeq \frac{2}{16\pi^2} \frac{\lambda_5}{M_{ij}^2} \ln \left(\frac{M_{N,ij}^2}{m^2(H^0)} \right). \tag{5.117}$$

Absorbing $\ln\left(\frac{M_{N,ij}^2}{m^2(H^0)}\right)$ into M_N^{-1} (which can be done without loss of generality) we can write

$$(\mathcal{M}_\nu)_{ij} = \frac{2\lambda_5}{16\pi^2} m_{l,i} \left(M_N^{-1}\right)_{ij} m_{l,j}. \tag{5.118}$$

Since we have a rough idea about the form of the neutrino mass matrix in the limit of zero CP-phase δ and small reactor angle θ_{13}, we can use it to get an idea about the elements of the RH neutrino mass matrix. It is interesting that all elements of this mass matrix can be determined.

5.10.3 The mechanism of radiative transmission

A numerical fit of the heavy neutrino mass matrices to current neutrino data is given in Ref. [14]. In both cases, normal and inverted mass hierarchy, there is a strong hierarchy in the heavy neutrino sector in a way similar to the charged lepton sector. This is what we label as the *radiative transmission of hierarchy* from the charged leptons to the heavy neutrinos (or vice versa). Note that this mechanism, given a certain form of M_N (with small mixings), naturally allows for large mixing angles in the SM lepton sector, that are not necessarily maximal. This is different from many other models, where in most cases only zero or maximal mixing is predicted.[10]

To see analytically why this happens, let us try to reconstruct M_N from the tri-bimaximal form for the PMNS-matrix [173, 174],

$$U_{\text{PMNS}} = \begin{pmatrix} \sqrt{\frac{2}{3}} & \frac{1}{\sqrt{3}} & 0 \\ -\frac{1}{\sqrt{6}} & \frac{1}{\sqrt{3}} & -\frac{1}{\sqrt{2}} \\ -\frac{1}{\sqrt{6}} & \frac{1}{\sqrt{3}} & \frac{1}{\sqrt{2}} \end{pmatrix}. \tag{5.119}$$

Using this and Eq. (5.118), we can write down M_N as function of λ_5 and of the light neutrino mass eigenvalues $m_{1,2,3}$. It is given by $\frac{\lambda_5}{6m_1m_2m_3}$ times

$$\begin{pmatrix} 2(m_1+2m_2)m_3m_e^2 & 2(m_1-m_2)m_3m_em_\mu & 2(m_1-m_2)m_3m_em_\tau \\ 2(m_1-m_2)m_3m_em_\mu & (3m_1m_2+m_2m_3+2m_1m_3)m_\mu^2 & (-3m_1m_2+m_2m_3+2m_1m_3)m_\mu m_\tau \\ 2(m_1-m_2)m_3m_em_\tau & (-3m_1m_2+m_2m_3+2m_1m_3)m_\mu m_\mu & (3m_1m_2+m_2m_3+2m_1m_3)m_\tau^2 \end{pmatrix}. \tag{5.120}$$

If we assume normal ($m_1 = p^2 m_0$, $m_2 = pm_0$, and $m_3 = m_0$, with small p) or inverted hierarchy ($m_1 = m_0$, $m_2 = m_0$, and $m_3 = pm_0$), the corresponding matrices will roughly look like

$$(M_N)_{\text{NH}} = \frac{\lambda_5}{6p^2m_0} \begin{pmatrix} 4m_e^2 & -2m_em_\mu & -2m_em_\tau \\ -2m_em_\mu & m_\mu^2 & m_\mu m_\tau \\ -2m_em_\tau & m_\mu m_\tau & m_\tau^2 \end{pmatrix} \tag{5.121}$$

and

$$(M_N)_{\text{IH}} = \frac{\lambda_5}{2pm_0} \begin{pmatrix} 2pm_e^2 & 0 & 0 \\ 0 & m_\mu^2 & -m_\mu m_\tau \\ 0 & -m_\mu m_\tau & m_\tau^2 \end{pmatrix}. \tag{5.122}$$

Note that the reconstruction of the matrices from Eqs. (5.121) and (5.122) has led us to heavy neutrino mass matrices which are hierarchical and stiff. Furthermore, the μ-τ symmetry [167]

[10] Note however, that there are also exceptions to this: E.g., the size of the mixing angle could be determined by underlying discrete symmetries [198], or it could arise from an anarchical pattern of the neutrino mass matrix [199].

from Eq. (5.120) translates into a pattern in the lower right 2×2-part of M_N. In all cases, having a light neutrino mass close to zero ($p \to 0$ in Eqs. (5.121) and (5.122)) can only increase this hierarchy, but not destroy it. Especially in Eq. (5.122) the 11-entry is fixed, which means that we will generically have one fixed heavy neutrino mass that is not too large. A similar situation happens for the quasi-degenerate case.

These mass matrices for the heavy neutrinos have a structure that is easily obtainable from the Froggat-Nielsen (FN) mechanism [200], by a $U(1)_H$ flavour symmetry with H charges $(0, 1, 2)$ for the third, second, and first generation right-handed lepton doublets. The LR- and $U(1)_H$-invariant Yukawa couplings in this case can be written as:

$$\mathcal{L}_{Y,H} = h_3^l \bar{l}_{3,L} \tilde{\Phi} l_{3,R} + h_2^l \bar{l}_{2,L} \tilde{\Phi} l_{2,R} \frac{\sigma}{M} + h_1^l \bar{l}_{1,L} \tilde{\Phi} l_{1,R} \left(\frac{\sigma}{M}\right)^2 + \left[\sum_{a,b=1,2,3} f_{ab} l_{a,R}^T \tilde{\Delta} l_{b,R} \left(\frac{\sigma}{M}\right)^{6-(a+b)} + h.c. \right]. \tag{5.123}$$

For an appropriate choice of $\frac{<\sigma>}{M}$ (roughly 1/20 in the NH-case), we get the desired hierarchy in both, the charged lepton masses as well as in the right-handed neutrino sector. This hierarchy then translates into a structure of the light neutrino mass matrix that naturally yields large mixing angles, although no values are excluded a priori.

The first results for this new model seem to be an encouraging, and it will be exiting to see if it survives further testing. In any case, it will be a nice playground for models that can predict flavour structure without invoking discrete flavour symmetries.

Chapter 6

Conclusions

In this thesis, some of the mysterious phenomena of the leptonic sector of the Standard Model of Elementary Particle Physics have been discussed. In the course of the text, we have treated unexplained measurements as well as New Physics.

After giving a brief review of the Standard Model in Chapter 2, we have started in Chapter 3 by discussing a phenomenon that is still unexplained, namely the measurement of a seemingly modulated decay law in Electron Capture decays of different highly charged ions. We have shown that, contrary to first claims, this phenomenon cannot be related to standard neutrino oscillations. This has been argued for using several different pictures and languages, which all led us to the same conclusion. The remaining possibility to cause such a result are Quantum Beats that arise from a splitting in the initial state. This possibility has its problems, too, but is up to now one of the very few viable attempts for an explanation.

Starting with Chapter 4 we have turned our focus to New Physics beyond the Standard Model. The first topic that has been discussed is the possible Majorana nature of the neutrino, which means that the neutrino might be identical to its anti-particle. If this is the case, rare decays like neutrino-less double beta decay will occur unless very unfortunate values of the parameters involved are present. After discussing the interplay of future measurements of such processes with other experiments that will yield information on the neutrino mass, we have performed a detailed calculation of one particular alternative double beta process, namely radiative double Electron Capture. This process can occur via the emission of one or more photons, and it is not a priori clear which mode is dominant. We have performed the calculation of both modes in the same framework to be able to compare the results. It turns out that in some cases the two-photon mode can indeed be favored, or at least be comparable to the emission of one single photon. We have shown this for isotopes with a relatively small Q-value, using an approximation for the two-photon case whose viability we have tested in the calculation of the one-photon mode.

In Chapter 5, we have discussed another phenomenon which generically occurs in theories beyond the Standard Model, namely the violation of lepton flavour. Since there is no deeper reason for lepton flavour to be a conserved quantum number, it is violated in many extensions of the Standard Model. We have first systematically investigated which criteria have to be fulfilled in order for lepton flavour to be conserved or violated. Indeed, one can reduce models, which seem to be relatively complicated from the first sight, to their essentials so that it is very easy to see if lepton flavour violation can occur in the respective model, or not. We have later on turned this logic around and have investigated how well models that have an explanation for patterns that occur in the flavour sector can be constrained by lepton flavour violations experiments. It turns out that models with an extended scalar sector very generically crash with phenomenology, once some structure is introduced (e.g., by discrete flavour symmetries), while they can easily pass all experimental bounds without this additional structure. We have

also shortly discussed a new mechanism that could explain such patterns.

Summing up, we have investigated three of the countless mysteries of the leptonic sector of particle physics. It is clear that, in spite of apparent successes of our theories, we still lack an understanding of many aspects of the elementary particles in Nature. Hopefully this thesis can at least contribute a bit to attack these questions and can be a small one of the many building blocks which are required to manufacture our immense "building" – understanding "what the world contains, In its innermost heart and finer veins".

List of Abbreviations

$0\nu\beta\beta$	=	Neutrino-less double beta decay
BSM	=	Physics beyond the Standard Model
CKM	=	Cabibbo-Kobayashi-Maskawa
EC	=	Electron Capture
$ECEC$	=	Double Electron Capture
ESR	=	Experimental Storage Ring
FCNCs	=	Flavour Changing Neutral Currents
FN	=	Froggat-Nielsen mechanism
FRS	=	Fragment Separator
GIM	=	Glashow-Iliopoulos-Maiani mechanism
GSI	=	GSI Helmholtzzentrum für Schwerionenforschung
HDM	=	Heidelberg-Moscow experiment
$\mathcal{IH}$/IH	=	Inverted Hierarchy
$\mathcal{INT}$	=	Intermediate
KK	=	Kaluza-Klein
LFV	=	Lepton Flavour Violation
LHC	=	Large Hadron Collider
LR	=	Left-right symmetric
MSSM	=	Minimal Supersymmetric Standard Model
mSUGRA	=	Minimal Supergravity
NH	=	Normal Hierarchy
NME	=	Nuclear Matrix Element
PMNS	=	Pontecorvo-Maki-Nagakawa-Sakata
QBs	=	Quantum Beats
$\mathcal{QD}$	=	Quasi-degenerate
QM	=	Quantum Mechanics
QFT	=	Quantum Field Theory
SM	=	Standard Model
SUSY	=	Supersymmetry
THDM	=	Two Higgs Doublet Model
UEDs	=	Universal Extra Dimensions
VEV	=	Vacuum Expectation Value

Summary of the general conditions for the absence of LFV

A summary of the general conditions necessary for the absence of lepton flavour violation is given in the subsequent table.

Model	Conditions for the absence of tree-level FCNCs (S/V)	Conditions for the absence of tree-level FC by doubly charged bosons (Sab/V)	Conditions for the absence of 1-loop flavour change	1-loop flavour change & GIM-suppression
SM	S) aut. Align Vab) FU	N/A	A: $(\nu_L,\, W_\mu^-)$, Align excl.	A: aut. GIM
Multi Higgs	S) Align	N/A	A: $(\nu^M_{\text{heavy}}/\nu_R,\, H_k^-)$, Align B: $(\nu_L/\nu^M_{\text{light}},\, H_k^-)$, Align excl. C: $(\nu_{\text{Dirac}},\, H_k^-)$, Align excl.	A: Align, mass deg. for ν^M_{heavy} B: aut. GIM C: Align
Z'	Va) Align	N/A	N/I	N/I
Triplet Higgs	N/A	Sa) Align excl.	N/I	N/I
331	S) Align Va) FU	Sab) Align V) Align	N/I	N/I
LR	S) Align Va) FU	Sab) Align	N/I	N/I
Isosinglets	Vb) FU	N/A	N/I	N/I
UEDs	N/A	N/A	A: $(\nu_{L(n)},\, W^-_{\mu(n)})$, Align excl. A: $(\nu_{R(n)},\, a^-_{(n)})$, Align excl. B: $(\nu_{L(n)},\, a^-_{(n)})$, Align excl. C: $(\nu_{R/L(n)},\, a^-_{(n)})$, Align excl.	A, B, C: aut. GIM
MSSM $+\nu_R$	N/A without R-parity	N/A	A: $((\tilde{\chi}^{-/0}_{A,R})',\, \tilde{\nu}'/\tilde{e}')$, Align B: $((\tilde{\chi}^{-/0}_{A,L})',\, \tilde{\nu}'/\tilde{e}')$, Align C: $((\tilde{\chi}^{-/0}_{A})',\, \tilde{\nu}'/\tilde{e}')$, Align	A, B, C: aut. Align, mass deg.

Summary table of the necessary conditions for the absence of LFV. (N/A: not applicable; N/I: not investigated, due to presence at tree-level; aut. Align: Alignment is automatic in this model; Align excl.: Alignment is excluded phenomenologically; Align: Alignment needs to be imposed; FU: flavour universality; aut. GIM: all GIM-conditions are automatically fulfilled; mass deg.: Mass degeneracy needs to be imposed)

Acknowledgments

Everybody who has ever written a Ph.D.-thesis will know that such a task is never something that is really done alone. In any case there will be people who gave support, in the form of knowledge, exchange, guidance, love, or by just being there. Although the support of these people is not always visible in the work that has been done, it has been there! Because work is done by humans and every human being needs to live – in and beyond his or her work. Of course, such important people have also been there in my case. And now it is time to say thank you! To those I mention explicitely – and to those I don't.

The first and definitely one of the most important persons to mention is my supervisor Manfred Lindner. Thank you for taking me to Heidelberg and for accepting me as Ph.D.-student! Thank you for the freedom you gave me to pursue my own ideas, and for the guidance whenever I needed it (and for several times on late Friday afternoons when you skipped something in favor of a discussion with me)! And: Thank you for encouraging me in the phases when I had doubts! I am also greatful that I had so many opportunities to learn a lot when going to summer schools (the most important one being the great Cargese school in 2007) and when doing research visits (going to Dubna really helped a lot!). You can be sure that I know very well what I owe to you.

I am also grateful to my thesis referees: One is again Manfred. The other one is Tilman Plehn: Thank you for immediately agreeing to be the second referee, and for your quick answer! My third and fourth examiner should be mentioned, too. A big thank you to Klaus Blaum and Werner Aeschbach-Hertig for taking the time for my defense.

Everything would not have turned out so nicely if there were no people to proofread the whole thing: Martina Abb, Alex Blum, and Joachim Kopp did a really good job! (It is amazing what I don't see anymore when I have read a text five times in a row...)

Of course, before such a thesis can be written, a lot of work has to be done! This is much more fun when having nice, intelligent, and reliable collaborators: Adisorn Adulpravitchai, Alexander Blum, Hendrik Kienert, Joachim Kopp, Manfred Lindner, Werner Maneschg, Rabi Mohapatra, Viviana Niro, Werner Rodejohann, and Fedor Šimkovic are the ones that deserve my gratitude. Especially two should be mentioned: Joachim, we had so many illuminating discussions! It has always been a pleasure to work with you and I hope we go on with it when we're reshuffled to whatever countries in this world. And Fedor, thank you for being very patient with me when I kept on pushing our project and when I was asking too many questions at once. I have really learned a lot from you, maybe even more than you think!

A lot of work has been done, but this is by far not everything. A lot of organisational obstancles had to be overcome, too, and whenever there was such a problem our secretary Anja Berneiser has been on the spot to help me. Anja, thank you very much for the countless small (and bigger) things you helped me with! And thank you for being the heart (or the sun ;-)) of our division. It was always great to spend five minutes in your office, being supplied with gummy bears and talking about the nice aspects of life.

Work is important, but the surrounding is, too. It is crucial to have nice colleagues for enjoying the daily life. This has been made especially easy for me, since I had really nice people

around me at work, and some of them are now much more than just colleagues! The first person to mention is Alex Blum, with whom I have shared an office for nearly the whole time of my Ph.D. Alex, am really grateful to Claudia that she kicked you out of her office so that we finally ended up sharing ours! ;-) It was a pleasure to have so many discussions with you – about physics, of course, but also about so many other things. We have even made an invention, the *travel counter*. The deal was that, whenever one of us went to some new place for at least one night, he had to bring a postcard or something similar. By this, we kept ourselves being active and we went to see the world! In the end I have won the bet (16 to 13), but I think we both have gained a lot from it!

A very big thank you also to Werner Maneschg. It was a pleasure to meet you here and I enjoyed the countless times when we had nice discussions together, but also our culinary experiences, and the fun we had. The same is true for Dusan Budjas (whose names I will never be able to spell correctly with all dashes and squiggles): We really had a cool time together, I enjoyed it so much! And thank you, Flo Kaether and Mark Heisel, for all the fun, the snooker, and the discussions about music and karate! Thank you, Triple M (Markus Michael Müller), for the joyful coffee breaks, and you, Marik Barnabé-Heider and Oleg Chkvorets, for the good times we had together. There are so many people in our division, and all should be mentioned! But this list would be much too long... Still, I also had a good time with: Christoph Aberle, Adisorn Adulpravitchai, Evgeny Akhmedov, James Barry, Anja Berneiser, Fedor Bezrukov, Hans Hettmansperger, Reinhard Hofacker, Andreas Hohenegger, Alex Kartavtsev, Joachim Kopp, Conradin Langbrandtner, Sebastian Lindemann, Viviana Niro, Josefa Oehm, Toshi Ota, Peter Peiffer, Werner Rodejohann, Michael Schmidt, Thomas Schwetz, Hardy Simgen, Marc Weber, and with all the ones I forgot to mention explicitely – this was not on purpose, but just because of my confusion when trying to make a complete list.

Natürlich gibt es auch Menschen jenseits der Arbeit, denen mein großer Dank gebührt! Zum einen sind einige sehr wichtige Freunde zu erwähnen: Lukas Sennefelder, danke, dass wir so lange befreundet sind! Du kennst mich so gut (auch wenn wir uns seltener sehen) und wusstest immer Rat, wenn ich dich gefragt habe. Andy Regler, du hälst es auch schon ewig mit mir aus! Und das, obwohl wir beide oft genug so viel Stress hatten, dass wir uns oft verpasst haben. Trotzdem habe ich die Zeit jedes Mal genossen! Matze Stecher, uiuiui, das war echt krass, als du auf einmal nach Australien abgehauen bist! Aber es war richtig klasse, als wir dich dort besucht haben, und sicher endest du früher oder später auch wieder in Deutschland. Diese Zeit werden wir nutzen! Daniel Czap, auch du warst immer nah, auch wenn du geographisch weit weg bist. Aber wir halten uns ja immer wieder per Telefon auf dem Laufenden und hin und wieder sehen wir uns ja auch! Marius Schulte, danke für die vielen schönen Diskussionen, die wir zusammen hatten. Und Simon Dietz danke dafür, dass du mich hin und wieder doch ein bisschen neidisch gemacht hast, dass ich nicht in Ingolstadt geblieben bin.

Danke an meine Eltern, Franz und Katharina Merle. Nein, nicht einfach danke, ein RIESEN DANKE!!! Ihr habt mich immer unterstützt, auch wenn ich nicht leicht war. Ihr standet hinter jeder meiner Entscheidungen und ich weiß wie gern ihr mich habt (und was ich euch alles verdanke). Seid euch gewiss, dass ich genauso für euch empfinde!

Danke auch an meine "zweite Familie", Maria, Paul und Sabine Abb. Dafür, dass ich mich bei euch immer so wohl gefühlt habe (und natürlich für Maria's Kochtipps! ;-)).

Das allerallergrößte Dankeschön gebührt aber meiner Freundin Martina Abb. Danke für all deine Liebe!!! Danke für die schöne Zeit, die wir miteinander hatten, und für die vielen Jahre, die noch folgen werden! Du hast mein Leben wirklich verändert. Und ohne dich wäre das alles so nie möglich gewesen. Ich liebe dich!!!

Bibliography

[1] Project Gutenberg Literary Archive Foundation. `http://www.gutenberg.org`; from the German drama *Faust* by J. W. v. Goethe; Translation by C. T. Brooks.

[2] **UA1** Collaboration, G. Arnison *et al.*, "Experimental observation of lepton pairs of invariant mass around 95 GeV/c^2 at the CERN SPS collider," *Phys. Lett.* **B126** (1983) 398–410.

[3] **D0** Collaboration, S. Abachi *et al.*, "Observation of the top quark," *Phys. Rev. Lett.* **74** (1995) 2632–2637, `hep-ex/9503003`.

[4] Brookhaven National Laboratory. `http://www.g-2.bnl.gov/`.

[5] G. Bertone, D. Hooper, and J. Silk, "Particle dark matter: Evidence, candidates and constraints," *Phys. Rept.* **405** (2005) 279–390, `hep-ph/0404175`.

[6] A. Riotto, "Theories of baryogenesis," `hep-ph/9807454`.

[7] S. P. Martin, "A Supersymmetry Primer," `arXiv:hep-ph/9709356`.

[8] CERN. `http://lhc.web.cern.ch/lhc/`.

[9] A. Blum and A. Merle, "General Conditions for Lepton Flavor Violation at Tree- and 1-Loop Level," *Phys. Rev.* **D77** (2008) 076005, `arXiv:0709.3294 [hep-ph]`.

[10] H. Kienert, J. Kopp, M. Lindner, and A. Merle, "The GSI anomaly," *J. Phys. Conf. Ser.* **136** (2008) 022049, `arXiv:0808.2389 [hep-ph]`.

[11] W. Maneschg, A. Merle, and W. Rodejohann, "Statistical Analysis of future Neutrino Mass Experiments including Neutrino-less Double Beta Decay," *Europhys. Lett.* **85** (2009) 51002, `arXiv:0812.0479 [hep-ph]`.

[12] A. Adulpravitchai, M. Lindner, and A. Merle, "Confronting Flavour Symmetries and extended Scalar Sectors with Lepton Flavour Violation Bounds," `arXiv:0907.2147 [hep-ph]`.

[13] A. Merle, "Why a splitting in the final state cannot explain the GSI-Oscillations," `arXiv:0907.3554 [hep-ph]`.

[14] A. Adulpravitchai, M. Lindner, A. Merle, and R. N. Mohapatra, "Radiative Transmission of Lepton Flavor Hierarchies," `arXiv:0908.0470 [hep-ph]`.

[15] **Particle Data Group** Collaboration, C. Amsler *et al.*, "Review of particle physics," *Phys. Lett.* **B667** (2008) 1.

[16] P. Minkowski, "$\mu \to e\gamma$ at a Rate of One Out of 1-Billion Muon Decays?," *Phys. Lett.* **B67** (1977) 421.

[17] T. Yanagida, "Horizontal gauge symmetry and masses of neutrinos,". In Proceedings of the Workshop on the Baryon Number of the Universe and Unified Theories, Tsukuba, Japan, 13-14 Feb 1979.

[18] M. Gell-Mann, P. Ramond, and R. Slansky, "Complex Spinors and Unified Theories,". Print-80-0576 (CERN).

[19] S. L. Glashow, "The Future of Elementary Particle Physics," *NATO Adv. Study Inst. Ser. B Phys.* **59** (1980) 687.

[20] R. N. Mohapatra and G. Senjanovic, "Neutrino mass and spontaneous parity nonconservation," *Phys. Rev. Lett.* **44** (1980) 912.

[21] V. Barger, D. Marfatia, and K. Whisnant, "Progress in the physics of massive neutrinos," *Int. J. Mod. Phys.* **E12** (2003) 569–647, `hep-ph/0308123`.

[22] M. Beuthe, "Oscillations of neutrinos and mesons in quantum field theory," *Phys. Rept.* **375** (2003) 105–218, `arXiv:hep-ph/0109119`.

[23] M. C. Gonzalez-Garcia and M. Maltoni, "Phenomenology with Massive Neutrinos," *Phys. Rept.* **460** (2008) 1–129, `arXiv:0704.1800 [hep-ph]`.

[24] R. N. Mohapatra *et al.*, "Theory of neutrinos: A white paper," *Rept. Prog. Phys.* **70** (2007) 1757–1867, `arXiv:hep-ph/0510213`.

[25] B. Povh, K. Rith, C. Scholz, and F. Zetsche, "Particles and nuclei: An Introduction to the physical concepts,". Berlin, Germany: Springer (1995) 340 p.

[26] J. F. Gunion, H. E. Haber, G. L. Kane, and S. Dawson, "The Higgs Hunter's Guide,". SCIPP-89/13.

[27] P. Langacker and M. Plumacher, "Flavor changing effects in theories with a heavy Z' boson with family non-universal couplings," *Phys. Rev.* **D62** (2000) 013006, `hep-ph/0001204`.

[28] T. Appelquist, H.-C. Cheng, and B. A. Dobrescu, "Bounds on universal extra dimensions," *Phys. Rev.* **D64** (2001) 035002, `hep-ph/0012100`.

[29] Y. A. Litvinov *et al.*, "Observation of Non-Exponential Orbital Electron Capture Decays of Hydrogen-Like ^{140}Pr and ^{142}Pm Ions," *Phys. Lett.* **B664** (2008) 162–168, `arXiv:0801.2079 [nucl-ex]`.

[30] A. N. Ivanov, R. Reda, and P. Kienle, "On the time–modulation of the K–shell electron capture decay of H-like $^{140}Pr^{58+}$ ions produced by neutrino–flavour mixing," `arXiv:0801.2121 [nucl-th]`.

[31] A. N. Ivanov, E. L. Kryshen, M. Pitschmann, and P. Kienle, "Neutrino masses from the Darmstadt oscillations," `arXiv:0804.1311 [nucl-th]`.

[32] A. N. Ivanov, E. L. Kryshen, M. Pitschmann, and P. Kienle, "Time Modulation of the β^+-Decay Rate of H-Like $^{140}Pr^{58+}$ Ions," *Phys. Rev. Lett.* **101** (2008) 182501.

[33] M. Faber, "Kinematics and Quantum Field Theory of the Neutrino Oscillations Observed in the Time-modulated Orbital Electron Capture Decay in an Ion Storage Ring," `arXiv:0801.3262 [nucl-th]`.

[34] H. J. Lipkin, "New method for studying neutrino mixing and mass differences," arXiv:0801.1465 [hep-ph].

[35] H. J. Lipkin, "The GSI method for studying neutrino mass differences - For Pedestrians," arXiv:0805.0435 [hep-ph].

[36] H. Kleinert and P. Kienle, "Neutrino-Pulsating Vacuum and Neutrino Mass Difference," arXiv:0803.2938 [nucl-th].

[37] P. M. Walker, "A neutrino's wobble?," *Nature* **453N7197** (2008) 864–865.

[38] H. J. Lipkin, "Theory of neutrino oscillations using condensed matter physics Including production process and energy-time uncertainty," arXiv:0905.1216 [hep-ph].

[39] A. N. Ivanov, P. Kienle, and M. Pitschmann, "Rates of K-shell Electron Capture Decays of ^{180}Re and ^{142}Pm Atoms," arXiv:0905.1904 [nucl-th].

[40] A. N. Ivanov and P. Kienle, "On the time modulation of the K-shell electron capture decay rates of H-like heavy ions at GSI experiments," *Phys. Rev. Lett.* **103** (2009) 062502, arXiv:0908.0877 [nucl-th].

[41] C. Giunti, "Comment on the Neutrino-Mixing Interpretation of the GSI Time Anomaly," arXiv:0801.4639 [hep-ph].

[42] C. Giunti, "Rates of Processes with Coherent Production of Different Particles and the GSI Time Anomaly," *Phys. Lett.* **B665** (2008) 92–94, arXiv:0805.0431 [hep-ph].

[43] C. Giunti, "Comment on 'A neutrino's wobble?'," arXiv:0807.3818 [hep-ph].

[44] H. Burkhardt, J. Lowe, J. Stephenson, G. J., T. Goldman, and B. H. J. McKellar, "Oscillations in the GSI electron capture experiment," arXiv:0804.1099 [hep-ph].

[45] M. Peshkin, "Comment on 'New method for studying neutrino mixing and mass differences'," arXiv:0804.4891 [hep-ph].

[46] M. Peshkin, "Comment on 'The GSI method for studying neutrino mass differences - For Pedestrians'," arXiv:0811.1765 [hep-ph].

[47] A. Gal, "Neutrinos do not oscillate yet at GSI," arXiv:0809.1213 [nucl-th].

[48] A. G. Cohen, S. L. Glashow, and Z. Ligeti, "Disentangling Neutrino Oscillations," arXiv:0810.4602 [hep-ph].

[49] C. Giunti, "The GSI Time Anomaly: Facts and Fiction," *Nucl. Phys. Proc. Suppl.* **188** (2009) 43–45, arXiv:0812.1887 [hep-ph].

[50] C. Giunti, "The GSI Time Anomaly: Facts and Fiction," arXiv:0905.4620 [hep-ph].

[51] V. V. Flambaum, "Comment on 'Time modulation of the K-shell electron capture decay rates of H-like heavy ions at GSI experiments', arXiv:0908.0877," arXiv:0908.2039 [nucl-th].

[52] G. Lambiase, G. Papini, and G. Scarpetta, "Spin-rotation coupling in non-exponential decay of hydrogenlike heavy ions," arXiv:0811.2302 [nucl-th].

[53] I. M. Pavlichenkov, "Hyperfine Level Splitting for Hydrogen-Like Ions due to Rotation-Spin Coupling," *Europhys. Lett.* **85** (2009) 40008, arXiv:0810.2898 [physics.atom-ph].

[54] M. Faber, A. N. Ivanov, P. Kienle, M. Pitschmann, and N. I. Troitskaya, "On the influence of the magnetic field of the GSI experimental storage ring on the time-modulation of the EC- decay rates of the H-like mother ions," arXiv:0906.3617 [nucl-th].

[55] V. I. Isakov, "On the possible mixing of the electron capture and the positron emission channels in nuclear decay," arXiv:0906.4219 [nucl-th].

[56] N. Winckler *et al.*, "Can Hyperfine Excitation explain the Observed Oscillation- Puzzle of Nuclear Orbital Electron Capture of Hydrogen-like Ions?," arXiv:0907.2277 [nucl-th].

[57] Y. A. Litvinov *et al.*, "Comment on the paper 'Search for oscillation of the electron-capture decay probability of ^{142}Pm' at arXiv:0807.0649v1," arXiv:0807.2308 [nucl-ex].

[58] P. A. Vetter *et al.*, "Search for Oscillation of the Electron-Capture Decay Probability of ^{142}Pm," *Phys. Lett.* **B670** (2008) 196–199, arXiv:0807.0649 [nucl-ex].

[59] T. Faestermann *et al.*, "Could the GSI Oscillations be Observed in a Standard Electron Capture Decay Experiment?," arXiv:0807.3297 [nucl-ex].

[60] Y. Litvinov. private communication.

[61] T. Radon *et al.*, "Schottky mass measurements of cooled nuclei and mass landscape of the new area of neutron-defficient sub-uranium nuclides,". GSI-REPORT-2001-06.

[62] F. Bosch. private communication.

[63] H. B. Mann and D. R. Whitney, "On a Test of Whether one of Two Random Variables is Stochastically Larger than the Other," *Ann. Math. Statist.* **18** (1947) 50–60.

[64] M. E. Peskin and D. V. Schroeder, "An Introduction to quantum field theory,". Reading, USA: Addison-Wesley (1995) 842 p.

[65] T. Young, "The Bakerian Lecture. Experiments and Calculations Relative to Physical Optics.," *Royal Society of London Proceedings Series I* **1** (1800) 131–132.

[66] R. P. Feynman and A. R. Hibbs, *Quantum Mechanics and Path Integrals.* McGraw-Hill, New York, 1965.

[67] C. Giunti, C. W. Kim, and U. W. Lee, "Coherence of neutrino oscillations in vacuum and matter in the wave packet treatment," *Phys. Lett.* **B274** (1992) 87–94.

[68] M. Steck *et al.*, "Electron cooling experiments at the ESR," *Nucl. Instr. Meth.* **A532** (2004) 357–365.

[69] F. Bosch *et al.*, "Electron cooling force measurements for highly charged ions in the ESR," *Hyperfine Interactions* **99** (1996) 277–283.

[70] GSI. http://www.gsi.de/forschung/ap/projects/esr_e.html.

[71] C. Giunti, "Coherence and wave packets in neutrino oscillations," *Found. Phys. Lett.* **17** (2004) 103–124, arXiv:hep-ph/0302026.

[72] A. N. Ivanov, M. Faber, R. Reda, and P. Kienle, "Weak decays of H-like ^{140}Pr^{58+} and He-like ^{140}Pr^{57+} ions," arXiv:0711.3184.

[73] W. Bambynek *et al.*, "Orbital electron capture by the nucleus," *Rev. Mod. Phys.* **49** (1977) 77–221.

[74] B. Stech. private communication.

[75] W. W. Chow, M. O. Scully, and J. O. Stoner, "Quantum-beat phenomena described by quantum electrodynamics and neoclassical theory," *Phys. Rev.* **A11** (1975) 1380–1388.

[76] A. N. Ivanov, E. L. Kryshen, M. Pitschmann, and P. Kienle, "Comments on 'Rates of processes with coherent production of different particles and the GSI time anomaly'by C. Giunti, Phys. Lett. B 665, 92 (2008), 0805.0431," `arXiv:0807.2750 [nucl-th]`.

[77] M. Steck *et al.*, "Anomalous temperature reduction of electron cooled heavy ion beams in the storage ring ESR," *Phys. Rev. Lett.* **77** (1996) 3803–3806.

[78] A. N. Ivanov, R. Reda, and P. Kienle, "Reply on "Comment on neutrino-mixing interpretation of the GSI time anomaly"by C. Giunti, arXiv:0801.4639 [nucl-th]," `arXiv:0803.1289`.

[79] J. Schechter and J. W. F. Valle, "Neutrino Decay and Spontaneous Violation of Lepton Number," *Phys. Rev.* **D25** (1982) 774.

[80] Z.-z. Xing, "Vanishing effective mass of the neutrinoless double beta decay?," *Phys. Rev.* **D68** (2003) 053002, `arXiv:hep-ph/0305195`.

[81] F. Simkovic and A. Faessler, "Distinguishing the $0\nu\beta\beta$ decay mechanisms," *Prog. Part. Nucl. Phys.* **48** (2002) 201–209, `arXiv:hep-ph/0112272`.

[82] M. Doi and T. Kotani, "Neutrinoless modes of double beta decay," *Prog. Theor. Phys.* **89** (1993) 139–160.

[83] H. V. Klapdor-Kleingrothaus *et al.*, "Latest Results from the Heidelberg-Moscow Double Beta Decay Experiment," *Eur. Phys. J.* **A12** (2001) 147–154, `arXiv:hep-ph/0103062`.

[84] **CUORICINO** Collaboration, C. Arnaboldi *et al.*, "Results from a search for the $0\nu\beta\beta-$decay of ^{130}Te," *Phys. Rev.* **C78** (2008) 035502, `arXiv:0802.3439 [hep-ex]`.

[85] A. S. Barabash, "NEMO-3 double beta decay experiment: Lastest results," `arXiv:hep-ex/0610025`.

[86] P. Vogel, "Neutrino Mass and Neutrinoless Double Beta Decay," `arXiv:0807.1559 [hep-ph]`.

[87] F. Simkovic, A. Faessler, H. Muther, V. Rodin, and M. Stauf, "The $0\nu\beta\beta$-decay nuclear matrix elements with self- consistent short-range correlations," `arXiv:0902.0331 [nucl-th]`.

[88] A. Faessler *et al.*, "QRPA uncertainties and their correlations in the analysis of neutrinoless double beta decay," `arXiv:0810.5733 [hep-ph]`.

[89] J. Suhonen and M. Kortelainen, "Nuclear matrix elements for double beta decay," *Int. J. Mod. Phys.* **E17** (2008) 1–11.

[90] J. Suhonen and M. Kortelainen, "Nuclear matrix elements for $0\nu\beta\beta$ decay: Recent advances," *AIP Conf. Proc.* **972** (2008) 128–136.

[91] V. I. Tretyak and Y. G. Zdesenko, "Tables of double beta decay data - an update," *Atom. Data Nucl. Data Tabl.* **80** (2002) 83–116.

[92] M. Lindner, A. Merle, and W. Rodejohann, "Improved limit on θ_{13} and implications for neutrino masses in neutrino-less double beta decay and cosmology," *Phys. Rev.* **D73** (2006) 053005, arXiv:hep-ph/0512143.

[93] A. Merle and W. Rodejohann, "Getting information on $|U_{e3}|^2$ from neutrino-less double beta decay," *Adv. High Energy Phys.* **2007** (2007) 82674, arXiv:hep-ph/0703135.

[94] I. Abt *et al.*, "A new Ge-76 double beta decay experiment at LNGS," arXiv:hep-ex/0404039.

[95] H. Simgen. private communication.

[96] S. Hannestad, "Primordial Neutrinos," *Ann. Rev. Nucl. Part. Sci.* **56** (2006) 137–161, arXiv:hep-ph/0602058.

[97] **KATRIN** Collaboration, A. Osipowicz *et al.*, "KATRIN: A next generation tritium beta decay experiment with sub-eV sensitivity for the electron neutrino mass," arXiv:hep-ex/0109033.

[98] O. Host, O. Lahav, F. B. Abdalla, and K. Eitel, "Forecasting neutrino masses from combining KATRIN and the CMB: Frequentist and Bayesian analyses," *Phys. Rev.* **D76** (2007) 113005, arXiv:0709.1317 [hep-ph].

[99] S. Pascoli, S. T. Petcov, and T. Schwetz, "The Absolute Neutrino Mass Scale, Neutrino Mass Spectrum, Majorana CP-Violation and Neutrinoless Double-Beta Decay," *Nucl. Phys.* **B734** (2006) 24–49, arXiv:hep-ph/0505226.

[100] A. Y. Ignatiev and B. H. J. McKellar, "Possible new interactions of neutrino and the KATRIN experiment," *Phys. Lett.* **B633** (2006) 89–92, arXiv:hep-ph/0506246.

[101] R. Fardon, A. E. Nelson, and N. Weiner, "Dark energy from mass varying neutrinos," *JCAP* **0410** (2004) 005, arXiv:astro-ph/0309800.

[102] R. D. Peccei, "Neutrino models of dark energy," *Phys. Rev.* **D71** (2005) 023527, arXiv:hep-ph/0411137.

[103] G. L. Fogli *et al.*, "Observables sensitive to absolute neutrino masses: A reappraisal after WMAP-3y and first MINOS results," *Phys. Rev.* **D75** (2007) 053001, arXiv:hep-ph/0608060.

[104] G. L. Fogli *et al.*, "Observables sensitive to absolute neutrino masses (Addendum)," *Phys. Rev.* **D78** (2008) 033010, arXiv:0805.2517 [hep-ph].

[105] H. V. Klapdor-Kleingrothaus, I. V. Krivosheina, A. Dietz, and O. Chkvorets, "Search for neutrinoless double beta decay with enriched ^{76}Ge in Gran Sasso 1990-2003," *Phys. Lett.* **B586** (2004) 198–212, arXiv:hep-ph/0404088.

[106] M. Doi and T. Kotani, "Neutrino emitting modes of double beta decay," *Prog. Theor. Phys.* **87** (1992) 1207–1232.

[107] Z. Sujkowski and S. Wycech, "Neutrino-less double electron capture: A tool to search for Majorana neutrinos," *Phys. Rev.* **C70** (2004) 052501, arXiv:hep-ph/0312040.

[108] F. Simkovic. private communication.

[109] J. D. Bjorken and S. D. Drell, "Relativistic Quantum Mechanis (German Translation),". Spektrum Akademischer Verlag, 1998, Heidelberg/Berlin, Germany, 312p.

[110] S. M. Bilenky and S. T. Petcov, "Massive Neutrinos and Neutrino Oscillations," *Rev. Mod. Phys.* **59** (1987) 671.

[111] M. Doi, T. Kotani, H. Nishiura, K. Okuda, and E. Takasugi, "Neutrino mass, the right-handed interaction and the double beta decay. I. Formalism," *Prog. Theor. Phys.* **66** (1981) 1739.

[112] P. Domin, S. Kovalenko, F. Simkovic, and S. V. Semenov, "Neutrino accompanied $\beta^{\pm}\beta^{\pm}$, β^{+}/EC and EC/EC processes within single state dominance hypothesis," *Nucl. Phys.* **A753** (2005) 337–363, arXiv:nucl-th/0411002.

[113] L. D. Landau and E. M. Lifshitz, "Textbook on Theoretical Physics Vol. 4: Quantum Electrodynamics (German Translation),". Akademie-Verlag, 1991, Berlin, Germany, 614p.

[114] M. Maggiore, "A Modern introduction to quantum field theory,". Oxford University Press, 2005. (Oxford Series in Physics, 12. ISBN 0 19 852073 5).

[115] R. Firestone. http://ie.lbl.gov/atomic/bind.pdf.

[116] O. Chkvorets, "Search for double beta decay with HPGe detectors at the Gran Sasso underground laboratory," arXiv:0812.1206 [nucl-ex].

[117] O. Chkvorets, M. Barnabe-Heider, K. Gusev, and S. Schonert, "Limit on radiative 0νECEC decay of ^{36}Ar,". GERDA Scientific / Technical Report: GSTR-06-019.

[118] F. Deppisch and H. Pas, "Pinning down the mechanism of neutrinoless double beta decay with measurements in different nuclei," *Phys. Rev. Lett.* **98** (2007) 232501, arXiv:hep-ph/0612165.

[119] K. Zuber, "COBRA: Double beta decay searches using CdTe detectors," *Phys. Lett.* **B519** (2001) 1–7, arXiv:nucl-ex/0105018.

[120] **COBRA** Collaboration, T. Bloxham *et al.*, "First results on double beta decay modes of Cd, Te and Zn isotopes with the COBRA experiment," *Phys. Rev.* **C76** (2007) 025501, arXiv:0707.2756 [nucl-ex].

[121] A. S. Barabash, F. Hubert, P. Hubert, and V. Umatov, "New limits on the beta+ EC and ECEC processes in Te-120," *J. Phys.* **G34** (2007) 1721–1728, arXiv:nucl-ex/0703020.

[122] H. Kiel, D. Munstermann, and K. Zuber, "A search for various double beta decay modes of Cd, Te and Zn isotopes," *Nucl. Phys.* **A723** (2003) 499–514, arXiv:nucl-ex/0301007.

[123] F. A. Danevich *et al.*, "ZnWO-4 crystals as detectors for 2beta decay and dark matter experiments," *Nucl. Instrum. Meth.* **A544** (2005) 553–564, arXiv:nucl-ex/0409014.

[124] P. Belli *et al.*, "New limits on 2beta+ decay processes in Cd-106," *Astropart. Phys.* **10** (1999) 115–120.

[125] O. Nachtmann, "Elementary Particle Physics: Concepts and Phenomena,". Berlin, Germany: Springer (1990) 559 p.

[126] **MEGA** Collaboration, M. L. Brooks *et al.*, "New limit for the family-number non-conserving decay $\mu^+ \to e^+\gamma$," *Phys. Rev. Lett.* **83** (1999) 1521–1524, `hep-ex/9905013`.

[127] **MEG** Collaboration, S. Ritt, "Status of the MEG experiment $\mu \to e\gamma$," *Nucl. Phys. Proc. Suppl.* **162** (2006) 279–282.

[128] T. P. Cheng and L. F. Li, "Gauge Theory of Elementary Particle Physics,". Oxford, UK: Clarendon (1984) 536 P. (Oxford Science Publications).

[129] T. P. Cheng and L. F. Li, "Gauge theory of elementary particle physics: Problems and solutions,". Oxford, UK: Clarendon (2000) 306 p.

[130] B. He, "Probing extra dimensions by lepton flavor nonconserving quantum loop effects,". UMI-30-74926.

[131] L. Lavoura, "General formulae for $f_1 \to f_2\gamma$," *Eur. Phys. J.* **C29** (2003) 191–195, `arXiv:hep-ph/0302221`.

[132] S. L. Glashow, J. Iliopoulos, and L. Maiani, "Weak Interactions with Lepton-Hadron Symmetry," *Phys. Rev.* **D2** (1970) 1285–1292.

[133] S. Antusch, C. Biggio, E. Fernandez-Martinez, M. B. Gavela, and J. Lopez-Pavon, "Unitarity of the Leptonic Mixing Matrix," *JHEP* **10** (2006) 084, `arXiv:hep-ph/0607020`.

[134] **Belle** Collaboration, K. Hayasaka *et al.*, "New search for $\tau \to \mu\gamma$ and $\tau \to e\gamma$ decays at Belle," *Phys. Lett.* **B666** (2008) 16–22, `arXiv:0705.0650 [hep-ex]`.

[135] **BABAR** Collaboration, B. Aubert *et al.*, "Search for lepton flavor violation in the decay $\tau^\pm \to e^\pm\gamma$," *Phys. Rev. Lett.* **96** (2006) 041801, `arXiv:hep-ex/0508012`.

[136] **SINDRUM** Collaboration, U. Bellgardt *et al.*, "Search for the Decay $\mu^+ \to e^+e^+e^-$," *Nucl. Phys.* **B299** (1988) 1.

[137] **SINDRUM II.** Collaboration, C. Dohmen *et al.*, "Test of lepton flavor conservation in $\mu \to e$ conversion on titanium," *Phys. Lett.* **B317** (1993) 631–636.

[138] M. Blanke, A. J. Buras, B. Duling, A. Poschenrieder, and C. Tarantino, "Charged Lepton Flavour Violation and $(g-2)_\mu$ in the Littlest Higgs Model with T-Parity: a clear Distinction from Supersymmetry," *JHEP* **05** (2007) 013, `hep-ph/0702136`.

[139] M. Raidal *et al.*, "Flavour physics of leptons and dipole moments," *Eur. Phys. J.* **C57** (2008) 13–182, `arXiv:0801.1826 [hep-ph]`.

[140] A. de Gouvea and J. Jenkins, "A Survey of Lepton Number Violation via Effective Operators," `arXiv:0708.1344 [hep-ph]`.

[141] S. L. Glashow and S. Weinberg, "Natural Conservation Laws for Neutral Currents," *Phys. Rev.* **D15** (1977) 1958.

[142] E. A. Paschos, "Diagonal Neutral Currents," *Phys. Rev.* **D15** (1977) 1966.

[143] B. W. Lee and R. E. Shrock, "Natural Suppression of Symmetry Violation in Gauge Theories: Muon - Lepton and Electron Lepton Number Nonconservation," *Phys. Rev.* **D16** (1977) 1444.

[144] C. Itzykson and J. B. Zuber, "Quantum Field Theory,". New York, USA: Mcgraw-hill (1980) 705 P.(International Series In Pure and Applied Physics).

[145] J. T. Liu and D. Ng, "Lepton flavor changing processes and CP violation in the 331 model," *Phys. Rev.* **D50** (1994) 548–557, `hep-ph/9401228`.

[146] D. L. Anderson and M. Sher, "3-3-1 models with unique lepton generations," *Phys. Rev.* **D72** (2005) 095014, `hep-ph/0509200`.

[147] C. Promberger, S. Schatt, and F. Schwab, "Flavor changing neutral current effects and CP violation in the minimal 3-3-1 model," `hep-ph/0702169`.

[148] N. G. Deshpande, J. F. Gunion, B. Kayser, and F. I. Olness, "Left-right symmetric electroweak models with triplet Higgs," *Phys. Rev.* **D44** (1991) 837–858.

[149] A. G. Akeroyd, M. Aoki, and Y. Okada, "Lepton flavour violating tau decays in the left-right symmetric model," `hep-ph/0610344`.

[150] G. C. Branco, D. Delepine, B. Nobre, and J. Santiago, "Extra dimensions, isosinglet charged leptons and neutrino factories," *Nucl. Phys.* **B657** (2003) 355–377, `arXiv:hep-ph/0209263`.

[151] F. Pisano and V. Pleitez, "An $SU(3) \times U(1)$ model for electroweak interactions," *Phys. Rev.* **D46** (1992) 410–417, `hep-ph/9206242`.

[152] A. De Rujula, H. Georgi, and S. L. Glashow, "A Theory of Flavor Mixing," *Ann. Phys.* **109** (1977) 258.

[153] A. J. Buras, M. Spranger, and A. Weiler, "The impact of universal extra dimensions on the unitarity triangle and rare K and B decays.," *Nucl. Phys.* **B660** (2003) 225–268, `hep-ph/0212143`.

[154] I. I. Bigi *et al.*, "Charged lepton radiative and B-meson double radiative decays in models with universal extra dimensions," `hep-ph/0603160`.

[155] J. Hisano, T. Moroi, K. Tobe, and M. Yamaguchi, "Lepton-Flavor Violation via Right-Handed Neutrino Yukawa Couplings in Supersymmetric Standard Model," *Phys. Rev.* **D53** (1996) 2442–2459, `hep-ph/9510309`.

[156] Z. Chacko and G. D. Kribs, "Constraints on lepton flavor violation in the MSSM from the muon anomalous magnetic moment measurement," *Phys. Rev.* **D64** (2001) 075015, `hep-ph/0104317`.

[157] Y. Nir and N. Seiberg, "Should squarks be degenerate?," *Phys. Lett.* **B309** (1993) 337–343, `hep-ph/9304307`.

[158] S. Dimopoulos and H. Georgi, "Softly Broken Supersymmetry and $SU(5)$," *Nucl. Phys.* **B193** (1981) 150.

[159] C. Hagedorn, *Flavored Model Building*. PhD thesis, Munich University of Technology, Munich, January, 2008.

[160] V. Barger, P. Langacker, M. McCaskey, M. J. Ramsey-Musolf, and G. Shaughnessy, "LHC Phenomenology of an Extended Standard Model with a Real Scalar Singlet," *Phys. Rev.* **D77** (2008) 035005, arXiv:0706.4311 [hep-ph].

[161] H. E. Haber and D. O'Neil, "Basis-independent methods for the two-Higgs-doublet model. II: The significance of $\tan\beta$," *Phys. Rev.* **D74** (2006) 015018, arXiv:hep-ph/0602242.

[162] R. Diaz, R. Martinez, and J. A. Rodriguez, "Lepton flavor violation in the two Higgs doublet model type III," *Phys. Rev.* **D63** (2001) 095007, arXiv:hep-ph/0010149.

[163] W. Grimus and L. Lavoura, "$S(3) \times Z(2)$ model for neutrino mass matrices," *JHEP* **08** (2005) 013, arXiv:hep-ph/0504153.

[164] W. Grimus and L. Lavoura, "A discrete symmetry group for maximal atmospheric neutrino mixing," *Phys. Lett.* **B572** (2003) 189–195, arXiv:hep-ph/0305046.

[165] H. Ishimori *et al.*, "D_4 Flavor Symmetry for Neutrino Masses and Mixing," *Phys. Lett.* **B662** (2008) 178–184, arXiv:0802.2310 [hep-ph].

[166] A. Adulpravitchai, A. Blum, and C. Hagedorn, "A Supersymmetric D_4 Model for mu-tau Symmetry," *JHEP* **03** (2009) 046, arXiv:0812.3799.

[167] T. Fukuyama and H. Nishiura, "Mass matrix of Majorana neutrinos," arXiv:hep-ph/9702253.

[168] E. Ma and G. Rajasekaran, "Softly broken A_4 symmetry for nearly degenerate neutrino masses," *Phys. Rev.* **D64** (2001) 113012, arXiv:hep-ph/0106291.

[169] K. S. Babu, E. Ma, and J. W. F. Valle, "Underlying A_4 symmetry for the neutrino mass matrix and the quark mixing matrix," *Phys. Lett.* **B552** (2003) 207–213, arXiv:hep-ph/0206292.

[170] G. Altarelli and F. Feruglio, "Tri-bimaximal neutrino mixing from discrete symmetry in extra dimensions," *Nucl. Phys.* **B720** (2005) 64–88, arXiv:hep-ph/0504165.

[171] G. Altarelli and F. Feruglio, "Tri-bimaximal neutrino mixing, A_4 and the modular symmetry," *Nucl.Phys* **B741** (2006) 215–235, arXiv:hep-ph/0512103.

[172] G. Altarelli, F. Feruglio, and Y. Lin, "Tri-bimaximal neutrino mixing from orbifolding," *Nucl. Phys.* **B775** (2007) 31–44, arXiv:hep-ph/0610165.

[173] P. F. Harrison, D. H. Perkins, and W. G. Scott, "Tri-bimaximal mixing and the neutrino oscillation data," *Phys. Lett.* **B530** (2002) 167, arXiv:hep-ph/0202074.

[174] S. Goswami, S. Petcov, S. Ray, and W. Rodejohann, "Large U_{e3} and Tri-bimaximal Mixing," arXiv:0907.2869 [hep-ph].

[175] E. Ma, "Verifiable radiative seesaw mechanism of neutrino mass and dark matter," *Phys. Rev.* **D73** (2006) 077301, arXiv:hep-ph/0601225.

[176] D. Aristizabal Sierra, J. Kubo, D. Restrepo, D. Suematsu, and O. Zapata, "Radiative seesaw: Warm dark matter, collider and lepton flavour violating signals," *Phys. Rev.* **D79** (2009) 013011, arXiv:0808.3340 [hep-ph].

[177] E. Ma, "Neutrino Mass: Mechanisms and Models," arXiv:0905.0221 [hep-ph].

[178] A. Zee, "A Theory of Lepton Number Violation, Neutrino Majorana Mass, and Oscillation," *Phys. Lett.* **B93** (1980) 389.

[179] K. S. Babu and E. Ma, "Natural Hierarchy of radiatively induced Majorana Neutrino Masses," *Phys. Rev. Lett.* **61** (1988) 674.

[180] A. Zee, "Quantum Numbers of Majorana Neutrino Masses," *Nucl. Phys.* **B264** (1986) 99.

[181] K. S. Babu, "Model of 'Calculable' Majorana Neutrino Masses," *Phys. Lett.* **B203** (1988) 132.

[182] D. Suematsu, T. Toma, and T. Yoshida, "Reconciliation of CDM abundance and $\mu \to e\gamma$ in a radiative seesaw model," `arXiv:0903.0287 [hep-ph]`.

[183] E. M. Dolle and S. Su, "The Inert Dark Matter," `arXiv:0906.1609 [hep-ph]`.

[184] D. Eriksson, J. Rathsman, and O. Stal, "2HDMC - Two-Higgs-Doublet Model Calculator Physics and Manual," `arXiv:0902.0851 [hep-ph]`.

[185] M. Hirsch, S. Morisi, and J. W. F. Valle, "Tri-bimaximal neutrino mixing and neutrinoless double beta decay," *Phys. Rev.* **D78** (2008) 093007, `arXiv:0804.1521 [hep-ph]`.

[186] M. C. Chen and S. F. King, "A_4 See-Saw Models and Form Dominance," *JHEP* **06** (2009) 072, `arXiv:0903.0125`.

[187] A. Raspereza, "Higgs search results," `arXiv:hep-ex/0209021`.

[188] W. Grimus, L. Lavoura, O. M. Ogreid, and P. Osland, "A precision constraint on multi-Higgs-doublet models," *J. Phys.* **G35** (2008) 075001, `arXiv:0711.4022 [hep-ph]`.

[189] R. Kitano, M. Koike, and Y. Okada, "Detailed calculation of lepton flavor violating muon electron conversion rate for various nuclei," *Phys. Rev.* **D66** (2002) 096002, `arXiv:hep-ph/0203110`.

[190] J. C. Pati and A. Salam, "Lepton Number as the Fourth Color," *Phys. Rev.* **D10** (1974) 275–289.

[191] R. N. Mohapatra and J. C. Pati, "Left-Right Gauge Symmetry and an Isoconjugate Model of CP Violation," *Phys. Rev.* **D11** (1975) 566–571.

[192] G. Senjanovic and R. N. Mohapatra, "Exact Left-Right Symmetry and Spontaneous Violation of Parity," *Phys. Rev.* **D12** (1975) 1502.

[193] R. N. Mohapatra and G. Senjanovic, "Neutrino Masses and Mixings in Gauge Models with Spontaneous Parity Violation," *Phys. Rev.* **D23** (1981) 165.

[194] W. Konetschny and W. Kummer, "Nonconservation of Total Lepton Number with Scalar Bosons," *Phys. Lett.* **B70** (1977) 433.

[195] R. E. Marshak and R. N. Mohapatra, "Selection Rules for Baryon Number Nonconservation in Gauge Models,". Invited talk given at Orbis Scientiae, Coral Gables, Fla., Jan 14-17, 1980.

[196] T. P. Cheng and L.-F. Li, "Neutrino Masses, Mixings and Oscillations in $SU(2) \times U(1)$ Models of Electroweak Interactions," *Phys. Rev.* **D22** (1980) 2860.

[197] G. Lazarides, Q. Shafi, and C. Wetterich, "Proton Lifetime and Fermion Masses in an SO(10) Model," *Nucl. Phys.* **B181** (1981) 287.

[198] A. Blum, C. Hagedorn, and A. Hohenegger, "θ_C from the Dihedral Flavor Symmetries D_7 and D_{14}," *JHEP* **03** (2008) 070, `arXiv:0710.5061 [hep-ph]`.

[199] N. Haba and H. Murayama, "Anarchy and hierarchy," *Phys. Rev.* **D63** (2001) 053010, `arXiv:hep-ph/0009174`.

[200] C. D. Froggatt and H. B. Nielsen, "Hierarchy of Quark Masses, Cabibbo Angles and CP Violation," *Nucl. Phys.* **B147** (1979) 277.